SUSCEPTIBILITY OF DS/FH, M-ARY DPSK TO PARTIAL- AND FULL-BAND NOISE, CW-TONE, AND PERIODIC FM JAMMING

A THESIS

Presented to

The Faculty of the Division of Graduate

Studies and Research

by

Richard A. Yost

In Partial Fulfillment

of the Requirements for the Degree

Doctor of Philosophy

in the School of Electrical Engineering

Georgia Institute of Technology

March 1978

SUSCEPTIBILITY OF DS/FH, M-ARY DPSK

TO PARTIAL- AND FULL-BAND NOISE,

CW-TONE, AND PERIODIC FM JAMMING

Approved:

R. H. Pettit, Chairman

A. [redacted]

J. L. Hammond

Date approved by chairman: 3-9-71

This dissertation is dedicated to

my mother,

Dortha A. Yost

and

to the memory of

my father,

Harold E. Yost

ACKNOWLEDGMENTS

It is my pleasure at this time to extend my sincere gratitude to my thesis advisor, Dr. Ray H. Pettit. The constant encouragement from and worthwhile discussions with Dr. Pettit were of significant personal and technical importance throughout the duration of this work.

I thank the members of the reading committee, Drs. Aubrey M. Bush and Joseph L. Hammond, for not only taking the time to review and comment on this thesis but also for the academic pleasure I received from their instructional endeavors.

I am pleased to acknowledge the partial financial support of the Office of the Assistant Chief of Staff for Studies and Analysis, Headquarters-U. S. Air Force. In addition, the financial support of the Callaway Foundation through the President's Fellowship and the Schlumberger Oil Company through the Schlumberger Fellowship for my first two years of graduate studies is greatly appreciated.

Gratitude is also extended to Mrs. Kathy Massett for her skillful typing and her infinite patience.

Finally, and most importantly, I wish to acknowledge the commitment, dedication, and emotional support of my wife, Sharon. This thesis is as much hers as it is mine.

TABLE OF CONTENTS

		PAGE
DEDICATION		ii
ACKNOWLEDGMENTS		iii
GLOSSARY OF SYMBOLS		vii
LIST OF TABLES		xix
LIST OF ILLUSTRATIONS		xxi
SUMMARY		xxvii
Chapter		
I.	INTRODUCTION	1
II.	ECM AND SPREAD SPECTRUM	7
III.	DPSK	25
IV.	THE SYSTEM MODEL	33
	Receiver Model Signal Model Noise Model IF_2 Bandpass Filter Model Jamming Model Spread Spectrum Model	
V.	CHARACTERIZATION OF THE SPREAD AND FILTERED INTERFERENCE	50
	Periodic FM Jamming Signal CW-Tone Jamming Signal Noise Jamming Signal	
VI.	GENERAL SUSCEPTIBILITY ANALYSIS	60
VII.	PROBABILITY OF ERROR FOR BINARY DPSK	74
	Periodic FM Jamming CW-Tone Jamming Noise Jamming	

		PAGE
VIII.	PROBABILITY OF ERROR FOR QUATERNARY DPSK	90
	Periodic FM Jamming CW-Tone Jamming Noise Jamming	
IX.	PROBABILITY OF ERROR FOR M-ARY DPSK	106
	Upper and Lower Bounds Periodic FM Jamming CW-Tone Jamming Noise Jamming	
X.	DEVELOPMENT OF TRACTABLE ERROR EXPRESSIONS	131
XI.	QUANTITATIVE PROCEDURES AND RESULTS	164
	Preliminaries Computational Organization Basis for Parametric Comparison General Results and Preliminary Conclusions Code Rate Dependence Hopping Slot Dependence and Partial-Band Jamming Effects Frequency Offset Dependence FM Modulation Index Dependence Gaussian Approximations M-ary DPSK	
XII.	SUMMARY, CONCLUSIONS, AND RECOMMENDATIONS	237
	Transmitter Strategy Jamming Strategy Processing Gain Definitions Gaussian Approximations Recommendations	
Appendix		
A.	FOURIER SERIES COEFFICIENTS OF LINEAR-SWEPT FM . . .	242
B.	ERROR EXPRESSIONS FOR DS/FH, BINARY DPSK SUBJECTED TO DEPENDENT INTERFERENCE	244
C.	FOURIER SERIES COEFFICIENTS OF A PSEUDO-RANDOM WAVEFORM	250
D.	SPECTRAL-DENSITY-REDUCTION-FACTOR FOR NOISE JAMMING	258
E.	PROOF THAT $PR(ERR\|JR,\overline{JP}) = PR(ERR\|\overline{JR},JP)$	265

PAGE

F. PRICE'S FUNCTION 274

G. DERIVATION OF $p_{\gamma|\phi_1}(\gamma|\phi_1)$ 276

H. STEPS LEADING TO ROSENBAUM'S EQUIVALENT EXPRESSION 282

I. PROOF OF THE EVEN DISTRIBUTION OF ERRORS 288

J. DETERMINATION OF THE GENERAL LOWER BOUND FOR M EVEN 296

K. CONDITIONS FOR ENVELOPE PERIODICITY 301

L. ENVELOPE CALCULATIONS 307

BIBLIOGRAPHY 311

VITA 317

GLOSSARY OF SYMBOLS

A	Maximum of the spread and filtered CW-tone envelope
A_x	RMS value of the spread and filtered FM envelope at the maxchip
$A_{ji}(t)$	Spread and filtered FM envelope in the i^{th} signaling interval
$[A_{ji}(t)]_{cw}$	Spread and filtered CW-tone envelope in the i^{th} signaling interval
$a_{ji}(t)$	Dimensionless quantity, $A_{ji}(t) \cdot (\frac{\sqrt{K_s}}{A_j})$
$a_{jicw}(t)$	Dimensionless quantity, $[A_{ji}(t)]_{cw} \cdot (\frac{\sqrt{K_s}}{A_j})$
A_1, A_2	Sampled, spread and filtered jamming signal envelopes
A_s	DPSK signal amplitude
A_j	Unscaled jamming signal amplitude
$A(\omega)$	Filter magnitude characteristic
A^+, A^-	Filter magnitudes
a_i	Amplitudes of a PR waveform, ± 1
a_n	Fourier series coefficients of a periodic FM signal
$\lvert a_n \rvert$	Magnitude of the Fourier series coefficients of a periodic FM signal

$\{\alpha_i\}$	Set of gaussian random variables
β	FM modulation index
b_K	Butterworth filter phase coefficients
$\binom{b}{a}$	Binomial coefficients, $\frac{b!}{a!(b-a)!}$
$C(u)$	Fresnel integral, $\int_o^u \cos(\pi t^2/2)\,dt$
$C_d(\tau)$	Unnormalized, discrete version of the autocorrelation function for a PR waveform
$C_c(\tau)$	Unnormalized, continuous version of the autocorrelation function for a PR waveform
c_m	Fourier series coefficients of a PR waveform
$\|c_m\|$	Magnitude of the Fourier series coefficients of a PR waveform
$\|c'_m\|$	Modified version of $\|c_m\|$
DS	Direct sequence
d_1, d_2	Distances
δ_{m0}	Kronecker delta, if m=0, then $\delta_{m0}=1$
δ_i^{ℓ}	Jamming parameter, equal to one if jamming signal is located in the ℓ^{th} hopping slot during the i^{th} signaling interval and zero otherwise
$E[\cdot]$	Expectation operator
E_b	Energy per bit
err	The event describing a decision error
$\mathrm{erf}(u)$	Error function, $\frac{2}{\sqrt{\pi}}\int_o^u \exp(-t^2)\,dt$

erfc(u)	Complementary error function, $\frac{2}{\sqrt{\pi}} \int_u^\infty \exp(-t^2)dt$
FH	Frequency-hopping
f	Frequency, in hertz
γ, α	Angles
H	The event describing that a frequency-hop has occurred between adjacent signaling intervals
$H(\omega)$	Filter transfer characteristic
I_h	Integer
$I_o(u)$	Modified Bessel function of the first kind and order zero, $\frac{1}{2\pi} \int_o^{2\pi} \exp(u \cos t)dt$
$I_\mu(u)$	Modified Bessel function of the first kind and order μ
J	Total jamming power, each jammed slot contains J/K_s units of power
J_o	One-sided, spectral density height of a noise jammer
JR, JP	Reference signal jammed, present signal jammed
JR, $\overline{JP}$	Reference signal jammed, present signal not jammed
$\overline{JR}$, JP	Reference signal not jammed, present signal jammed
$\overline{JR}$, $\overline{JP}$	Reference signal not jammed, present signal not jammed
$j_i^\ell(t)$	Jamming signal located in the ℓ^{th} hopping slot during the i^{th} signaling interval

$j_i(t)$	Dehopped jamming signal in the i^{th} signaling interval
$j_{is}(t)$	DS-spread and dehopped jamming signal in the i^{th} signaling interval
$j_{isf}(t)$	Filtered, DS-spread, and dehopped jamming signal in the i^{th} signaling interval
$[j_i^{\ell}(t)]_{cw}$	CW-tone jamming signal located in the ℓ^{th} frequency hopping slot during the i^{th} signaling interval
$[j_i(t)]_{cw}$	Dehopped, CW-tone jamming signal in the i^{th} signaling interval
$[j_{is}(t)]_{cw}$	DS-spread and dehopped, CW-tone jamming signal in the i^{th} signaling interval
$[j_{isf}(t)]_{cw}$	Filtered, DS-spread, and dehopped, CW-tone jamming signal in the i^{th} signaling interval.
K	Butterworth filter order
K_j	A constant
K_s	Number of hopping slots containing jamming signals ($1 \leq K_s \leq N_s$)
k	Any one of the M possible DPSK waveforms, (0,1, . . . ,M-1)
k_p	One of the p phase shifts of the PR waveform
M	Number of distinct DPSK waveforms (M phases) being transmitted
m(t)	Periodic, modulating waveform

$\{m_i\}$	Mean values of $\{\alpha_i\}$
N	Thermal noise power
N_1, N_2, N_3	Integers
N_j	Total noise jamming power
N_j'	Total noise jamming power at the demodulator input
N_r	Number of signaling intervals over which the jamming envelope repeats
N_o	One-sided spectral density of the white, gaussian thermal noise
N_s	Number of frequency-hopping slots
$n_i(t)$	Sample function from a white gaussian noise random process located in the i^{th} signaling interval
$n_{is}(t)$	DS-spread noise process in the i^{th} signaling interval
$n_{if}(t)$	Narrowband-filtered, white gaussian noise process in the i^{th} signaling interval
PR	Pseudo-random
PN	Pseudo-noise
P_1, P_2	Random variables
P_k	A'priori probabilities (k=0,1, . . . ,M-1)
P_{R_j}	Probability that the received signal falls in the error subregion R_j
$P_{\mu,\nu}(a,b;r)$	Price's function [53]
$P_p[\lambda]$	Half-plane probability function for the present signal

$P_r[\lambda]$	Half-plane probability function for the reference signal
$P_{\lvert\theta\rvert}(\theta)$	Probability distribution function of the magnitude of θ
$Pr(JR,JP)$	Probability that both the reference and present signals are jammed
$Pr(JR,\overline{JP})$	Probability that the reference signal is jammed and the present signal is not jammed
$Pr(\overline{JR},JP)$	Probability that the reference signal is not jammed and the present signal is jammed
$Pr(\overline{JR},\overline{JP})$	Probability that both the reference and present signals are not jammed
$Pr(err)$	Probability of error
$Pr(err\lvert JR,JP)$	Probability of error when both the reference and present signals are jammed
$Pr(err\lvert JR,\overline{JP})$	Probability of error when the reference signal is jammed and the present signal is not jammed
$Pr(err\lvert\overline{JR},JP)$	Probability of error when the reference signal is not jammed and the present signal is jammed
$Pr(err\lvert\overline{JR},\overline{JP})$	Probability of error when both the reference and present signals are not jammed
$P^u(err)$	Upper bound to the probability of error
$P^\ell(err)$	Lower bound to the probability of error
$P_{BN}(\cdot,\cdot)$	Probability of error for a binary coding format and noise jamming

$P_{QN}(\cdot,\cdot)$	Probability of error for a quaternary coding format and noise jamming
$P_N^u(\cdot,\cdot)$	Upper bound to the probability of error for an M-ary coding format and noise jamming
$P_N^\ell(\cdot,\cdot)$	Lower bound to the probability of error for an M-ary coding format and noise jamming
$P_{BCW}(\cdot,\cdot)$	Probability of error for a binary coding format and CW-tone jamming
$P_{QCW}(\cdot,\cdot)$	Probability of error for a quaternary coding format and CW-tone jamming
$P_{CW}^u(\cdot,\cdot)$	Upper bound to the probability of error for an M-ary coding format and CW-tone jamming
$P_{CW}^\ell(\cdot,\cdot)$	Lower bound to the probability of error for an M-ary coding format and CW-tone jamming
$P_{BFM}(\cdot,\cdot)$	Probability of error for a binary coding format and FM jamming
$P_{QFM}(\cdot,\cdot)$	Probability of error for a quaternary coding format and FM jamming
$P_{FM}^u(\cdot,\cdot)$	Upper bound to the probability of error for an M-ary coding format and FM jamming
$P_{FM}^\ell(\cdot,\cdot)$	Lower bound to the probability of error for an M-ary coding format and FM jamming
$P_J(\text{err})$	Probability of error for any coding format and any jamming (e.g. J=BFM for binary coding and FM jamming)

$P_{AVG,J}(err)$	True average error probability for any coding format and any jammer (e.g. J=BFM for binary coding and FM jamming)
$P_J(err,n,k_p)$	Probability of error for any coding format and any jamming (e.g. J=BFM for binary coding and FM jamming) showing the dependence on the sample time (n) and PR phase shift (k_p)
$p(t)$	PR waveform
p	Number of chips in one period of the PR code
ϕ_{ji}^{ℓ}	Random phase of the jamming signal located in the ℓ^{th} hopping slot during the i^{th} signaling interval
ϕ_{ji}	Random phase of the dehopped jamming signal during the i^{th} signaling interval
ϕ_1, ϕ_2	Sampled, spread and filtered jamming signal phases
$\Delta\phi$	Phase slippage of the spread and filtered jamming signal from one interval to the next
$\Phi_{ji}(t)$	Spread and filtered FM phase in the i^{th} signaling interval
$[\Phi_{ji}(t)]_{cw}$	Spread and filtered CW-tone phase in the i^{th} signaling interval
ϕ_n	Phase of the periodic FM, Fourier series coefficients
ϕ_m	Phase of the PR waveform, Fourier series coefficients

$Q(c,d)$	Marcum-Q function, $\int_d^\infty t \cdot \exp[-(\frac{t^2+c^2}{2})] \cdot I_o(ct)dt$
Q_1, Q_2	Random variables
$\vec{R}_1, \vec{R}_2$	Noise and interference corrupted received phasors
R_1, R_2	Ricean random variables
R_j, R'_j	Error subregions in an M-ary decision region diagram
R_c	Code rate
R_I	Information (symbol) rate
$r_i(t)$	Received signal located in the i^{th} signaling interval
$r_{id}(t)$	Dehopped, received signal located in the i^{th} signaling interval
$r_{ids}(t)$	Despread and dehopped, received signal located in the i^{th} signaling interval
$r_{idsf}(t)$	Filtered, despread, and dehopped received signal located in the i^{th} signaling interval
ρ	Signal-plus-interference-to-noise ratio
S	Average signal power
$S(u)$	Fresnel integral, $\int_o^u \sin(\pi t^2/2)dt$
S_c	Code slip ratio, ω_p/ω_b
S_j	Jamming slip ratio, ω_m/ω_b

S_n	Spectral-density-reduction factor
$Si(u)$	Sine integral, $\int_o^u \frac{\sin(t)}{t}\,dt$
$S_p(f)$	Continuous version of the PR waveform spectral density
$S_j(f)$	Spectral density of the noise jamming signal
$S_{js}(f)$	Spectral density of the DS-spread, noise jamming signal
$S_{jw}(f)$	Spectral density of a white noise jamming signal
$\frac{S}{J}$, SNR	Signal-to-noise power ratio
$\frac{S}{N}$, SJR	Signal-to-jamming power ratio
$(\frac{S}{N})_D$, $(\frac{S}{J})_D$	SNR and SJR at the demodulator input
$(\frac{S}{N})_F$, $(\frac{S}{J})_F$	SNR and SJR at the frequency-dehopping output
$(\frac{S}{N})_R$, $(\frac{S}{J})_R$	SNR and SJR at the receiver input
$si(u)$	Relative of the Sine integral, $-\int_o^u \frac{\sin(t)}{t}\,dt$
$s_i(t)$	DPSK signal in the i^{th} signaling interval
$s_{si}(t)$	DS-spread, DPSK signal in the i^{th} signaling interval
$s_{hsi}(t)$	Frequency-hopped, DS-spread, DPSK signal in the i^{th} signaling interval

T_b	Duration of signaling interval
T_c	Duration of one PR chip
T_{f_j}	Fundamental period of the time function $\rho_j(t)$
T_m	Period of FM modulating function, m(t)
T_p	Period of PR waveform, $T_p = pT_c$
t_o	Offset parameter
t_s	Sampling time
θ	Random angle between an uncorrupted reference and the actual reference
θ^+, θ^-	Filter phases
θ_i	DPSK signal phase in the i^{th} signaling interval
$\hat{\theta}_i$	Estimate of the DPSK signal phase in the i^{th} signaling interval
$\theta(\omega)$	Filter phase characteristic
u_1, u_2, u_3	Integers
(u,v)	Coordinate of the tip of a phasor
v_1, v_2, v_3	Integers
W_{fo}	Frequency offset parameter
ω	Arbitrary frequency, radians/sec
ω_c	Carrier frequency, radians/sec
ω_{f_j}	Fundamental frequency (in radians/sec) of the time function $\rho_j(t)$, $\omega_{f_j} = 2\pi/T_{f_j}$

ω_j	Dehopped jamming frequency (radians/sec)
ω_j^{ℓ}	Frequency-hopped jamming frequency (radians/sec)
ω_m	Fundamental frequency (in radians/sec) of the FM modulating function m(t), $\omega_m = 2\pi/T_m$
ω_p	Fundamental frequency (in radians/sec) of the PR waveform, $\omega_p = 2\pi/pT_c$
$\{\omega_j\}$	Frequency content of the time function $\rho_j(t)$
X,Y,Z	Random variables
x	Uniformly distributed random variable over $(0,2\pi)$ (sometimes referred to as the offset parameter) and related to the actual offset parameter by $x = 2\pi t_o/T_m$
x_i, y_i	Gaussian random variables
x_r, x_p	Offset parameters for the reference and present jamming signals
$x_i(t), y_i(t)$	Slowly varying, statistically independent, zero mean gaussian random processes in the i^{th} signaling interval
χ_1, χ_2	Random variables
ξ	Angle

LIST OF TABLES

TABLE		PAGE
1	Error Expressions for DS/FH, Binary DPSK With Noise Jamming	155
2	Error Expressions for DS/FH, Quaternary DPSK With Noise Jamming	156
3	Upper Bound Error Expressions for DS/FH, M-ary DPSK with Noise Jamming	157
4	Error Expressions for DS/FH, Binary DPSK With CW-Tone Jamming	158
5	Error Expressions for DS/FH, Quaternary DPSK With CW-Tone Jamming	159
6	Upper Bound Error Expressions for DS/FH, M-ary DPSK With CW-Tone Jamming	160
7	Error Expressions for DS/FH, Binary DPSK with FM Jamming	161
8	Error Expressions for DS/FH, Quaternary DPSK with FM Jamming	162
9	Upper Bound Error Expressions for DS/FH, M-ary DPSK With FM Jamming	163
10	Signal Power Increase Required to Maintain the Jam-Free Error Rate in a Spot and Barrage Jamming Environment With S/J=0 dB	200
11	Signal Power Increase Required to Maintain the Jam-Free Error Rate in a Spot and Swept-Spot Jamming Environment With S/J=0 dB	203
12	Assumed and True DS Processing Gains for a Noise Jamming Environment with an Error Rate of 10^{-5} and S/N=12 dB	209
13	Assumed and Minimum DS Processing Gains for a Co-channel, CW-tone Jamming Environment with an Error Rate of 10^{-5} and S/N=12 dB	209

LIST OF TABLES

TABLE		PAGE
14	Thermal-Noise-Limiting Error Rate for S/J=8 dB and S/N=12 dB	211
15	Assumed and True FH Processing Gains for a Noise Jamming Environment with an Error Rate of 10^{-4} and S/N=12 dB	219
16	Assumed and True FH Processing Gains for a Co-channel, CW-Tone Jamming Environment with an Error Rate of 10^{-4} and S/N=12 dB	220
17	CW-Tone Jamming Frequencies Causing the Most System Degradation as a Function of the PR-Code Period . . .	224

LIST OF ILLUSTRATIONS

FIGURE		PAGE
1	Spread Spectrum Transmission/Reception	10
2	Generic Direct Sequence Transmitter/Receiver	12
3	Interference Rejection Capability of Spread Spectrum Signaling	14
4	Generic Frequency-Hopping Transmitter/Receiver . . .	16
5	Overall System Transmission/Reception	34
6	Receiver Model	35
7	Modulation Waveforms Illustrating the Offset Parameter	44
8	Signal, Interference, and Noise Phasors at Adjacent Sampling Times for a Transmitted "0"	66
9	Reference Flow Graph for Binary DPSK	75
10	Signal, Interference, and Noise Phasors at Adjacent Sampling Times for a Transmitted "0" and M=4	91
11	Reference Flow Graph for Quaternary DPSK	95
12	Nondetailed, Double-Exposure Phasor Diagram Depicting the Shaded Region (BOA')	108
13	Double-Exposure Phasor Diagram Depicting the Regions Required in the Lower Bound Derivation	113
14	Reference Flow Graph for M-ary DPSK	118
15	Comparison of Upper Bound and Average Error Rates for Cochannel, CW-Tone Jamming with p=7, S_c=1, and S/J= 0.0,5.0 dB	137
16	Comparison of Upper Bound and Average Error Rates for Cochannel, CW-Tone Jamming with p=31, S_c=1, and S/J= 0.0,5.0 dB	138

LIST OF ILLUSTRATIONS

FIGURE		PAGE
17	Comparison of Upper Bound and Average Error Rates for Cochannel, CW-Tone Jamming with p=7, S_c=1, and S/N=10.0,15.0 dB	139
18	Comparison of Upper Bound and Average Error Rates for Cochannel, CW-Tone Jamming with p=31, S_c=1, and S/N=10.0,15.0 dB	140
19	Offset Parameter Dependence at the Maxchip for FM Jamming with p=7, S_c=1, S_j=1, β=1, and S/J=0.0, 5.0 dB	144
20	Offset Parameter Dependence at the Maxchip for FM Jamming with p=7, S_c=1, S_j=1, β=1, and S/N=10.0, 15.0 dB	145
21	Offset Parameter Dependence at the Maxchip for FM Jamming with p=7, S_c=1, S_j=1, β=2, and S/J=0.0, 5.0 dB	147
22	Offset Parameter Dependence at the Maxchip for FM Jamming with p=7, S_c=1, S_j=1, β=2, and S/N=10.0, 15.0 dB	148
23	Bound Deviation vs S/N, S/J, and M for Noise Jamming	151
24	Bound Deviation vs S/N, S/J, and M for CW-Tone Jamming	152
25	Bound Deviation vs S/N, S/J, and M for FM Jamming . .	153
26	Probability of Error vs S/N for Binary DPSK in a White Gaussian Noise Environment (Jamless Case or S/J=∞)	173
27	Probability of Error for High S/J and DS/FH, Binary DPSK Regardless of the Jamming Type	174
28	Reference Curves Without DS and vs S/N: FH, Binary DPSK; Noise Jamming; N_s=2,K_s=1	176
29	Reference Curves Without DS and vs S/J: FH, Binary DPSK; Noise Jamming; N_s=2,K_s=1	177

LIST OF ILLUSTRATIONS

FIGURE		PAGE
30	Reference Curves Without DS and vs S/N: FH, Binary DPSK; Cochannel, CW-Tone Jamming; N_s=2, K_s=1	178
31	Reference Curves Without DS and vs S/J: FH, Binary DPSK; Cochannel, CW-Tone Jamming; N_s=2, K_s=1	179
32	Reference Curves Without DS and vs S/N: FH, Binary DPSK; Cochannel, Linear FM Jamming; β=1, S_j=1, K=1, N_s=2, K_s=1	180
33	Reference Curves Without DS and vs S/J: FH, Binary DPSK; Cochannel, Linear FM Jamming; β=1, S_j=1, K=1, N_s=2, K_s=1	181
34	Reference Curves Without DS/FH and vs S/N: Binary DPSK; Noise Jamming	183
35	Reference Curves Without DS/FH and vs S/J: Binary DPSK; Noise Jamming	184
36	Reference Curves Without DS/FH and vs S/N: Binary DPSK; Cochannel CW-Tone Jamming	185
37	Reference Curves Without DS/FH and vs S/J: Binary DPSK; Cochannel CW-Tone Jamming	186
38	Reference Curves Without DS/FH and vs S/N: Binary DPSK; Cochannel, Linear FM Jamming; β=1, S_j=1, K=1	187
39	Reference Curves Without DS/FH and vs S/J: Binary DPSK; Cochannel, Linear FM Jamming; β=1, S_j=1, K=1	188
40	Probability of Error vs S/N: DS/FH, Binary DPSK; Noise Jamming; p=31, S_c=1, N_s=2, K_s=1	190
41	Probability of Error vs S/J: DS/FH, Binary DPSK; Noise Jamming; p=31, S_c=1, N_s=2, K_s=1	191
42	Probability of Error vs S/N: DS/FH, Binary DPSK; Cochannel, CW-Tone Jamming; p=31, S_c=1, K=1, N_s=2, K_s=1	192

LIST OF ILLUSTRATIONS

FIGURE		PAGE
43	Probability of Error vs S/J: DS/FH, Binary DPSK; Cochannel, CW-Tone Jamming; p=31, S_c=1, K=1, N_s=2, K_s=1	193
44	Probability of Error vs S/N: DS/FH, Binary DPSK; Cochannel, Linear FM Jamming; p=31, S_c=1, β=1, S_j=1, K=1, N_s=2, K_s=1	194
45	Probability of Error vs S/J: DS/FH, Binary DPSK; Cochannel, Linear FM Jamming; p=31, S_c=1, β=1, S_j=1, K=1, N_s=2, K_s=1	195
46	Comparison of Spot (Cochannel, CW-Tone) and Barrage (Noise) Jamming Error Rates vs S/N: DS/FH Binary DPSK; p=31, S_c=1, K=1, N_s=2, K_s=1	198
47	Comparison of Spot (Cochannel, CW-Tone) and Barrage (Noise) Jamming Error Rates vs S/J: DS/FH, Binary DPSK; p=31, S_c=1, K=1, N_s=2, K_s=1	199
48	Comparison of Spot (Cochannel, CW-Tone) and Swept-Spot (Cochannel, Linear FM) Jamming Error Rates vs S/N: DS/FH, Binary DPSK; p=31, S_c=1, β=1, S_j=1, K=1, N_s=2, K_s=1	201
49	Comparison of Spot (Cochannel, CW-Tone) and Swept-Spot (Cochannel, Linear FM) Jamming Error Rates vs S/J: DS/FH, Binary DPSK; p=31, S_c=1, β=1, S_j=1, K=1, N_s=2, K_s=1	202
50	Dependence of the Probability of Error vs S/J on the Code Rate (~p): DS/FH, Binary DPSK; Noise Jamming; S/N=12 dB, S_c=1, N_s=2, K_s=1	206
51	Dependence of the Probability of Error vs S/J on the Code Rate (~p): DS/FH, Binary DPSK; Cochannel, CW-Tone Jamming; S/N=12 dB, S_c=1, K=1, N_s=2, K_s=1	207
52	Dependence of the Probability of Error vs S/J on N_s and K_s ($1 \le K_s \le 50$): DS/FH, Binary DPSK; Noise Jamming; S/N=12 dB, p=31, S_c=1	213
53	Dependence of the Probability of Error vs S/J on N_s and K_s ($50 \le K_s \le 500$): DS/FH, Binary DPSK; Noise Jamming; S/N=12 dB, p=31, S_c=1	214

LIST OF ILLUSTRATIONS

FIGURE		PAGE
54	Dependence of the Probability of Error vs S/J on N_s and K_s ($1 \le K_s \le 50$): DS/FH, Binary DPSK; Cochannel, CW-Tone Jamming; S/N=12 dB, p=31, S_c=1, K=1	215
55	Dependence of the Probability of Error vs S/J on N_s and K_s ($50 \le K_s \le 500$): DS/FH, Binary DPSK; Cochannel, CW-Tone Jamming; S/N=12 dB, p=31, S_c=1, K=1	216
56	Dependence of the Probability of Error vs S/J on the Frequency Offset Parameter, W_{fo}: DS/FH, Binary DPSK; CW-Tone Jamming; p=31, S_c=1, K=1, N_s=2, K_s=1	223
57	Magnitude Spectrum of a Spread, CW-Tone Jamming Signal	226
58	Dependence of the Probability of Error vs S/N on β: The Uppermost Curve Represents β=0, and Each Succeeding Curve Represents β=0.5,1,2,3,4, and 5 With S/J=0 dB, p=31, S_c=1, S_j=1, K=1, N_s=2, K_s=1	227
59	Dependence of the Probability of Error vs S/J on β: The Uppermost Curve Represents β=0 and Each Succeeding Curve Represents β=0.5,1,2,3,4, and 5 With S/N= 10 dB, p=31, S_c=1, S_j=1, K=1, N_s=2, K_s=1	228
60	Comparison of Gaussian Approximation to Average Error Rate vs S/J: DS/FH, Binary DPSK; Cochannel, CW-Tone Jamming; S/N=10 dB, p=15, S_c=1, K=1, N_s=2, K_s=1	230
61	Comparison of Gaussian Approximation to Average Error Rate vs S/J: DS/FH, Binary DPSK; Cochannel, CW-Tone Jamming; S/N=10 dB, p=31, S_c=1, K=1, N_s=2, K_s=1	231
62	Upper and Lower Bounds for M-ary (M=4,8) DPSK: DS/FH; Noise Jamming; S/J=5 dB, p=31, S_c=1, N_s=2, K_s=1	233
63	Upper and Lower Bounds for M-ary (M=4,8) DPSK: DS/FH; Noise Jamming; S/N=12 dB, p=31, S_c=1, N_s=2, K_s=1	234

LIST OF ILLUSTRATIONS

FIGURE		PAGE
64	Upper and Lower Bounds at the Maxchip for M-ary (M=4,8) DPSK: DS/FH; Cochannel, CW-Tone Jamming; S/J=5 dB, p=31, S_c=1, K=1, N_s=2, K_s=1	235
65	Upper and Lower Bounds at the Maxchip for M-ary (M=4,8) DPSK: DS/FH; Cochannel, CW-Tone Jamming; S/N=12 dB, p=31, S_c=1, K=1, N_s=2, K_s=1	236
66	Basic Waveshape for Each PR Chip	251
67	Continuous Version of the Unnormalized Autocorrelation Function for a PR Code Sequence Consisting of Elements ±1	251
68	Spectral Density of a Wideband Noise Jammer ($\frac{1}{T} \leq \frac{1}{T_c} = R_c$)	259
69	Continuous Version of the Well Known Discrete Spectral Density for a PR Waveform of Amplitude ±1 . . .	259
70	Spectral Density of a Spread Noise Jammer Over the Frequency Range ($-R_c/2$, $R_c/2$)	263
71	Double Exposure Phasor Diagram for a Jammed Reference Signal (JR)	266
72	Double Exposure Phasor Diagram for a Jammed Present Signal (JP)	266
73	Region Containing the Event $\gamma_r - \gamma_p \leq \eta$ for $-2\pi \leq \eta \leq 0$ . . .	269
74	Region Containing the Event $\gamma_r - \gamma_p > \eta$ for $0 \leq \eta \leq 2\pi$ . . .	269
75	Quadrature Noise Components Properly Aligned With the Interference-Corrupted Desired Signal Phasor $\vec{Z}$	277
76	Illustration of the Regions Required by Eq. (H-4) . .	285
77	Double-Exposure Phasor Diagram Depicting the Equally-Spaced Error Regions, E_1 and E_2	290
78	Illustration of the M-ary Decision Regions With Appropriately Defined Error Subregions	297

SUMMARY

Electrical communication systems requiring electromagnetic radiation to transfer information are inherently susceptible to unfriendly detection and interference. As a result, spread spectrum signaling schemes have been proposed to combat these unfriendly intentions.

The analysis contained herein is a theoretical and numerical characterization of the susceptibility of a direct sequence/frequency-hopped, M-ary differential-phase-shift-keying (DPSK) system subjected to thermal noise and to partial- and full-band white gaussian noise, CW-tone, and periodically-modulated FM jamming. Theoretically, expressions for the system susceptibility in terms of the receiver probability of error are individually derived for each of the three jamming signals and for M=2,4, and M>4. In the development of these expressions, no use is made of equating the spread interference to additional gaussian noise of equal power, a practice commonly invoked but theoretically unproven. Exact expressions for M=2 and 4 are developed whereas complexity dictates the use of very accurate bounding techniques for M>4. All expressions ultimately depend on the signal, noise, interference and receiver parameters.

The theoretical analysis leads to rather involved average-error-probability expressions. In order to provide the methodology required to perform extensive parametric studies, a simplification of these involved expressions is developed for the CW-tone and periodic FM jamming cases. The simplification is accomplished by appropriately choosing

the jamming amplitude or a function of the jamming amplitude to produce an upper bound to the average error rate. No simplification is required for the noise jamming situation.

In order to show the feasibility of using the simplified expressions for exhaustive parametric studies, a typical study is graphically presented and extensively discussed. Graphical illustrations include plotting probability of error for each jamming signal as a function of the signal-to-noise power ratio or the signal-to-jamming power ratio. Other parameters include the direct sequence code rate, the number of frequency-hopping slots, the number of jamming signals, the FM modulation index, and the frequency offset of the jamming signal. The discussion which parallels these illustrations includes a comparison of the three jamming signals, the dependence of the error rate on the direct sequence code rate, the choice of a partial- or full-band jamming strategy, and the effects of non-cochannel interference.

Tentative conclusions from this study indicate that a CW-tone interference is significantly more destructive to the DPSK system than noise jamming and slightly more destructive than linear-swept FM jamming. It is also shown that a partial-band jamming strategy may, in many situations, produce larger degradations in system performance. Because of the direct-sequence-spreading, the maintenance of a cochannel interference is not as critical as in the nonspread situation and in fact a non-cochannel interference produces a larger probability of error.

Spread spectrum signaling schemes are normally compared and judged through a figure-of-merit referred to as the processing gain. Certain shortcomings in this figure-of-merit are brought out in this

analysis by comparing the assumed gain and the actual processing gain.

CHAPTER I

INTRODUCTION

Increased usage of electromagnetic waves for information transfer has placed great strains on existing electronic communication systems and increasing demands on systems in the development stage. Not only must these systems be designed to meet the basic requirements of reliable and rapid information transfer, but also have the capability of dealing with the larger amount of interference created by this use. Furthermore, communication systems requiring electromagnetic waves to link the source and destination are inherently susceptible to unfriendly detection and interference. This places an even greater strain on a system since the maintenance of a covert (secret) or secure information transfer depends heavily on these unfriendly intentions. To determine the effects and susceptibility of a communication to such extreme operating conditions, an analytical and numerical performance study of a particular system has been completed. The specifics of the system and interference are delayed at the present time in order to present a few instructive and introductive generalities.

The types of interference possibly encountered by a system may be categorized into two classes. The first class consists of those interferences with a natural origin. Such interferences include thermal noise, atmospheric disturbances, and multipath transmissions, to name a few. Man-made interference, both deliberate and unintentional,

comprise the second class. Unintentional interference may result from any electrical signal whose main purpose is not the disruption of another communication system. On the other hand, deliberate, man-made interference is intentional, the intent being to corrupt or destroy the reliability and security of another system. Such interferences are commonly used by military adversaries for the specific purpose of disrupting an unfriendly communication system. Because of this use, the deliberate (intentional) interference is generally referred to as electrical jamming, or in a possibly more familiar term, electronic countermeasures (ECM).

In order to minimize or eliminate the destructive effects which an ECM tactic or any interference may impose on a system, a new class of signaling schemes has been developed. This class is referred to as Spread Spectrum (SS) and is comprised of signals which use a much wider bandwidth than is required for conventional transmission. Two such spread spectrum techniques, which are discussed in Chapter II, are direct sequence (DS) and frequency-hopping (FH). When used to specifically combat an ECM threat, spread spectrum signaling becomes an important portion of the broader area concerned with general, anti-ECM methods, otherwise known as electronic counter-countermeasures (ECCM). The use of steerable-null antennas is another prominent type of ECCM.

Spread spectrum is usually used in conjunction with a conventional, digital, information-transferral scheme. Those digital signaling techniques more often used are amplitude-shift-keying (ASK), frequency-shift-keying (FSK), phase-shift-keying (PSK), and differential-phase-shift-keying (DPSK). The implementational simplicity of ASK in a non-fading environment is rather attractive but the performance

improvement of FSK, PSK, and DPSK is much more appealing. Ideal FSK and PSK require exact knowledge of the carrier phase for proper demodulation. If the receiver has the capability of generating a reference signal (exact carrier frequency and phase), PSK is preferred over FSK because of the PSK antipodal signaling scheme as opposed to the orthogonal scheme used by FSK. Due to the receiver size and cost or the transmission medium, it may not be feasible or possible to generate a perfect reference. In such cases DPSK is widely used since the DPSK reference is merely the signal in the previous signaling interval. In addition to its receiver simplicity and for large signal-to-noise ratios, DPSK also approaches the performance of the ideal PSK scheme in a white, gaussian noise environment. Thus, the overall use of DPSK is quite justified and important.

As pointed out earlier, the demand in some cases is such that information must be transmitted at as high a data rate as possible. In order to accomplish this, binary signaling schemes may be waived for the more general M-ary coding format. This is not to say that the use of binary signaling will cease, for an end is clearly not in sight. However, certain high data rate requirements may place the M-ary format into the forefront. For example, Rockwell's microwave digital radio model (MDR-11) [1] operates at a data rate of 90 Mbps and incorporates an 8-ary PSK scheme. Another practical M-ary modem is the 8-ary FSK signaling structure utilized in both the uplink and downlink of the LES 8/9 experimental satellite system [2]. Even though an increase in M is usually accompanied by the need to increase the signal-to-noise

ratio or the bandwidth for a specified system performance, the necessity to communicate more rapidly may require the increase in M.

Before any communication system is developed, its theoretical performance for the type of transmission environment most likely to be encountered must be determined. The theoretical analysis is quite justified in lieu of the more costly and time consuming experimental and simulation studies. In the absence of any ECCM tactic, the performance analyses of the above digital techniques have quite heavily incorporated the effects of natural interferences, but to a much lesser extent the effects of ECM. Due to the increase in sophisticated electronic countermeasures, detailed analyses of these effects on the conventional digital schemes, as well as those schemes incorporating spread spectrum, must be established to determine the resultant system performance.

As a step in this direction, a theoretical and numerical analysis is undertaken to determine the susceptibility of DS/FH, M-ary DPSK to thermal noise and to a variety of ECM environments such as: wideband, white gaussian noise; continuous wave tone (CW-tone) jamming; and periodic FM interference. Theoretically, mathematical equations describing the performance (via probability of error) of binary, quaternary, and M-ary (M>4), DS/FH DPSK systems under the influence of each of the jamming signals are derived. Numerically, a computer program is developed to evaluate these equations, thus providing the methodology to carry out extensive parametric studies.

This analysis serves basically a two-fold purpose. First, an ECM strategist can, from this analysis, determine how destructive particular jamming signals are to a DS/FH, M-ary DPSK system. Secondly,

because this system may be designed to counter certain ECM threats, an ECCM strategist will have the means of describing the beneficial results such a system may produce. In other words, the results obtainable from this study can indicate the destructive effects of ECM as well as the constructive effects of ECCM.

The report is henceforth divided into four stages:

Stage 1: Explanation

Stage 2: System Modeling and Signal Characterization

Stage 3: Theoretical Derivations

Stage 4: Calculations and Results

The explanation stage describes in more detail ECM and the ECCM tactic of spread spectrum signaling. Both of these items are covered in Chapter II. Also included in Stage 1 is Chapter III, which presents an historical background of and relevant analyses concerned with DPSK.

An important part of any analysis of this type is the system modeling, hence Stage 2. Certain assumptions and specific models to be used in the remainder of this work are, respectively, pointed out and presented in Chapter IV. Because of the signal processing performed by the system model, characterization of certain signals (specifically the jamming signals) is imperative and sufficiently covered in Chapter V.

The actual mathematical calculations comprise Stage 3 and are presented in Chapters VI-IX. A very general analytical technique is presented in Chapter VI, and because of its complexity, serves only as a motivational tool for the more specific results of Chapters VII-IX. Different analytical techniques are required for M=2,4, and greater than 4, hence a separate chapter is devoted to each, with the results

in Chapters VII, VIII, and IX, respectively. Due to the number of specific jamming cases throughout Chapters VII-IX, a rigid organization is required and explicitly explained at the beginning of each chapter. In addition, each chapter contains a helpful flowchart (Figures 9, 11, and 14) indicating the precise location of each case considered.

Chapters X, XI, and XII comprise the final stage. Chapter X provides the necessary simplification of the expressions derived in Chapters VII-IX and hence shows the feasibility of using these expressions for extensive parametric studies. Tables 1-9 summarize the simplified expressions for each of the cases in Chapters VII-IX. Quantitative methods and typical results are presented in Chapter XI, with Chapter XII summarizing the conclusions and recommending future research.

CHAPTER II

ECM AND SPREAD SPECTRUM

Any study concerned with the effects of ECM and spread spectrum signaling would be incomplete without a complete description of these items. Attention is initially focused on ECM, followed by an introduction to the ECCM tactic of spread spectrum signaling.

Any electronic technique utilized for the specific purpose of corrupting or destroying the ability of a communication system to transfer information is referred to as an electronic countermeasure (ECM). Electronic countermeasures are generally grouped into two areas, interference jamming and deception jamming, respectively depending on their destructive or deceptive intentions.

Interference jamming may involve the use of sophisticated electrical signals to impede the reception of information. Applications of this type of ECM typically are the jamming of enemy radar, voice and video communications, and missile-guidance systems. Though the variety of interference jamming signals is large, it is possible to categorize these signals into the following classes:

(1) Spot Jamming - A signal whose jamming power density is highly concentrated within the bandwidth of the receiver (e.g. CW-tone).

(2) Broad-Band Barrage Jamming - In contrast to spot jamming, barrage jamming uses a signal

with a low jamming power density. Its power is spread over a large bandwidth, usually at least equivalent to the receiver's operating bandwidth (e.g. wideband gaussian noise).

(3) Swept-Spot Jamming - A compromise between barrage and spot jamming wherein a high power density signal is swept over the entire operating bandwidth (e.g. periodic FM).

A very interesting jamming signal for analysis purposes is the periodically-modulated FM signal since the barrage and spot jamming signals can be incorporated in the FM signal by the appropriate choices of the FM signal parameters (power, modulation index).

Comprising the second group of ECM tactics are the deception jamming signals. In deception jamming, an adversary attempts to feed erroneous information into a communication system rather than trying to destroy the system reception capability. An example of such jamming would be the transmission of false range and rate information by an aircraft to camouflage its actual position and speed. Unlike interference jamming, deception jamming requires the knowledge of the type of information being sought by the communication system in order that the appropriate false information might be transmitted.

The work discussed herein considers the interference jamming case only and in particular, white gaussian noise jamming, CW-tone jamming, and periodic FM jamming. The effects of these three jamming signals on DS/FH, M-ary DPSK are discussed in the bulk of this paper, but for the present, spread spectrum signaling is introduced.

Spread spectrum is the general classification given to a set of signaling schemes that use a much larger-than-required bandwidth to transmit information. Bandwidths on the order of 10^4 to 10^6 times as large as the information bandwidth are common, and though this large bandwidth may be devastating to spectrum conservation, the performance benefits obtained with spread spectrum far outweigh the cost in bandwidth for many applications.

Dixon has acquainted a vast audience to the generalities of spread spectrum signaling through a tutorial paper [3] and a recently published text [4]. The text [4] is the first attempt at a fairly comprehensive, non-mathematical presentation of spread spectrum, though the AGARD Lecture Series [5] and a symposium sponsored by the Naval Electronics Laboratory Center [6] had already initiated such a presentation. The recent appearance of these presentations clearly exemplifies the interest in and future involvement of spread spectrum techniques.

A generic spread spectrum system is shown in Figure 1; it can be seen that the spectrum spreading portion of the system is a separate entity, or simply, an addition to a conventional communication system. The conventionally-modulated signal has its bandwidth spread just prior to transmission. At the receiver and before any conventional demodulation, the transmitted spectrum is despread, resulting in the original conventionally-modulated waveform. In many cases, it is quite difficult to distinguish between the spreading operation and the conventional modulation, but for discussional and analytical purposes, the above convention is certainly accurate.

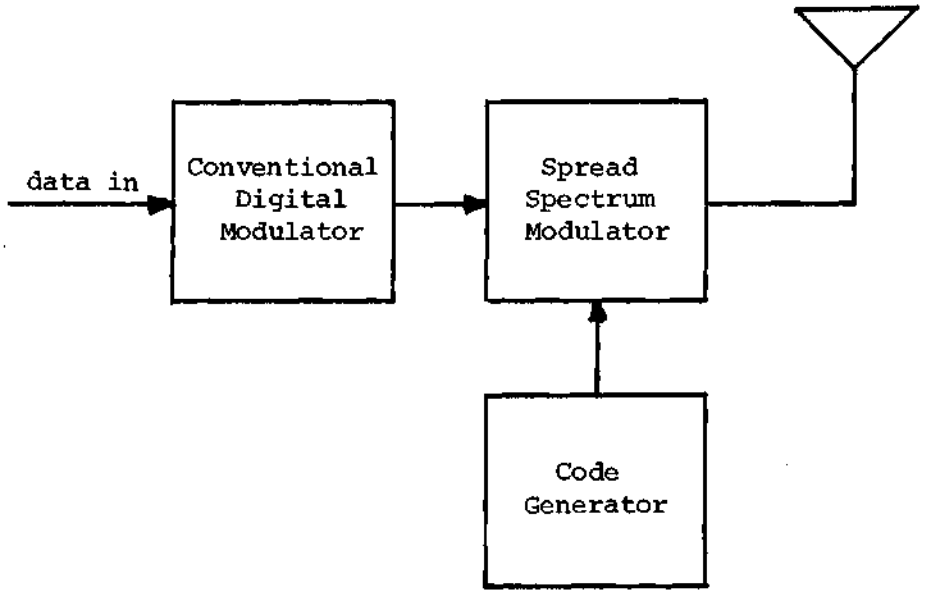

(a) Generic Spread Spectrum Transmitter

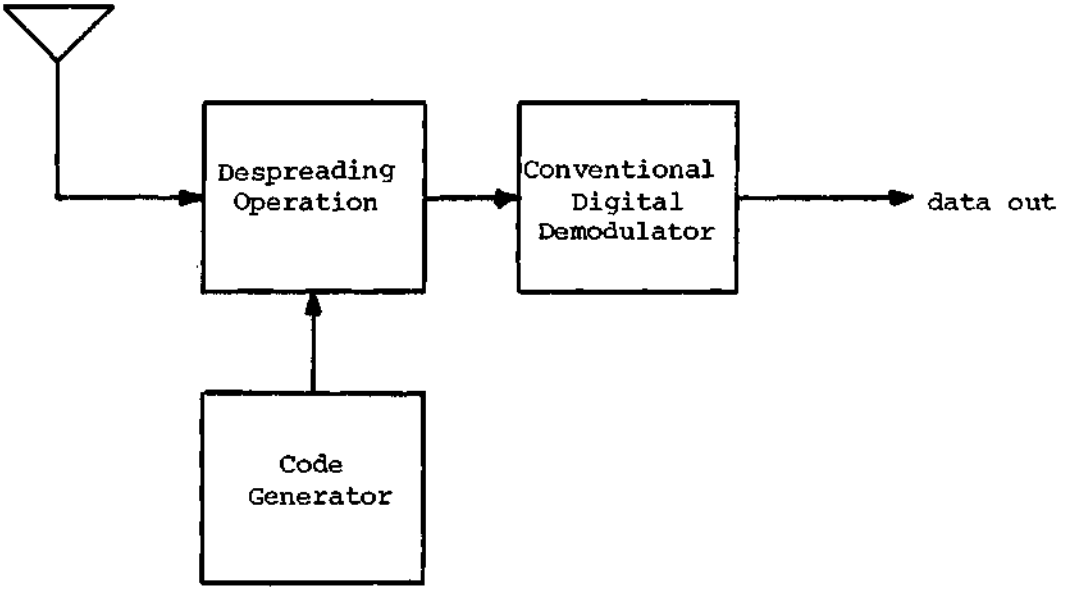

(b) Generic Spread Spectrum Receiver

FIGURE 1. Spread Spectrum Transmission/Reception

The usual basis for either the spreading or despreading operations is the generation of a pseudo-random (PR) code that is periodic and, to the casual observer, seemingly random. Pseudo-random codes may be either linear or nonlinear but the more widely used codes are the linear codes, specifically, maximal-length PR codes. Without precise knowledge of the PR code, it is impossible to recover the conventionally-modulated signal and hence the basic information. A somewhat private communication system may be designed around this fact provided the transmitter and prescribed receiver(s) are the only system(s) having the proper PR code knowledge. The desired receiver must have the capability of generating the PR code and the ability to determine the code phase since the extraction of the desired information depends on proper synchronization being obtained and maintained. This problem of synchronization is a major implementational hurdle [6-9] which must be overcome to insure accurate information transfer. Only precise synchronized systems are considered in this work.

To appreciate the significance of the PR code basis and to show how the PR code is used, it is appropriate to introduce two of the more widely used spread spectrum techniques: direct sequence (DS; sometimes referred to as pseudo-noise, PN) and frequency-hopping (FH). Because these two techniques are germane to the work contained herein, a detailed discussion is presented for them. Nevertheless, it should be pointed out that other spread spectrum techniques exist. Two such techniques are time hopping (TH) and the "chirp" method, both of which are also important and briefly covered in [4].

Direct sequence (DS) spread spectrum, as shown in Figure 2, is

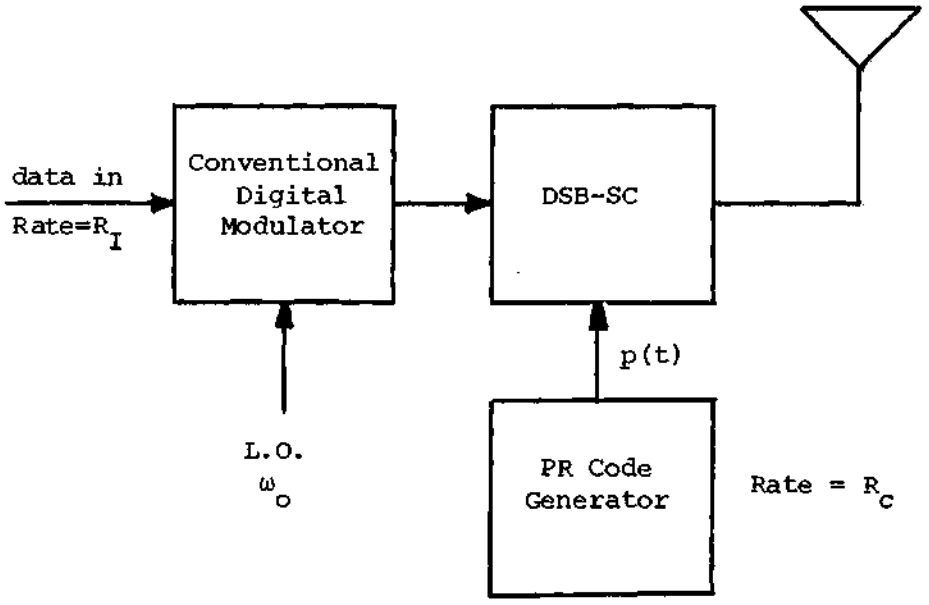

(a) DS Transmitter

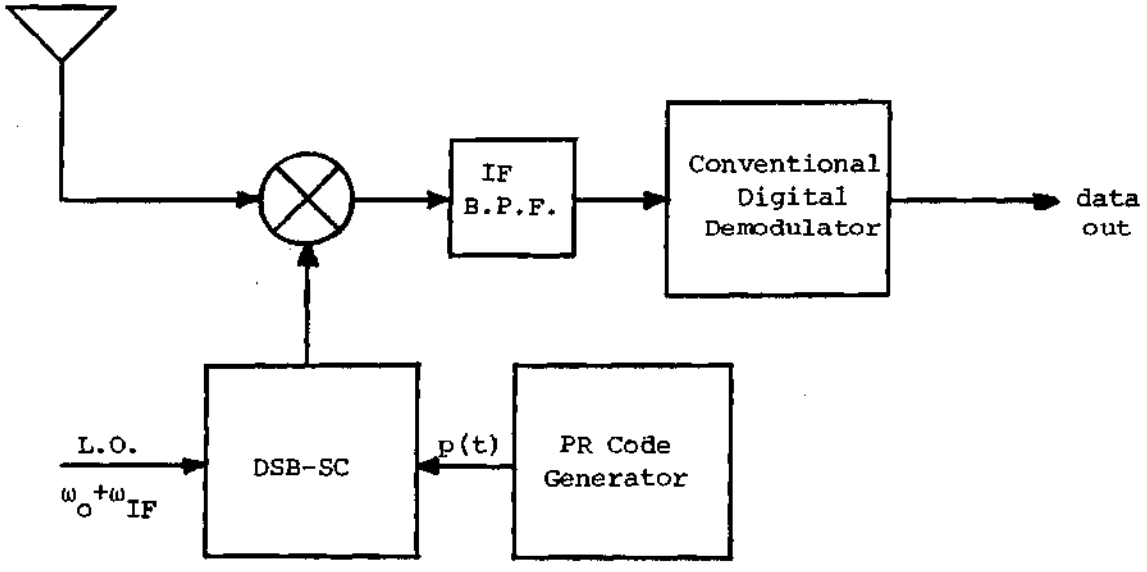

(b) DS Receiver

FIGURE 2. Generic Direct Sequence Transmitter/Receiver

so called because the PR code directly biphase, or quadraphase modulates the previous conventionally-modulated signal. For example, basic information may be modulated via conventional PSK, and upon biphase modulating this PSK signal by the PR code sequence, a new PSK signal is produced. If the code rate (R_c) were much larger than the information (symbol) rate (R_I), the new PSK signal would have a corresponding larger RF bandwidth than the original PSK signal. This bandwidth expansion is under the complete control of the PR code, specifically the code rate; as the code rate decreases or increases, the RF bandwidth respectively decreases or increases.

An exact replica of the PR code must be generated and synchronously maintained at the receiver in order that the spreading can be properly removed. Such synchronization techniques may include the transmission of a prescribed preamble or the use of a matched filter to extract the sync information directly from the modulated signal. A general discussion of different techniques may be found in [4-9]. By proper correlation of the received signal with the exact PR code replica, proper removal of the spectrum spreading is accomplished. It is this correlation process which illustrates the power of spread spectrum communications for the process coherently extracts (despreads) the conventional signal while at the same time decorrelates (spreads) any interference not possessing the exact PR code sequence information. By correlating the PR code sequence with the interference, the interference power is spread out, thereby producing less interference power in the information bandwidth than would have been anticipated if spread spectrum had not been used. This reduction in interference power, as illustrated in Figure 3, is responsible for the performance increase of spread

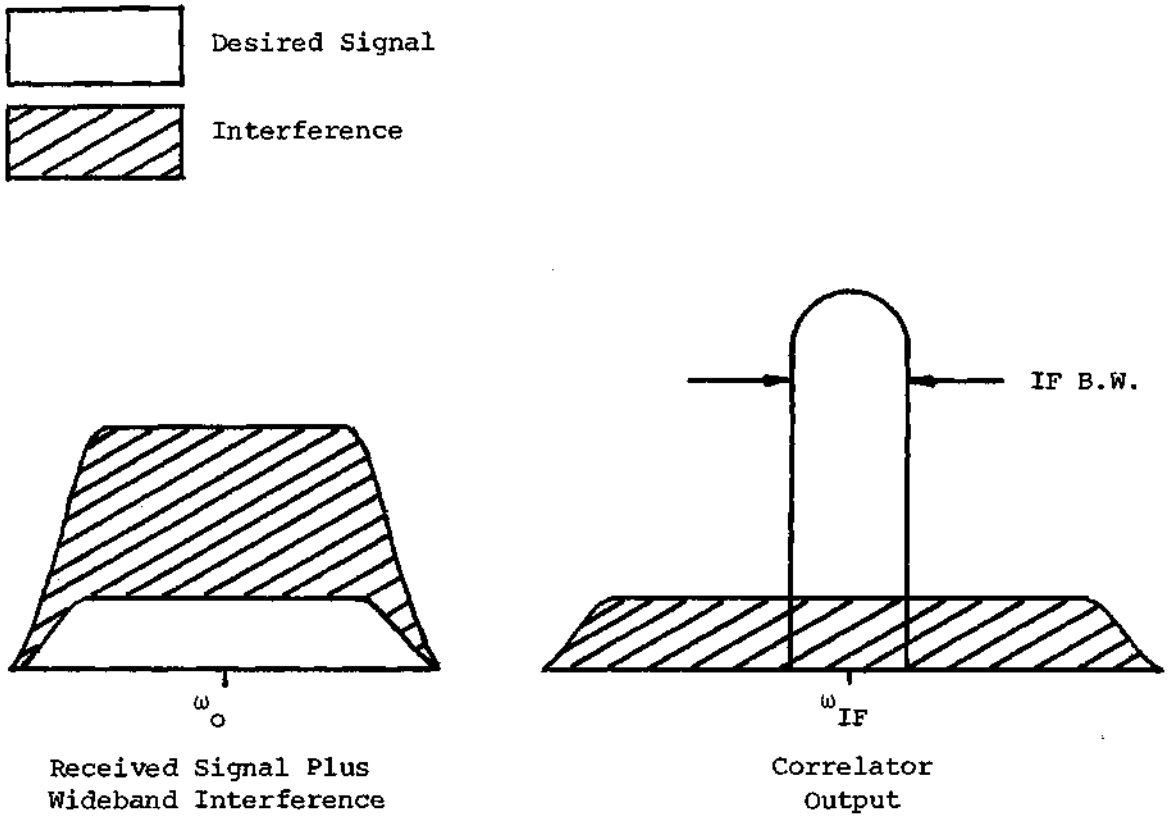

(a) Wideband Interference

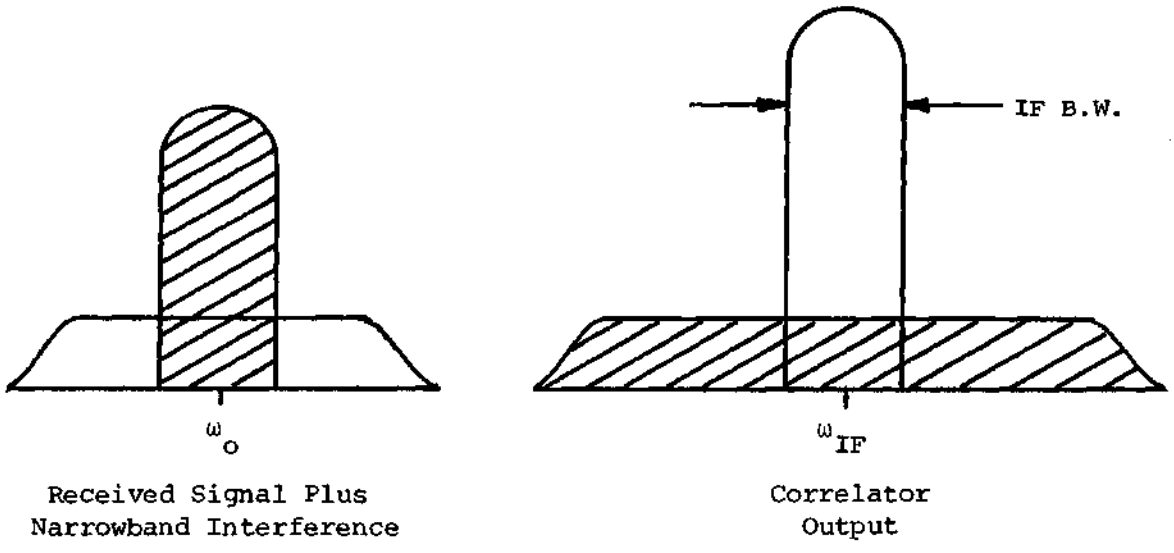

(b) Narrowband Interference

FIGURE 3. Interference Rejection Capability of Spread Spectrum Signaling

spectrum communications, and in particular, DS signaling.

Frequency-hopping (FH) spread spectrum possesses similar properties with DS; the main similarity being the correlation process required at the receiver. The main difference between FH and DS signaling can be seen in Figure 4, where it is shown that the FH-PR code does not directly affect the conventionally-modulated signal as does the DS-PR code, but in fact, initially goes through a code-to-frequency transformation. An FH system produces a spreading effect by pseudo-randomly hopping the final carrier frequency over a wide range of prescribed frequencies. The hopping pattern and hopping rate are determined by the FH-PR code and code rate, respectively.

With this ability to change the carrier frequency, it is difficult for an adversary to not only locate the specific carrier frequency at any time (covert communications) but also to jam that particular frequency at the right time. In a constant jamming-power situation, the adversary is forced to decrease his power density to cover the entire band of possible frequencies, or use a high power density jamming signal over a portion of the band. In either case, the adversary must accept a smaller probability of creating an error.

There are two basic differences between DS and FH signaling as currently practiced: the code rate and the time to acquire synchronization. Code rates for DS are usually much higher than those for FH. This is due to the relatively slow frequency synthesizers which only permit code rates on the order of 100 kbps [10] as opposed to DS modulators operating near 200 Mbps. Higher code rates are certainly more desirable from an anti-interference point of view but create some

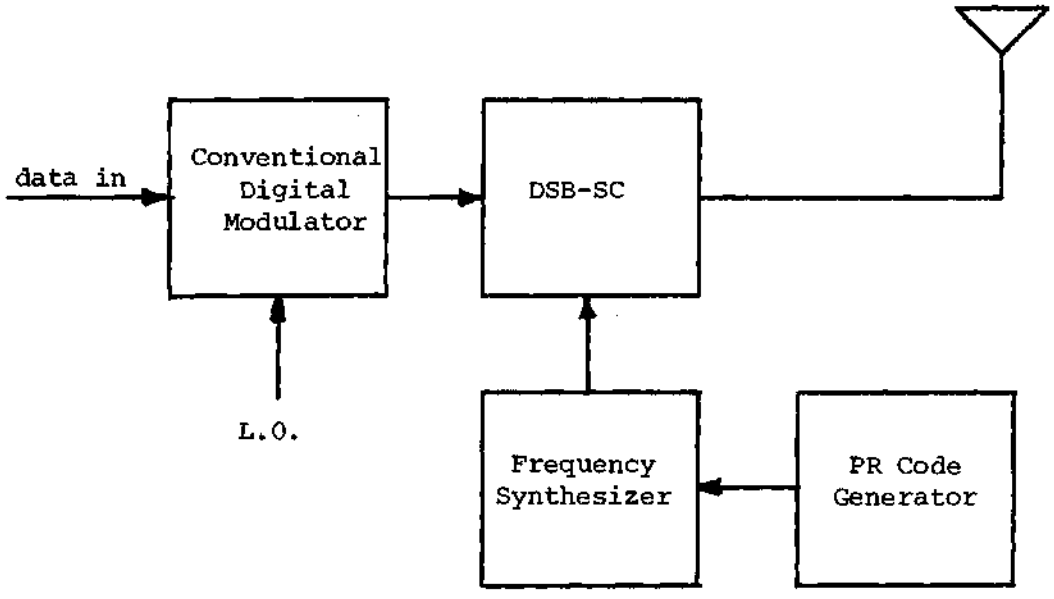

(a) FH Transmitter

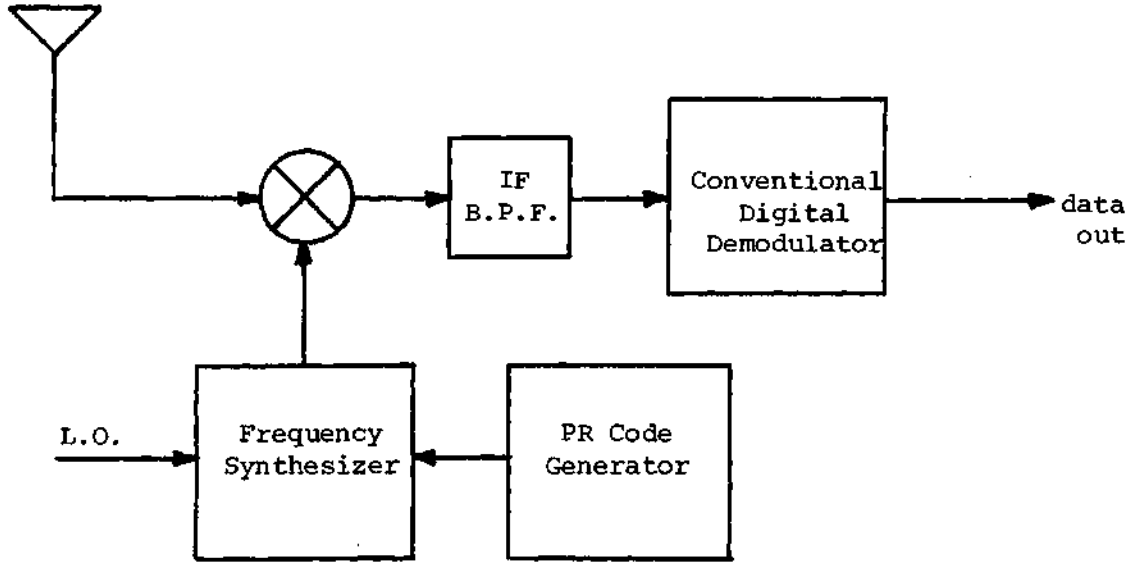

(b) FH Receiver

FIGURE 4. Generic Frequency-Hopping Transmitter/Receiver

initial acquisition problems. This leads to the second current difference between DS and FH; the initial acquisition time for FH is much smaller than that for DS. Typical acquisition times are on the order of 1 ms for FH and 2-3 seconds for DS [10]. The difference is a direct consequence of the acquisition time being proportional to the PR code rate and the initial uncertainty (code length in seconds). In some cases, the changes of the code rate and/or code length (in seconds) cannot be made independently of one another. For example, an increase in the code rate for a sequence would automatically decrease the code length (in seconds) of the sequence provided a single code sequence is considered before and after the rate and length change. These two effects would cancel each other, and the acquisition time would be unaffected. However, if the code length (in seconds) would remain constant and the code rate increased, no longer is the same code sequence considered. In this case the acquisition time would increase.

Other differences exist between DS and FH and will be highlighted shortly. The presentation of these differences is important because it exemplifies the complementary nature of the two techniques; where one technique may not be suitable for an application, the other may be quite appropriate and vice versa. An example of this would be the use of spread spectrum as a navigational tool in a multiple-access environment. Because of the higher code rates, DS is a likely candidate for very accurate time-of-arrival measurements. However, the "near-far" problem[1]

[1]The "near-far" problem is associated with a nearby friendly or jamming transmitter of small power disrupting the transmission of information from a distant transmitter.

discourages the use of DS in certain multiple-access environments and encourages the use of FH. The complementary nature of these two techniques suggests a combination (hybrid) of DS and FH to accomodate both the navigation and multiple-access problems.

Another example of this complementary nature, and more germane to this work, concerns the effects of different interferences on those systems incorporating either DS or FH. In a binary FH-FSK system, suppose one CW-tone interferer were located within the hopping bandwidth and appears in one of the two receiver filters after the dehopping operation. If the interference power exceeds the signal power and the CW-tone is located in the filter not containing the actual signal, an error will nearly always be made. By using DS in conjunction with FH in this case, a reduction in interference power within the filter is accomplished and errors reduced. The DS spreading places some interference power at other hopping frequencies, but the power is less dense than before, resulting in the "spillover" causing an insignificant degradation in system performance. This example is evidence of the fact that separately, DS and FH signaling techniques are affected differently by different jamming signals. The important result from this example is that these interference effects may be minimized by using the best of both methods, particularly a hybrid DS/FH spread spectrum technique.

The Joint Tactical Information Distribution System (JTIDS) [11], which is intended to be the major tactical communications net from the 1980's on, is a prime example of the use of a hybrid DS/FH scheme. Paraphrasing [11], hardware limitations cause processing improvement to be more easily obtained and less costly if the improvement is acquired

through a hybrid scheme as opposed to one individual scheme.

In summary, these examples presented above have heuristically explained the complementary benefits incurred by a hybrid DS/FH spread spectrum scheme. Because of these benefits, a basis has been formed for motivating the use of a hybrid spread spectrum technique in the work herein. For this work, a conventional M-ary DPSK signal will have its bandwidth spread by a technique involving the combination of DS and FH with the resulting system performance evaluated analytically and graphically.

In order to show the wide-ranging significance of spread spectrum usage and the utility of this study, a set of applications is listed.

(1) Anti-Jamming Capabilities - Because of the despreading operation at the receiver, any uncorrelated interference will be spread out and thus create less power in the IF bandwidth following the correlation device. This decrease in interference power is an indication of the interference rejection capability of the system.

(2) Multiple-Access Capability - In satellite communications, a number of users must simultaneously use the same satellite. Each user may be given a different FH-PR or DS-PR code. In the FH case, it is hoped that the probability of two users occupying the same frequency band is very small, thus making

the mutual interference negligible. If each user were given a different DS-PR code and transmission occurred over the same frequency interval, all undesired signals would be spread out and the desired signal despread by the specific code. If either the probability of simultaneous frequency-band-occupation or the DS spread interference were small, a large number of users may operate in the same satellite.

(3) Multipath Tolerance - Frequency-hopping is already akin to the well known frequency diversity techniques but the use of DS to combat multipath is not as widely known, though of equal importance. Any DS multipath signals arriving at least one code-bit interval late will be spread out rather than despread by the correlation process. This spreading is a result of the multipath code being uncorrelated with the receiver-generated PR code replica. The multipath signal appears as any other interference impinging upon the receiver. Direct sequence signaling to combat multipath is of a discriminatory nature since the receiver discriminates against any time shifted PR codes.

(4) High Resolution Ranging - By determining the time it takes a DS spread spectrum signal to transit the distance to and from an object, it is possible to estimate the range to the object. The determination of the time-of-arrival is accomplished by observing the initial time difference between the receiver-generated PR code replica and the received signal's PR code during the synchronization of the incoming signal. Due to the inherent wide bandwidth of a DS signal, the time-of-arrival resolution is very high.

(5) Identification - Each user of a large communication system may have a different PR code sequence, similar to the multiple-access system. Because of this uniqueness, the identification of any user is accomplished via the determination of the PR code being used. In addition to the identification capability, one is also able to selectively call or discretely address a particular user by generating the unique code of that user.

(6) Message Privacy - Without proper knowledge of the PR code sequence, an adversary cannot properly despread the incoming spread spectrum signal. This prohibits access to the

conventionally-modulated signal, or in some cases, the baseband information itself. A message privacy system is sometimes referred to as a secure communication system. It is important to note that while linear PR codes are widely used for interference rejection, navigation, and other applications, they do not provide a secure communication environment because an adversary can theoretically decipher the code once a short sequential set of 2n+1 (n = number of shift-register stages needed to generate the code) bits from the sequence is known [4]. To secure a communication system, nonlinear PR codes are used.[1]

(7) Low Detectability - Spread spectrum modulation results in a low power density signal with statistical properties similar to noise. As a result, the transmitted signal is very difficult to detect and covert communications is achieved.

(8) Power Flux Density Reduction - In order to meet international guidelines limiting the power flux density impinging on the surface of the earth, certain satellite communication

[1]This work will emphasize linear PR codes, specifically maximal-length PR codes, but the work is general enough to consider nonlinear, periodic codes as well.

> systems (space shuttle tracking and relay system) have resorted to reducing the power flux density by means of wideband, spread spectrum signaling schemes [12,13].

Because the immediate concern of this study is the interference rejection capability of spread spectrum communications, the amount or degree of rejection possible is a rather significant quantity. The most widely accepted measure of this quantity, termed the system processing gain, is given by the ratio of the RF bandwidth to the information bandwidth. Heuristically, this definition may be considered to be the ratio of the amount of interference power in the RF bandwidth before the despreading operation to the interference power in the IF bandwidth after the despreading operation. This reduction in power is referred to as a gain, and specifically, the despreading or processing gain. For DS signaling, the ratio is the PR code rate over the symbol rate, and for FH, the ratio is identical to the number of hopping frequencies used.

The processing gain is a rough estimate of the improvement provided by spread spectrum usage, and it continues to be a heavily relied upon design parameter. The true performance gain, as compared to the "processing gain" is and must be of great interest for the analysis of existing and proposed systems. Glazer [14] writes that "while processing gain conveys a rough idea of the performance of the signaling system, accurate comparisons and specifications require the use of more precise figures of merit." This statement is substantiated by the results obtained by Pettit [15] for frequency-hopped, noncoherent frequency-shift-keying (FH-NCFSK) in a partial-band noise, tone or swept-FM jamming

environment. Pettit's findings [15] included an example for which an expected processing gain of 27 dB was shown to be an actual processing gain of 6 dB, approximately. The actual gain was observed to be dependent upon the acceptable error rate, the type of jamming, and the jamming strategy. With this in mind, it is clear that more careful evaluations will be required for certain critically important systems now in the development stage.

CHAPTER III

DPSK

Differential-Phase-Shift-Keying (DPSK) is a conventional, coherent signaling scheme very similar to its closest relative, phase-shift-keying (PSK) [16]. In DPSK, digital information (e.g. a "0" or a "1") is conveyed in the phase changes between successive pulses (signals in adjacent signaling intervals) unlike the PSK method of conveying information with the absolute phase of each pulse. For example, instead of absolutely associating the symbols 0 and 1 respectively with the phases 0 and 180, the binary DPSK method may associate the symbol 0 with the event of two successive pulses of identical phase and the symbol 1 with the event of two successive pulses being 180° out of phase. M-ary DPSK signaling is quite similar to this binary case, the difference being that a group of $\log_2 M$ symbols is associated with two successive pulses whose phase difference is one of M prespecified phases.

In addition to the differential-coding-of-data difference, the main difference between DPSK and PSK lies in the method used in deriving the reference signal for coherent detection. Whereas the PSK reference is nominally an exact replica of the carrier signal, the DPSK reference is simply the previous signal or combination of previous signals. Differential-phase-shift-keying performance is compromised because the reference used is corrupted by interference (thermal noise and jamming

signals), unlike the accurate, interference-free reference used in ideal PSK demodulation. Despite the performance compromise, DPSK remains useful because the requirement of generating a reference has been eliminated, thereby creating a less complex receiver.

In M-ary digital communication systems, with M-ary DPSK included among these, the transmitter selects one of M waveforms to transmit during a specified signaling interval. For DPSK, the waveform is a sinusoid having one of M prespecified phases. The receiver attempts to decide which of the M waveforms was transmitted during each signaling interval. Because the received signal is corrupted by interference, the receiver will occasionally decide incorrectly. The randomness of the corrupting interference and the assumed randomness of the transmitted waveforms prohibit an exact determination of the number of errors. This randomness leads to a probabilistic estimation of the number of errors with the estimation being commonly referred to as the average probability of error. Usage of the average probability of error as a performance measure is common practice as can be witnessed by the following historical discussion of M-ary DPSK.

As reported in [17], Doelz [18] was responsible for the development of DPSK while the Collins "Kineplex" system [17] introduced the practicality of such a signaling scheme. Theoretical analysis of binary DPSK in a white gaussian noise environment was reported by Lawton [19] and presented generally by Cahn [20]. The end result of these analyses revealed the probability of error for binary DPSK to be

$$Pr(err) = \frac{1}{2} \exp(-E_b/N_o) \qquad (3\text{-}1)$$

where

E_b = energy per received bit

N_o = single-sided noise power spectral density

Due to the noisy reference used by DPSK, its performance as given in Eq. (3-1) is not as favorable as the ideal PSK performance [16]:

$$Pr(err) = \frac{1}{2} \operatorname{erfc}[\sqrt{E_b/N_o}] \tag{3-2}$$

where

$$\operatorname{erfc}[x] \triangleq \frac{2}{\sqrt{\pi}} \int_x^{\infty} e^{-t^2} dt \tag{3-3}$$

As the signal-to-noise ratio (E_b/N_o) becomes large (>10 dB), the difference in the required E_b/N_o is less than 1 dB for the same probability of error. In other words, for a DPSK system operating in a high E_b/N_o region, receiver complexity is significantly reduced at little expense in system performance.

The above analyses are for the case of white gaussian noise interference only and are applicable to the binary (M=2) DPSK signaling scheme. They are too restrictive and in fact are misleading for systems which operate in an ECM environment, as well as for many nonmilitary systems. In addition, because of requirements for higher data rates, M-ary (M>2) systems are becoming increasingly popular. Therefore, to insure proper design of future systems and to gain a better understanding of the performance of existing systems, more general analyses are

necessary. A discussion of the extension of the white gaussian noise case to more complicated interferences is initially presented, followed by the historical background concerning the binary-to-M-ary extension.

Rosenbaum [21] made the first step in the interference-extension direction by considering a binary DPSK system subjected to a single, cochannel, randomly-phased, sinusoidal interference. Probability of error expressions were developed and graphically illustrated. As a further extension of the single sinusoidal case, Rosenbaum [22] analyzed the situation in which the interference could be modeled as a sum of independently-phased sinusoids, or multiple CW-tone interference. Two interesting contributions were produced by Rosenbaum's multiple, CW-tone interference report [22]. The first contribution, although a hypothesis, states that the maximum system degradation occurs whenever a constant interference power is equally distributed among the multiple interferers. Prabhu [23] reached the same conclusion for an ideal PSK system, but likewise could not provide a proof. Rosenbaum's [22] second contribution involved avoiding the common assumption of representing the multiple, CW-tone interference by additional gaussian noise of equal power, a representation quite often performed but unjustified. The pessimism generated by Rosenbaum [22] of such a representation was substantiated when a three-decade performance difference between the two methods was witnessed. One additional item of major importance involves the assumption of phase independence of the multiple CW-tones. Since certain interferences of interest are periodic and therefore may be represented in a Fourier series [24], one might attempt to employ for them the above results of multiple, CW-tone interference. However, this would not be

expected to produce valid results as evidenced by the fact that the sinusoids of the Fourier series do not have random phases, but instead exhibit definite phase relationships.

Other analyses have included the effects of signal multipath on the performance of binary DPSK transmitted over distant radio links [25] and the direct adaptability of these results to the analysis of single, CW-tone interference [26]. Telephone-line effects, and in general, bandlimited channel effects on the performance of binary DPSK were analyzed by Bussgang and Leiter [27] with Shimbo, et al. [28] developing the mathematical basis for determining intersymbol interference degradations. Because of the nature of DPSK demodulation, errors may often occur in pairs. This situation was considered by Goldman in his multiple-error performance analysis [29].

Military communication systems often must operate in highly sophisticated environments. To establish the performance of such systems, specifically the binary DPSK scheme, Lowery [30] developed the susceptibility equations of binary DPSK subjected to periodic FM interference. In [30], the Fourier series representation of the periodic FM interference formed the basis for the useful results which were obtained. Interest in this type of interference had previously been noted [31] and more recently continued in Pettit's extensive analysis of NCFSK [32].

As stated previously, the requirement of higher data rates necessitates the extension of binary to M-ary DPSK. Initially, M-ary DPSK analyses were restricted solely to the quaternary (M=4) case rather than the more general M>2 case. The interest in this case was due to the development of the "Kineplex" system [17] which is a 4-phase DPSK

system. Certain nonrigorous performance analyses [33,34] were performed for this case. Fleck and Trabka [35] waived these specifics and generalized the analysis to an arbitrary M-phase DPSK system in white gaussian noise. The probability of error expression obtained by Fleck and Trabka [35] was in the form of a rather complicated double integral. A simplified and an approximate analysis for high signal-to-noise ratios was carried out by Arthurs and Dym [36].

Again the white gaussian noise assumption is very restrictive, creating the need to allow for increased interference complexity. A study of atmospheric noise effects was undertaken by Halton and Spalding [37] and the performance of quaternary DPSK subjected to a single, CW-tone interference by Rosenbaum [21]. A generalization of the single, CW-tone interference case for 4-ary DPSK was obtained for M-ary DPSK, with the expressions being upper bounds to, rather than exact expressions for, the probability of error [38]. Castellani, et al. [39] considered the effects of intersymbol interference on M-ary DPSK signaling, while the practical, finite-width thresholds of the receiver were taken into consideration by Prabhu [40].

Because of the increased emphasis being placed on communications electronic warfare [41], the analysis of M-ary DPSK systems utilizing spread spectrum signaling techniques has become quite important. The initial step toward such an analysis has included in a cursory fashion only, DS, FH, and DS/FH spread spectrum techniques with binary and quaternary DPSK as the conventional modulating schemes [42,43]. These systems have been subjected to partial-band white gaussian noise and single and multiple CW-tone interference. A few other analyses [44-51]

of spread spectrum techniques have also been produced for a variety of situations, covering FSK, PSK, NCFSK, and DPSK. The analysis technique used by [42,43] is based on the assumption that the interference at the output of the DS correlator is equivalent to white gaussian noise of equal power. Using this assumption and covering the cases for which the interference power is much greater than the thermal noise power, the analysis [42] completely eliminates the effects due to thermal noise. This elimination cannot be justified because in the absence of thermal noise it is possible to increase the DS code rate without bound and obtain an infinite processing gain. Since the thermal noise level directly affects the choice of the code rate, such a simplifying assumption is not desirable.

A hidden consequence of this gaussian equivalence assumption is the fact that the analysis is valid only for those DS codes which have a very long period (in chips and in seconds). In many cases, shorter length codes are used to decrease the initial time uncertainty and hence the acquisition time. The above analyses [42] would not be expected to accurately predict the performance of a system using these shorter length codes.

The other drawbacks of these analyses are the restriction of M to be less than or equal to four and the inclusion of only rather simple interferences. Higher data rates being required by modern modems and the eventual use of these systems in sophisticated jamming environments necessitate analyses which treat the general M-ary case and other interferences such as periodic FM.

In order to remain as general as possible this study does not use

the white gaussian noise equivalent assumption nor does it eliminate the thermal effects. An analysis technique which does not rely upon either of these assumptions is developed and utilized. The research does not restrict M to be less than or equal to four but rather allows M to be arbitrary and utilizes a more complicated jamming signal, periodic FM, which includes the CW-tone interference as a special case.

CHAPTER IV

THE SYSTEM MODEL

The actual, but still general, DS/FH, M-ary DPSK transmission/reception system is illustrated in Figure 5. It is the purpose of this chapter to analytically describe this system in detail.

Receiver Model

The receiver shown in Figure 6 has as its input, during the i^{th} signaling interval, a signal of the form

$$r_i(t) = s_{hsi}(t) + \sum_{\ell=1}^{N_s} \delta_i^{\ell} j_i^{\ell}(t) + n_i(t) \qquad (4\text{-}1)$$

in which:

(a) $s_{hsi}(t)$ is the frequency-hopped and direct sequence spread, M-ary DPSK signal in the i^{th} signaling interval;

(b) $j_i^{\ell}(t)$ is the jamming signal located within the bandwidth ($\sim 2R_c$, R_c = code rate) of the ℓ^{th} frequency-hopping slot during the i^{th} signaling interval;

(c) δ_i^{ℓ} is equal to 1 if the ℓ^{th} hopping slot during the i^{th} signaling interval contains a jamming signal and is equal to 0 if no jamming signal is present;

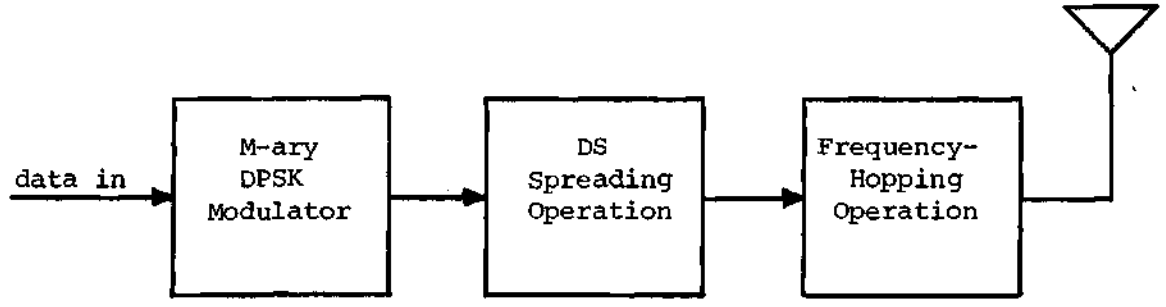

(a) DS/FH, M-ary DPSK Transmitter

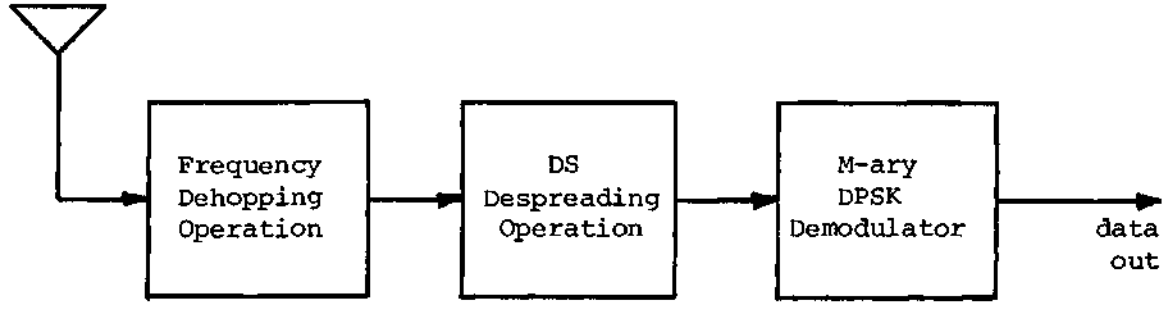

(b) DS/FH, M-ary DPSK Receiver

FIGURE 5. Overall System Transmission/Reception

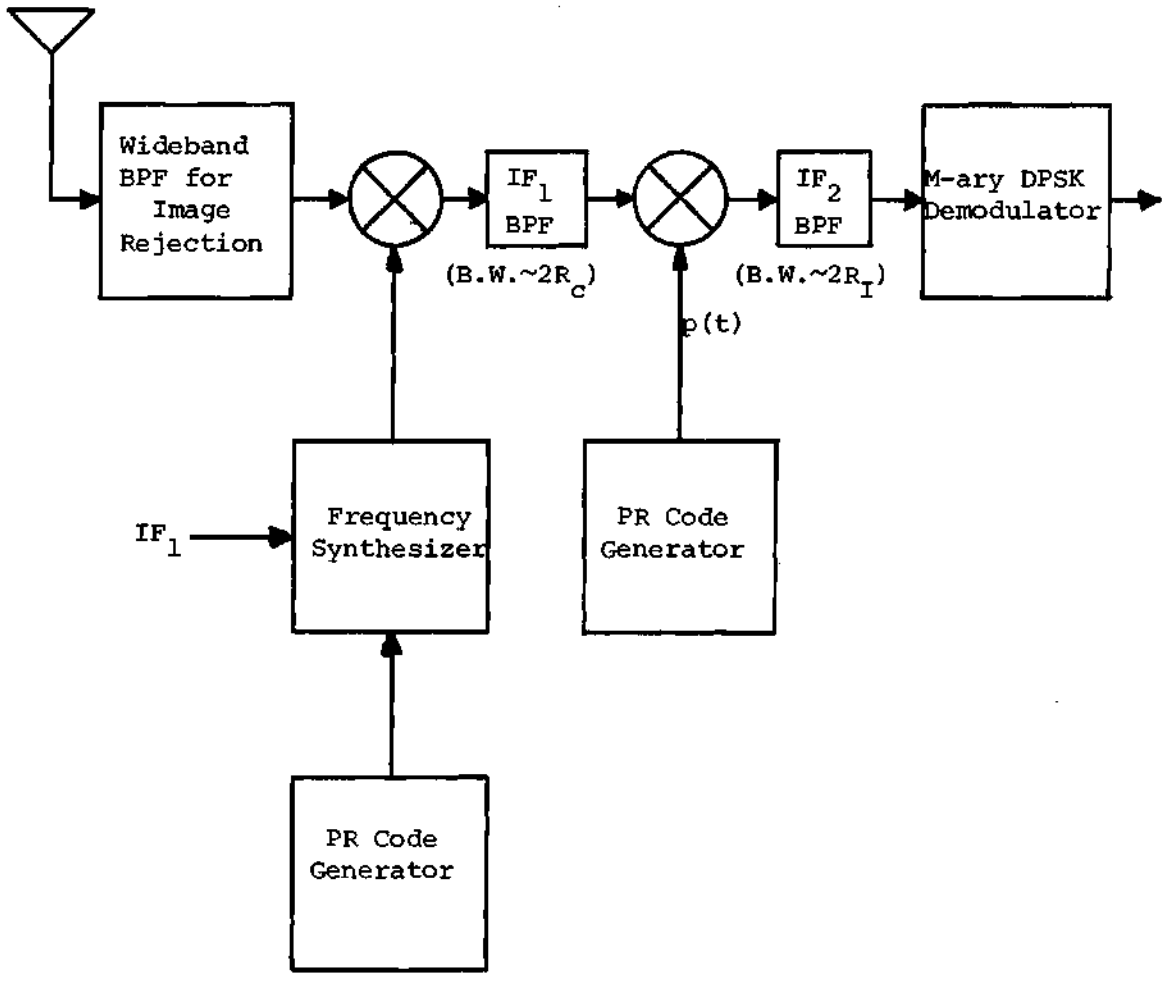

FIGURE 6. Receiver Model

(d) $n_i(t)$ is a sample function from a white gaussian noise random process with one-sided spectral density, N_o, and located in the i^{th} signaling interval;

(e) N_s is the number of frequency-hopping slots.

Due to the fact that frequency-hopping rates and signaling rates are of the same order of magnitude for many cases of interest, the time between frequency hops is assumed to be equal to the signal duration (T_b), and the actual frequency changes assumed to coincide with a signaling change. This permits the carrier frequency to remain constant over each signaling interval and allows the interference within the signaling interval to be composed of the jamming signal from one hopping slot.

Upon entering the receiver, the received signal is filtered and then dehopped. The wideband filtering operation merely eliminates any image frequencies that may be translated to the IF_1 bandpass filter (BPF) bandwidth and has no effect on the desired signal or the jamming signal which might happen to be located in the same frequency slot. The noise term is also assumed to be unaltered because of the wide bandwidth.

The dehopping operation is assumed identical to and synchronized with the hopping operation at the transmitter. If the desired DS-spread signal $s_{si}(t)$ were located within the m^{th} frequency-hopping slot and a jamming signal $j_i^m(t)$ were present in the same slot, the dehopping operation would simultaneously translate both signals to the IF_1 bandwidth. The IF_1 filter is assumed to be wideband ($\sim 2R_c$) and hence capable of passing these two signals unaltered. All other jamming signals ($\ell \neq m$)

located in the unused hopping slots are eliminated by the IF_1 filter. For analysis purposes, the wideness of the IF_1 filter bandwidth permits the assumption that over the range of frequencies of interest an identical noise spectral density exists at the input and output. The dehopped, received signal during the i^{th} signaling interval, and located at the IF_1 filter output, may be written as

$$r_{id}(t) = s_{si}(t) + j_i(t) + n_i(t) \tag{4-2}$$

where $j_i(t)$ is the jamming signal located in the same hopping slot containing the desired signal and which occurs during the i^{th} signaling interval.

The dehopped, received signal as described in Eq. (4-2) is accurately characterized only if a jamming signal is present in the same hopping slot as the desired signal during the i^{th} signaling interval. If no jamming signal were present in the slot (partial band jamming), there would be no jamming signal present in the IF_1 bandwidth. Consequently,

$$r_{id}(t) = s_{si}(t) + n_i(t) \tag{4-3}$$

At this point, $r_{id}(t)$ is then DS despread by the correlation process. This despreading operation is also assumed identical to and synchronized with the DS spreading at the transmitter. Perfect and complete recovery of the original M-ary DPSK signal in the i^{th} signaling interval, $s_i(t)$, is then possible. In addition, the correlation

process spreads the bandwidth of the possibly-present jamming signal and the noise process. The output of the correlator takes the form

$$r_{ids}(t) = s_i(t) + j_{is}(t) + n_{is}(t) \qquad \text{(jammer present)} \qquad (4\text{-}4)$$

or

$$r_{ids}(t) = s_i(t) + n_{is}(t) \qquad \text{(jammer absent)} \qquad (4\text{-}5)$$

in which:

(a) $j_{is}(t)$ is the DS-spread jamming signal in the i^{th} signaling interval;

(b) $n_{is}(t)$ is the DS-spread noise process in the i^{th} signaling interval.

It will be assumed throughout this analysis that $n_{is}(t) = n_i(t)$. This assumption is possible since $n_i(t)$ has a flat spectrum for nearly all frequencies of interest and any modulation (multiplication) will only alter the magnitude of the spectrum and not its shape. The magnitude alteration is so small that it is neglected. Therefore, the dehopped and despread, received signal may be written as

$$r_{ids}(t) = s_i(t) + j_{is}(t) + n_i(t) \qquad \text{(jammer present)} \qquad (4\text{-}6)$$

or

$$r_{ids}(t) = s_i(t) + n_i(t) \qquad \text{(jammer absent)} \tag{4-7}$$

The IF_2 filtering is a narrowband operation (B.W. $\sim 2R_I$) and is assumed to have no effect on the DPSK signal, $s_i(t)$. In other words, all significant frequency components of $s_i(t)$ are passed unaltered. As for the spread jamming signal and the white gaussian noise, the filter will reduce their effect on the subsequent demodulation process. The IF_2 filtered, dehopped, and despread received signal is written as

$$r_{idsf}(t) = s_i(t) + j_{isf}(t) + n_{if}(t) \qquad \text{(jammer present)} \tag{4-8}$$

or

$$r_{idsf}(t) = s_i(t) + n_{if}(t) \qquad \text{(jammer absent)} \tag{4-9}$$

in which:

(a) $j_{isf}(t)$ is the filtered, DS spread jamming signal located in the i^{th} signaling interval;

(b) $n_{if}(t)$ is a narrowband gaussian noise process in the i^{th} signaling interval.

Lastly, an M-ary DPSK demodulator accepts signals in two adjacent signaling intervals and using the former signal as the reference, decides which of the M phases was transmitted in the latter signal.

Signal Model

The M-ary DPSK signal in the i^{th} signaling interval is represented as

$$s_i(t) = A_s \cos(\omega_c t + \theta_i) \tag{4-10}$$

where θ_i may take on any phase of the form $\frac{2\pi k}{M}$ $(k = 0,1,2,\ldots,M-1)$ and ω_c may be considered the carrier frequency of the conventional DPSK modulated signal and the center frequency of the IF_1 and IF_2 bandpass filters.

Noise Model

The IF_2 bandpass filter output, $n_{if}(t)$, for the white gaussian noise input, $n_i(t)$, is expressible in the usual quadrature components [16,52] as

$$n_{if}(t) = x_i(t)\cos\omega_c t - y_i(t)\sin\omega_c t \tag{4-11}$$

where $x_i(t)$ and $y_i(t)$ are statistically independent, zero mean gaussian random processes with average power N and located in the i^{th} signaling interval. It will also be assumed that

$$E(n_{if}(t)n_{jf}(t)) = 0 \qquad (i \neq j)$$

IF_2 Bandpass Filter Model

Bandpass filtering is accomplished by adjusting the signal

magnitude by $A(\omega)$ and the signal phase by $\theta(\omega)$. The overall transfer function of the IF_2-BPF is expressible as

$$H(\omega) = A(\omega)\exp(-j\theta(\omega)) \tag{4-12}$$

where it is assumed that

$$A(\omega_c + \omega) = A(\omega_c - \omega) \tag{4-13}$$

and

$$\theta(\omega_c + \omega) = -\theta(\omega_c - \omega) \tag{4-14}$$

Jamming Model

Three types of jamming signals are presented here: periodic FM; CW-tone; and noise jamming. Due to its generality, the periodic FM interfering signal is considered first.

The constant amplitude, periodically-modulated FM signal located within the ℓ^{th} frequency-hopping slot during the i^{th} signaling interval is represented mathematically as

$$j_i^{\ell}(t) = \frac{A_j}{\sqrt{K_s}} \cos[\omega_j^{\ell} t + \phi_{ji}^{\ell} + K_j \int_o^t m(\tau)d\tau] \tag{4-15}$$

where:

(a) $\frac{A_j^2}{2}$ is the total jamming power;

(b) K_s is the number of hopping slots containing jamming signals ($1 \le K_s \le N_s$);

(c) ω_j^{ℓ} is the frequency (in radians per second) of the jamming signal located in the ℓ^{th} hopping slot;

(d) ϕ_{ji}^{ℓ} is the random phase of the jamming signal located in the ℓ^{th} hopping slot during the i^{th} signaling interval and is uniformly distributed on $(0,2\pi)$;

(e) $m(\tau)$ is a periodic waveform with period $T_m = 2\pi/\omega_m$;

(f) K_j is a constant and related to the modulation index (β) by $\beta = \frac{K_j}{\omega_m} |m(\tau)|_{max}$.

There is at most one jamming signal located within each of the hopping slots; the total number of possible jamming signals is equal to the number of hopping slots (N_s). The amplitude of the FM signal in Eq. (4-15) is scaled in such a manner that the jammer power is equally distributed among the K_s jamming signals, with each signal containing a power of $A_j^2/2K_s$.

As described in the receiver model, at most one jamming signal is permitted to be within the bandwidth of the IF_1 filter during the i^{th} signaling interval. With the notation presented in the receiver model and Eq. (4-15), the i^{th} signaling interval contains a jamming signal of the form

$$j_i(t) = \frac{A_j}{\sqrt{K_s}} \cos[\omega_j t + \phi_{ji} + K_j \int_o^t m(\tau)d\tau] \qquad (4\text{-}16)$$

in which:

(a) ω_j is the frequency (in radians per second) of the dehopped and IF_1 filtered jamming signal;

(b) ϕ_{ji} is a random phase, uniformly distributed on $(0,2\pi)$.

There is no justification in assuming that the signaling interval coincides with the beginning of the jamming sweep. To compensate for this, an additional variable, t_o, termed the offset parameter, is included in the modulating function definition. Figure 7 illustrates this parameter for two typical modulating functions. Because of its unknown nature, t_o may be assumed to be uniformly distributed over the modulating-signal period T_m. For familiarity, a new random variable may be defined as

$$x = \frac{2\pi t_o}{T_m} \qquad (4\text{-}17)$$

where, according to this definition, x is uniformly distributed on $(0,2\pi)$.

Because $m(\tau)$ is a periodic function, $j_i(t)$ may be expanded into a Fourier series. This representation simplifies the very complex structure of Eq. (4-16). The end result is

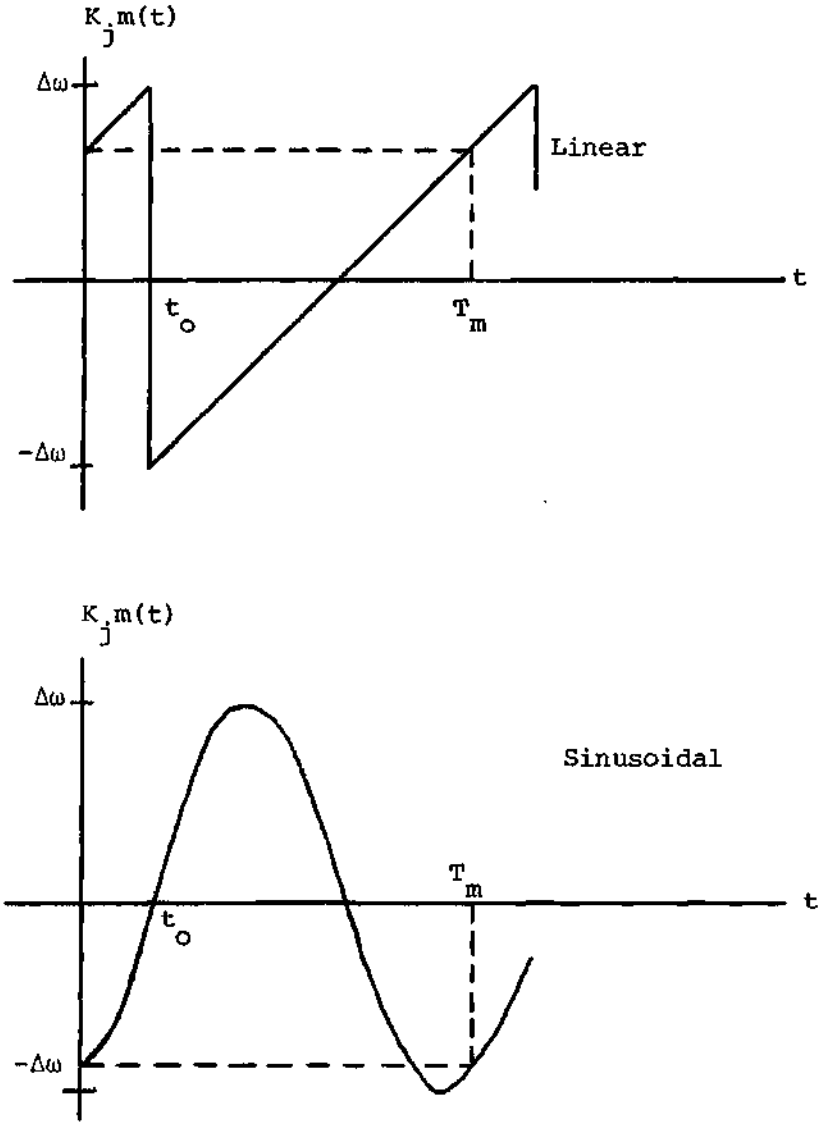

FIGURE 7. Modulation Waveforms Illustrating the Offset Parameter

$$j_i(t) = \frac{A_j}{\sqrt{K_s}} \sum_{n=-\infty}^{\infty} |a_n| \cos[(\omega_j + n\omega_m)t + \phi_{ji} + \phi_n] \qquad (4\text{-}18)$$

where

$$|a_n| = \{[\text{Real}(a_n)]^2 + [\text{Imag}(a_n)]^2\}^{\frac{1}{2}}$$

$$\phi_n = \arctan\{\text{Imag}(a_n)/\text{Real}(a_n)\} \qquad (4\text{-}19)$$

with

$$a_n = \frac{1}{T_m} \int_{t_i}^{t_i+T_m} \exp[jK_j \int_o^t m(\tau,x)d\tau] \exp[-jn\omega_m t]dt \qquad (4\text{-}20)$$

It should be emphasized that although the coefficients a_n do not explicitly show the dependence on the offset parameter x, this dependence does exist and is depicted in the integrand of Eq. (4-20).

For the linear sweep of Figure 7, Lowery [30] has evaluated the coefficients. Appendix A contains the coefficient expressions derived by [30]. The coefficients for other periodic waveforms can be determined, with some results appearing in Middleton [24].

If the modulation index were set to zero (β=0), the jamming signal would reduce to a single sinusoid of the form

$$j_i(t) = \frac{A_j}{\sqrt{K_s}} \cos[\omega_j t + \phi_{ji}] \qquad (4\text{-}21)$$

No Fourier series expansion is required here since Eq. (4-21) is presently in its most basic form.

To include a barrage jamming situation, simply redefine $j_i(t)$ to be

$$j_i(t) = n_{ji}(t) \tag{4-22}$$

where $n_{ji}(t)$ is an additional gaussian noise process with a constant spectral density over the IF_1 bandwidth ($2R_c$). The total jamming power per slot of this signal is N_j/K_s, where N_j represents the total noise jamming power.

Spread Spectrum Model

A combination of two types of spread spectrum techniques is used: direct sequence (DS) and frequency-hopping (FH). Because of the spread spectrum modulation process, DS is mathematically the more complicated to model, whereas FH is simply a translation of frequency components.

The frequency-hopping effects are incorporated into the analysis by a two-step process. In the first step, because there may not be a jamming signal within each hopping slot (partial-band jamming), it is quite possible that either the dehopped reference signal or the dehopped present signal will not be affected by a jamming signal. Therefore, four cases must be considered depending on the presence or absence of a jammer in the reference or present signaling interval. Secondly, the probabilities of a jamming signal influencing the reference and/or present signal must be accounted for in order to average out the effects of the four individual cases. This averaging is accomplished in the last step of the probability of error evaluation. In addition to these

effects and because the carrier frequency changes from one interval to the next, it will be assumed that the jamming signals affecting two adjacent signaling intervals are independent. This is certainly not a very restrictive assumption except in the special and extreme case of operating in only one frequency slot (i.e. no FH), where the adjacent-interval jamming signals are actually dependent. Because the present study is to illustrate the effects of FH, the dependent jamming situation is not considered, though some preliminary work is included in Appendix B.

The DS spread spectrum effects must be modeled at the onset of the evaluation. Chapter V illustrates the direct use of this modeling. Since DS modulation is performed by biphase modulating (multiplying) the DPSK waveform by a PR waveform, the same process at the receiver removes the DS effects from the desired signal. At the same time, this process affects the jamming signal, and in fact spreads the jamming signal bandwidth. In order to determine the DS effects on a jamming signal without having to resort to simply equating the spread jamming signal to additional gaussian noise of equal power, a Fourier series representation of the PR waveform is used.

Due to its periodicity, a maximal-length PR waveform may be expanded into a Fourier series, thus giving rise to a suitable representation for the purposes of this study. The Fourier series representation of the PR waveform, p(t), is

$$p(t) = \sum_{m=-\infty}^{\infty} c_m \exp(jm\omega_p t) \qquad (4\text{-}23)$$

where

$$\omega_p = \frac{2\pi}{T_p} = \frac{2\pi}{pT_c}$$

$\frac{1}{T_c}$ = chip rate of the PR waveform

p = number of chips in one period of the PR waveform

and

$$c_m = \frac{1}{pT_c}\int_{t_o}^{t_o+pT_c} p(t)\exp(-jm\omega_p t)\,dt \tag{4-24}$$

Alternatively, Eq. (4-23) may be written as

$$p(t) = \sum_{m=-\infty}^{\infty} |c_m| \exp(j(m\omega_p t + \phi_m)) \tag{4-25}$$

with

$$|c_m| = \{[\text{Real}(c_m)]^2 + [\text{Imag}(c_m)]^2\}^{1/2}$$

$$\phi_m = \arctan\{\text{Imag}(c_m)/\text{Real}(c_m)\} \tag{4-26}$$

or, as Appendix C suggests, as

$$p(t) = \sum_{m=0}^{\infty} |c'_m| \cos(m\omega_p t + \phi_m) \tag{4-27}$$

where

$$|c'_m| = \begin{cases} |c_o| & m=0 \\ 2|c_m| & m\neq 0 \end{cases} \qquad (4\text{-}28)$$

CHAPTER V

CHARACTERIZATION OF THE SPREAD AND FILTERED INTERFERENCE

An accurate characterization of the DS-spread and narrowband-filtered interference at the input to the DPSK demodulator must be developed. Such a characterization is accomplished in this chapter for each of the three jamming signals under consideration.

Because the white gaussian noise has previously been characterized in the commonly used quadrature representation (with respect to ω_c), a similar representation for the interference is quite appropriate. The envelope and phase of the interference with respect to ω_c will also be derived.

Periodic FM Jamming Signal

Since biphase modulation of the FM jamming signal by the PR waveform is identical to multiplying the signal and waveform, the DS-spread, FM jamming signal is written as

$$j_{is}(t) = j_i(t)p(t)$$

$$= \frac{A_j}{\sqrt{K_s}} \sum_{m=0}^{\infty} \sum_{n=-\infty}^{\infty} |a_n||c'_m| \{\cos[(\omega_j + n\omega_m)t + \phi_{ji} + \phi_n] \cdot \cos[m\omega_p t + \phi_m]\} \qquad (5\text{-}1)$$

After using the trigonometric identity

$$\cos A \cdot \cos B = \frac{1}{2}\cos(A+B) + \frac{1}{2}\cos(A-B) \ ,$$

Eq. (5-1) becomes

$$j_{is}(t) = \frac{A_j}{2\sqrt{K_s}} \sum_{m=0}^{\infty} \sum_{n=-\infty}^{\infty} |a_n||c'_m| \{\cos[(\omega_j + n\omega_m + m\omega_p)t + \phi_{ji} + \phi_n + \phi_m]$$

$$+ \cos[(\omega_j + n\omega_m - m\omega_p)t + \phi_{ji} + \phi_n - \phi_m]\} \qquad (5\text{-}2)$$

In order to obtain the output of the narrowband filter (IF_2) for the input $j_{is}(t)$, each frequency component of Eq. (5-2) must be modified by the filter amplitude and phase characteristics. Therefore, the DS-spread and filtered FM interference becomes

$$j_{isf}(t) = \frac{A_j}{2\sqrt{K_s}} \sum_{m=0}^{\infty} \sum_{n=-\infty}^{\infty} |a_n||c'_m| \cdot$$

$$\{A^+ \cos[(\omega_j + n\omega_m + m\omega_p)t + \phi_{ji} + \phi_n + \phi_m - \theta^+]$$

$$+ A^- \cos[(\omega_j + n\omega_m - m\omega_p)t + \phi_{ji} + \phi_n - \phi_m - \theta^-]\} \qquad (5\text{-}3)$$

where from Eq. (4-12)

$$A^+ \triangleq A(\omega_j + n\omega_m + m\omega_p)$$

$$A^- \triangleq A(\omega_j + n\omega_m - m\omega_p)$$

$$\theta^+ \triangleq \theta(\omega_j + n\omega_m + m\omega_p)$$

$$\theta^- \triangleq \theta(\omega_j + n\omega_m - m\omega_p) \qquad (5\text{-}4)$$

To achieve the goal of representing the spread and filtered interference with respect to the carrier frequency, the following definitions are introduced:

$$\text{(a)}\quad \rho_1(t) \triangleq (\omega_j - \omega_c + n\omega_m + m\omega_p)t + \phi_n + \phi_m - \theta^+ \tag{5-5}$$

$$\text{(b)}\quad \rho_2(t) \triangleq (\omega_j - \omega_c + n\omega_m - m\omega_p)t + \phi_n - \phi_m - \theta^- \tag{5-6}$$

Substituting Eqs. (5-5) and (5-6) into Eq. (5-3), the spread and filtered interference is written as

$$j_{isf}(t) = \frac{A_j}{2\sqrt{K_s}} \sum_{m=0}^{\infty} \sum_{n=-\infty}^{\infty} |a_n||c'_m| \{A^+ \cos[\omega_c t + \phi_{ji} + \rho_1(t)] + A^- \cos[\omega_c t + \phi_{ji} + \rho_2(t)]\} \tag{5-7}$$

Further manipulation of Eq. (5-7) with trigonometric identities produces

$$j_{isf}(t) = \{\frac{A_j}{2\sqrt{K_s}} \sum_{m=0}^{\infty} \sum_{n=-\infty}^{\infty} |a_n||c'_m| (A^+ \cos[\rho_1(t)] + A^- \cos[\rho_2(t)])\} \cos[\omega_c t + \phi_{ji}]$$
$$- \{\frac{A_j}{2\sqrt{K_s}} \sum_{m=0}^{\infty} \sum_{n=-\infty}^{\infty} |a_n||c'_m| (A^+ \sin[\rho_1(t)] + A^- \sin[\rho_2(t)])\} \sin[\omega_c t + \phi_{ji}] \tag{5-8}$$

Any function of the form

$$f(t) = F_1(t)\cos[\omega_c t + \phi] + F_2(t)\sin[\omega_c t + \phi]$$

is redefinable as

$$f(t) = F(t)\cos[\omega_c t + \phi + \Phi_f(t)]$$

where

$$F(t) = \sqrt{F_1^2(t) + F_2^2(t)}$$

and

$$\Phi_f(t) = -\arctan[F_2(t)/F_1(t)] \ .$$

Therefore, $j_{isf}(t)$ can be simplified to

$$j_{isf}(t) = A_{ji}(t)\cos[\omega_c t + \phi_{ji} + \Phi_{ji}(t)] \qquad (5\text{-}9)$$

where

$$A_{ji}(t) = \frac{A_j}{2\sqrt{K_s}}\left\{\left[\sum_{m=0}^{\infty}\sum_{n=-\infty}^{\infty}|a_n||c'_m|\,(A^+\cos[\rho_1(t)]+A^-\cos[\rho_2(t)])\right]^2\right.$$

$$\left. + \left[\sum_{m=0}^{\infty}\sum_{n=-\infty}^{\infty}|a_n||c'_m|\,(A^+\sin[\rho_1(t)]+A^-\sin[\rho_2(t)])\right]^2\right\}^{1/2} \qquad (5\text{-}10)$$

and

$$\Phi_{ji}(t) = \arctan\left\{\frac{\sum_{m=0}^{\infty}\sum_{n=-\infty}^{\infty}|a_n||c'_m|(A^+\sin[\rho_1(t)]+A^-\sin[\rho_2(t)])}{\sum_{m=0}^{\infty}\sum_{n=-\infty}^{\infty}|a_n||c'_m|(A^+\cos[\rho_1(t)]+A^-\cos[\rho_2(t)])}\right\} \quad (5\text{-}11)$$

For eventual use, it is beneficial to rewrite Eq. (5-10) as

$$A_{ji}(t) = \frac{A_j}{\sqrt{K_s}}a_{ji}(t) \quad (5\text{-}12)$$

where $a_{ji}(t)$ is a dimensionless quantity and equal to

$$a_{ji}(t) = \frac{1}{2}\left\{\left[\sum_{m=0}^{\infty}\sum_{n=-\infty}^{\infty}|a_n||c'_m|(A^+\cos[\rho_1(t)]+A^-\cos[\rho_2(t)])\right]^2 + \left[\sum_{m=0}^{\infty}\sum_{n=-\infty}^{\infty}|a_n||c'_m|(A^+\sin[\rho_1(t)]+A^-\sin[\rho_2(t)])\right]^2\right\}^{\frac{1}{2}} \quad (5\text{-}13)$$

Furthermore, the envelope and phase representation of Eq. (5-9) may be placed into the desired quadrature form by expanding the cosine term to obtain

$$j_{isf}(t) = (A_{ji}(t)\cos[\phi_{ji} + \Phi_{ji}(t)])\cos\omega_c t - (A_{ji}(t)\sin[\phi_{ji} + \Phi_{ji}(t)])\sin\omega_c t \quad (5\text{-}14)$$

CW-Tone Jamming Signal

In many cases, the jamming signal may consist of a constant amplitude sinusoid (CW-tone) of the form

$$[j_i(t)]_{cw} = \frac{A_j}{\sqrt{K_s}} \cos[\omega_j t + \phi_{ji}] \tag{5-15}$$

The DS-spread, CW-tone signal becomes

$$\begin{aligned}
[j_{is}(t)]_{cw} &= [j_i(t)]_{cw} p(t) \\
&= \frac{A_j}{\sqrt{K_s}} \sum_{m=0}^{\infty} |c'_m| \{\cos[\omega_j t+\phi_{ji}] \cos[m\omega_p t+\phi_m]\} \\
&= \frac{A_j}{2\sqrt{K_s}} \sum_{m=0}^{\infty} |c'_m| \{\cos[(\omega_j+m\omega_p)t+\phi_{ji}+\phi_m] \\
&\qquad + \cos[(\omega_j-m\omega_p)t+\phi_{ji}-\phi_m]\}
\end{aligned} \tag{5-16}$$

Again, the IF_2 filtered output for the input defined in Eq. (5-15) is obtained by modifying each frequency component by the appropriate amplitude and phase. The filtered and DS-spread, CW-tone jamming signal may then be written as

$$\begin{aligned}
[j_{isf}(t)]_{cw} = \frac{A_j}{2\sqrt{K_s}} \sum_{m=0}^{\infty} |c'_m| \{&A^+_{cw} \cos[(\omega_j+m\omega_p)t+\phi_{ji}+\phi_m-\theta^+_{cw}] \\
&+ A^-_{cw} \cos[(\omega_j-m\omega_p)t+\phi_{ji}-\phi_m-\theta^-_{cw}]\}
\end{aligned} \tag{5-17}$$

where from Eq. (4-12)

$$A_{cw}^{+} \triangleq A(\omega_j + m\omega_p)$$

$$A_{cw}^{-} \triangleq A(\omega_j - m\omega_p)$$

$$\theta_{cw}^{+} \triangleq \theta(\omega_j + m\omega_p)$$

$$\theta_{cw}^{-} \triangleq \theta(\omega_j - m\omega_p) \qquad (5\text{-}18)$$

Two new parameters

$$\rho_3(t) \triangleq (\omega_j - \omega_c + m\omega_p)t + \phi_m - \theta_{cw}^{+} \qquad (5\text{-}19)$$

and

$$\rho_4(t) \triangleq (\omega_j - \omega_c - m\omega_p)t - \phi_m - \theta_{cw}^{-} \qquad (5\text{-}20)$$

are introduced and upon substituting these parameters into Eq. (5-17), gives

$$[j_{isf}(t)]_{cw} = \frac{A_j}{2\sqrt{K_s}} \sum_{m=0}^{\infty} |c'_m| \{A_{cw}^{+}\cos[\omega_c t+\phi_{ji}+\rho_3(t)] + A_{cw}^{-}\cos[\omega_c t+\phi_{ji}+\rho_4(t)]\}$$

$$= \left\{\frac{A_j}{2\sqrt{K_s}} \sum_{m=0}^{\infty} |c'_m| (A_{cw}^{+}\cos[\rho_3(t)]+A_{cw}^{-}\cos[\rho_4(t)])\right\} \cos[\omega_c t+\phi_j]$$

$$- \left\{\frac{A_j}{2\sqrt{K_s}} \sum_{m=0}^{\infty} |c'_m| (A_{cw}^{+}\sin[\rho_3(t)]+A_{cw}^{-}\sin[\rho_4(t)])\right\} \sin[\omega_c t+\phi_j] \qquad (5\text{-}21)$$

With the same reasoning which led to Eq. (5-9), Eq. (5-21) can be placed in the envelope and phase representation with the result being

$$[j_{isf}(t)]_{cw} = [A_{ji}(t)]_{cw}\cos[\omega_c t + \phi_{ji} + [\Phi_{ji}(t)]_{cw}] \tag{5-22}$$

where

$$[A_{ji}(t)]_{cw} = \frac{A_j}{2\sqrt{K_s}}\left\{\left[\sum_{m=0}^{\infty}|c'_m|\,(A^+_{cw}\cos[\rho_3(t)]+A^-_{cw}\cos[\rho_4(t)])\right]^2 + \left[\sum_{m=0}^{\infty}|c'_m|\,(A^+_{cw}\sin[\rho_3(t)]+A^-_{cw}\sin[\rho_4(t)])\right]^2\right\}^{\frac{1}{2}} \tag{5-23}$$

and

$$[\Phi_{ji}(t)]_{cw} = \arctan\left\{\frac{\sum_{m=0}^{\infty}|c'_m|\,(A^+_{cw}\sin[\rho_3(t)]+A^-_{cw}\sin[\rho_4(t)])}{\sum_{m=0}^{\infty}|c'_m|\,(A^+_{cw}\cos[\rho_3(t)]+A^-_{cw}\cos[\rho_4(t)])}\right\} \tag{5-24}$$

Again, it is beneficial to rewrite Eq. (5-23) as

$$[A_{ji}(t)]_{cw} = \frac{A_j}{\sqrt{K_s}}\,a_{jicw}(t) \tag{5-25}$$

where $a_{jicw}(t)$ is a dimensionless quantity and equal to

$$a_{jicw}(t) = \frac{1}{2}\left\{\left[\sum_{m=0}^{\infty}|c'_m|\,(A^{+}\cos[\rho_3(t)]+A^{-}\cos[\rho_4(t)])\right]^2 + \left[\sum_{m=0}^{\infty}|c'_m|\,(A^{+}\sin[\rho_3(t)]+A^{-}\sin[\rho_4(t)])\right]^2\right\}^{\frac{1}{2}} \qquad (5\text{-}26)$$

The required quadrature representation is determined by expanding the cosine term of Eq. (5-22) to obtain

$$[j_{isf}(t)]_{cw} = ([A_{ji}(t)]_{cw}\cos[\phi_{ji} + [\Phi_{ji}(t)]_{cw}])\cos\omega_c t - ([A_{ji}(t)]_{cw}\sin[\phi_{ji} + [\Phi_{ji}(t)]_{cw}])\sin\omega_c t \qquad (5\text{-}27)$$

As an interesting and informative sidenote, if the CW-tone jammer were a cochannel interference ($\omega_j=\omega_c$), the identities

$$\rho_3(t) = -\rho_4(t)$$

and

$$A^{+}_{cw} = A^{-}_{cw}$$

are produced. With these identities, Eq. (5-23) reduces to

$$[A_{ji}(t)]_{cw} = \frac{A_j}{\sqrt{K_s}}\sum_{m=0}^{\infty}|c'_m|A^{+}_{cw}\cos[m\omega_p t + \phi_m - \theta^{+}_{cw}]$$

which is none other than a filtered version of p(t), the PR waveform.

Noise Jamming Signal

In the noise jamming model description, it was stated that the noise jammer has a constant spectral density over the DS-spread bandwidth ($2R_c$) and zero elsewhere. This applies for each frequency slot in which a noise jammer is located. Because the noise jamming signal is modeled as a bandlimited interference, the DS-correlation process at the receiver will spread the signal out and reduce its spectral density value at the center of the band. This is unlike the thermal noise situation for in that model, the thermal noise is not strictly bandlimited and hence its spectral density value at the center of the band is negligibly affected by the correlation process. The modeling constraint placed on the noise jamming bandwidth causes the spectral density value at the center of the band to be scaled by a factor. This factor, known as the spectral-density-reduction-factor and denoted as S_n, is determined in Appendix D to be

$$S_n = .902823349530 \tag{5-28}$$

In other words, if the noise jamming had a constant spectral density height of $J_o/2$ before the correlation process, it would have a spectral height of $S_nJ_o/2$ at the center of the IF_2-BPF. Of course, the spectral density of the spread noise jammer would no longer be constant, but over the narrowband region of the IF_2-BPF it can be assumed constant (see Appendix D) with a value of $S_nJ_o/2$.

CHAPTER VI

GENERAL SUSCEPTIBILITY ANALYSIS

Based on the system model described in Chapter IV, the fundamental task becomes the derivation of the expressions for the probability of error. These expressions must depend in some manner on the signal, noise, interference and receiver parameters. In this chapter, the general M-ary, probability of error expressions requiring evaluation are established. The results are quite complex and ultimately serve a motivational purpose only. However, their presentation at this point remains instructive nonetheless. Throughout this chapter, certain notation used extensively in the remainder of the study will be presented.

The M-ary DPSK demodulator uses the signal $r_{(i-1)dsf}(t)$ in the $(i-1)^{th}$ signaling interval as the reference for the signal $r_{idsf}(t)$ in the i^{th} signaling interval. If $\theta_i=0$, a correct decision is made provided the estimate of θ_i, $\hat{\theta}_i$, is located within the interval $(-\pi/M, \pi/M)$. That is

$$\begin{aligned} \Pr(\text{correct decision} \mid \text{"0" sent}) &= \Pr(C \mid \text{"0" sent}) \\ &= \Pr(-\pi/M < \hat{\theta}_i < \pi/M \mid \text{"0" sent}) \\ &= 1 - \Pr(\text{error} \mid \text{"0" sent}) \\ &= 1 - \Pr(\text{err} \mid \text{"0" sent}) \end{aligned} \tag{6-1}$$

or

$$\begin{aligned} \Pr(\text{err}|\text{"0" sent}) &= 1 - \Pr(-\pi/M < \hat{\theta}_i < \pi/M|\text{"0" sent}) \\ &= 1 - \Pr(|\hat{\theta}_i| < \pi/M|\text{"0" sent}) \\ &= \Pr(|\hat{\theta}_i| > \pi/M|\text{"0" sent}) \end{aligned} \tag{6-2}$$

In general

$$\begin{aligned} \Pr(\text{err}|\tfrac{\text{"2}\pi k\text{"}}{M} \text{ sent}) &\triangleq \Pr(\text{err}|\text{"k"}) \\ &= \Pr(|\hat{\theta}_i - \tfrac{2\pi k}{M}| > \tfrac{\pi}{M}|\text{"k"}) \end{aligned} \tag{6-3}$$

Denoting $\Pr(\text{"0" sent})$ by P_0 and in general $\Pr(\frac{\text{"2}\pi k\text{"}}{M} \text{ sent})$ by P_k, the total probability of error is

$$\begin{aligned} \Pr(\text{err}) &= \sum_{k=0}^{M-1} P_k \Pr(\text{err}|\text{"k"}) \\ &= \sum_{k=0}^{M-1} P_k \Pr(|\hat{\theta}_i - \tfrac{2\pi k}{M}| > \tfrac{\pi}{M}|\text{"k"}) \end{aligned} \tag{6-4}$$

For the special but very common and important case of equal apriori probabilities ($P_k = 1/M$), Eq. (6-4) reduces to

$$\Pr(\text{err}) = \frac{1}{M} \sum_{k=0}^{M-1} \Pr(|\hat{\theta}_i - \tfrac{2\pi k}{M}| > \tfrac{\pi}{M}|\text{"k"}) \tag{6-5}$$

The derivation of the probability in Eq. (6-5) is the fundamental task. The main approach used in this derivation is to individually

determine the probability for the four cases of the presence or absence of a jammer in the $(i-1)^{th}$ signaling interval (reference signal) or the i^{th} signaling interval (present signal). That is, probability of error expressions must be individually derived for the following cases

CASE	JAMMER PRESENT IN REFERENCE SIGNAL (JR)	JAMMER PRESENT IN PRESENT SIGNAL (JP)
1	YES	YES
2	YES	NO
3	NO	YES
4	NO	NO

The probabilities requiring evaluation are ($\overline{A}$ refers to the complement of the event A):

$$\text{(a)}\quad \Pr(\text{err}|\text{JR},\text{JP}) = \frac{1}{M}\sum_{k=0}^{M-1} \Pr\left(\left|\hat{\theta}_i - \frac{2\pi k}{M}\right| > \frac{\pi}{M}\middle|\text{"k"},\text{JR},\text{JP}\right)$$

$$\text{(b)}\quad \Pr(\text{err}|\text{JR},\overline{\text{JP}}) = \frac{1}{M}\sum_{k=0}^{M-1} \Pr\left(\left|\hat{\theta}_i - \frac{2\pi k}{M}\right| > \frac{\pi}{M}\middle|\text{"k"},\text{JR},\overline{\text{JP}}\right)$$

$$\text{(c)}\quad \Pr(\text{err}|\overline{\text{JR}},\text{JP}) = \frac{1}{M}\sum_{k=0}^{M-1} \Pr\left(\left|\hat{\theta}_i - \frac{2\pi k}{M}\right| > \frac{\pi}{M}\middle|\text{"k"},\overline{\text{JR}},\text{JP}\right)$$

$$\text{(d)}\quad \Pr(\text{err}|\overline{\text{JR}},\overline{\text{JP}}) = \frac{1}{M}\sum_{k=0}^{M-1} \Pr\left(\left|\hat{\theta}_i - \frac{2\pi k}{M}\right| > \frac{\pi}{M}\middle|\text{"k"},\overline{\text{JR}},\overline{\text{JP}}\right) \qquad (6\text{-}6)$$

If there are N_s hopping slots with K_s $(1 \le K_s \le N_s)$ of those slots jammed, the probability that a slot contains a jamming signal is K_s/N_s. Consequently, the probability that a slot is not jammed is

$(N_s-K_s)/N_s$. Furthermore, if the jammer is allowed an additional degree of sophistication, specifically the capability of frequency-hopping, the use of a jammed or unjammed slot during one interval is completely independent of the use of a jammed or unjammed slot during the next interval. Hence

$$\begin{aligned} \Pr(JR,JP) &= (K_s/N_s)^2 \\ \Pr(JR,\overline{JP}) &= K_s(N_s-K_s)/N_s^2 \\ \Pr(\overline{JR},JP) &= (N_s-K_s)K_s/N_s^2 \\ \Pr(\overline{JR},\overline{JP}) &= ((N_s-K_s)/N_s)^2 \end{aligned} \tag{6-7}$$

The frequency-hopping capability of a jammer is certainly more likely since a fixed-frequency jammer is more easily detected and thwarted. Therefore, this research is concerned only with those jammers which have the frequency-hopping capability. Nevertheless, the discrete probabilities for a fixed-frequency situation are

$$\begin{aligned} \Pr(JR,JP) &= \left(\frac{K_s}{N_s}\right)\left(\frac{K_s-1}{N_s-1}\right) \\ \Pr(JR,\overline{JP}) &= \left(\frac{K_s}{N_s}\right)\left(\frac{N_s-K_s}{N_s-1}\right) \\ \Pr(\overline{JR},JP) &= \left(\frac{N_s-K_s}{N_s}\right)\left(\frac{K_s}{N_s-1}\right) \\ \Pr(\overline{JR},\overline{JP}) &= \left(\frac{N_s-K_s}{N_s}\right)\left(\frac{N_s-K_s-1}{N_s-1}\right) \end{aligned} \tag{6-8}$$

The overall probability of error may now be written from Eqs. (6-6) and (6-7) as

$$\begin{aligned} Pr(err) = {} & Pr(err|JR,JP)Pr(JR,JP)+Pr(err|JR,\overline{JP})Pr(JR,\overline{JP}) \\ & + Pr(err|\overline{JR},JP)Pr(\overline{JR},JP)+Pr(err|\overline{JR},\overline{JP})Pr(\overline{JR},\overline{JP}) \\ = {} & Pr(err|JR,JP)[(K_s/N_s)^2]+Pr(err|JR,\overline{JP})[K_s(N_s-K_s)/N_s^2] \\ & + Pr(err|\overline{JR},JP)[(N_s-K_s)K_s/N_s^2]+Pr(err|\overline{JR},\overline{JP})[((N_s-K_s)/N_s)^2] \end{aligned} \tag{6-9}$$

The general analytical development required to derive the specific probabilities in Eq. (6-9) is now introduced.

To remain as general as possible, it will be initially assumed that the two adjacent signaling intervals are independently jammed with periodic, FM interference. The DPSK demodulator input during the i^{th} signaling interval is

$$r_{idsf}(t) = s_i(t) + j_{isf}(t) + n_{if}(t) \tag{6-10}$$

It will prove very useful from this point on to change the notation concerning the i^{th} signaling interval to a notation which refers to the signal in that interval. The i^{th} signaling interval has been referred to as the interval containing the present (p) signal, therefore the (i) notation is changed to (p). With this change in mind and the models of Chapter IV, Eq. (6-10) becomes

$$r_{pdsf}(t) = r_{idsf}(t)$$

$$= A_s\cos[\omega_c t + \theta_p] + A_{jp}(t)\cos[\omega_c t + \phi_{jp} + \phi_{jp}(t)]$$

$$+ x_p(t)\cos[\omega_c t] - y_p(t)\sin[\omega_c t] \qquad (6\text{-}11)$$

where $A_{jp}(t)$ and $\phi_{jp}(t)$ are the envelope and phase, respectively, of the spread and filtered, FM signal corrupting the present signal. Likewise, for the reference signal in the $(i-1)^{th}$ signaling interval, the analytical description is

$$r_{rdsf}(t) = r_{(i-1)dsf}(t) = s_{(i-1)}(t) + j_{(i-1)sf}(t) + n_{(i-1)f}(t)$$

$$= s_r(t) + j_{rsf}(t) + n_{rf}(t)$$

$$= A_s\cos[\omega_c t + \theta_r] + A_{jr}(t)\cos[\omega_c t + \phi_{jr} + \phi_{jr}(t)]$$

$$+ x_r(t)\cos[\omega_c t] - y_r(t)\sin[\omega_c t] \qquad (6\text{-}12)$$

where the analogous notation for the reference (r) signal has been used.

Assuming without a loss of generality that a "0" was sent (set $\theta_p = \theta_r = 0$), it is possible to view the decoding process on a "double exposure" phasor diagram. This is accomplished by overlaying two adjacent received phasors (with respect to $\cos\omega_c t$ and $\sin\omega_c t$) on one diagram. Such a diagram is illustrated in Figure 8 where the definitions

$$A_1 = A_{jr}(t_s - T_b) \qquad x_1 = x_r(t_s - T_b)$$

$$A_2 = A_{jp}(t_s) \qquad y_1 = -y_r(t_s - T_b)$$

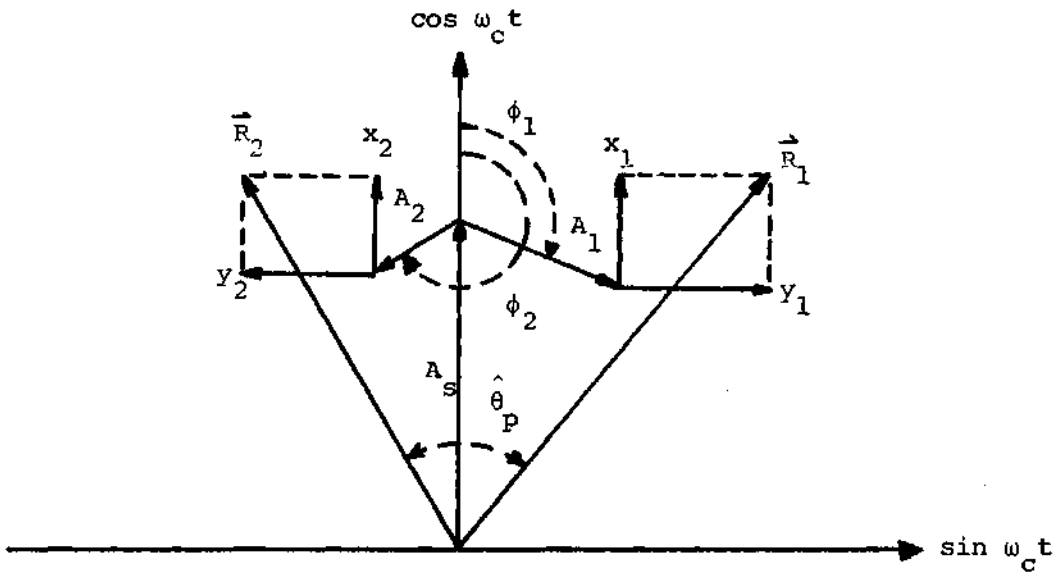

FIGURE 8. Signal, Interference, and Noise Phasors at Adjacent Sampling Times for a Transmitted "0"

$$\phi_1 = \phi_{jr} + \Phi_{jr}(t_s - T_b) \qquad x_2 = x_p(t_s)$$

$$\phi_2 = \phi_{jp} + \Phi_{jp}(t_s) \qquad y_2 = -y_p(t_s) \tag{6-13}$$

are used. The variables t_s and T_b are, respectively, the sample time and the duration of the signaling interval.

The decision boundaries, given that a "0" was sent, are located at $\pm\pi/M$ from the reference phasor. Therefore, if $-\pi/M < \hat{\theta}_p < \pi/M$, or equivalently, $\cos\hat{\theta}_p > \cos(\pi/M)$, a correct decision will be made. On the other hand, an error is made if $\cos\hat{\theta}_p < \cos(\pi/M)$. Thus

$$\Pr(\text{err}|\text{"0"},JR,JP) = \Pr(\cos\hat{\theta}_p < \cos(\pi/M)\,|\,\text{"0"},JR,JP) \tag{6-14}$$

is the probability requiring evaluation.

Note that with (A·B is the familiar dot product)

$$\cos(\hat{\theta}_p) = \vec{R}_1 \cdot \vec{R}_2 / |\vec{R}_1||\vec{R}_2|$$

an error will be made if

$$\vec{R}_1 \cdot \vec{R}_2 < |\vec{R}_1||\vec{R}_2|\cos(\pi/M) \tag{6-15}$$

where from Figure 8,

$$\vec{R}_1 \cdot \vec{R}_2 = (A_s + x_1 + A_1\cos\phi_1)(A_s + x_2 + A_2\cos\phi_2)$$

$$+ (y_1 + A_1\sin\phi_1)(y_2 + A_2\sin\phi_2) \tag{6-16}$$

$$|\vec{R}_1|^2 = (A_s + x_1 + A_1\cos\phi_1)^2 + (y_1 + A_1\sin\phi_1)^2 \tag{6-17}$$

and

$$|\vec{R}_2|^2 = (A_s + x_2 + A_2\cos\phi_2)^2 + (y_2 + A_2\sin\phi_2)^2 \tag{6-18}$$

The definitions

$$\begin{aligned} P_1 &\triangleq A_s + x_1 + A_1\cos\phi_1 \\ P_2 &\triangleq A_s + x_2 + A_2\cos\phi_2 \\ Q_1 &\triangleq y_1 + A_1\sin\phi_1 \\ Q_2 &\triangleq y_2 + A_2\sin\phi_2 \end{aligned} \tag{6-19}$$

transform the error event in Eq. (6-15) into

$$X \triangleq P_1P_2 + Q_1Q_2 < \sqrt{(P_1^2 + Q_1^2)(P_2^2 + Q_2^2)}\cos(\pi/M) \triangleq Y \tag{6-20}$$

The probability of the event in Eq. (6-20) is desired.

To say the least, Eq. (6-20) is a rather complicated event although considerable simplification is possible for M=2. In order to establish a more structured event, a few manipulations on Eq. (6-20) are now considered. Initially, square both sides of the inequality in Eq. (6-20). Since X may be less than zero, the squaring operation may prevent the inequality from remaining valid. Therefore, two cases, one for X positive and the other for X negative, must be considered. For these two cases, the probability of the event X<Y is now written as

$$\Pr(X<Y) = \Pr(X<Y|X<0)\Pr(X<0) + \Pr(X<Y|X>0)\Pr(X>0)$$
$$= \Pr(X<0) + \Pr(X<Y|X>0)\Pr(X>0) \qquad (6\text{-}21)$$

where the fact that Y is always greater than or equal to zero has been used. The first probability in Eq. (6-21), $\Pr(X<0)$, is none other than the binary (M=2), FM (JR,JP) jamming error probability and is seemingly much less complicated than $\Pr(X<Y|X>0)\Pr(X>0) = \Pr(X<Y,X>0)$. Therefore, focus is now placed on developing this latter joint probability.

For X>0, Eq. (6-20) can be transformed into the equivalent event

$$X \sin(\pi/M) < \cos(\pi/M) \begin{cases} Z & Z>0 \\ -Z & Z<0 \end{cases} \qquad (6\text{-}22)$$

where

$$Z = P_1Q_2 - P_2Q_1$$

Therefore,

$$\Pr(X<Y,X>0) = \Pr(X \sin(\pi/M)<Z \cos(\pi/M), X>0, Z>0)$$
$$+ \Pr(X \sin(\pi/M)< -Z \cos(\pi/M), X>0, Z<0) \qquad (6\text{-}23)$$

With the directly proven identity

$$ab + cd = \frac{1}{4}[(a+b)^2 + (c+d)^2 - (a-b)^2 - (c-d)^2] \qquad (6\text{-}24)$$

X and Z can be redefined as

$$X \sin(\pi/M) = (P_1P_2 + Q_1Q_2)\sin(\pi/M)$$

$$= \frac{1}{4}[(P_1 + P_2)^2 + (Q_1 + Q_2)^2 - (P_1 - P_2)^2 - (Q_1 - Q_2)^2]\sin(\pi/M) \qquad (6\text{-}25)$$

and

$$Z \cos(\pi/M) = (P_1Q_2 - P_2Q_1)\cos(\pi/M)$$

$$= \frac{1}{4}[(P_1 + Q_2)^2 + (P_2 - Q_1)^2 - (P_1 - Q_2)^2 - (P_2 + Q_1)^2]\cos(\pi/M) \qquad (6\text{-}26)$$

The definitions

$$\alpha_1 \triangleq (P_1+P_2)\sqrt{\sin(\pi/M)} \qquad \alpha_5 \triangleq (P_1+Q_2)\sqrt{\cos(\pi/M)}$$

$$\alpha_2 \triangleq (Q_1+Q_2)\sqrt{\sin(\pi/M)} \qquad \alpha_6 \triangleq (P_2-Q_1)\sqrt{\cos(\pi/M)}$$

$$\alpha_3 \triangleq (P_1-P_2)\sqrt{\sin(\pi/M)} \qquad \alpha_7 \triangleq (P_1-Q_2)\sqrt{\cos(\pi/M)}$$

$$\alpha_4 \triangleq (Q_1-Q_2)\sqrt{\sin(\pi/M)} \qquad \alpha_8 \triangleq (P_2+Q_1)\sqrt{\cos(\pi/M)} \qquad (6\text{-}27)$$

are now introduced and are so defined that upon conditioning the probability in Eq. (6-23) on x_r, x_p, ϕ_1, and ϕ_2, $\{\alpha_i: i=1,2,\ldots,8\}$ become a set of gaussian random variables with mean values

$$m_1 \triangleq E[\alpha_1] = (2A_s + A_1\cos\phi_1 + A_2\cos\phi_2)\sqrt{\sin(\pi/M)}$$

$$m_2 \triangleq E[\alpha_2] = (A_1\sin\phi_1 + A_2\sin\phi_2)\sqrt{\sin(\pi/M)}$$

$$m_3 \triangleq E[\alpha_3] = (A_1\cos\phi_1 - A_2\cos\phi_2)\sqrt{\sin(\pi/M)}$$

$$m_4 \triangleq E[\alpha_4] = (A_1\sin\phi_1 - A_2\sin\phi_2)\sqrt{\sin(\pi/M)}$$

$$m_5 \triangleq E[\alpha_5] = (A_s + A_1\cos\phi_1 + A_2\sin\phi_2)\sqrt{\cos(\pi/M)}$$

$$m_6 \triangleq E[\alpha_6] = (A_s - A_1\sin\phi_1 + A_2\cos\phi_2)\sqrt{\cos(\pi/M)}$$

$$m_7 \triangleq E[\alpha_7] = (A_s + A_1\cos\phi_1 - A_2\sin\phi_2)\sqrt{\cos(\pi/M)}$$

$$m_8 \triangleq E[\alpha_8] = (A_s + A_1\sin\phi_1 + A_2\cos\phi_2)\sqrt{\cos(\pi/M)} \qquad (6\text{-}28)$$

and variances

$$\sigma_i^2 \triangleq E[(\alpha_i - m_i)^2] = 2N\begin{cases}\sin(\pi/M) & i=1,2,3,4\\ \cos(\pi/M) & i=5,6,7,8\end{cases} \qquad (6\text{-}29)$$

Therefore, the conditional probability becomes

$$\Pr(X<Y, X>0 \mid x_r, x_p, \phi_1, \phi_2)$$

$$= \Pr(\alpha_1^2+\alpha_2^2-\alpha_3^2-\alpha_4^2<\alpha_5^2+\alpha_6^2-\alpha_7^2-\alpha_8^2,$$

$$\alpha_1^2+\alpha_2^2-\alpha_3^2-\alpha_4^2>0, \alpha_5^2+\alpha_6^2-\alpha_7^2-\alpha_8^2>0 \mid x_r, x_p, \phi_1, \phi_2)$$

$$+ \Pr(\alpha_1^2+\alpha_2^2-\alpha_3^2-\alpha_4^2<\alpha_7^2+\alpha_8^2-\alpha_5^2-\alpha_6^2,$$

$$\alpha_1^2+\alpha_2^2-\alpha_3^2-\alpha_4^2>0,\alpha_7^2+\alpha_8^2-\alpha_5^2-\alpha_6^2>0|x_r,x_p,\phi_1,\phi_2)$$

$$= \Pr(\chi_1<\chi_2,\chi_1>0,\chi_2>0|x_r,x_p,\phi_1,\phi_2)$$

$$+ \Pr(\chi_1<-\chi_2,\chi_1>0,\chi_2<0|x_r,x_p,\phi_1,\phi_2) \qquad (6\text{-}30)$$

where

$$\chi_1 \triangleq \alpha_1^2 + \alpha_2^2 - \alpha_3^2 - \alpha_4^2$$

$$\chi_2 \triangleq \alpha_5^2 + \alpha_6^2 - \alpha_7^2 - \alpha_8^2 \qquad (6\text{-}31)$$

For the conditioning in Eq. (6-30), the random variables χ_1 and χ_2 are individually described as the difference between two independent, noncentral, Chi-Square variates. Unfortunately, χ_1 and χ_2 are not necessarily independent, thereby eliminating the needed joint density function from being equal to the product of the marginal density functions. In hopes of circumventing this dependence, a transformation was performed on the random variables, $\alpha_i (i = 1,2,\ldots,8)$, to obtain a set of independent random variables. However, the eventual error event for this transformation proved as unwieldy as the event in Eq. (6-30). Hence, for this general analytical technique it is not known at this time if a closed form expression exists for the probability in Eq. (6-30) and furthermore the probabilities in Eq. (6-9). In lieu of this situation, other methods of attack are required. The approach proposed here is to

consider the probability of error for M=2, 4 and M>4 individually and to present analytical techniques leading to accurate and numerically tractable expressions. The binary, quaternary, and M>4 cases are separately, and respectively, considered in Chapters VII, VIII, and IX.

CHAPTER VII

PROBABILITY OF ERROR FOR BINARY DPSK

Depending on the type of interference considered, this chapter is divided into three sections: periodic FM jamming; CW-tone jamming; and noise jamming. Binary DPSK probability of error expressions are derived in these sections for the four subcases, which are (JR,JP), $(JR,\overline{JP})$, $(\overline{JR},JP)$, and $(\overline{JR},\overline{JP})$. In Appendix E, it is shown that the $(JR,\overline{JP})$ and $(\overline{JR},JP)$ subcases produce identical results. Thus, the $(JR,\overline{JP})$ and $(\overline{JR},JP)$ subcases are condensed into one subcase, that being the $(\overline{JR},JP)$ subcase.

As pointed out in Chapter VI, great simplification of the general analysis is possible for the binary (M=2) case. Because of this simplification, the same analytical technique used in the general analysis will be used here. The periodic FM jamming, (JR,JP) subcase is considered first because the results obtained serve as an analytical foundation for the remaining subcases. Extensive use of the performance of binary DPSK in a white gaussian noise environment (Eq. 3-1) will be made throughout.

Figure 9 summarizes the organization of this chapter and serves as a quick reference guide to the individual subcases.

Periodic FM Jamming

In Chapter VI, the inequality

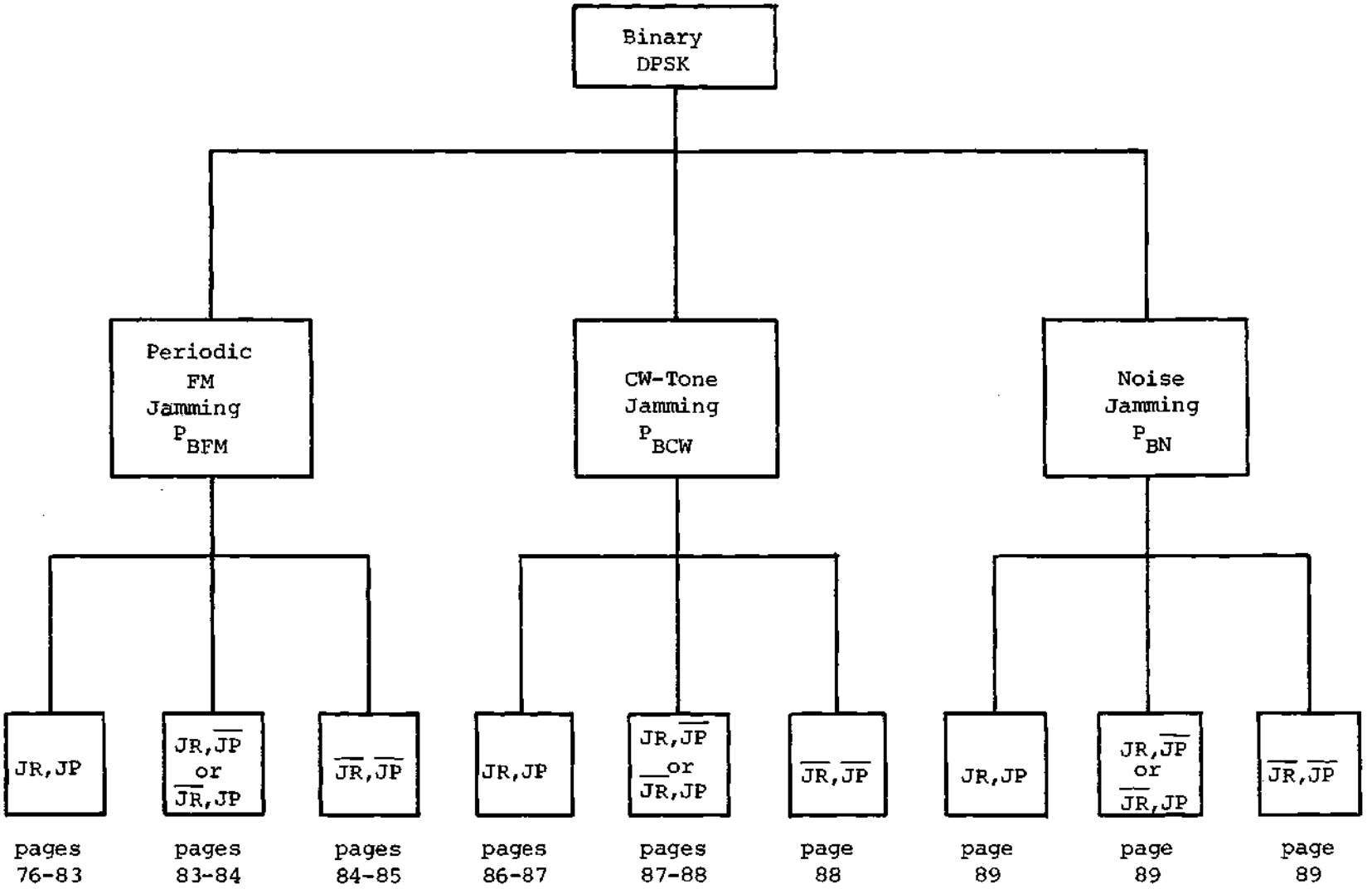

FIGURE 9. Reference Flow Graph for Binary DPSK

$$P_1P_2 + Q_1Q_2 < \sqrt{(P_1^2+Q_1^2)(P_2^2+Q_2^2)}\cos(\pi/M) \tag{7-1}$$

where

$$\begin{aligned} P_1 &= A_s + x_1 + A_1\cos\phi_1 \\ P_2 &= A_s + x_2 + A_2\cos\phi_2 \\ Q_1 &= \quad y_1 + A_1\sin\phi_1 \\ Q_2 &= \quad y_2 + A_2\sin\phi_2 \end{aligned} \tag{7-2}$$

could not be significantly simplified unless M=2. For the binary situation, Eq. (7-1) becomes

$$P_1P_2 + Q_1Q_2 < 0 \tag{7-3}$$

It is the purpose of this section to determine the probability of the event in Eq. (7-3) for each of the subcases when the interference is a periodic FM signal.

(JR,JP)

Recall from Chapter VI that the event defined in Eq. (7-1), or alternatively for the binary situation Eq. (7-3), was conditioned without a loss of generality on the event of the data bit "0" being transmitted. As a result of this conditioning and Eq. (7-3), the conditional probability of error for this binary, FM subcase is

$$P_{BFM}(JR,JP,"0") \triangleq Pr(err|JR,JP,"0")$$

$$= Pr(P_1P_2 + Q_1Q_2 < 0|JR,JP,"0") \qquad (7\text{-}4)$$

With the aid of Eq. (6-24) the error event in Eq. (7-3) is transformable into

$$(P_1 + P_2)^2 + (Q_1 + Q_2)^2 - (P_1 - P_2)^2 - (Q_1 - Q_2)^2 < 0$$

Thus,

$$P_{BFM}(JR,JP,"0") = Pr[(P_1+P_2)^2+(Q_1+Q_2)^2-(P_1-P_2)^2-(Q_1-Q_2)^2<0|JR,JP,"0"]$$

$$= Pr[(P_1+P_2)^2+(Q_1+Q_2)^2<(P_1-P_2)^2+(Q_1-Q_2)^2|JR,JP,"0"] \qquad (7\text{-}5)$$

Note that P_1,P_2,Q_1, and Q_2 become independent gaussian random variables when the defined quantities of Eq. (7-2) are conditioned on the variates x_r, x_p, ϕ_1, and ϕ_2. With the definitions

$$\alpha_1 = P_1+P_2 \qquad \alpha_3 = P_1-P_2$$

$$\alpha_2 = Q_1+Q_2 \qquad \alpha_4 = Q_1-Q_2$$

and the above conditioning, then

$$P_{BFM}(JR,JP,"0",x_r,x_p,\phi_1,\phi_2)$$

$$= \Pr\left[(P_1+P_2)^2+(Q_1+Q_2)^2 < (P_1-P_2)^2+(Q_1-Q_2)^2 \,\middle|\, JR, JP, "0", x_r, x_p, \phi_1, \phi_2\right]$$

$$= \Pr\left[\alpha_1^2+\alpha_2^2 < \alpha_3^2+\alpha_4^2 \,\middle|\, JR, JP, "0", x_r, x_p, \phi_1, \phi_2\right] \qquad (7\text{-}6)$$

The set, $\{\alpha_i\}$ contains elements which are also independent gaussian random variables with mean values

$$\begin{aligned} m_1 &\triangleq E[\alpha_1] = 2A_s + A_1\cos\phi_1 + A_2\cos\phi_2 \\ m_2 &\triangleq E[\alpha_2] = A_1\sin\phi_1 + A_2\sin\phi_2 \\ m_3 &\triangleq E[\alpha_3] = A_1\cos\phi_1 - A_2\cos\phi_2 \\ m_4 &\triangleq E[\alpha_4] = A_1\sin\phi_1 - A_2\sin\phi_2 \end{aligned} \qquad (7\text{-}7)$$

and variances

$$\sigma_i^2 \triangleq E[(\alpha_i - m_i)^2] = 2N \qquad (i=1,2,3,4) \qquad (7\text{-}8)$$

Since both sides of the inequality

$$\alpha_1^2 + \alpha_2^2 < \alpha_3^2 + \alpha_4^2$$

are positive, the positive square root may be taken. This operation leaves the probability of Eq. (7-6) absolutely unchanged and rewritten as

$$P_{BFM}(JR,JP,"0",x_r,x_p,\phi_1,\phi_2)$$

$$= Pr(\sqrt{\alpha_1^2+\alpha_2^2} < \sqrt{\alpha_3^2+\alpha_4^2} \,|\, JR,JP,"0",x_r,x_p,\phi_1,\phi_2)$$

$$= Pr(R_1<R_2 \,|\, JR,JP,"0",x_r,x_p,\phi_1,\phi_2) \qquad (7\text{-}9)$$

where the definitions

$$R_1 = \sqrt{\alpha_1^2 + \alpha_2^2}$$

$$R_2 = \sqrt{\alpha_3^2 + \alpha_4^2} \qquad (7\text{-}10)$$

have been introduced. It is well known [16] that the random variables R_1 and R_2, conditioned on the variates x_r, x_p, ϕ_1, and ϕ_2, are independent and Rician distributed with marginal density functions

$$p_{R_1}(r_1) = \frac{r_1}{2N} \exp\left[-\frac{r_1^2+m_1^2+m_2^2}{4N}\right] \cdot I_o\left[\frac{r_1\sqrt{m_1^2+m_2^2}}{2N}\right] \quad r_1 \geq 0 \qquad (7\text{-}11)$$

and

$$p_{R_2}(r_2) = \frac{r_2}{2N} \exp\left[-\frac{r_2^2+m_3^2+m_4^2}{4N}\right] \cdot I_o\left[\frac{r_2\sqrt{m_3^2+m_4^2}}{2N}\right] \quad r_2 \geq 0 \qquad (7\text{-}12)$$

where $I_o[\cdot]$ is the modified Bessel function of the first kind and zero order. The conditioning is implied in Eqs. (7-11) and (7-12) through the parameters m_1, m_2, m_3, and m_4 but is suppressed at this time for clarity.

With the conditional probabilistic description of R_1 and R_2, Eq. (7-9) becomes

$$P_{BFM}(JR,JP,"0",x_r,x_p,\phi_1,\phi_2)$$

$$= \int_o^\infty p_{R_2}(r_2) \int_o^{r_2} p_{R_1}(r_1)dr_1dr_2$$

$$= \left(\frac{1}{2N}\right)^2 \int_o^\infty \left\{ r_2 \exp\left[-\frac{r_2^2+m_3^2+m_4^2}{4N}\right] I_o\left[\frac{r_2\sqrt{m_3^2+m_4^2}}{2N}\right] \cdot \right.$$

$$\left. \int_o^{r_2} r_1 \exp\left[-\frac{r_1^2+m_1^2+m_2^2}{4N}\right] I_o\left[\frac{r_1\sqrt{m_1^2+m_2^2}}{2N}\right] dr_1 \right\} dr_2 \qquad (7\text{-}13)$$

The change of variables

$$u = \frac{r_1}{\sqrt{2N}} \qquad v = \frac{r_2}{\sqrt{2N}}$$

transforms Eq. (7-13) into

$$P_{BFM}(JR,JP,"0",x_r,x_p,\phi_1,\phi_2)$$

$$= \int_o^\infty \left\{ v \exp\left[-\frac{1}{2}\left(v^2 + \frac{m_3^2+m_4^2}{2N}\right)\right] I_o\left[v\sqrt{\frac{m_3^2+m_4^2}{2N}}\right] \cdot \right.$$

$$\left. \int_o^v u \exp\left[-\frac{1}{2}\left(u^2 + \frac{m_1^2+m_2^2}{2N}\right)\right] I_o\left[u\sqrt{\frac{m_1^2+m_2^2}{2N}}\right] du \right\} dv \qquad (7\text{-}14)$$

From Appendix F, Eq. (7-14) is seen to be equivalent to Price's

function [53], $P_{\mu,\nu}[a,b;r]$, with

$$\mu = \nu = 0$$

$$a = \sqrt{\frac{m_3^2+m_4^2}{2N}}$$

$$b = \sqrt{\frac{m_1^2+m_2^2}{2N}}$$

$$r = 1$$

Thus

$$P_{BFM}(JR,JP,"0",x_r,x_p,\phi_1,\phi_2)$$

$$= P_{0,0}\left[\sqrt{\frac{m_3^2+m_4^2}{2N}}\ ,\ \sqrt{\frac{m_1^2+m_2^2}{2N}}\ ;\ 1\right]$$

$$= Q\left[\frac{1}{2}\sqrt{\frac{m_3^2+m_4^2}{N}}\ ,\ \frac{1}{2}\sqrt{\frac{m_1^2+m_2^2}{N}}\right]$$

$$- \frac{1}{2}\exp\left[-\frac{1}{8N}(m_1^2+m_2^2+m_3^2+m_4^2)\right] I_o\left[\frac{1}{4N}\sqrt{(m_1^2+m_2^2)(m_3^2+m_4^2)}\right] \qquad (7\text{-}15)$$

where Q(c,d) is the Marcum-Q function defined by

$$Q(c,d) \triangleq \int_d^\infty t \exp[-\frac{1}{2}(t^2+c^2)] I_o[ct]dt$$

Substituting [54]

$$Q[\sqrt{\gamma}\,,\sqrt{\lambda}\,] - \frac{1}{2}\exp[-\frac{\gamma+\lambda}{2}]I_o[\sqrt{\gamma\lambda}\,]$$

$$= \frac{1}{2}\{1 - Q[\sqrt{\lambda}\,,\sqrt{\gamma}\,] + Q[\sqrt{\gamma}\,,\sqrt{\lambda}\,]\} \tag{7-16}$$

into Eq. (7-15) results in a conditional probability of the form

$$P_{BFM}(JR,JP,"0",x_r,x_p,\phi_1,\phi_2)$$

$$= \frac{1}{2}\left\{1 - Q\left[\frac{1}{2}\sqrt{\frac{m_1^2+m_2^2}{N}}\,,\frac{1}{2}\sqrt{\frac{m_3^2+m_4^2}{N}}\,\right]\right.$$

$$\left. + Q\left[\frac{1}{2}\sqrt{\frac{m_3^2+m_4^2}{N}}\,,\frac{1}{2}\sqrt{\frac{m_1^2+m_2^2}{N}}\,\right]\right\} \tag{7-17}$$

where after using Eq. (7-7)

$$m_1^2+m_2^2 = 4A_s^2+4A_s(A_1\cos\phi_1+A_2\cos\phi_2)+2A_1A_2\cos(\phi_1-\phi_2)+A_1^2+A_2^2$$

$$m_3^2+m_4^2 = A_1^2+A_2^2-2A_1A_2\cos(\phi_1-\phi_2) \tag{7-18}$$

Recall, the dependence of Eq. (7-17) on x_r and x_p is implicitly contained within A_1 and A_2 through the Fourier series coefficients a_n.

The conditioning in Eq. (7-17) is removed by averaging over the variables x_r, x_p, ϕ_1 and ϕ_2. Thus

$$P_{BFM}(JR,JP,"0") = \left(\frac{1}{2\pi}\right)^4 \int_0^{2\pi}\int_0^{2\pi}\int_0^{2\pi}\int_0^{2\pi} P_{BFM}(JR,JP,"0",x_r,x_p,\phi_1,\phi_2)$$

$$dx_r,dx_p,d\phi_1,d\phi_2 \qquad (7\text{-}19)$$

Equation (7-19) is an accurate but complex expression for the probability of error of this subcase. As will be shown in Chapter X, this complexity can be and is significantly reduced.

Because the interference-plus-noise is independent from one signaling interval to the next, the error expression in Eq. (7-19) must then be valid regardless of the data symbol. Hence,

$$P_{BFM}(JR,JP) = P_{BFM}(JR,JP,"0") \qquad (7\text{-}20)$$

<u>$(JR,\overline{JP})$ or $(\overline{JR},JP)$</u>

Only the latter subcase $(\overline{JR},JP)$ is specifically considered here because the subcases produce identical results.

The (JR,JP) subcase analysis just completed has formed a basis from which the immediate subcase analysis will draw. In fact, Eqs. (7-17) and (7-18) are directly applicable here but with $A_1=0$ since only the present signal is jammed. In other words

$$P_{BFM}(\overline{JR},JP,"0",x_p,\phi_2) = P_{BFM}(JR,JP,"0",x_r,x_p,\phi_1,\phi_2)\Big|_{A_1=0}$$

$$= \frac{1}{2}\left\{1 - Q\left[\frac{1}{2}\sqrt{\frac{m_1^2+m_2^2}{N}}\ ,\ \frac{1}{2}\sqrt{\frac{m_3^2+m_4^2}{N}}\right] + Q\left[\frac{1}{2}\sqrt{\frac{m_3^2+m_4^2}{N}}\ ,\ \frac{1}{2}\sqrt{\frac{m_1^2+m_2^2}{N}}\right]\right\} \qquad (7\text{-}21)$$

where now

$$m_1^2 + m_2^2 = 4A_s^2 + 4A_sA_2\cos\phi_2 + A_2^2$$

$$m_3^2 + m_4^2 = A_2^2 \tag{7-22}$$

Since one jamming signal alone is present, the eventual averaging operation is confined to a two-fold average over x_p and ϕ_2. Also, as in the previous subcase, the conditional error probability in Eq. (7-21) must be data-symbol-independent since the interference-plus-noise is independent from interval to interval. The final result is

$$\begin{aligned} P_{BFM}(\overline{JR},JP) &= P_{BFM}(JR,\overline{JP}) \\ &= P_{BFM}(\overline{JR},JP,\text{"0"}) \\ &= \left(\frac{1}{2\pi}\right)^2 \int_0^{2\pi}\int_0^{2\pi} P_{BFM}(\overline{JR},JP,\text{"0"},x_p,\phi_2)\,dx_p\,d\phi_2 \end{aligned} \tag{7-23}$$

where the integrand is defined in Eq. (7-21).

$\underline{\overline{JR},\overline{JP}}$

Neither the reference nor the present signal is jammed in this subcase. As a result, the only disruptive signal is the noise term. Thus, the probability of error expression is simply written as

$$P_{BFM}(\overline{JR},\overline{JP}) = \frac{1}{2}\exp\left[-\frac{A_s^2}{2N}\right] \tag{7-24}$$

Equation (7-24) can be obtained directly from Eq. (3-1) or by setting $A_2=0$ in Eq. (7-22) and substituting the result into Eq. (7-21).

CW-Tone Jamming

Results from the analysis carried out for the FM jamming subcases (M=2) can be directly applied here but rather than

$$A_1 = A_{jr}(t_s-T_b)$$

$$A_2 = A_{jp}(t_s)$$

$$\phi_1 = \phi_{jr} + \Phi_{jr}(t_s-T_b)$$

$$\phi_2 = \phi_{jp} + \Phi_{jp}(t_s-T_b)$$

the definitions

$$A_1 = [A_{jr}(t_s-T_b)]_{cw}$$

$$A_2 = [A_{jp}(t_s)]_{cw}$$

$$\phi_1 = \phi_{jr} + [\Phi_{jr}(t_s-T_b)]_{cw}$$

$$\phi_2 = \phi_{jp} + [\Phi_{jp}(t_s)]_{cw} \qquad (7-25)$$

are required. Again, ϕ_{jr} and ϕ_{jp} are uniformly distributed over the interval $(0,2\pi)$, making ϕ_1 and ϕ_2 also uniformly distributed (modulo - 2π) over the same interval. As a further difference, there is no offset parameter dependence.

The individual subcases are now considered.

JR,JP

Equation (7-17) is directly applicable in this case but with A_1 and A_2 being defined by Eq. (7-25). The error expression becomes

$$P_{BCW}(JR,JP,"0",\phi_1,\phi_2)$$

$$= P_{BFM}(JR,JP,"0",x_r,x_p,\phi_1,\phi_2)\Big|_{\substack{A_1=[A_{jr}(t_s-T_b)]_{cw} \\ A_2=[A_{jp}(t_s)]_{cw}}}$$

$$= \frac{1}{2}\left\{1 - Q\left[\frac{1}{2}\sqrt{\frac{m_1^2+m_2^2}{N}}\ ,\ \frac{1}{2}\sqrt{\frac{m_3^2+m_4^2}{N}}\ \right]\right.$$

$$\left. + Q\left[\frac{1}{2}\sqrt{\frac{m_3^2+m_4^2}{N}}\ ,\ \frac{1}{2}\sqrt{\frac{m_1^2+m_2^2}{N}}\ \right]\right\} \qquad (7\text{-}26)$$

In Eq. (7-26), the relations

$$m_1^2+m_2^2 = 4A_s^2+4A_s(A_1\cos\phi_1+A_2\cos\phi_2)+2A_1A_2\cos(\phi_1-\phi_2)+A_1^2+A_2^2$$

$$m_3^2+m_4^2 = A_1^2+A_2^2-2A_1A_2\cos(\phi_1-\phi_2) \qquad (7\text{-}27)$$

are used. It is again emphasized that the jamming amplitudes in Eq. (7-27) are CW-tone jamming amplitudes and are different from those used throughout the FM analysis.

Interference-plus-noise independence from interval-to-interval eliminates the data dependence, and by averaging over the uniform

phases, the error expression becomes

$$P_{BCW}(JR,JP) = P_{BCW}(JR,JP,"0")$$

$$= \left(\frac{1}{2\pi}\right)^2 \int_0^{2\pi}\int_0^{2\pi} P_{BCW}(JR,JP,"0",\phi_1,\phi_2)d\phi_1 d\phi_2 \qquad (7\text{-}28)$$

where the integrand is defined by Eqs. (7-26) and (7-27).

JR,$\overline{JP}$ or $\overline{JR}$,JP

From Eq. (7-26), the conditional error expression for the $\overline{JR}$,JP subcase is

$$P_{BCW}(\overline{JR},JP,"0",\phi_2) = P_{BCW}(JR,JP,"0",\phi_1,\phi_2)\Big|_{A_1=0}$$

$$= \frac{1}{2}\left\{1 - Q\left[\frac{1}{2}\sqrt{\frac{m_1^2+m_2^2}{N}}\ ,\ \frac{1}{2}\sqrt{\frac{m_3^2+m_4^2}{N}}\right]\right.$$

$$\left. + Q\left[\frac{1}{2}\sqrt{\frac{m_3^2+m_4^2}{N}}\ ,\ \frac{1}{2}\sqrt{\frac{m_1^2+m_2^2}{N}}\right]\right\} \qquad (7\text{-}29)$$

with

$$m_1^2 + m_2^2 = 4A_s + 4A_sA_2\cos\phi_2 + A_2^2$$

$$m_3^2 + m_4^2 = A_2^2 \qquad (7\text{-}30)$$

The data symbol dependence is removed as before and by averaging over the random phase ϕ_2, the probability of error for the $\overline{JR}$,JP (or

$JR,\overline{JP}$) subcase becomes

$$P_{BCW}(\overline{JR},JP) = P_{BCW}(\overline{JR},JP,"0")$$

$$= \frac{1}{2\pi}\int_{o}^{2\pi} P_{BCW}(JR,JP,"0",\phi_2)d\phi_2 \qquad (7\text{-}31)$$

where the integrand is defined by Eqs. (7-29) and (7-30).

$\overline{JR},\overline{JP}$

Only the thermal noise term degrades the system in this case, thus

$$P_{BCW}(\overline{JR},\overline{JP}) = P_{BFM}(\overline{JR},\overline{JP}) = \frac{1}{2}\exp[-\frac{A_s^2}{2N}] \qquad (7\text{-}32)$$

Noise Jamming

Assume a total jamming power of N_j. Since the jammer is operating in only K_s slots, the jamming power per jammed slot is simply N_j/K_s. In Chapter V, it was noted that a noise jammer has its power reduced by the factor S_n (= .902823349530) during the DS correlation process. Hence, the effective noise jamming power per jammed slot becomes S_nN_j/K_s, and the power within the narrowband bandwidth, $S_nN_j\omega_b/(K_s p\omega_p) = N_j'$.

If both signaling intervals are jammed, the total noise power (thermal plus jamming) is $N+N_j'$, while a total noise power of $N+N_j'/2$ is obtained when only one interval is jammed. Therefore, the individual subcases can be considered straightforwardly.

JR,JP

$$P_{BN}(JR,JP) = \frac{1}{2} \exp\left[- \frac{A_s^2}{2(N+N'_j)} \right] \tag{7-33}$$

JR,$\overline{JP}$ or $\overline{JR}$,JP

$$P_{BN}(JR,\overline{JP}) = P_{BN}(\overline{JR},JP)$$

$$= \frac{1}{2} \exp\left[- \frac{A_s^2}{2(N+N'_j/2)} \right] \tag{7-34}$$

$\overline{JR},\overline{JP}$

$$P_{BN}(\overline{JR},\overline{JP}) = \frac{1}{2} \exp\left[- \frac{A_s^2}{2N} \right] \tag{7-35}$$

CHAPTER VIII

PROBABILITY OF ERROR FOR QUATERNARY DPSK

A different analytical technique from that which was used for the binary case will be used here for the quaternary (M=4) case. In general the method involves conditioning on not only x_r, x_p, ϕ_1, and ϕ_2 (where applicable) but also on the phase angle between the signal-plus-reference-interference and the reference signal. This angle is denoted by γ in Figure 10 and has been shown [Appendix G or 16] to have a conditional probability density function of

$$p_{\gamma|\phi_1}(\gamma|\phi_1) = \frac{1}{2\pi}\exp[-\rho]\{1 + \sqrt{\rho\pi}\cos\gamma\exp[\rho\cos^2\gamma]\cdot (1 + \operatorname{erf}[\sqrt{\rho}\cos\gamma])\} \tag{8-1}$$

with

$$\rho = \frac{|\vec{Z}|^2}{2N} = \frac{1}{2N}\{(A_s + A_1\cos\phi_1)^2 + (A_1\sin\phi_1)^2\} \tag{8-2}$$

and where

$$\operatorname{erf}[u] = \frac{2}{\sqrt{\pi}}\int_0^u \exp(-t^2)dt$$

is the well known error function. Without a loss of generality, a "0" may be assumed to be sent. Therefore, the conditional probability of

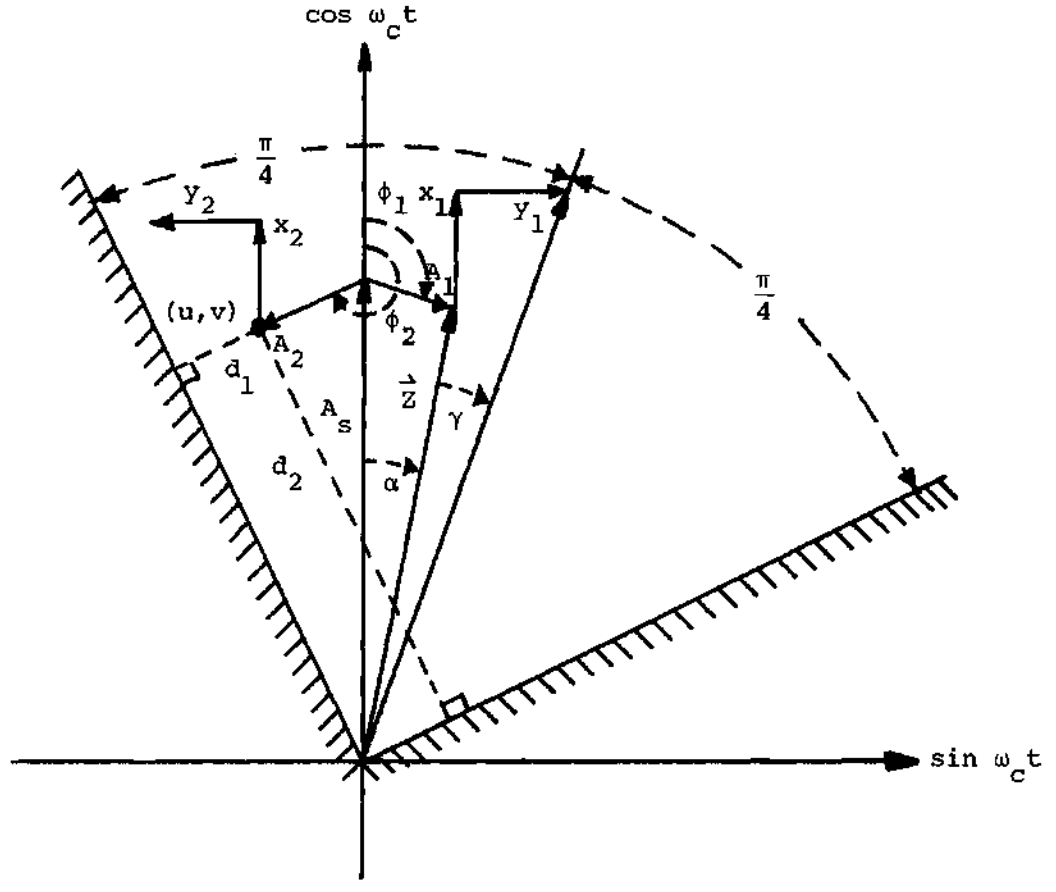

FIGURE 10. Signal, Interference, and Noise Phasors at Adjacent Sampling Times for a Transmitted "0" and M=4

error is the probability that the noise vectors x_2 and y_2 displace the present signal-plus-interference into the error region (outside of the bordered region in Figure 10). The final average probability of error is then obtained by removing all conditioning.

Certain parameters depicted in Figure 10 are important in this chapter and are considered now. Let the tip of the present signal-plus-interference phasor be characterized by the coordinates (u,v), where the coordinate u is the displacement of the tip along the horizontal axis and the coordinate v is the displacement of the tip along the vertical axis. In terms of the signal and interference parameters, these coordinates are

$$u = -A_2\sin(\phi_2-\pi) = A_2\sin\phi_2$$

$$v = A_s - A_2\cos(\phi_2-\pi) = A_s + A_2\cos\phi_2$$

The distance from the origin to the tip of the present signal-plus-interference phasor is defined to be

$$h \triangleq \sqrt{u^2+v^2}$$

Define the angle ξ, not shown in Figure 10, as the angle between the present signal phasor and the present signal-plus-interference phasor. Notice that ξ is related to u, v, and h by

$$\cos\xi = v/h$$

and

$$\sin \xi = u/h$$

Distance d_1 is then equal to

$$d_1 = h \sin[\frac{\pi}{4} - (\alpha+\gamma) + \xi]$$

$$= h\{\sin[\frac{\pi}{4} -\alpha-\gamma]\cos(\xi)+\cos[\frac{\pi}{4}-\alpha-\gamma]\sin(\xi)\}$$

$$= -v \sin[\alpha+\gamma- \frac{\pi}{4}]+u \cos[\alpha+\gamma- \frac{\pi}{4}]$$

$$= -(A_s+A_2\cos\phi_2)\sin[\alpha+\gamma - \frac{\pi}{4}]+(A_2\sin\phi_2)\cos[\alpha+\gamma - \frac{\pi}{4}] \qquad (8\text{-}3)$$

and distance d_2 equal to

$$d_2 = h \cos[\frac{\pi}{4} -(\alpha+\gamma)+\xi]$$

$$= h\{\cos[\frac{\pi}{4}- \alpha-\gamma]\cos(\xi)-\sin[\frac{\pi}{4}- \alpha-\gamma]\sin(\xi)\}$$

$$= v \cos[\frac{\pi}{4}- \alpha-\gamma]-u \sin[\frac{\pi}{4}- \alpha-\gamma]$$

$$= v \sin[\alpha+\gamma + \frac{\pi}{4}]-u \cos[\alpha+\gamma + \frac{\pi}{4}]$$

$$= (A_s+A_2\cos\phi_2)\sin[\alpha+\gamma + \frac{\pi}{4}]-(A_2\sin\phi_2)\cos[\alpha+\gamma + \frac{\pi}{4}] \qquad (8\text{-}4)$$

where it is evident that

$$\alpha = \arctan\left[\frac{A_1 \sin\phi_1}{A_s + A_1 \cos\phi_1}\right] \tag{8-5}$$

These defined quantities will be used extensively throughout this chapter in developing the appropriate probability of error expressions. As in Chapter VII, this chapter is also divided into three sections, each of which depends on the type of jamming signal present: periodic FM jamming; CW-tone jamming; and noise jamming. Each subcase (JR,JP; JR,$\overline{\text{JP}}$; $\overline{\text{JR}}$,JP; $\overline{\text{JR}}$,$\overline{\text{JP}}$) will be individually considered in each section and the corresponding error expression derived. Since the two subcases, (JR,$\overline{\text{JP}}$) and ($\overline{\text{JR}}$,JP), produce identical results, only the ($\overline{\text{JR}}$,JP) subcase is given detailed treatment. Figure 11 is provided for a quick reference guide to the individual sections.

Periodic FM Jamming

The (JR,JP) subcase result will again be used as a basis for developing probability of error expressions for the other FM subcases and the other two jamming signals. Therefore, the (JR,JP) subcase is considered first.

JR,JP

To begin with, the probability of error will be conditioned on the random variables x_r, x_p, ϕ_1, ϕ_2, and γ. Because of their independent orthogonal representation, the noise components x_2 and y_2 may be chosen to be colinear with the perpendicular boundary distances d_1 and d_2, respectively. With this orientation, the conditional probability of error for the (JR,JP) subcase is

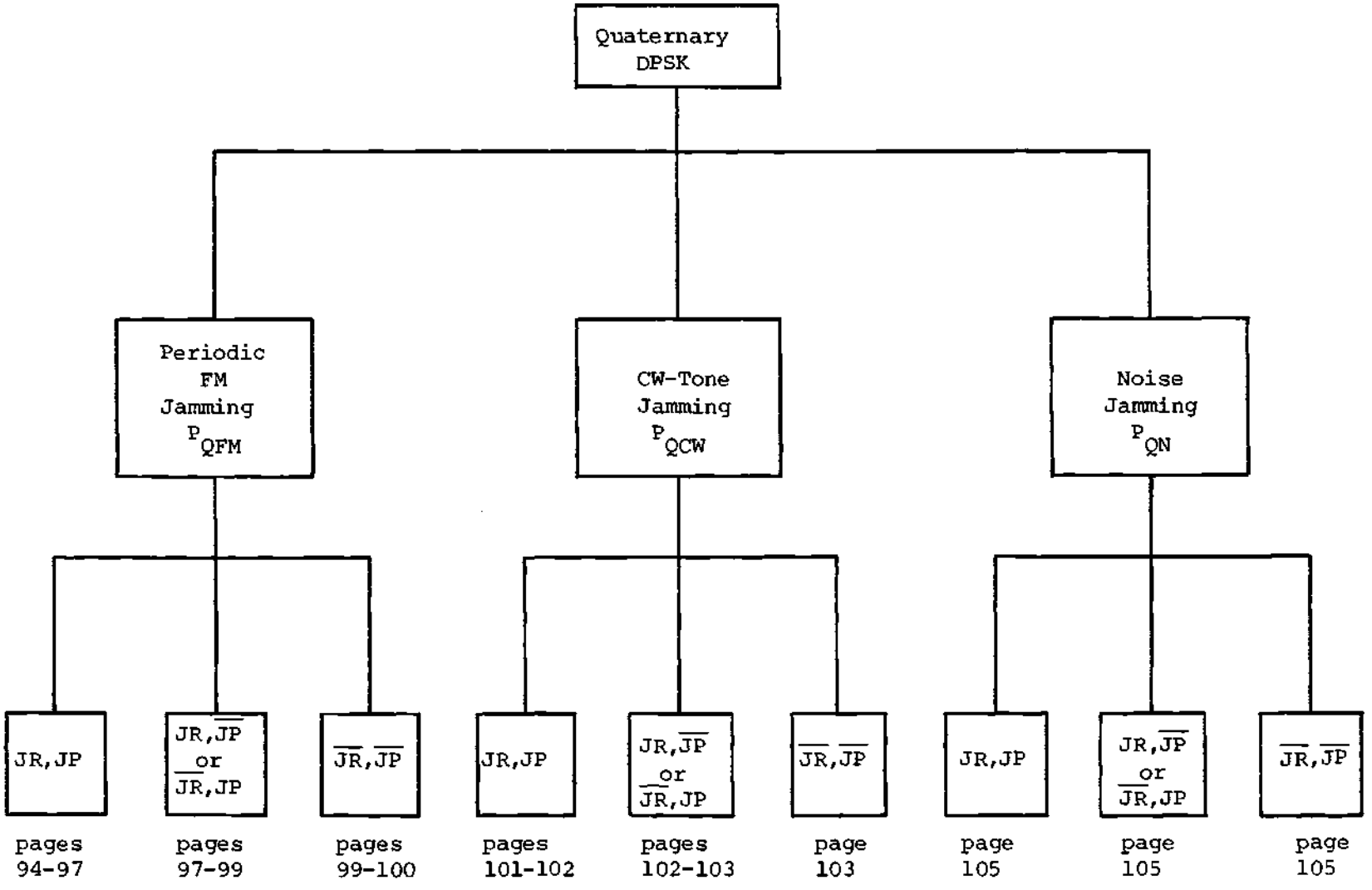

FIGURE 11. Reference Flow Graph for Quaternary DPSK

$$P_{QFM}(JR,JP,"0",x_r,x_p,\phi_1,\phi_2,\gamma)$$

$$= Pr(x_2<-d_2)+Pr(y_2>d_1)-Pr(x_2<-d_2)Pr(y_2>d_1)$$

$$= Pr(x_2>d_2)+Pr(y_2>d_1)-Pr(x_2>d_2)Pr(y_2>d_1)$$

$$= 1 - Pr(x_2\leq d_2) + 1 - Pr(y_2\leq d_1)$$

$$-[1 - Pr(x_2\leq d_2)][1 - Pr(y_2\leq d_1)]$$

$$= 2 - Pr(x_2\leq d_2)-Pr(y_2\leq d_1)$$

$$-[1 - Pr(x_2\leq d_2)][1 - Pr(y_2\leq d_1)]$$

$$= 1 - Pr(x_2\leq d_2)Pr(y_2\leq d_1)$$

$$= 1 - \frac{1}{4}\left\{1 + \text{erf}\left[\frac{d_2}{\sqrt{2N}}\right]\right\}\left\{1 + \text{erf}\left[\frac{d_1}{\sqrt{2N}}\right]\right\} \qquad (8\text{-}6)$$

Equation (8-6) may be further manipulated with the help of the complementary error function identity

$$\text{erfc}[u] = 1 - \text{erf}[u]$$

to obtain

$$P_{QFM}(JR,JP,"0",x_r,x_p,\phi_1,\phi_2,\gamma)$$

$$= \frac{1}{2}\,\text{erfc}\left[\frac{d_1}{\sqrt{2N}}\right] + \frac{1}{2}\,\text{erfc}\left[\frac{d_2}{\sqrt{2N}}\right] - \frac{1}{4}\,\text{erfc}\left[\frac{d_1}{\sqrt{2N}}\right]\text{erfc}\left[\frac{d_2}{\sqrt{2N}}\right] \qquad (8\text{-}7)$$

where

$$d_1 = -(A_s+A_2\cos\phi_2)\sin[\alpha+\gamma-\tfrac{\pi}{4}]+(A_2\sin\phi_2)\cos[\alpha+\gamma-\tfrac{\pi}{4}]$$

$$d_2 = (A_s+A_2\cos\phi_2)\sin[\alpha+\gamma+\tfrac{\pi}{4}]-(A_2\sin\phi_2)\cos[\alpha+\gamma+\tfrac{\pi}{4}] \qquad (8\text{-}8)$$

The conditioning may now be removed by averaging over the parameters x_r, x_p, ϕ_1, ϕ_2, and γ. The result is

$$P_{QFM}(JR,JP,"0")$$

$$= (\tfrac{1}{2\pi})^4 \int_0^{2\pi}\int_0^{2\pi}\int_0^{2\pi}\int_0^{2\pi} d\phi_1 d\phi_2 dx_r dx_p \int_{-\pi}^{\pi} P_{QFM}(JR,JP,"0",x_r,x_p,\phi_1,\phi_2,\gamma) \cdot$$

$$P_{\gamma|\phi_1}(\gamma|\phi_1)d\gamma \qquad (8\text{-}9)$$

where the integrand of the innermost integral is the product of Eqs. (8-1) and (8-7). Equation (8-9) will be greatly simplified in Chapter X.

The data symbol dependence is removed by noting that the noise-plus-interference is independent from interval-to-interval. Thus,

$$P_{QFM}(JR,JP) = P_{QFM}(JR,JP,"0") \qquad (8\text{-}10)$$

<u>$(JR,\overline{JP})$ or $(\overline{JR},JP)$</u>

Equations (8-7) and (8-8) are directly applicable here but with $A_1=0$, which yields an expression that is independent of x_r and ϕ_1. In other words

$$P_{QFM}(\overline{JR},JP,"0",x_p,\phi_2,\gamma)$$

$$= P_{QFM}(JR,JP,"0",x_r,x_p,\phi_1,\phi_2,\gamma)\Big|_{A_1=0}$$

$$= \frac{1}{2}\,\mathrm{erfc}\left[\frac{d_1}{\sqrt{2N}}\right] + \frac{1}{2}\,\mathrm{erfc}\left[\frac{d_2}{\sqrt{2N}}\right] - \frac{1}{4}\,\mathrm{erfc}\left[\frac{d_1}{\sqrt{2N}}\right]\mathrm{erfc}\left[\frac{d_2}{\sqrt{2N}}\right] \qquad (8\text{-}11)$$

For this subcase, $\alpha=0$ so that

$$d_1 = -(A_s+A_2\cos\phi_2)\sin[\gamma-\tfrac{\pi}{4}]+(A_2\sin\phi_2)\cos[\gamma-\tfrac{\pi}{4}]$$

$$d_2 = (A_s+A_2\cos\phi_2)\sin[\gamma+\tfrac{\pi}{4}]-(A_2\sin\phi_2)\cos[\gamma+\tfrac{\pi}{4}] \qquad (8\text{-}12)$$

The noise-plus-interference is again adjacent-interval-independent so that

$$P_{QFM}(\overline{JR},JP) = P_{QFM}(JR,\overline{JP})$$

$$= P_{QFM}(\overline{JR},JP,"0")$$

$$= \left(\frac{1}{2\pi}\right)^2 \int_0^{2\pi}\int_0^{2\pi} dx_p\,d\phi_2 \int_{-\pi}^{\pi} P_{QFM}(\overline{JR},JP,"0",x_p,\phi_2,\gamma)\,p_{\gamma|\phi_1}(\gamma|\phi_1)\,d\gamma \qquad (8\text{-}13)$$

where the integrand of the innermost integral is the product of the functions defined in Eqs. (8-1) and (8-11). In this situation though, Eq. (8-2) becomes

$$\rho = \frac{A_s^2}{2N}$$

Again, Chapter X will provide a reduction in the complexity of Eq. (8-13).

$\overline{JR},\overline{JP}$

Neither interval is jammed in this subcase, thus requiring

$$A_1 = A_2 = 0$$

and hence eliminating any dependence of the error expressions on x_r, x_p, ϕ_1, or ϕ_2. From Eqs. (8-7) and (8-8),

$$P_{QFM}(\overline{JR},\overline{JP}) = \int_{-\pi}^{\pi} P_{QFM}(JR,JP,"0",x_r,x_p,\phi_1,\phi_2,\gamma) \Big|_{\substack{A_1=0\\A_2=0}} p_{\gamma|\phi_1}(\gamma|\phi_1)\,d\gamma \qquad (8\text{-}14)$$

where

$$P_{QFM}(\overline{JR},\overline{JP},"0") = P_{QFM}(JR,JP,"0",x_r,x_p,\phi_1,\phi_2,\gamma) \Big|_{\substack{A_1=0\\A_2=0}}$$

$$= \frac{1}{2}\,\mathrm{erfc}\left[\frac{d_1}{\sqrt{2N}}\right] + \frac{1}{2}\,\mathrm{erfc}\left[\frac{d_2}{\sqrt{2N}}\right] - \frac{1}{4}\,\mathrm{erfc}\left[\frac{d_1}{\sqrt{2N}}\right]\mathrm{erfc}\left[\frac{d_2}{\sqrt{2N}}\right] \qquad (8\text{-}15)$$

with

$$d_1 = -A_s \sin\left[\gamma - \frac{\pi}{4}\right]$$

$$d_2 = A_s \sin\left[\gamma + \frac{\pi}{4}\right] \qquad (8\text{-}16)$$

The function $p_{\gamma|\phi_1}(\gamma|\phi_1)$ is defined in Eq. (8-1) but here

$$\rho = \frac{A_s^2}{2N}$$

CW-Tone Jamming

A direct application of the results from the FM jamming section (M=4) is possible here since a CW-tone signal is a specialized FM signal. It must be pointed out that although the parameters A_1, A_2, ϕ_1, ϕ_2 are used in this section, their definitions are different from those used in the FM section. In fact,

$$\begin{aligned} A_1 &= [A_{jr}(t_s - T_b)]_{cw} \\ A_2 &= [A_{jp}(t_s)]_{cw} \\ \phi_1 &= \phi_{jr} + [\Phi_{jr}(t_s - T_b)]_{cw} \\ \phi_2 &= \phi_{jp} + [\Phi_{jp}(t_s)]_{cw} \end{aligned} \tag{8-17}$$

The parameters ϕ_1 and ϕ_2 do remain uniformly distributed over the interval $(0,2\pi)$ despite the new definitions.

Any results from the FM jamming section which are used here must reflect the functional independence the CW-tone expressions exhibit in regards to the offset parameters. This is due to the fact that an offset parameter affects only an FM jamming signal.

The individual subcases are now considered.

JR,JP

Equation (8-7) is directly applicable for this subcase but with the proper modifications set forth by Eq. (8-17). The conditional error expression becomes

$$P_{QCW}(JR,JP,"0",\phi_1,\phi_2,\gamma)$$

$$= P_{QFM}(JR,JP,"0",x_r,x_p,\phi_1,\phi_2,\gamma)\Big|_{\substack{A_1 = [A_{jr}(t_s-T_b)]_{cw} \\ A_2 = [A_{jp}(t_s)]_{cw}}}$$

$$= \frac{1}{2}\,\mathrm{erfc}\left[\frac{d_1}{\sqrt{2N}}\right] + \frac{1}{2}\,\mathrm{erfc}\left[\frac{d_2}{\sqrt{2N}}\right] - \frac{1}{4}\,\mathrm{erfc}\left[\frac{d_1}{\sqrt{2N}}\right]\mathrm{erfc}\left[\frac{d_2}{\sqrt{2N}}\right] \tag{8-18}$$

The distances d_1 and d_2 are defined in Eq. (8-8) but with A_1 and A_2 modified according to Eq. (8-17). For completeness, the distances are

$$d_1 = -(A_s+A_2\cos\phi_2)\sin[\alpha+\gamma-\tfrac{\pi}{4}] + (A_2\sin\phi_2)\cos[\alpha+\gamma-\tfrac{\pi}{4}]$$

$$d_2 = (A_s+A_2\cos\phi_2)\sin[\alpha+\gamma+\tfrac{\pi}{4}] - (A_2\sin\phi_2)\cos[\alpha+\gamma+\tfrac{\pi}{4}] \tag{8-19}$$

Ultimately, the unconditional error expression becomes

$$P_{QCW}(JR,JP) = P_{QCW}(JR,JP,"0")$$

$$= \left(\frac{1}{2\pi}\right)^2 \int_0^{2\pi}\int_0^{2\pi} d\phi_1 d\phi_2 \int_{-\pi}^{\pi} P_{QCW}(JR,JP,"0",\phi_1,\phi_2,\gamma)\,p_{\gamma|\phi_1}(\gamma|\phi_1)\,d\gamma \tag{8-20}$$

where the innermost integrand is defined by the product of Eqs. (8-1) and (8-18).

JR,$\overline{JP}$ or $\overline{JR}$,JP

For the $\overline{JR}$,JP subcase, there is no jamming signal in the reference interval, hence $A_1=0$. With this fact, the distances of Eq. (8-19) are

$$d_1 = -(A_s+A_2\cos\phi_2)\sin[\gamma - \tfrac{\pi}{4}] + (A_2\sin\phi_2)\cos[\gamma - \tfrac{\pi}{4}]$$

$$d_2 = (A_s+A_2\cos\phi_2)\sin[\gamma + \tfrac{\pi}{4}] - (A_2\sin\phi_2)\cos[\gamma + \tfrac{\pi}{4}] \qquad (8\text{-}21)$$

and the error expression becomes

$$P_{QCW}(\overline{JR},JP,"0",\phi_2,\gamma) = P_{QCW}(JR,JP,"0",\phi_1,\phi_2,\gamma)\Big|_{A_1=0}$$

$$= \frac{1}{2}\operatorname{erfc}\left[\frac{d_1}{\sqrt{2N}}\right] + \frac{1}{2}\operatorname{erfc}\left[\frac{d_2}{\sqrt{2N}}\right] - \frac{1}{4}\operatorname{erfc}\left[\frac{d_1}{\sqrt{2N}}\right]\operatorname{erfc}\left[\frac{d_2}{\sqrt{2N}}\right] \qquad (8\text{-}22)$$

Equations (8-1) and (8-22) may now be used in conjunction with the data independence to produce

$$P_{QCW}(\overline{JR},JP) = P_{QCW}(\overline{JR},JP,"0")$$

$$= \frac{1}{2\pi}\int_0^{2\pi} d\phi_2 \int_{-\pi}^{\pi} P_{QCW}(\overline{JR},JP,"0",\phi_2,\gamma)P_{\gamma|\phi_1}(\gamma|\phi_1)d\gamma \qquad (8\text{-}23)$$

where the parameter ρ in Eq. (8-2) is required to be

$$\rho = \frac{A_s^2}{2N}$$

$\overline{JR},\overline{JP}$

Since $A_1 = A_2 = 0$, then

$$P_{QCW}(\overline{JR},\overline{JP}) = P_{QFM}(\overline{JR},\overline{JP}) \tag{8-24}$$

where $P_{QFM}(\overline{JR},\overline{JP})$ is defined in Eqs. (8-14) ~ (8-16).

Noise Jamming

The effective jamming power immediately following the joint process of DS correlation and narrowband filtering (IF_2) is $N_j' = N_j S_n \omega_b/(K_s p \omega_p)$, where N_j is the total jamming power and S_n is the reduction factor introduced by the correlation process. This jamming power will simply add to the thermal noise power N. The results from the quaternary, $FM(\overline{JR},\overline{JP})$ subcase may be used here. Care must be exercised as to which interval the jamming power is located, for the parameter

$$\rho = \frac{A_s^2}{2N}$$

and the function

$$P(\gamma) \triangleq \frac{1}{2}\,\mathrm{erfc}\left[\frac{d_1}{\sqrt{2N}}\right] + \frac{1}{2}\,\mathrm{erfc}\left[\frac{d_2}{\sqrt{2N}}\right] - \frac{1}{4}\,\mathrm{erfc}\left[\frac{d_1}{\sqrt{2N}}\right]\mathrm{erfc}\left[\frac{d_2}{\sqrt{2N}}\right] \tag{8-25}$$

change accordingly. The dependence of $P(\gamma)$ on γ is implicitly contained in d_1 and d_2 where

$$d_1 = -A_s \sin[\gamma - \frac{\pi}{4}]$$

$$d_2 = A_s \sin[\gamma + \frac{\pi}{4}]$$

If the jamming signal were present in the reference interval, then

$$\rho_1 \triangleq \rho \Big|_{N \to N+N'_j} = \frac{A_s^2}{2(N+N'_j)}$$

and

$$P_1(\gamma) \triangleq P(\gamma) \quad .$$

On the other hand,

$$\rho_2 \triangleq \rho = \frac{A_s^2}{2N}$$

and

$$P_2(\gamma) \triangleq P(\gamma) \Big|_{N \to N+N'_j}$$

when the present interval is jammed.

The results for the individual subcases may be written directly from the above discussion and are considered now. In all subcases, $p_{\gamma|\phi_1}(\gamma|\phi_1)$ is defined in Eq. (8-1).

JR,JP

$$P_{QN}(JR,JP) = \int_{-\pi}^{\pi} P_2(\gamma) p_{\gamma|\phi_1}(\gamma|\phi_1)\, d\gamma \tag{8-26}$$

with $\rho=\rho_1$.

JR,$\overline{JP}$ or $\overline{JR}$,JP

$$P_{QN}(JR,\overline{JP}) = P_{QN}(\overline{JR},JP)$$

$$= \int_{-\pi}^{\pi} P_2(\gamma) p_{\gamma|\phi_1}(\gamma|\phi_1)\, d\gamma \tag{8-27}$$

with $\rho=\rho_2$.

$\overline{JR},\overline{JP}$

$$P_{QN}(\overline{JR},\overline{JP}) = \int_{-\pi}^{\pi} P_1(\gamma) p_{\gamma|\phi_1}(\gamma|\phi_1)\, d\gamma \tag{8-28}$$

with $\rho=\rho_2$.

Notice that

$$P_{QN}(\overline{JR},\overline{JP}) = P_{QCW}(\overline{JR},\overline{JP}) = P_{QFM}(\overline{JR},\overline{JP})$$

CHAPTER IX

PROBABILITY OF ERROR FOR M-ARY DPSK

Because of the complexity which the general M-ary analysis introduced for arbitrary M, lower and upper bounds for M>4 are useful as alternate solutions. Developing such bounds is clearly not new to the error analysis of digital communication systems and is, in fact, an established research area [55]. The key to any bounding technique is the accuracy to which the bound(s) approximate the actual probability of error. With both upper and lower bounds calculated, this accuracy is known immediately. The bounds developed here are shown to have an increasing accuracy as the signal-to-noise ratio, signal-to-jamming ratio, or M, either separately or simultaneously increase. The generalities of the bounds are now presented, followed immediately by the specifics for the individual subcases of each jamming signal.

Upper and Lower Bounds

The upper bound will be henceforth denoted as

$$P^{u}(\text{err}) > \Pr(\text{err})$$

and when conditioned momentarily on the offset parameters x_r and x_p (for the most general jamming signal) as

$$P^{u}(\text{err}|x_r,x_p) > \Pr(\text{err}|x_r,x_p)$$

The offset parameter conditioning produces what is referred to as circularly symmetric interference. Circular symmetry implies that the interference envelope and phase at any one time be independent and that the probability density function of the phase be uniform over $(0,2\pi)$. The circular symmetry is certainly applicable here because the envelopes, $A_{jp}(t)$ and $A_{jr}(t)$, and the phases, $\Phi_{jp}(t)$ and $\Phi_{jr}(t)$ are constant at any one time when conditioned on the offset parameters. The overall jamming phases at this time

$$\phi_{jp} + \Phi_{jp}(t_s)$$

and

$$\phi_{jr} + \Phi_{jr}(t_s - T_b)$$

are both uniformly distributed (modulo-2π) over the interval $(0,2\pi)$, and independent of the respective envelopes, $A_{jp}(t_s)$ and $A_{jr}(t_s-T_b)$. Hence the conditional interference must be circularly symmetric. Furthermore, the conditional interference-plus-noise (noise alone is circularly symmetric [52]) is an overall, circularly symmetric signal. This is the result in which the sum of independent, circularly symmetric random variables yields a circularly symmetric random variable [52].

Consider Figure 12, where the line labeled reference (REF) is the interference-plus-noise corrupted signal from the previous signaling interval. The specific noise and interference components for the

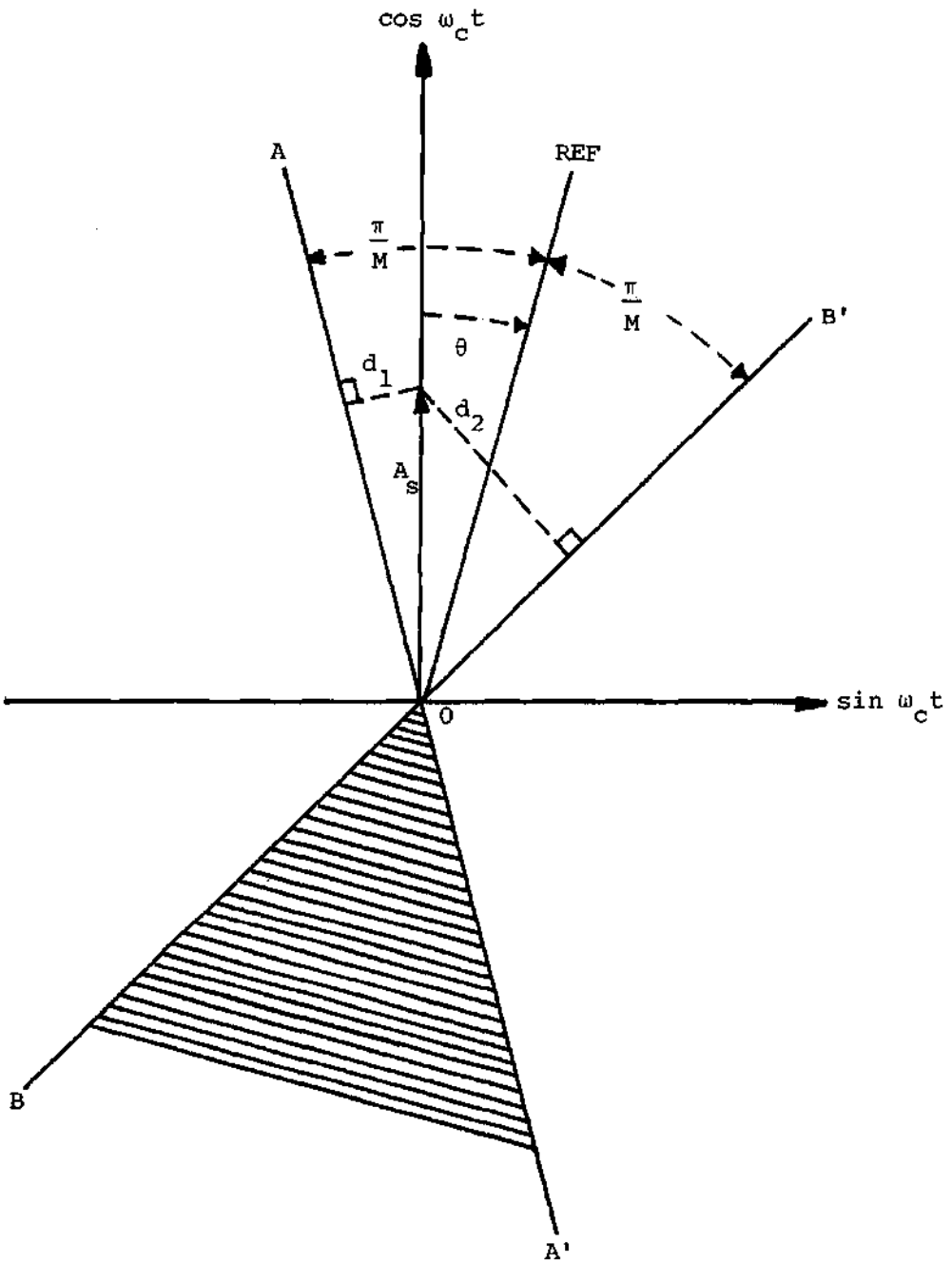

FIGURE 12. Nondetailed, Double-Exposure Phasor Diagram Depicting the Shaded Region (BOA')

reference have been eliminated in this figure for simplicity. In addition, assume without a loss of generality that the next data symbol is a "0". From Figure 12, two distances may be defined. These are

$$d_1 = A_s\cos(\theta+\theta_c) \tag{9-1}$$

and

$$d_2 = A_s\cos(\theta-\theta_c) \tag{9-2}$$

where

$$\theta_c \triangleq \frac{\pi}{2} - \frac{\pi}{M}$$

Because of the circularly symmetric interference-plus-noise, the conditional probability of error is dependent only upon the distances d_1 and d_2 rather than the orientation of the reference, and consequently the orientation of the decision boundaries. With this in mind, the union bound may be invoked to yield

$$\begin{aligned} P^u(\text{err}\,|\,\text{"0"},\theta,x_r,x_p) &= P_p[d_1] + P_p[d_2] \\ &= P_p[A_s\cos(\theta+\theta_c)] \\ &\quad + P_p[A_s\cos(\theta-\theta_c)] \end{aligned} \tag{9-3}$$

where $P_p[\lambda]$ is the so-called half-plane probability function [22] for

the present signal and is defined for $\lambda>0$ to be the probability that the interference-plus-noise phasor lies in the half-plane located a distance of λ from the mean of the phasor. For $\lambda<0$, the half-plane probability function is defined to be the probability that the interference-plus-noise phasor lies in the half-plane containing the mean of the phasor. With the addition of the two terms in Eq. (9-3), an upper bound to the true conditional probability of error is obtained because the shaded, error region (bounded by B'OA') in Figure 12 is added in twice. Notice that as M increases, the shaded region becomes smaller and the bound tighter.

The properties of the half-plane probability function are [22]

$$\lim_{\lambda\to\infty} P_p[\lambda] = 0$$

$$\lim_{\lambda\to-\infty} P_p[\lambda] = 1$$

$$P_p[0] = \frac{1}{2}$$

$$P_p[\lambda] + P_p[-\lambda] = 1 \tag{9-4}$$

With the θ dependence averaged out, Eq. (9-3) becomes

$$P^u(\text{err}|\text{"0"},x_r,x_p) = \int_{-\pi}^{\pi} p_\theta(\theta)\{P_p[A_s\cos(\theta+\theta_c)] + P_p[A_s\cos(\theta-\theta_c)]\}d\theta \tag{9-5}$$

where $p_\theta(\theta)$ is the probability density function of the random phase θ.

In order to circumvent the required knowledge of $p_\theta(\theta)$, Rosenbaum [22] has shown (the steps are repeated in Appendix H) that an equivalent expression is

$$P^u(\text{err}|\text{"0"},x_r,x_p) = 2\,P_r[A_s] - 2A_s\int_o^{\pi/2} P_r'[A_s\sin\theta]\{P_p[A_s\cos(\theta+\theta_c)]+P_p[A_s\cos(\theta-\theta_c)]\}\cos\theta d\theta \quad (9\text{-}6)$$

where $P_r[\lambda]$ is the half-plane probability function defined for the reference signal and $P_r'[\lambda]$ is the first derivative of $P_r[\lambda]$ with respect to λ. The dependence of Eq. (9-6) on the variables x_r and x_p is an implicit dependence at this point and will remain so for the time being.

To obtain the true upper bound, Eq. (9-5) must be averaged over the conditional variables, resulting in

$$P^u(\text{err}) = \left(\frac{1}{2\pi}\right)^2 \int_o^{2\pi}\int_o^{2\pi} P^u(\text{err}|\text{"0"},x_r,x_p)dx_r dx_p \quad (9\text{-}7)$$

where the interference-plus-noise independence has been used to eliminate the conditioning on "0". The final step in evaluating Eq. (9-7) is to determine the present and reference half-plane probabilities. This step is best accomplished on an individual subcase basis and is done so immediately following the general discussion of the lower bound.

With the upper bound firmly established in Eq. (9-7), it is appropriate to develop the lower bound at this time. At first a trivial lower bound is presented and then the steps leading to a tighter bound are developed. In both instances, the upper bound previously determined

will be used extensively. Therefore only its notation will be used and any offset parameter conditioning or averaging will be assumed to have been completed prior to its use here.

It is evident from Figure 12 that a trivial lower bound would be

$$P^{\ell}(\text{err}) = \frac{1}{2} P^{u}(\text{err}) < \Pr(\text{err}) \tag{9-8}$$

Due to its computational simplicity (at least once the upper bound is known), this lower bound is rather attractive. However, the constant 50% deviation from the upper bound may not be suitable for many applications requiring more accurate approximations. A closer look at Figure 12 will provide a much tighter lower bound.

For simplicity, consider the M=4 case and the familiar diagram illustrated in Figure 13. Figure 13 is a slightly modified version of Figure 12 in that certain regions (U,V,W,X,Y,Z) have been specified. From Figure 13, it can be seen that

$$\begin{aligned}\Pr(\text{err}) = {} & \Pr(U) + \Pr(V) + \Pr(W) + \\ & \Pr(X) + \Pr(Y) + \Pr(Z)\end{aligned} \tag{9-9}$$

and

$$\begin{aligned}P^{u}(\text{err}\,|\,\text{"0"}) = {} & \Pr(U) + \Pr(V) + \Pr(Y) + \Pr(Z) \\ & + 2[\Pr(W) + \Pr(X)]\end{aligned} \tag{9-10}$$

where Pr(i) is the probability that the signal-plus-interference-plus

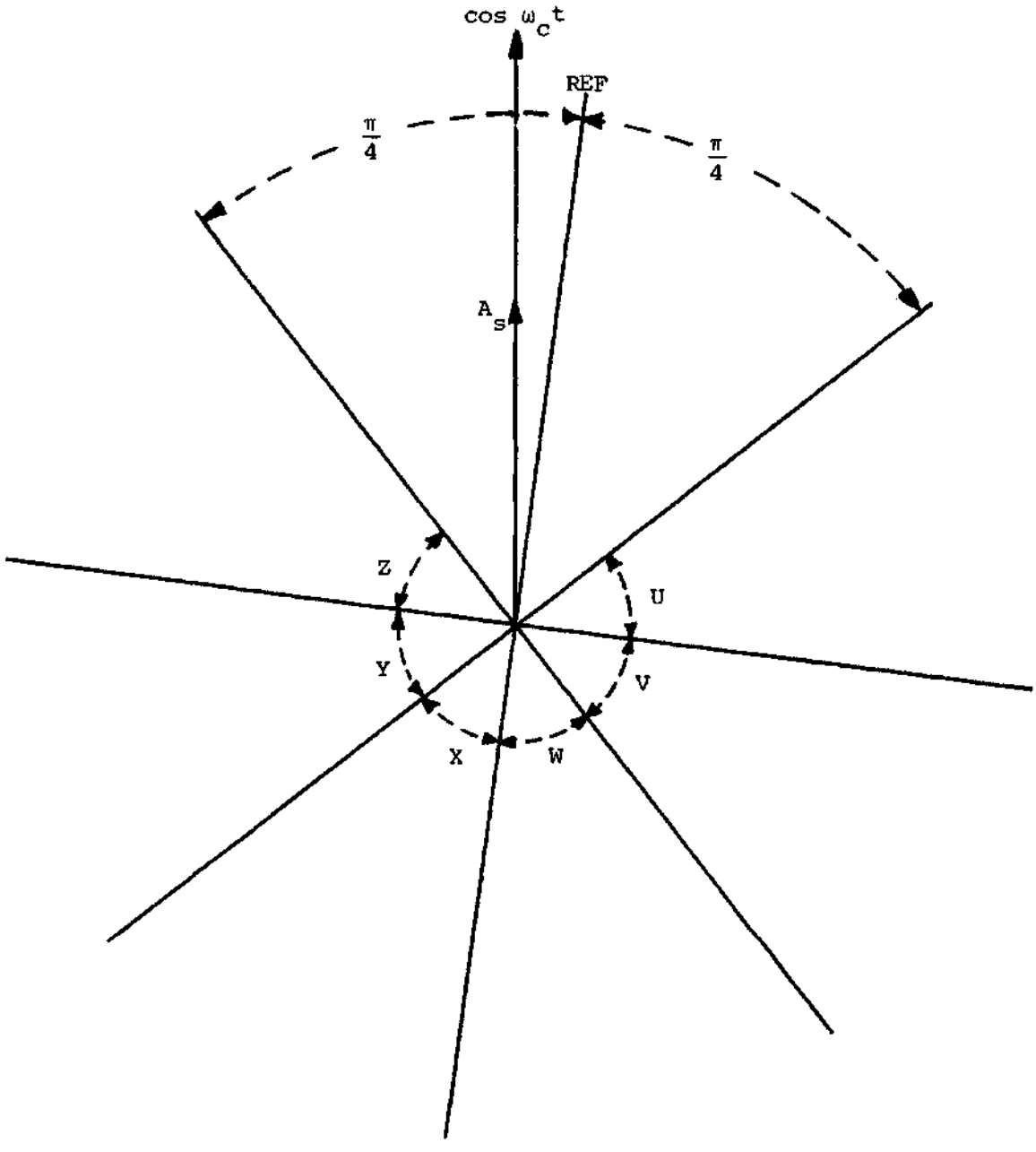

FIGURE 13. Double-Exposure Phasor Diagram Depicting the Regions Required in the Lower Bound Derivation

noise falls in region i.

Consider the probability

$$P^{u}(\text{err}|\text{"0"}) - \frac{1}{2}[Pr(V) + Pr(W) + Pr(X) + Pr(Y)] \tag{9-11}$$

On the average, it is known (see Appendix I) that

$$Pr(V) = Pr(Y)$$

$$Pr(W) = Pr(X)$$

thereby transforming Eq. (9-11) into

$$P^{u}(\text{err}|\text{"0"}) - Pr(V) - Pr(W) \tag{9-12}$$

Substitute Eq. (9-10) into Eq. (9-12) and obtain

$$Pr(U) + Pr(Y) + Pr(Z) + Pr(W) + 2Pr(X) \tag{9-13}$$

Notice that the only region left out of the quantity in Eq. (9-13) is the region V. Since the region V (or Y) is closer to the error-free region, it is much more likely to contain the corrupted signal than is region X. Therefore,

$$Pr(V) > Pr(X)$$

and

$$P^{u}(\text{err}|\text{"0"}) = \frac{1}{2}[Pr(V) + Pr(W) + Pr(X) + Pr(Y)]$$

$$= Pr(U) + Pr(Y) + Pr(Z) + Pr(W) + 2Pr(X)$$

$$< Pr(U) + Pr(V) + Pr(W) + Pr(X) + Pr(Y) + Pr(Z)$$

$$= Pr(\text{err}|\text{"0"}) \qquad (9\text{-}14)$$

In other words, the sought after lower bound is

$$P^{\ell}(\text{err}|\text{"0"}) = P^{u}(\text{err}|\text{"0"}) - \frac{1}{2}[Pr(V) + Pr(W) + Pr(X) + Pr(Y)] \qquad (9\text{-}15)$$

It is apparent from Figure 13 that the term

$$Pr(V) + Pr(W) + Pr(X) + Pr(Y)$$

is simply the error probability for the binary case. Thus

$$P^{\ell}(\text{err}|\text{"0"}) + P^{u}(\text{err}|\text{"0"}) - \frac{1}{2} P_{B}(\text{err}|\text{"0"}) \qquad (9\text{-}16)$$

where $P_{B}(\text{err}|\text{"0"})$ is the binary error probability for any of the subcases in Chapter VII.

The above analysis for M=4 is straightforwardly extended (see Appendix J) to the arbitrary M (even) case and is found to be

$$P^{\ell}(\text{err}|\text{"0"}) = P^{u}(\text{err}|\text{"0"}) - \frac{2}{M} P_B(\text{err}|\text{"0"}) \tag{9-17}$$

After the data symbol dependence is removed, the lower bound becomes

$$\begin{aligned} P^{\ell}(\text{err}) &= P^{\ell}(\text{err}|\text{"0"}) \\ &= P^{u}(\text{err}) - \frac{2}{M} P_B(\text{err}) \end{aligned} \tag{9-18}$$

From Eq. (9-18) it is seen that as M increases, $\frac{2}{M} P_B(\text{err})$ becomes smaller and the bounds more accurate. Furthermore, as the signal-to-noise or signal-to-jamming ratios become larger, $P_B(\text{err})$ gets smaller, and, again the bounds more accurate.

In summary and with Eqs. (9-7) and (9-18), the actual probability of error is bounded by

$$P^{\ell}(\text{err}) = P^{u}(\text{err}) - \frac{2}{M} P_B(\text{err}) < Pr(\text{err}) < P^{u}(\text{err}) \tag{9-19}$$

It is now time to calculate the lower and upper bounds for the individual subcases of all three jamming signals. Since the binary error probability required for the lower bound has already been determined (Chapter VII), the remaining quantity needed by both bounds is the upper bound. Therefore, the analysis henceforth is concerned with the determination of the upper bound for each of the subcases. However, as Eqs. (9-6) and (9-7) indicate, the actual task is to derive the reference and present half-plane probability functions. Once these functions are known for each subcase, the upper bound expression is

simultaneously known.

The remainder of this chapter deals with the determination of the half-plane probabilities and is organized in an identical manner as Chapters VII and VIII. Figure 14 is provided as a quick reference guide to the individual subcases.

Periodic FM Jamming

The determination of $P_r[\lambda]$ and $P_p[\lambda]$ for each of the individual subcases follows a very definite analytical path. First, the circular symmetry assumption is used to rotate lines BB' or AA' around the tip of the desired signal phasor until they are parallel with the inphase ($\cos\omega_c t$) or quadrature-phase ($\sin\omega_c t$) axes. This enables the analysis to eliminate either the inphase or quadrature-phase interference-plus-noise because of its irrelevance. Secondly, the half-plane probability functions are conditioned on the phases ϕ_1 or ϕ_2, respectively depending on whether the reference or present probability function is being sought. The third step involves calculating the probability that the interference-plus-noise is greater than some quantity, designated for the time being as λ. Finally, the functions are averaged over the appropriate phase to produce either $P_r[\lambda]$ or $P_p[\lambda]$. It is also mandatory that the half-plane probabilities be conditioned on x_r or x_p. However, the conditioning notation is temporarily suppressed when determining $P_r[\lambda]$ and $P_p[\lambda]$, and will resurface at the appropriate time.

JR,JP

Without a loss in generality, the line AA' is rotated to be parallel with the inphase axis. The ϕ_2-conditioned half-plane

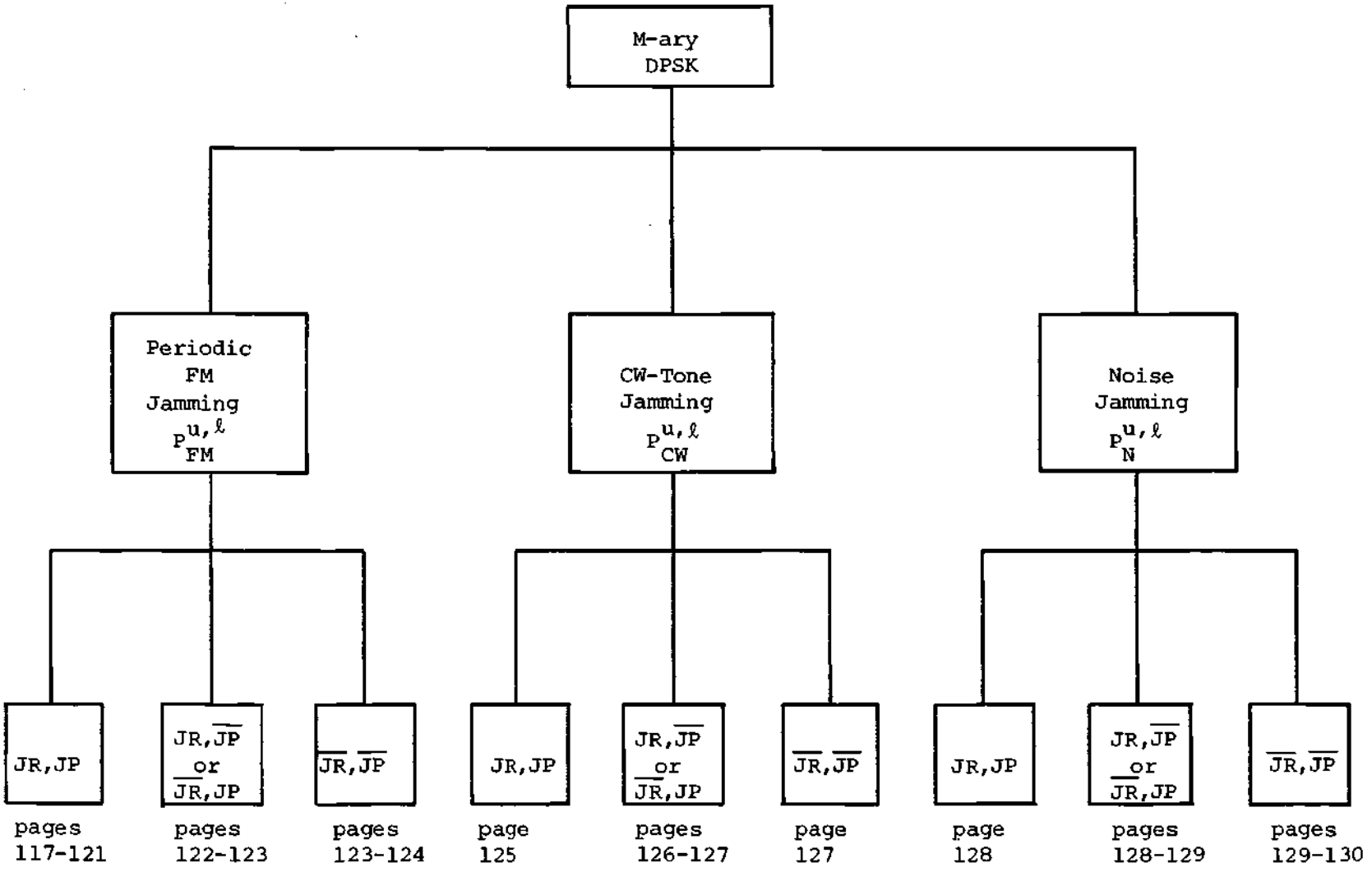

FIGURE 14. Reference Flow Graph for M-ary DPSK

probability function for the present signaling interval is

$$P_p[JR,JP,\phi_2,\lambda] \triangleq P_p[\lambda|\phi_2,JR,JP]$$

$$= Pr(y_2 + A_2\sin\phi_2 > \lambda|\phi_2,JR,JP) \qquad (9\text{-}20)$$

where y_2, as defined in Chapter VI, is a zero mean, gaussian random variable with a variance of N. Since y_2 is the only random quantity in the conditioned event

$$y_2 + A_2\sin\phi_2 > \lambda$$

Eq. (9-20) becomes

$$P_p[JR,JP,\phi_2,\lambda] = Pr(y_2 > \lambda - A_2\sin\phi_2|\phi_2,JR,JP)$$

$$= \frac{1}{2}\,\mathrm{erfc}\left[\frac{1}{\sqrt{2N}}\,(\lambda - A_2\sin\phi_2)\right] \qquad (9\text{-}21)$$

The ϕ_2-conditioning is removed by taking the statistical expectation with respect to ϕ_2. The result is

$$P_p[JR,JP,\lambda] = E_{\phi_2}\left\{\frac{1}{2}\,\mathrm{erfc}\left[\frac{1}{\sqrt{2N}}\,(\lambda - A_2\sin\phi_2)\right]\right\}$$

$$= \frac{1}{4\pi}\int_0^{2\pi}\mathrm{erfc}\left[\frac{1}{\sqrt{2N}}\,(\lambda - A_2\sin\phi_2)\right]d\phi_2$$

$$= \frac{1}{2\pi}\int_{-\pi/2}^{\pi/2}\mathrm{erfc}\left[\frac{1}{\sqrt{2N}}\,(\lambda - A_2\sin\phi_2)\right]d\phi_2 \qquad (9\text{-}22)$$

Though different in its application, Eq. (9-22) is identical to a result obtained by Rosenbaum [22]. In that case, Eq. (9-22) was evaluated by expanding $\text{erfc}[x + f(\phi_2)]$ in a Taylor series about the point x and the expectation performed term-by-term. By evaluating the expectation in this manner an integration had been eliminated. Unfortunately, the price that was paid was the restrictions imposed on the values $\lambda/\sqrt{2N}$ ($\lambda \sim A_s$) and $A_2/\sqrt{2N}$. Without the appropriate restrictions, the Taylor series had problems of converging to the correct value. The incorrectness was due to the large values which some of the series terms reached, resulting in intolerable, large round-off errors. Based on these parameter restrictions for the series method, the integration in Eq. (9-22) is retained.

The reference signaling interval has a half-plane probability function that is similarly determined to be (rotate line BB')

$$P_r[JR,JP,\lambda] = \frac{1}{2\pi}\int_{-\pi/2}^{\pi/2} \text{erfc}\left[\frac{1}{\sqrt{2N}}(\lambda - A_1\sin\phi_1)\right] d\phi_1 \qquad (9\text{-}23)$$

The derivative of Eq. (9-23) with respect to λ is

$$P_r'[JR,JP,\lambda] = \frac{-1}{(\pi)^{3/2}} \cdot \frac{1}{\sqrt{2N}}\int_{-\pi/2}^{\pi/2} \exp\left[-\frac{1}{2N}(\lambda - A_1\sin\phi_1)^2\right] d\phi_1 \qquad (9\text{-}24)$$

With the result in Eq. (9-6), the conditional upper bound for this FM subcase is

$$P_{FM}^{u}(JR,JP,"0",x_r,x_p)$$

$$= 2\,P_r[JR,JP,A_s] - 2A_s\int_0^{\pi/2} P_r'[JR,JP,A_s\sin\theta]\cdot$$

$$\{P_p[JR,JP,A_s\cos(\theta+\theta_c)] + P_p[JR,JP,A_s\cos(\theta-\theta_c)]\}\cos\theta d\theta \qquad (9\text{-}25)$$

where $P_p[JR,JP,\cdot]$, $P_r[JR,JP,\cdot]$ and $P_r'[JR,JP,\cdot]$ are defined by Eqs. (9-22)-(9-24). Since the parameters x_r and x_p implicitly influence Eqs. (9-22)-(9-24) through A_1 and A_2, Eq. (9-25) must be averaged over these two parameters. The data dependence is automatically removed since the interference-plus-noise is interval-to-interval independent so that the true upper bound for this (JR,JP) subcase is written as

$$P_{FM}^{u}(JR,JP) = P_{FM}^{u}(JR,JP,"0")$$

$$= \left(\frac{1}{2\pi}\right)^2 \int_0^{2\pi}\int_0^{2\pi} P_{FM}^{u}(JR,JP,"0",x_r,x_p)dx_r dx_p \qquad (9\text{-}26)$$

where the integrand is defined by Eqs. (9-22)-(9-25). Equation (9-26) will be greatly simplified in Chapter X.

The lower bound for this subcase is directly written from Eqs. (9-18), (9-26) and (7-20) as

$$P_{FM}^{\ell}(JR,JP) = P_{FM}^{u}(JR,JP) - \frac{2}{M}P_{BFM}(JR,JP) \qquad (9\text{-}27)$$

JR,$\overline{JP}$ or $\overline{JR}$,JP

Only the ($\overline{JR}$,JP) subcase is considered here because the two subcases produce identical results. Equation (9-26) is directly applicable here but since $A_1=0$, the upper bound becomes

$$P_{FM}^{\dot{u}}(\overline{JR},JP,"0",x_p)$$

$$= 2\,P_r[\overline{JR},JP,A_s] - 2A_s\int_o^{\pi/2} P_r'[\overline{JR},JP,A_s\sin\theta]\cdot$$

$$\{P_p[\overline{JR},JP,A_s\cos(\theta+\theta_c)] + P_p[\overline{JR},JP,A_s\cos(\theta-\theta_c)]\}\cos\theta d\theta \qquad (9\text{-}28)$$

where from Eqs. (9-22)-(9-24)

$$P_p[\overline{JR},JP,\lambda] = \frac{1}{2\pi}\int_{-\pi/2}^{\pi/2} \operatorname{erfc}[\frac{1}{\sqrt{2N}}(\lambda - A_2\sin\phi_2)]d\phi_2 \qquad (9\text{-}29)$$

$$P_r[\overline{JR},JP,\lambda] = \frac{1}{2}\operatorname{erfc}[\frac{\lambda}{\sqrt{2N}}] \qquad (9\text{-}30)$$

$$P_r'[\overline{JR},JP,\lambda] = \frac{-1}{\sqrt{\pi}}\cdot\frac{1}{\sqrt{2N}}\exp[-\frac{\lambda^2}{2N}] \qquad (9\text{-}31)$$

The conditional upper bound defined in Eq. (9-28) is actually data symbol independent so that

$$P_{FM}^{u}(\overline{JR},JP) = P_{FM}^{u}(\overline{JR},JP,"0")$$

$$= \frac{1}{2\pi}\int_{o}^{2\pi} P_{FM}^{u}(\overline{JR},JP,"0",x_p)\,dx_p \qquad (9\text{-}32)$$

where the integrand is defined by Eqs. (9-28)-(9-31). As before, Chapter X will provide a simplification of Eq. (9-32).

For this subcase and from Eqs. (9-18), (9-32) and (7-23), the lower bound is

$$P_{FM}^{\ell}(\overline{JR},JP) = P_{FM}^{u}(\overline{JR},JP) - \frac{2}{M} P_{BFM}(\overline{JR},JP) \qquad (9\text{-}33)$$

$\underline{\overline{JR},\overline{JP}}$

No jamming signal is located in either interval, hence $A_1=A_2=0$. This fact then eliminates all offset parameter dependence. The half-plane probability functions are written as

$$P_p[\overline{JR},\overline{JP},\lambda] = \frac{1}{2}\,\mathrm{erfc}\left[\frac{\lambda}{\sqrt{2N}}\right] \qquad (9\text{-}34)$$

$$P_r[\overline{JR},\overline{JP},\lambda] = \frac{1}{2}\,\mathrm{erfc}\left[\frac{\lambda}{\sqrt{2N}}\right] \qquad (9\text{-}35)$$

$$P_r'[\overline{JR},\overline{JP},\lambda] = \frac{-1}{\sqrt{\pi}} \cdot \frac{1}{\sqrt{2N}} \exp\left[-\frac{\lambda^2}{2N}\right] \qquad (9\text{-}36)$$

These definitions of $P_p[\overline{JR},\overline{JP},\cdot]$, $P_r[\overline{JR},\overline{JP},\cdot]$, and $P_r'[\overline{JR},\overline{JP},\cdot]$ are then used in Eq. (9-6) to obtain

$$P^{u}_{FM}(\overline{JR},\overline{JP}) = P^{u}_{FM}(\overline{JR},\overline{JP},\text{"0"})$$

$$= 2\ P_r[\overline{JR},\overline{JP},A_s] - 2\ A_s \int_0^{\pi/2} P'_r[\overline{JR},\overline{JP},A_s\sin\theta] \cdot$$

$$\{P_p[\overline{JR},\overline{JP},A_s\cos(\theta+\theta_c)] + P_p[\overline{JR},\overline{JP},A_s\cos(\theta-\theta_c)]\}\cos\theta d\theta \qquad (9\text{-}37)$$

From Eqs. (9-18), (9-37) and (7-24), the lower bound is expressed as

$$P^{\ell}_{FM}(\overline{JR},\overline{JP}) = P^{u}_{FM}(\overline{JR},\overline{JP}) - \frac{2}{M} P_{BFM}(\overline{JR},\overline{JP}) \qquad (9\text{-}38)$$

CW-Tone Jamming

Extensive use of the results in the FM jamming section (M>4) are made throughout the individual CW-tone jamming subcases. The parameters A_1, A_2, ϕ_1, and ϕ_2 are frequently used as before but must be redefined as

$$A_1 = [A_{jr}(t_s - T_b)]_{cw}$$

$$A_2 = [A_{jp}(t_s)]_{cw}$$

$$\phi_1 = \phi_{jr} + [\Phi_{jr}(t_s - T_b)]_{cw}$$

$$\phi_2 = \phi_{jp} + [\Phi_{jp}(t_s)]_{cw} \qquad (9\text{-}39)$$

There is no offset parameter dependence since the jamming signal is a single sinusoid. The individual subcases are now considered.

JR,JP

$$P^{u}_{CW}(JR,JP) = P^{u}_{CW}(JR,JP,"0")$$

$$= P^{u}_{FM}(JR,JP,"0",x_r,x_p)\Big|_{\substack{A_1 = [A_{jr}(t_s-T_b)]_{cw} \\ A_2 = [A_{jp}(t_s)]_{cw}}}$$

$$= 2\,P_r[JR,JP,A_s] - 2\,A_s\int_o^{\pi/2} P'_r[JR,JP,A_s\sin\theta]\cdot$$

$$\{P_p[JR,JP,A_s\cos(\theta+\theta_c] + P_p[JR,JP,A_s\cos(\theta-\theta_c)]\}\cos\theta d\theta \qquad (9\text{-}40)$$

where

$$P_p[JR,JP,\lambda] = \frac{1}{2\pi}\int_{-\pi/2}^{\pi/2} \operatorname{erfc}[\frac{1}{\sqrt{2N}}(\lambda-A_2\sin\phi_2)]d\phi_2 \qquad (9\text{-}41)$$

$$P_r[JR,JP,\lambda] = \frac{1}{2\pi}\int_{-\pi/2}^{\pi/2} \operatorname{erfc}[\frac{1}{\sqrt{2N}}(\lambda-A_1\sin\phi_1)]d\phi_1 \qquad (9\text{-}42)$$

$$P'_r[JR,JP,\lambda] = \frac{-1}{(\pi)^{3/2}}\cdot\frac{1}{\sqrt{2N}}\int_{-\pi/2}^{\pi/2} \exp[-\frac{1}{2N}(\lambda-A_1\sin\phi_1)^2]d\phi_1 \qquad (9\text{-}43)$$

The lower bound becomes

$$P^{\ell}_{CW}(JR,JP) = P^{u}_{CW}(JR,JP) - \frac{2}{M}P_{BCW}(JR,JP) \qquad (9\text{-}44)$$

where Eqs. (9-18), (9-40), and (7-28) have been used.

JR,$\overline{JP}$ or $\overline{JR}$,JP

For this subcase, Eq. (9-39) is still necessary but with $A_1=0$ ($\overline{JR}$,JP subcase). With this condition, Eqs. (9-41)-(9-43) are modified to be

$$P_p[\overline{JR},JP,\lambda] = \frac{1}{2\pi}\int_{-\pi/2}^{\pi/2} \text{erfc}[\frac{1}{\sqrt{2N}}(\lambda-A_2\sin\phi_2)]d\phi_2 \tag{9-45}$$

$$P_r[\overline{JR},JP,\lambda] = \frac{1}{2}\,\text{erfc}[\frac{\lambda}{\sqrt{2N}}] \tag{9-46}$$

$$P_r'[JR,JP,\lambda] = \frac{-1}{\sqrt{\pi}} \cdot \frac{1}{\sqrt{2N}} \exp[-\frac{\lambda^2}{2N}] \tag{9-47}$$

The unconditional upper bound for this subcase is then

$$P_{CW}^u(\overline{JR},JP) = P_{CW}^u(\overline{JR},JP,"0")$$

$$= P_{CW}^u(JR,JP)\Big|_{A_1=0}$$

$$= 2\,P_r[\overline{JR},JP,A_s] - 2A_s\int_o^{\pi/2} P_r'[\overline{JR},JP,A_s\sin\theta] \cdot$$

$$\{P_p[\overline{JR},JP,A_s\cos(\theta+\theta_c)] + P_p[\overline{JR},JP,A_s\cos(\theta-\theta_c)]\}\cos\theta d\theta \tag{9-48}$$

where the definitions in Eqs. (9-45)-(9-47) are required.

With Eqs. (9-18), (9-48) and (7-31), the lower bound becomes

$$P_{CW}^{\ell}(\overline{JR},JP) = P_{CW}^{u}(\overline{JR},JP) - \frac{2}{M} P_{BCW}(\overline{JR},JP) \tag{9-49}$$

$\overline{JR},\overline{JP}$

The amplitudes for this unjammed case are $A_1=A_2=0$. Therefore

$$P_{CW}^{u}(\overline{JR},\overline{JP}) = P_{CW}^{u}(\overline{JR},\overline{JP},"0") = P_{FM}^{u}(\overline{JR},\overline{JP}) \tag{9-50}$$

where $P_{FM}^{u}(\overline{JR},\overline{JP})$ is defined by Eqs. (9-34)-(9-37).

It must also be true that

$$P_{CW}^{\ell}(\overline{JR},\overline{JP}) = P_{FM}^{\ell}(\overline{JR},\overline{JP}) \quad . \tag{9-51}$$

Equation (9-38) defines $P_{FM}^{\ell}(\overline{JR},\overline{JP})$.

Noise Jamming

If a jammer outputs a total noise power of N_j watts, the jamming power at the input to the DPSK demodulator must then be $N_j' = S_n N_j w_b/(K_s \cdot pw_p)$, where S_n is the reduction factor defined previously. This power simply adds to the existing thermal noise term in the reference or present half-plane probability functions provided the reference or present signaling interval is jammed, respectively.

For each subcase the upper bound is generally written as

$$P_N^u(\cdot,\cdot) = 2\,P_r[\cdot,\cdot,A_s] - 2\,A_s \int_o^{\pi/2} P_r'(\cdot,\cdot,A_s\sin\theta] \cdot$$

$$\{P_p[\cdot,\cdot,A_s\cos(\theta+\theta_c)] + P_p[\cdot,\cdot,A_s\cos(\theta-\theta_c)]\}\cos\theta d\theta \tag{9-52}$$

It is the functions $P_p[\cdot,\cdot,\cdot]$, $P_r[\cdot,\cdot,\cdot]$, and $P'_r[\cdot,\cdot,\cdot]$ which are different for each subcase.

In each of the following subcases, only the half-plane probability expressions are given since the general upper bound of Eq. (9-52) applies to all subcases. Equations (9-41)-(9-43) are used but with $A_1=A_2=0$.

JR,JP

The half-plane probability functions are

$$P_p[JR,JP,\lambda] = \frac{1}{2}\,\mathrm{erfc}\left[\frac{\lambda}{\sqrt{2(N+N'_j)}}\right] \tag{9-53}$$

$$P_r[JR,JP,\lambda] = \frac{1}{2}\,\mathrm{erfc}\left[\frac{\lambda}{\sqrt{2(N+N'_j)}}\right] \tag{9-54}$$

$$P'_r[JR,JP,\lambda] = \frac{-1}{\sqrt{\pi}}\sqrt{\frac{1}{2(N+N'_j)}}\,\exp\left[\frac{-\lambda^2}{2(N+N'_j)}\right] \tag{9-55}$$

With Eqs. (9-18) and (7-33), the lower bound is

$$P_N^{\ell}(JR,JP) = P_N^{u}(JR,JP) - \frac{2}{M}\,P_{BN}(JR,JP) \tag{9-56}$$

JR,$\overline{JP}$ or $\overline{JR}$,JP

The half-plane probability functions are

$$P_p[\overline{JR},JP,\lambda] = \frac{1}{2}\,\mathrm{erfc}\left[\frac{\lambda}{\sqrt{2(N+N'_j)}}\right] \tag{9-57}$$

$$P_r[\overline{JR},JP,\lambda] = \frac{1}{2}\,\mathrm{erfc}\left[\frac{\lambda}{\sqrt{2N}}\right] \tag{9-58}$$

$$P'_r[\overline{JR},JP,\lambda] = \frac{-1}{\sqrt{\pi}} \cdot \frac{1}{\sqrt{2N}} \exp\left[\frac{-\lambda^2}{2N}\right] \tag{9-59}$$

With Eqs. (9-18) and (7-34), the lower bound is

$$P_N^{\ell}(\overline{JR},JP) = P_N^{u}(\overline{JR},JP) - \frac{2}{M} P_{BN}(\overline{JR},JP) \tag{9-60}$$

$\underline{\overline{JR},\overline{JP}}$

The half-plane probability functions are

$$P_p[\overline{JR},\overline{JP},\lambda] = \frac{1}{2}\,\mathrm{erfc}\left[\frac{\lambda}{\sqrt{2N}}\right] \tag{9-61}$$

$$P_r[\overline{JR},\overline{JP},\lambda] = \frac{1}{2}\,\mathrm{erfc}\left[\frac{\lambda}{\sqrt{2N}}\right] \tag{9-62}$$

$$P'_r[\overline{JR},\overline{JP},\lambda] = \frac{-1}{\sqrt{\pi}} \cdot \frac{1}{\sqrt{2N}} \exp\left[\frac{-\lambda^2}{2N}\right] \tag{9-63}$$

With Eqs. (9-18) and (7-35), the lower bound is

$$P_N^{\ell}(\overline{JR},\overline{JP}) = P_N^{u}(\overline{JR},\overline{JP}) - \frac{2}{M} P_{BN}(\overline{JR},\overline{JP}) \tag{9-64}$$

Note that

$$P_N^u(\overline{JR},\overline{JP}) = P_{CW}^u(\overline{JR},\overline{JP}) = P_{FM}^u(\overline{JR},\overline{JP})$$

and

$$P_N^\ell(\overline{JR},\overline{JP}) = P_{CW}^\ell(\overline{JR},\overline{JP}) = P_{FM}^\ell(\overline{JR},\overline{JP})$$

CHAPTER X

DEVELOPMENT OF TRACTABLE ERROR EXPRESSIONS

With the specific subcase results derived in Chapters VII-IX, the total probability of error may be written as

$$\begin{aligned} P_J(\text{err}) = \quad & P_J(JR,JP)\Pr(JR,JP) \\ & + 2\, P_J(\overline{JR},JP)\Pr(\overline{JR},JP) \\ & + \quad P_J(\overline{JR},\overline{JP})\Pr(\overline{JR},\overline{JP}) \end{aligned} \tag{10-1}$$

where J represents any of the subscripts introduced in those chapters (e.g. J may be BFM for binary DPSK, FM jamming). If the definitions (from Eq. (6-7))

$$\Pr(JR,JP) = \left(\frac{K_s}{N_s}\right)^2$$

$$\Pr(\overline{JR},JP) = \frac{(N_s-K_s)K_s}{N_s^2}$$

$$\Pr(\overline{JR},\overline{JP}) = \left(\frac{N_s-K_s}{N_s}\right)^2$$

are used, Eq. (10-1) becomes

$$P_J(\text{err}) = P_J(JR,JP)\left(\frac{K_s}{N_s}\right)^2 + 2\,P_J(\overline{JR},JP)\,\frac{(N_s-K_s)K_s}{N_s^2} + P_J(\overline{JR},\overline{JP})\left(\frac{N_s-K_s}{N_s}\right)^2 \qquad (10\text{-}2)$$

Unfortunately, the general probability of error expression in Eq. (10-2) does not necessarily describe the average error rate of the DPSK system. This is due to the dependence of the parameters A_1 and A_2 on the sampling times and the phase of p(t) at those sampling times. In fact, if these parameters are not identical at each sampling time and for every phase shift of p(t) at those sampling times, the error rates will change from one sampling time to the next and, more than likely, from one phase shift of p(t) to the next. Therefore, in order to classify any of the error rates as average error rates, the error expressions must be evaluated for an infinite sequence of sampling times and, at each sample time, for p different code phases. This infinite number of error probabilities is then averaged to obtain the true average error probability, which is mathematically written as

$$P_{AVG,J}(\text{err}) = \lim_{N\to\infty} \frac{1}{N} \sum_{n=1}^{N} \left[\frac{1}{p} \sum_{k_p=1}^{p} P_J(\text{err},n,k_p) \right] \qquad (10\text{-}3)$$

In Eq. (10-3), the dependence on the sample time (n) and the phase (k_p) has been justifiably inserted because of the redefinitions

$$A_1 = A_{jr}((n-1)T_b, k_p)$$

$$A_2 = A_{jp}(nT_b, k_p) \qquad (10\text{-}4)$$

The two-variable dependence introduced into the FM envelopes of Eq. (10-4) should not be considered an unqualified mathematical deviation from the previously used one-variable convention (i.e. $A_{jp}(nT_b)$), but rather as a more complete description of the envelopes. Similar envelope notation is available for the CW-tone envelopes. In addition, there are no envelope variations for the noise jamming case, thereby making Eq. (10-2) the actual average error rate for all noise jamming situations.

To say the least, Eq. (10-3) is numerically rather cumbersome to evaluate. Because of this, certain steps must be taken to minimize or eliminate the computations required by Eq. (10-3). The remaining portion of this chapter is devoted to developing accurate and computationally efficient methods to circumvent the problem posed by the nature of Eq. (10-3). As an additional result of the method used, some of the complex expressions in Chapters VII-IX are significantly reduced.

One method of reducing the complexity of Eq. (10-3) is to consider a restrictive class of PR waveforms and jamming signals that requires the envelope functions to return to their initial values after a finite number (N_r) of signaling intervals. With such a repetition, Eq. (10-3) is reduced to two finite summations of the form

$$P_{AVG,J}(err) = \frac{1}{N_r} \sum_{n=1}^{N_r} \left[\frac{1}{p} \sum_{k_p=1}^{p} P_J(err, n, k_p) \right] \qquad (10\text{-}5)$$

The conditions under which the envelopes are periodic over N_r intervals are developed in Appendix K, where it is shown that the greatest simplification (N_r=1) is possible when

$$W_{fo} \triangleq \frac{\omega_j - \omega_c}{\omega_b} = \text{integer} \tag{10-6}$$

$$S_j \triangleq \frac{\omega_m}{\omega_b} = \text{positive integer} \tag{10-7}$$

and

$$S_c \triangleq \frac{\omega_p}{\omega_b} = \text{positive integer} \tag{10-8}$$

where

$$\omega_b = \frac{2\pi}{T_b} \quad .$$

The parameters W_{fo}, S_j, and S_c are referred to as the frequency offset, the jamming slip ratio, and the code slip ratio, respectively.

Though this method is valid and not too restrictive in some situations [30], here it imposes not only modeling inconsistencies but also very restrictive parameter variations. In the first place, this analysis has assumed that the interferences occuring in adjacent signaling intervals arise from different hopping slots and hence are independent; if the envelopes are to be periodic over a finite number of signaling intervals, some dependence would be required. Secondly, the

restrictions on W_{fo} and S_j are not too rigid, but maintaining integer values for S_c eliminates many practical situations which require long PR codes. These longer codes are usually accompanied by a decrease in ω_p such that $\omega_p < \omega_b$. Furthermore, this method does nothing to reduce the code phase averaging. A method is now introduced to eliminate these disadvantages.

Equation (10-3) can be reduced to an average over one probability by simply choosing one of the possible envelope values (one each for A_1 and A_2) and using it to calculate the probability of error. This method certainly eliminates Eq. (10-3) but provides a result having an unknown relationship with respect to the true average error probability. However, if this one envelope value were the maximum or minimum of all possible values, an upper bound or lower bound to the average probability of error could be obtained, respectively. With both the upper and lower bounds known, the true average probability of error would be known to within certain easily calculated limits.

Because the envelope maximum (minimum) is used to generate an (a) upper (lower) bound to the average error rate, a common question asked is: How much of an effect do changes in the envelope maximum (minimum), and correspondingly the upper (lower) bound, have on the true average error rate? For this study and in the first place, the envelope maximum and minimum have approximately an identical chance of occurring as any other envelope value since the p phase shifts are equally likely and the variation of the envelope about each phase shift is very small. In fact, for CW-tone jamming, the envelope at each phase shift is constant.

Secondly, evidence has indicated that changes in the envelope maximum will affect and in most cases dictate the corresponding changes in the average error rate much more than the changes in the envelope minimum. This is due in part to the fact that as the envelope minimum becomes smaller, the jamming efforts become overshadowed by the thermal noise effects, causing the jamless, probability-of-error curve to be reached. When this happens, any pertubation of the jamming parameters is witnessed only in the changes of the upper bound and the corresponding changes in the average probability of error. Furthermore, additional evidence has shown that the average error probability is closer to the upper bound than to the lower bound, thereby attaching more credence to the large effect the envelope maximum has on the average error rate. In fact, though the lower bound does indicate somewhat the best attainable performance, its usefulness as a lower bound is limited to very specific cases and henceforth will not be considered.

In order to illustrate and substantiate the claims just professed, Figures 15-18, which involve CW-tone jamming, are presented. Figures 15 and 16 should be viewed as a pair, as should Figures 17 and 18, since in the former two the error rates are plotted versus signal-to-noise ratio (S/N) with the signal-to-jamming ratio (S/J) as a parameter whereas in the latter two, the roles of S/N and S/J are reversed. The only difference between Figures 15 and 16 and between Figures 17 and 18 is that p is equal to seven in Figures 15 and 17 and equal to thirty-one in Figures 16 and 18. It is seen in comparing each of the pairs of figures that as p increases (S_c fixed) the error curves must and do shift to the left. The important consideration here is that the upper

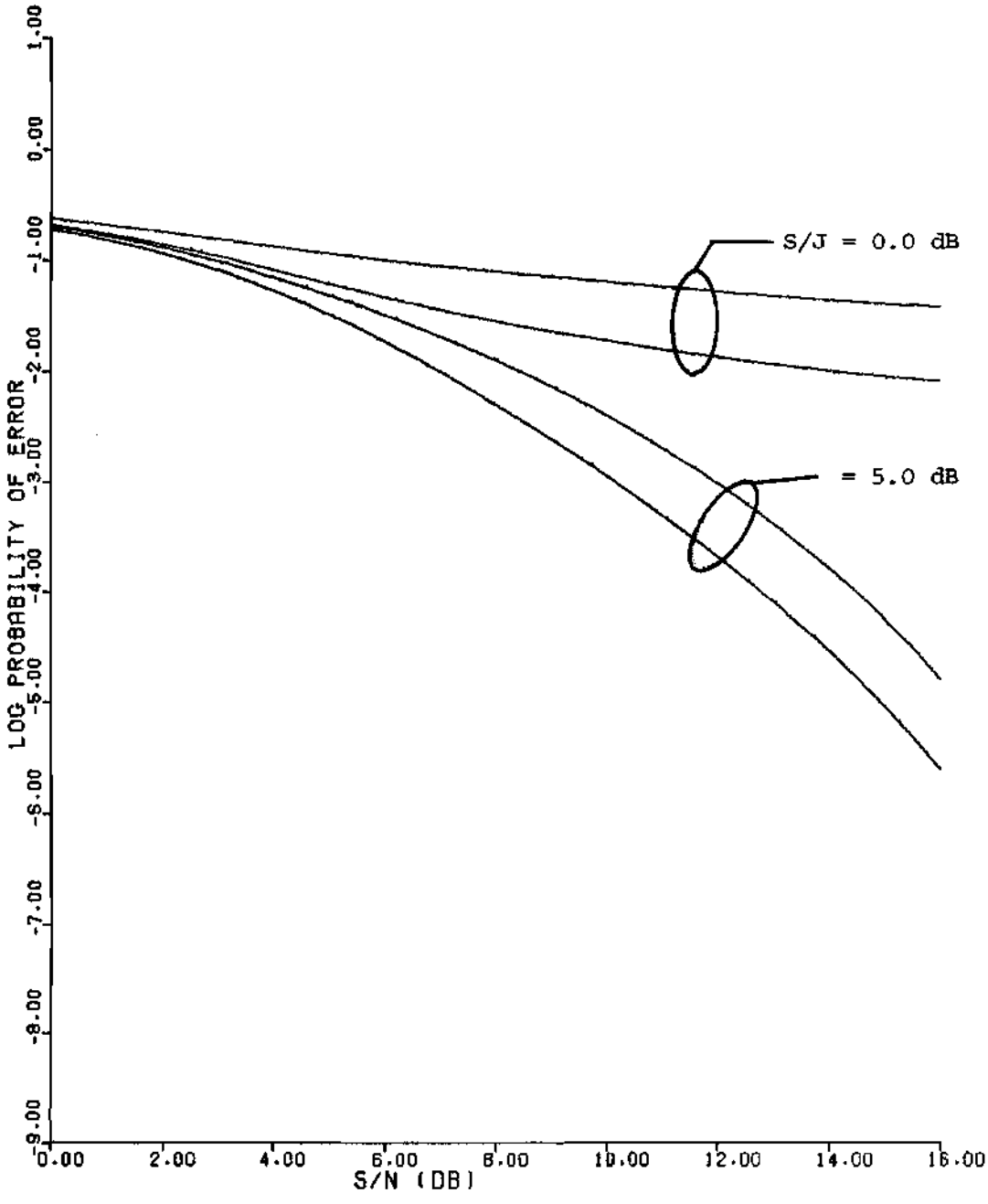

FIGURE 15. Comparison of Upper Bound and Average Error Rate for Cochannel, CW-Tone Jamming with p=7, S_c=1, and S/J = 0.0,5.0 dB

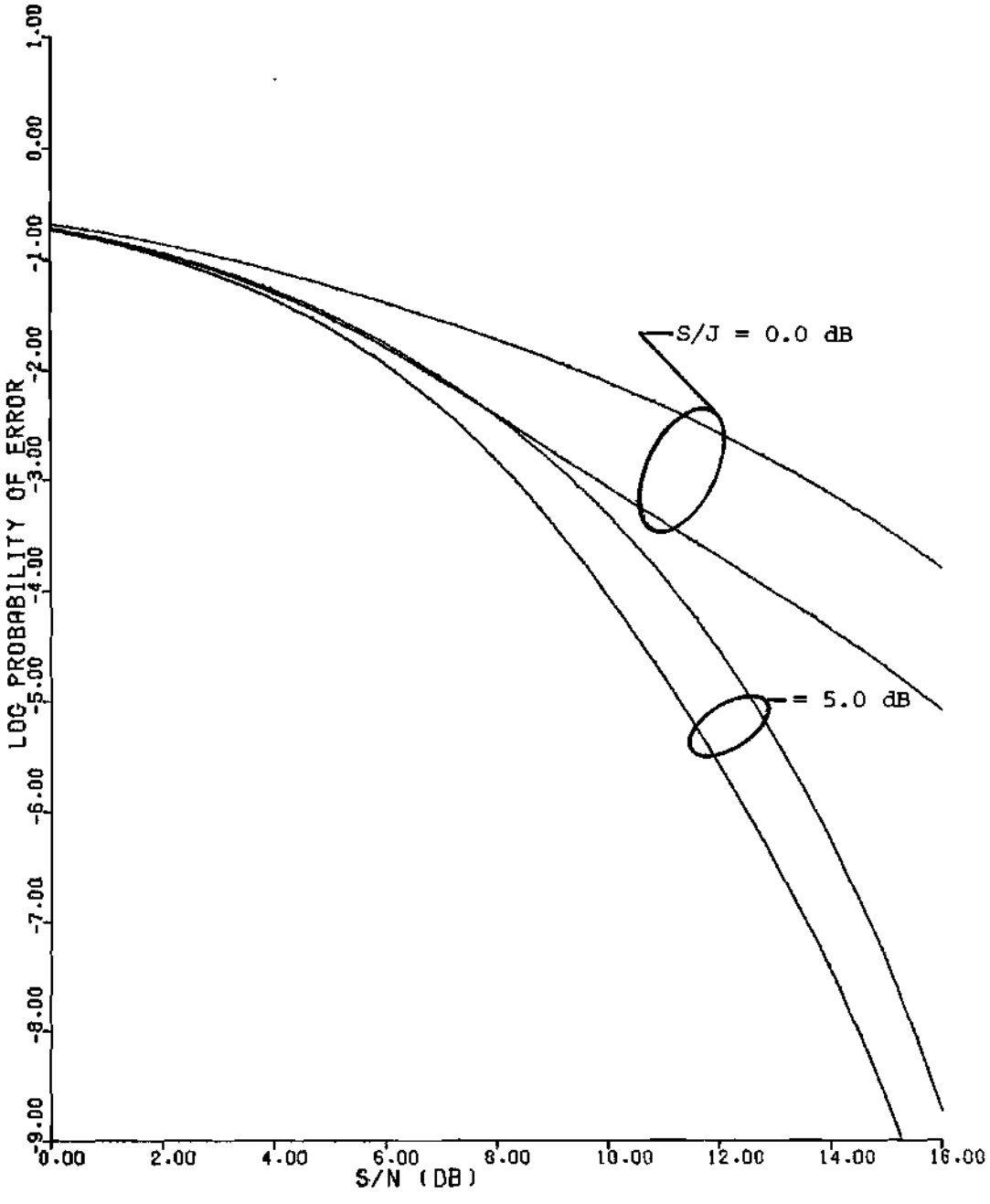

FIGURE 16. Comparison of Upper Bound and Average Error Rates for Cochannel, CW-Tone Jamming with p=31, S_c=1, and S/J = 0.0,5.0 dB

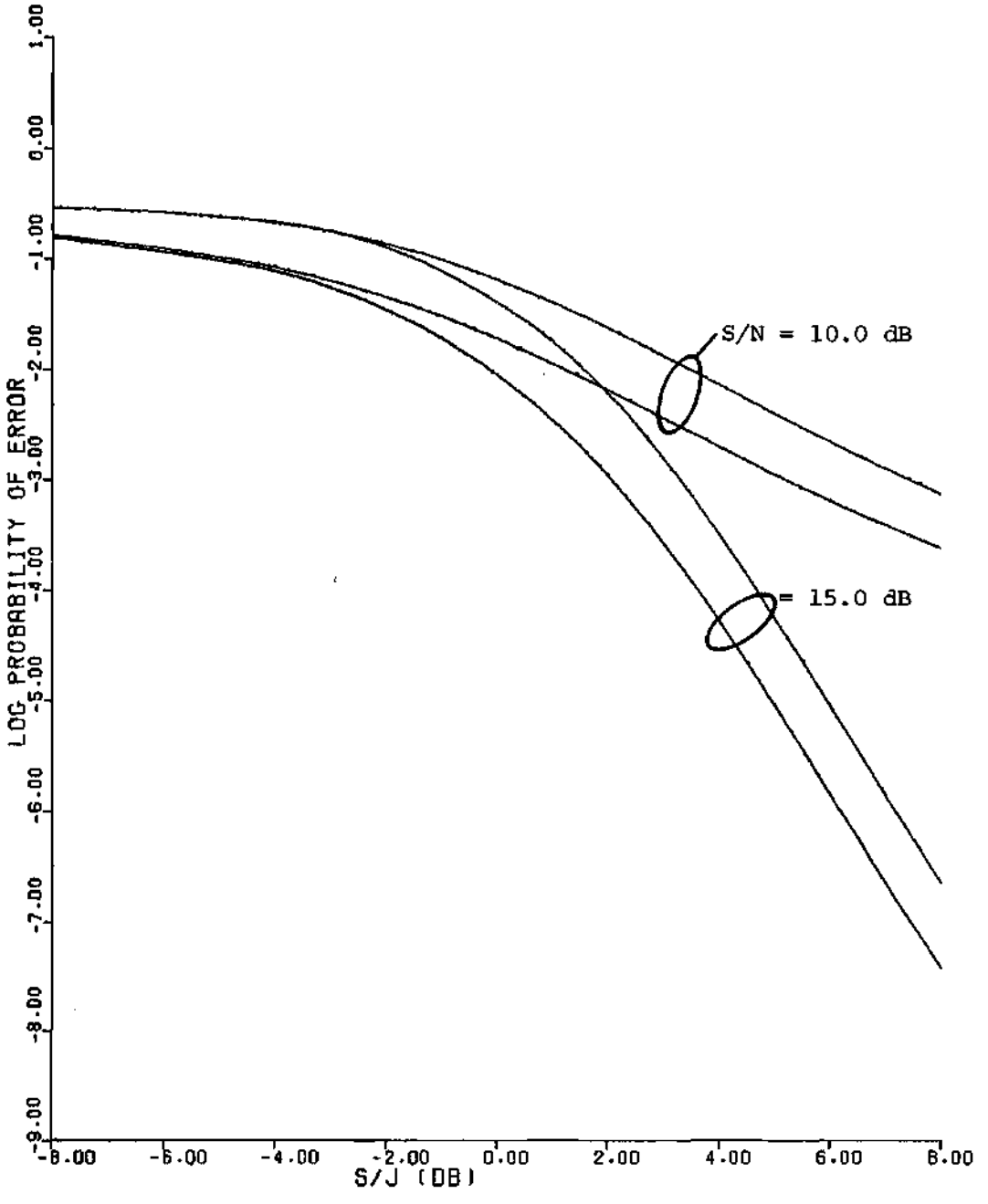

FIGURE 17. Comparison of Upper Bound and Average Error Rates for Cochannel, CW-Tone Jamming with p=7, S_c=1, and S/N = 10.0,15.0 dB

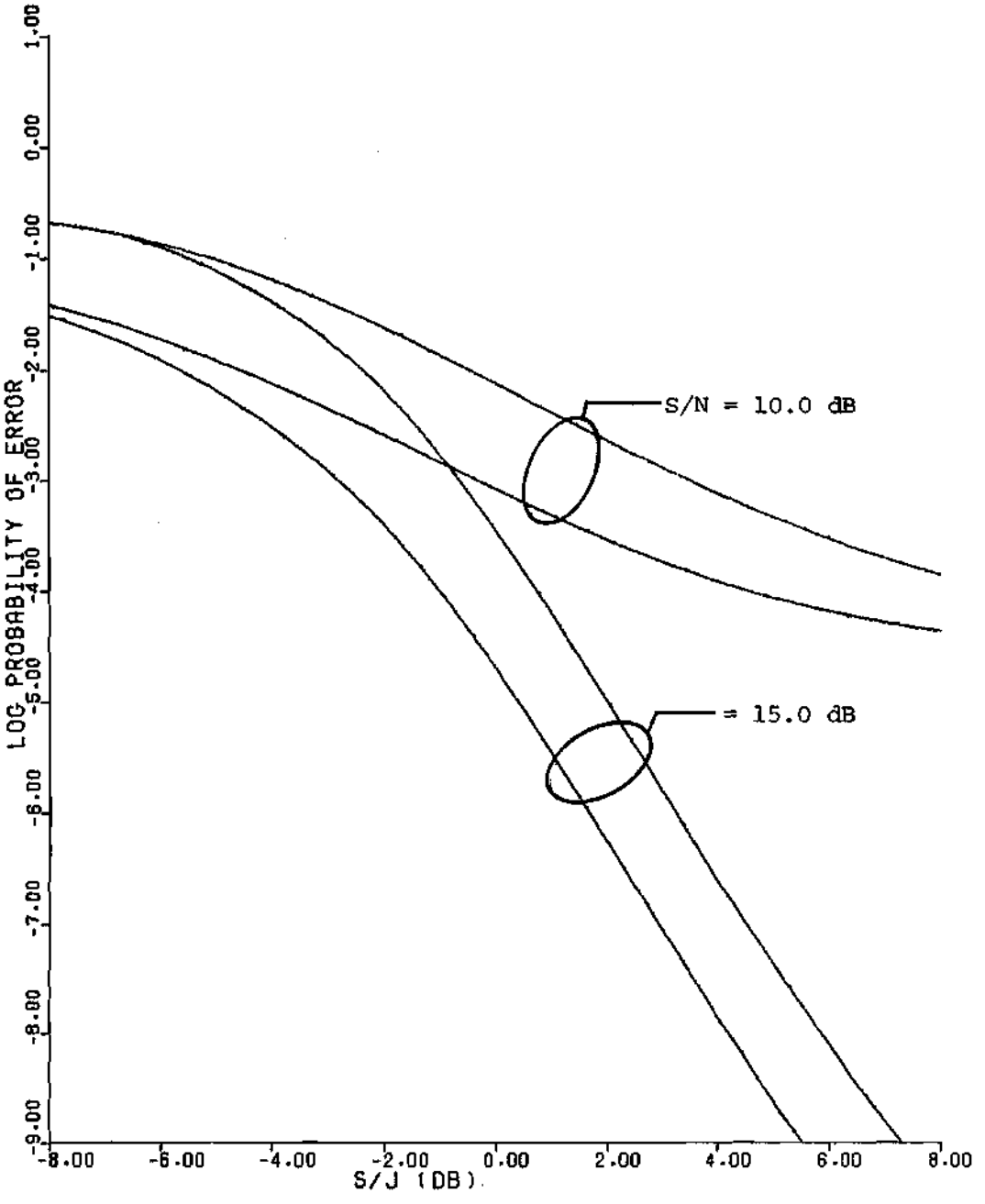

FIGURE 18. Comparison of Upper Bound and Average Error Rates for Cochannel CW-Tone Jamming with p=31, S_c=1, and S/N = 10.0,15.0 dB

bound is relatively close to the true average and that the corresponding shifts of the upper bound and the average due to parameter and power variations are nearly equal. For example, assume a constant error probability of 10^{-4} (-4.0 on the ordinate axis) and an S/J of 5.0 dB. As Figures 15 and 16 indicate, the average error curve shifts approximately 3.0 dB to the left when p increases whereas the upper bound curve shifts about 3.5 dB. For the same error rate but with an S/N of 15.0 dB, Figures 17 and 18 show respective shifts of approximately 4.5 dB and 4.1 dB for the average error rate and upper bound curves.

With the closeness and nearly equal changes of the two error rates, the upper bound is a useful criterion for extensive parametric studies. Furthermore, from a computational point of view, the upper bound expression is clearly more desirable since its computation time is 10-100 times less than that required to compute the average (at least for p=7,31). This becomes a considerable savings in time and money when a large parametric study is undertaken.

The above discussion and illustrations, while providing evidence in an engineering sense, obviously do not completely prove the conjectures that the upper bound is close to the average error rate and that any changes occur approximately equal. There may exist some cases where the closeness or the identical behavior is not as well substantiated. Nonetheless, the upper bound remains a useful tool for parametric studies. If the true average error rate were required, it most certainly could be calculated, though at large expense, using the methods and techniques described above.

The actual determination of the maximum of the envelope will now be discussed. For completeness, the envelope minimum calculation will also be considered. The calculation of these values is totally dictated by the type of jamming signal present. In the simplest case, the jamming signal is a constant amplitude CW-tone. After this signal is passed through the DS correlator and the narrowband filter, the envelope is simply a filtered version of p(t). Because the start of the signaling interval is guaranteed to coincide with the beginning of a PR code chip (synchronous generation), there are only p possible sampled envelope values which can occur. A particular value depends on the phase shift (or chip) of the PR waveform at the sampling time. There exists one phase shift (or chip), henceforth referred to as the "maxchip," which produces the envelope maximum. Correspondingly, one phase shift ("minchip") produces the envelope minimum. Each of these is determined by calculating the envelope for each of the possible phase shifts and performing a comparison of the envelope values.

For an FM jamming signal, there are also p different, PR waveform phase shifts possible at any one time. However, in contrast to the CW-tone case, the envelope also depends on the offset parameter. Therefore, in order to determine the maximum and minimum of the envelope for the FM case, the variation of the envelope due to the offset parameter must be monitored at each of the p phase shifts. Corresponding to each of the p phase shifts, there exists an offset parameter value which maximizes the envelope for that phase shift and a value which minimizes the envelope for the same phase shift. These two offset parameter values are given the names, "maxoffset" and "minoffset," respectively.

The absolute maximum of all FM envelope values would be that value occuring for the maxchip and maxoffset simultaneously. Likewise, the absolute minimum envelope value would occur whenever the minchip and minoffset coincided.

As the error expressions for the FM cases of Chapters VII-IX indicate, the offset parameters were to have been averaged over. Due to the maximization approach proposed here, this averaging is no longer required and those expressions which created numerical problems because of this averaging have now been reduced to more computationally efficient expressions.

To insure that the offset parameter maximization creates only a minor, additional deviation (in addition to the PR-chip maximization) between the upper bound and the average error rate, the dependence of the error probability on the offset parameter at the maxchip was investigated. As an illustration of the typical offset parameter dependence, refer to Figures 19 and 20. The difference between these two figures is that in Figure 19, S/N is used as the abscissa variable and S/J as the parameter, whereas the roles are reversed in Figure 20. In each figure there are two sets of curves, corresponding to two different parameter values. For the time being consider only the upper and lower bounds for each parameter value. The upper and lower bound curves are a result of using the maxoffset and minoffset, respectively, at the maxchip. In other words, the phase shift (maxchip) which produces the maximum envelope value is sampled and for that phase shift the offset parameters which produce the maximum and minimum envelope value are used.

The key result from these curves is that the upper and lower

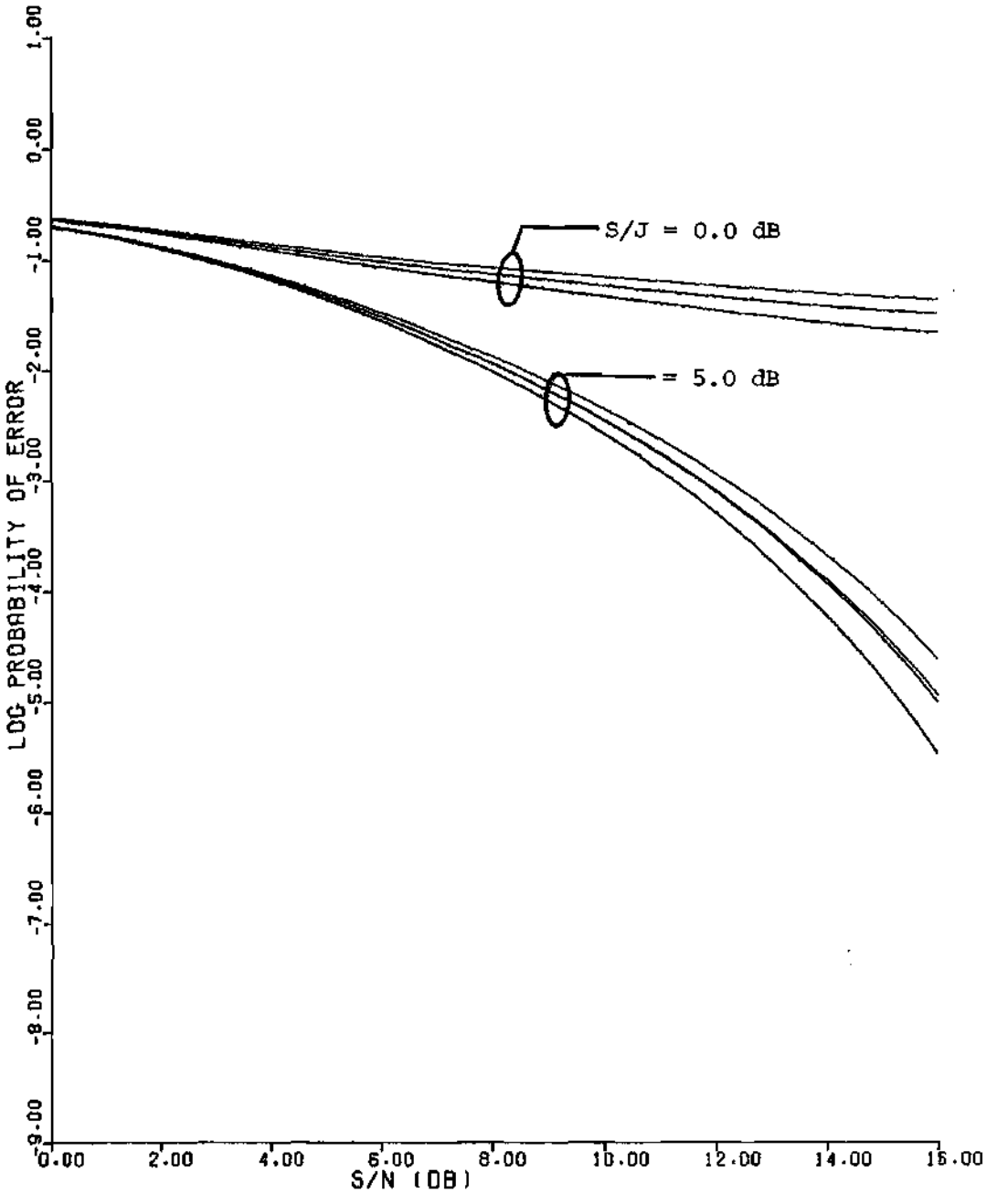

FIGURE 19. Offset Parameter Dependence at the Maxchip for FM Jamming with p=7, S_c=1, S_j=1, β=1 and S/J = 0.0,5.0 dB

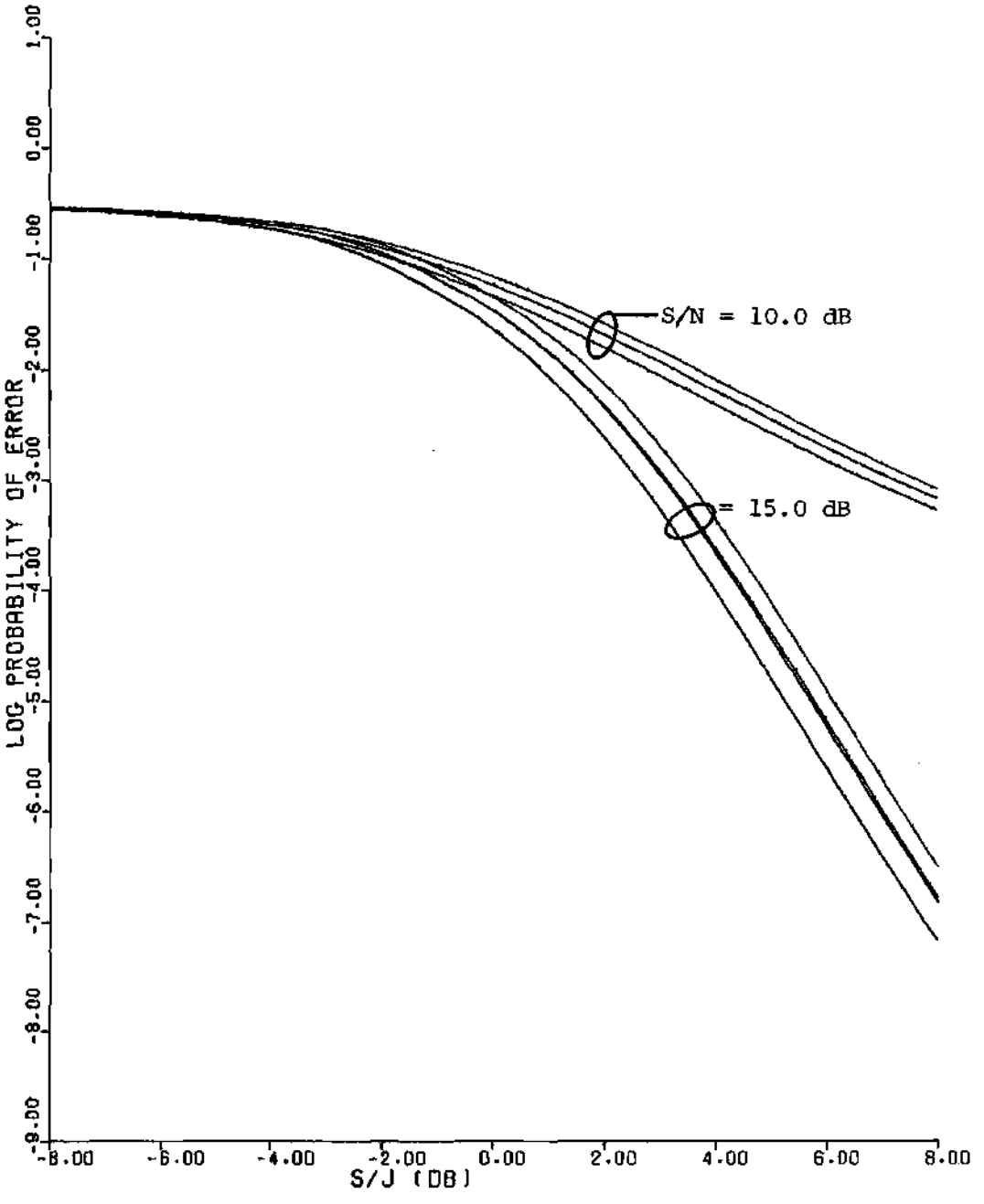

FIGURE 20. Offset Parameter Dependence at the Maxchip for FM Jamming with p=7, S_c=1, S_j=1, β=1, and S/N = 10.0, 15.0 dB

bounds for the maxchip (due to the maxoffset and minoffset) are reasonably tight bounds. This tightness indicates a lack of strong offset parameter dependence. For a wide variation of system and jamming variables this same tightness prevails. Nonetheless, for some variable values, the dependence becomes more pronounced. For example, in Figures 21 and 22, β is taken to be two, in contrast to the β=1 curves of Figures 19 and 20. The increase in the modulation index has caused the bounds to deviate somewhat. This latter case, however, is not included in the practical cases of interest, since it would not be realistic to expect the jammer to spread his bandwidth and hence reduce the jamming power within the narrowband filter bandwidth.

Because of this weak offset parameter dependence, there is no need to average over the offset parameter. Nonetheless, if it were possible to approximate this average, a slightly more accurate analysis would result. An approximation has been developed with the specific results depicted as the additional curves constrained by the bounds in Figures 19-22. The actual probability of error averaged over the offset parameter at the maxchip was determined and is graphed as the curve nearest the upper bound for each parameter value. This holds for each set of curves. In addition to the average error curve, there is also one other curve constrained within the bounds of each set. This curve is the approximated average and is so obtained by determining the RMS value of the possible envelope values at the maxchip and then calculating the error rate for this value. In other words, instead of determining an average probability, the probability based on an average envelope is determined. In some cases (e.g. the S/J=0.0 set for Figure

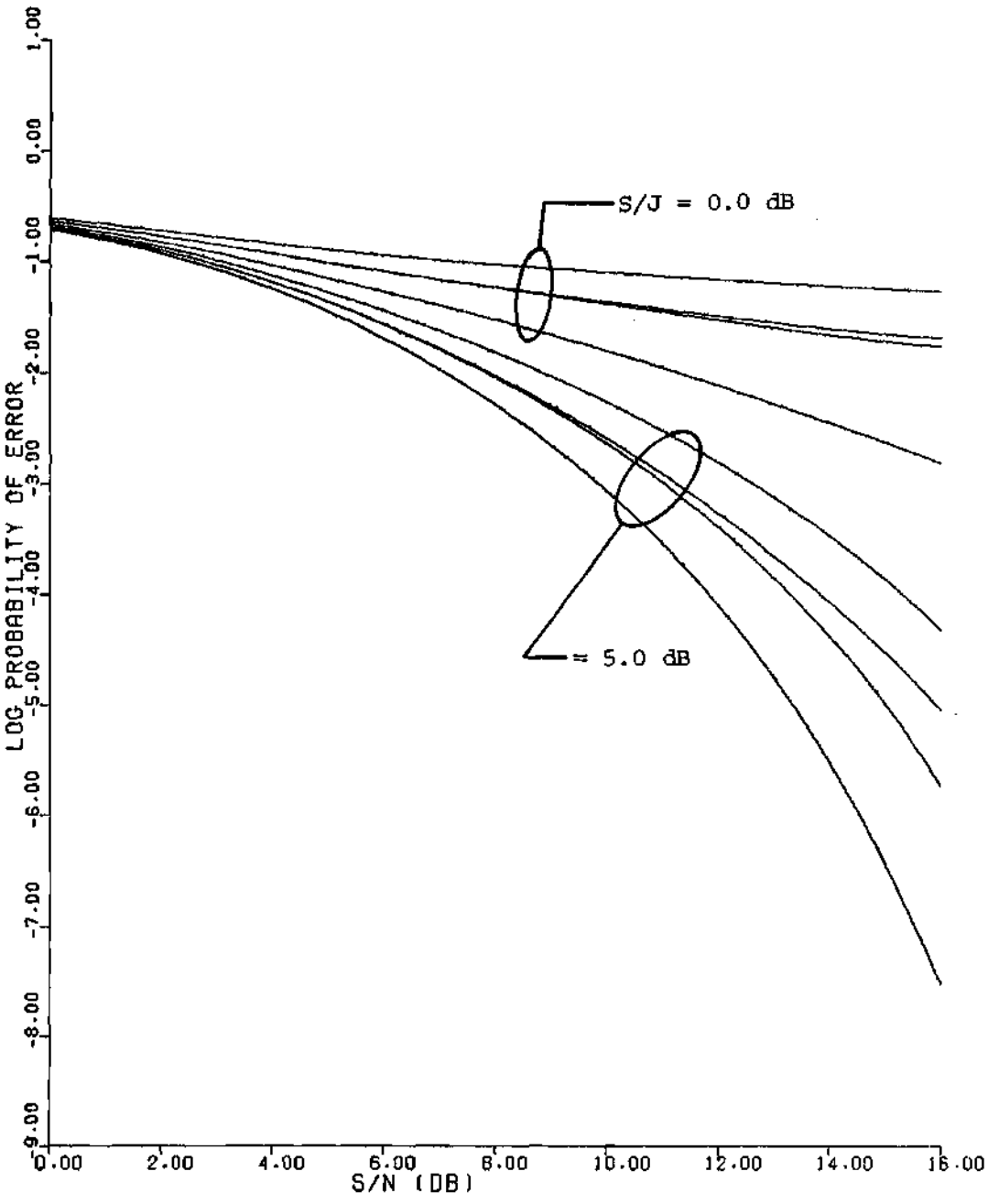

FIGURE 21. Offset Parameter Dependence at the Maxchip for FM Jamming with p=7, S_c=1, S_j=1, β=2, and S/J= 0.0,5.0 dB

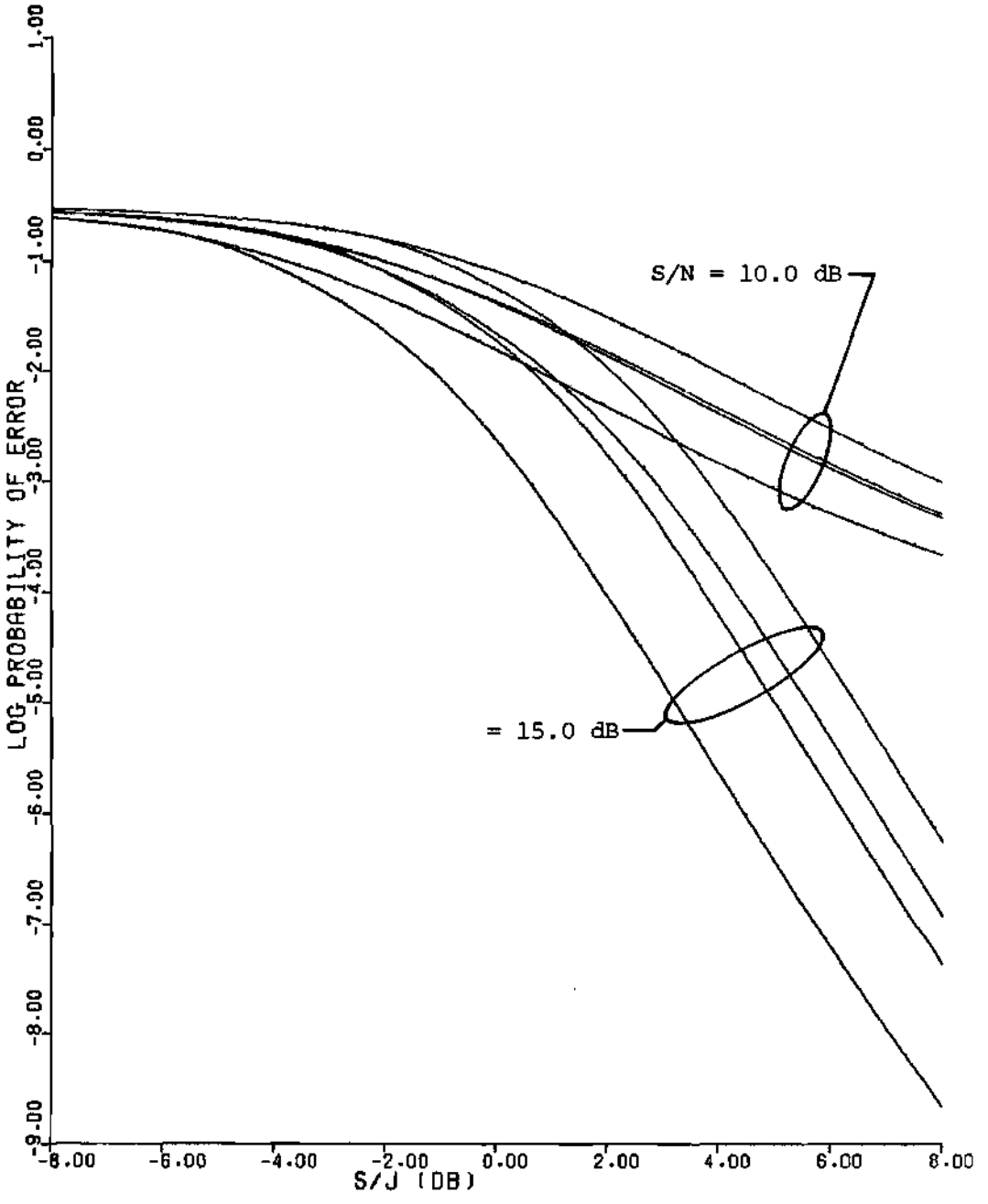

FIGURE 22. Offset Parameter Dependence at the Maxchip for FM Jamming with p=7, S_c=1, S_j=1, β=2, and S/N = 10.0,15.0 dB

19) the approximation and actual average are too close to be distinguished. Again, the accuracy of this approximation depends on the particular parameter values chosen, but for the values of interest for the practical cases, it is a good approximation.

In summary, any offset-parameter averaging required by the expressions in Chapters VII-IX may be eliminated. One argument for its elimination is based on using the absolute maximum (maxchip-maxoffset) envelope value. Upon investigating the variation of the error rate as a function of the offset parameter at the different phase shifts (in particular the maxchip) it was found that only a weak dependence existed. In fact, the offset-parameter averaging process could be approximated by evaluating the conditional error expressions (Chapters VII-IX) with the RMS value of the envelope at those phase shifts. Therefore, the goal of the "maximum" amplitude search for the FM case became the location of the maxchip and then, for this phase shift, the determination of the RMS value of the envelope variation.

In lieu of the envelope calculations just discussed, the bounding techniques presented in Chapter IX for M>4 ultimately serve as upper and lower bounds to the error rate which would be obtained for the maxchip envelope value. The upper and lower bounds in Chapter IX and calculated for the envelope value at the maxchip and minchip, respectively, do provide an overall upper and lower bound to the average error rate for M>4. However, since the bounds for the error rate at the maxchip is the main concern here, the tightness of these bounds, both of which are calculated at the maxchip, is significant. The deviation of these bounds from the true error rate at the maxchip is negligible. This

fact is illustrated in Figures 23-25 where, for each jamming signal, the log of the difference between the upper and lower bounds (bound deviation) is plotted for two values of the signal-to-jamming-power ratio and for M=4, 8, and 16. It is generally concluded, as expected from Chapter IX, that as M, S/J, or S/N increase, the bounds become tighter. Thus, only a reasonably small difference exists between the maxchip error rate and the bounds to that rate.

Before leaving this chapter, a few additional comments are required. Even with the elimination of the offset parameter averaging, it should be noted that the numerical computation required by the quaternary subcases is still substantial. For example, in the CW-tone $(\overline{JR},JP)$ subcase, an adaptive integration routine is required to accurately compute the expression. The generation of one curve for this subcase took 500 seconds, whereas a computation time of only 5 seconds was required to evaluate the very tight lower and upper bounds to the maxchip error rate. Therefore the bounds developed for M>4 are also used for M=4.

The simplifications discussed in this chapter, including the fact that $A_1=A_2$ for maximization, result in efficiently-computable expressions. These expressions for each subcase of Chapters VII-IX are summarized in Tables 1-9, where for a quick reference, the specific tables are:

TABLE 1: BINARY, NOISE JAMMING

TABLE 2: QUATERNARY, NOISE JAMMING

TABLE 3: M>4, NOISE JAMMING

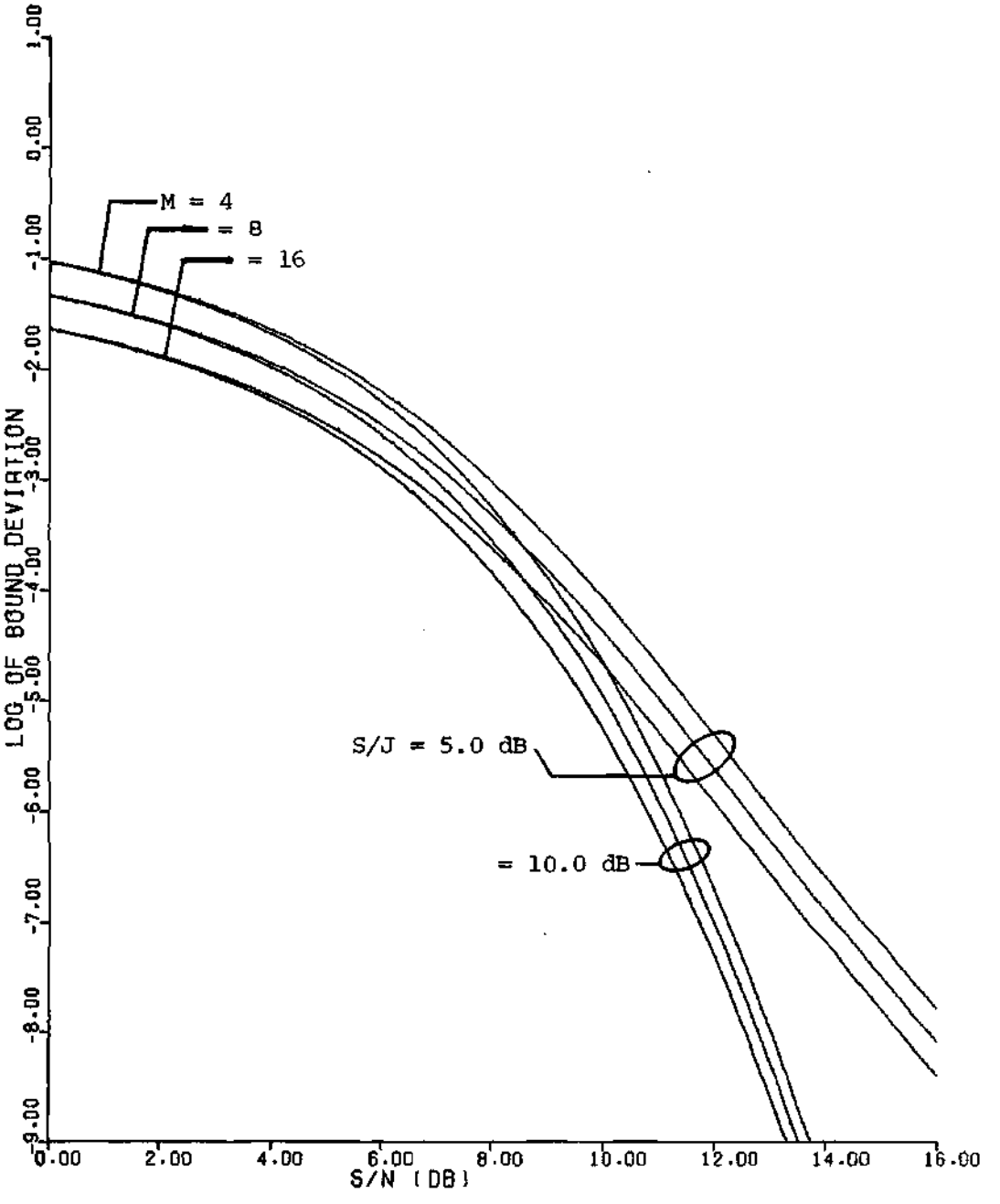

FIGURE 23. Bound Deviation vs S/N, S/J, and M for Noise Jamming

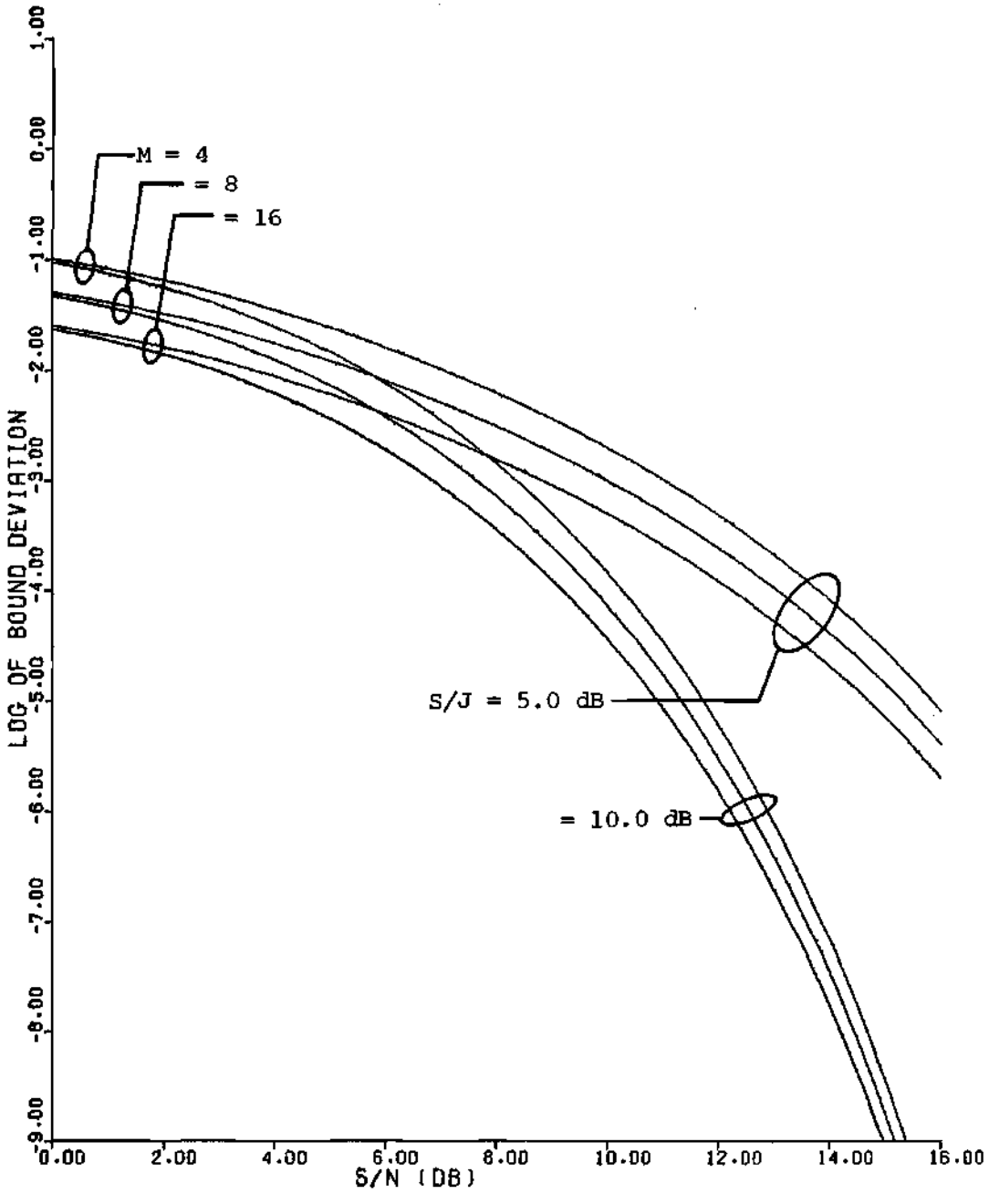

FIGURE 24. Bound Deivation vs S/N, S/J, and M for CW-Tone Jamming

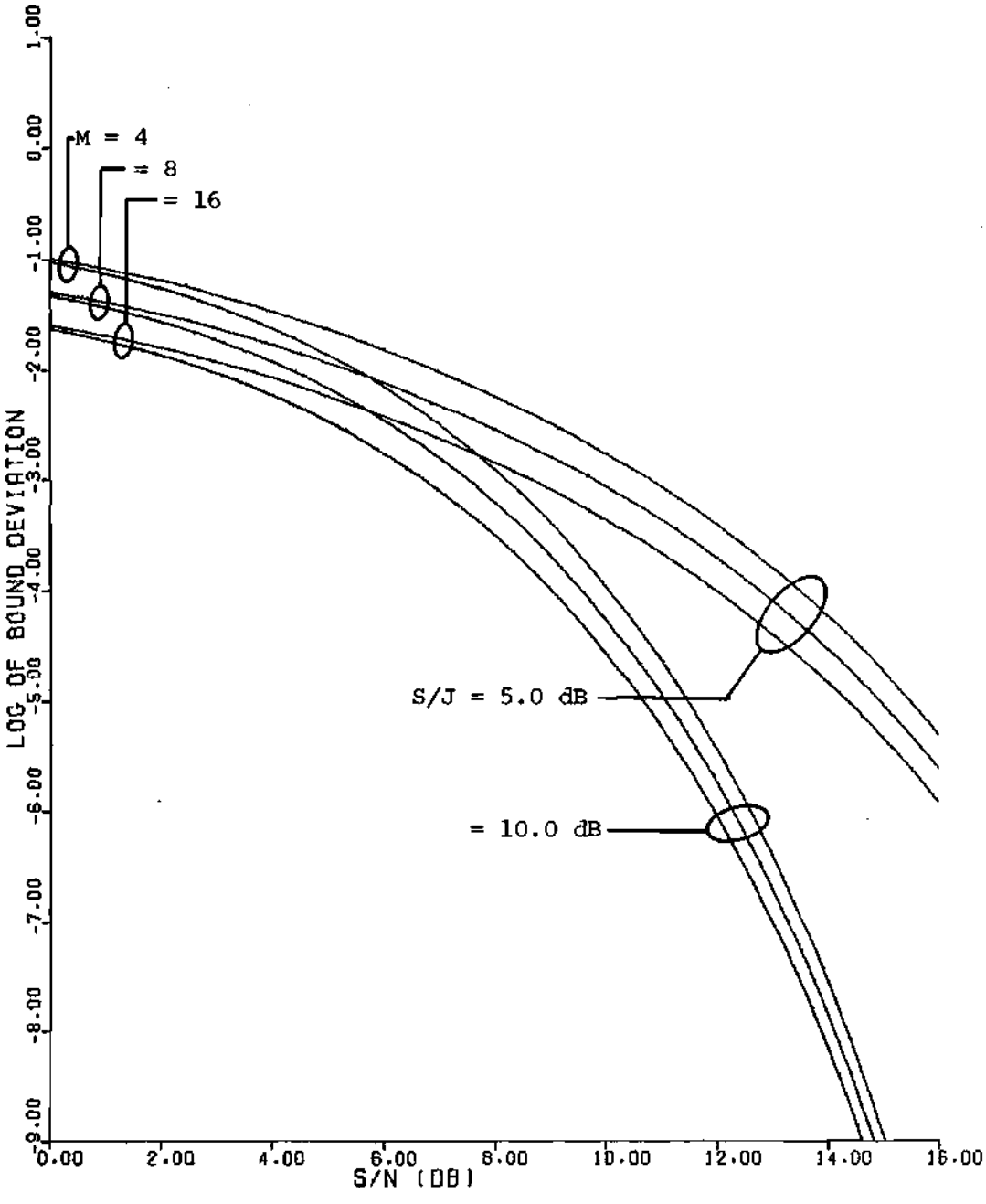

FIGURE 25. Bound Deviation vs S/N, S/J, and M for FM Jamming

TABLE 4: BINARY, CW-TONE JAMMING

TABLE 5: QUATERNARY, CW-TONE JAMMING

TABLE 6: M>4, CW-TONE JAMMING

TABLE 7: BINARY, FM JAMMING

TABLE 8: QUATERNARY, FM JAMMING

TABLE 9: M>4, FM JAMMING

In these tables the notation

$$A = a_{jicw}(t) \text{ at the maxchip}$$

and

$$A_x = \text{RMS}(a_{ji}(t) \text{ at the maxchip})$$

is used.

TABLE 1. Error Expressions for DS/FH, Binary DPSK with Noise Jamming

$P_{BN}(\overline{JR},\overline{JP})$	$\frac{1}{2}\exp[-\frac{1}{2}\frac{A_s^2}{N}]$
$P_{BN}(JR,\overline{JP})$ OR $P_{BN}(\overline{JR},JP)$	$\frac{1}{2}\exp[-\frac{1}{2}(\frac{A_s^2}{N+N_j'/2})]$
$P_{BN}(JR,JP)$	$\frac{1}{2}\exp[-\frac{1}{2}(\frac{A_s^2}{N+N_j'})]$

TABLE 2. Error Expressions for DS/FH, Quaternary DPSK with Noise Jamming

$P_{QN}(\overline{JR},\overline{JP})$	USE $P_N^u(\overline{JR},\overline{JP})$ IN TABLE 3
$P_{QN}(JR,\overline{JP})$ OR $P_{QN}(\overline{JR},JP)$	USE $P_N^u(JR,\overline{JP})$ OR $P_N^u(\overline{JR},JP)$ IN TABLE 3
$P_{QN}(JR,JP)$	USE $P_N^u(JR,JP)$ IN TABLE 3

TABLE 3. Upper Bound Error Expressions for DS/FH, M-ary DPSK with Noise Jamming

$P_N^u(\overline{JR},\overline{JP})$	$\text{erfc}[\frac{A_s}{\sqrt{2N}}] + \frac{A_s}{\sqrt{2N\pi}} \int_o^{\pi/2} \exp(-\frac{A_s^2}{2N}\sin^2\theta)\{\text{erfc}[\frac{A_s}{\sqrt{2N}}\cos(\theta+\theta_c)] + \text{erfc}[\frac{A_s}{\sqrt{2N}}\cos(\theta-\theta_c)]\}\cos\theta d\theta$
$P_N^u(JR,\overline{JP})$ OR $P_N^u(\overline{JR},JP)$	$\text{erfc}[\frac{A_s}{\sqrt{2N}}] + \frac{A_s}{\sqrt{2N\pi}} \int_o^{\pi/2} \exp(-\frac{A_s^2}{2N}\sin^2\theta) \cdot \{\text{erfc}[\frac{A_s}{\sqrt{2(N+N_j')}}\cos(\theta+\theta_c)] + \text{erfc}[\frac{A_s}{\sqrt{2(N+N_j')}}\cos(\theta-\theta_c)]\}\cos\theta d\theta$
$P_N^u(JR,JP)$	$\text{erfc}[\frac{A_s}{\sqrt{2(N+N_j')}}] + \frac{A_s}{\sqrt{2(N+N_j')\pi}} \int_o^{\pi/2} \exp(-\frac{A_s^2}{2(N+N_j')}\sin^2\theta) \cdot \{\text{erfc}[\frac{A_s}{\sqrt{2(N+N_j')}}\cos(\theta+\theta_c)] + \text{erfc}[\frac{A_s}{\sqrt{2(N+N_j')}}\cos(\theta-\theta_c)]\}\cos\theta d\theta$

TABLE 4. Error Expressions for DS/FH Binary DPSK with CW-Tone Jamming

$P_{BCW}(\overline{JR},\overline{JP})$	$\frac{1}{2}\exp[-\frac{A_s^2}{2N}]$
$P_{BCW}(JR,\overline{JP})$ OR $P_{BCW}(\overline{JR},JP)$	$\frac{1}{2\pi}\int_o^{\pi}\{1-Q[\frac{1}{2}\sqrt{\frac{4A_s^2+4A_sA\cos\phi_1+A^2}{N}}\ ,\ \frac{1}{2}\frac{A}{\sqrt{N}}]+Q[\frac{1}{2}\frac{A}{\sqrt{N}}\ ,\ \frac{1}{2}\sqrt{\frac{4A_s^2+4A_sA\cos\phi_1+A^2}{N}}]\}d\phi_1$
$P_{BCW}(JR,JP)$	$(\frac{1}{2\pi})^2\int_o^{2\pi}\int_o^{2\pi}\frac{1}{2}\{1-Q[\frac{1}{2}\sqrt{\frac{m_1^2+m_2^2}{N}}\ ,\ \frac{1}{2}\sqrt{\frac{m_3^2+m_4^2}{N}}]+Q[\frac{1}{2}\sqrt{\frac{m_3^2+m_4^2}{N}}\ ,\ \frac{1}{2}\sqrt{\frac{m_1^2+m_2^2}{N}}]\}d\phi_1d\phi_2$ $m_1^2+m_2^2 = 4A_s^2+4A_sA(\cos\phi_1+\cos\phi_2)+2A^2\cos(\phi_1-\phi_2)+2A^2$ $m_3^2+m_4^2 = 2A^2-2A^2\cos(\phi_1-\phi_2)$

TABLE 5. Error Expressions for DS/FH, Quaternary DPSK With CW-Tone Jamming

$P_{QCW}(\overline{JR},\overline{JP})$	USE $P^{u}_{CW}(\overline{JR},\overline{JP})$ IN TABLE 6
$P_{QCW}(JR,\overline{JP})$ OR $P_{QCW}(\overline{JR},JP)$	USE $P^{u}_{CW}(JR,\overline{JP})$ OR $P^{u}_{CW}(\overline{JR},JP)$ IN TABLE 6
$P_{QCW}(JR,JP)$	USE $P^{u}_{CW}(JR,JP)$ IN TABLE 6

TABLE 6. Upper Bound Error Expressions for DS/FH, M-ary, DPSK With CW-Tone Jamming

$P_{CW}^{u}(\overline{JR},\overline{JP})$	$\operatorname{erfc}\left[\frac{A_s}{\sqrt{2N}}\right] + \frac{A_s}{\sqrt{2N\pi}} \int_0^{\pi/2} \exp\left(-\frac{A_s^2}{2N}\sin^2\theta\right)\left\{\operatorname{erfc}\left[\frac{A_s}{\sqrt{2N}}\cos(\theta+\theta_c)\right] + \operatorname{erfc}\left[\frac{A_s}{\sqrt{2N}}\cos(\theta-\theta_c)\right]\right\}\cos\theta\, d\theta$
$P_{CW}^{u}(JR,\overline{JP})$ OR $P_{CW}^{u}(\overline{JR},JP)$	$\operatorname{erfc}\left[\frac{A_s}{\sqrt{2N}}\right] + \frac{A_s}{\sqrt{2N\pi}} \int_0^{\pi/2} \exp\left(-\frac{A_s^2}{2N}\sin^2\theta\right)\left\{\frac{1}{2\pi}\int_0^{2\pi}\left(\operatorname{erfc}\left[\frac{A_s}{\sqrt{2N}}\cos(\theta+\theta_c) - \frac{A}{\sqrt{2N}}\sin\phi_2\right] + \operatorname{erfc}\left[\frac{A_s}{\sqrt{2N}}\cos(\theta-\theta_c) - \frac{A}{\sqrt{2N}}\sin\phi_2\right]\right) d\phi_2\right\}\cos\theta\, d\theta$
$P_{CW}^{u}(JR,JP)$	$\frac{1}{2\pi}\int_0^{2\pi} \operatorname{erfc}\left[\frac{A_s}{\sqrt{2N}} - \frac{A}{\sqrt{2N}}\sin\phi_1\right] d\phi_1 + \frac{A_s}{\sqrt{2N\pi^3}} \int_0^{\pi/2}\left\{\int_0^{2\pi} \exp\left[-\left(\frac{A_s}{\sqrt{2N}}\sin\theta - \frac{A}{\sqrt{2N}}\sin\phi_1\right)^2\right] d\phi_1\right\} \cdot \left\{\frac{1}{4\pi}\int_0^{2\pi}\left(\operatorname{erfc}\left[\frac{A_s}{\sqrt{2N}}\cos(\theta+\theta_c) - \frac{A}{\sqrt{2N}}\sin\phi_2\right] + \operatorname{erfc}\left[\frac{A_s}{\sqrt{2N}}\cos(\theta-\theta_c) - \frac{A}{\sqrt{2N}}\sin\phi_2\right]\right) d\phi_2\right\} \cdot \cos\theta\, d\theta$

TABLE 7. Error Expressions for DS/FH, Binary DPSK With FM Jamming

$P_{BFM}(\overline{JR},\overline{JP})$	$\frac{1}{2}\exp[-\frac{A_s^2}{2N}]$
$P_{BFM}(JR,\overline{JP})$ OR $P_{BFM}(\overline{JR},JP)$	$\frac{1}{2\pi}\int_o^{\pi}\{1-Q[\frac{1}{2}\sqrt{\frac{4A_s^2+4A_sA_x\cos\phi_1+A_x^2}{N}}\ ,\ \frac{1}{2}\frac{A_x}{\sqrt{N}}]$ $+Q[\frac{1}{2}\frac{A_x}{\sqrt{N}}\ ,\ \frac{1}{2}\sqrt{\frac{4A_s^2+4A_sA_x\cos\phi_1+A_x^2}{N}}]\}d\phi_1$
$P_{BFM}(JR,JP)$	$(\frac{1}{2\pi})^2\int_o^{2\pi}\int_o^{2\pi}\frac{1}{2}\{1-Q[\frac{1}{2}\sqrt{\frac{m_1^2+m_2^2}{N}}\ ,\ \frac{1}{2}\sqrt{\frac{m_3^2+m_4^2}{N}}]$ $+Q[\frac{1}{2}\sqrt{\frac{m_3^2+m_4^2}{N}}\ ,\ \frac{1}{2}\sqrt{\frac{m_1^2+m_2^2}{N}}]\}d\phi_1 d\phi_2$ $m_1^2+m_2^2 = 4A_s^2+4A_sA_x(\cos\phi_1+\cos\phi_2)+2A_x^2\cos(\phi_1-\phi_2)+2A_x^2$ $m_3^2+m_4^2 = 2A_x^2-2A_x^2\cos(\phi_1-\phi_2)$

TABLE 8. Error Expressions for DS/FH, Quaternary DPSK With FM Jamming

$P_{QFM}(\overline{JR},\overline{JP})$	USE $P^{u}_{FM}(\overline{JR},\overline{JP})$ IN TABLE 9
$P_{QFM}(JR,\overline{JP})$ OR $P_{QFM}(\overline{JR},JP)$	USE $P^{u}_{FM}(JR,\overline{JP})$ OR $P^{u}_{FM}(\overline{JR},JP)$ IN TABLE 9
$P_{QFM}(JR,JP)$	USE $P^{u}_{FM}(JR,JP)$ IN TABLE 9

TABLE 9. Upper Bound Error Expressions for DS/FH, M-ary DPSK With FM Jamming

$P^u_{FM}(\overline{JR},\overline{JP})$	$\operatorname{erfc}[\frac{A_s}{\sqrt{2N}}] + \frac{A_s}{\sqrt{2N\pi}} \int_o^{\pi/2} \exp(-\frac{A_s^2}{2N}\sin^2\theta)\{\operatorname{erfc}[\frac{A_s}{\sqrt{2N}}\cos(\theta+\theta_c)] + \operatorname{erfc}[\frac{A_s}{\sqrt{2N}}\cos(\theta-\theta_c)]\}\cos\theta d\theta$
$P^u_{FM}(JR,\overline{JP})$ OR $P^u_{FM}(\overline{JR},JP)$	$\operatorname{erfc}[\frac{A_s}{\sqrt{2N}}] + \frac{A_s}{\sqrt{2N\pi}} \int_o^{\pi/2} \exp(-\frac{A_s^2}{2N}\sin^2\theta) \cdot \{\frac{1}{2\pi}\int_o^{2\pi} (\operatorname{erfc}[\frac{A_s}{\sqrt{2N}}\cos(\theta+\theta_c) - \frac{A_x}{\sqrt{2N}}\sin\phi_2] + \operatorname{erfc}[\frac{A_s}{\sqrt{2N}}\cos(\theta-\theta_c) - \frac{A_x}{\sqrt{2N}}\sin\phi_2])d\phi_2\}\cos\theta d\theta$
$P^u_{FM}(JR,JP)$	$\frac{1}{2\pi}\int_o^{2\pi} \operatorname{erfc}[\frac{A_s}{\sqrt{2N}} - \frac{A_x}{\sqrt{2N}}\sin\phi_1]d\phi_1 + \frac{A_s}{\sqrt{2N\pi^3}} \int_o^{\pi/2} \{\int_o^{2\pi} \exp[-(\frac{A_s}{\sqrt{2N}}\sin\theta - \frac{A_x}{\sqrt{2N}}\sin\phi_1)]d\phi_1\} \cdot \{\frac{1}{4\pi}\int_o^{2\pi} (\operatorname{erfc}[\frac{A_s}{\sqrt{2N}}\cos(\theta+\theta_c) - \frac{A_x}{\sqrt{2N}}\sin\phi_2] + \operatorname{erfc}[\frac{A_s}{\sqrt{2N}}\cos(\theta-\theta_c) - \frac{A_s}{\sqrt{2N}}\sin\phi_2])d\phi_2\} \cdot \cos\theta d\theta$

CHAPTER XI

QUANTITATIVE PROCEDURES AND RESULTS

Because of the complexity exhibited by the majority of the subcases in Tables 1-9, closed form expressions for those subcases containing integrals are either unknown at this time or impossible to obtain. Therefore, numerical techniques are required to evaluate these complex expressions. It is the purpose of this chapter to present the numerical techniques involved, to illustrate the results of a typical analytical study, and to draw tentative conclusions as to the best system/jamming strategies.

Preliminaries

A few basic and important facts must be emphasized at this point. They are:

(1) The point in the system model at which the thermal noise and jamming powers are measured is very critical. Since demodulation systems require specific thermal noise limitations, it is normal to refer the thermal noise power to the input of the demodulation system. Therefore, for this analysis the signal-to-noise ratio (SNR), written as

$$\left(\frac{S}{N}\right)_D \triangleq \frac{A_s^2}{2N} \tag{11-1}$$

is that ratio measured at the demodulator input. If needed, the SNR at the output of the dehopping system or at the receiver input may be determined once $(S/N)_D$ is known. In fact, the frequency-dehopping output SNR is

$$\left(\frac{S}{N}\right)_F = \left(\frac{\omega_b}{p\omega_p}\right)\left(\frac{S}{N}\right)_D = \left(\frac{1}{pS_c}\right)\left(\frac{S}{N}\right)_D \tag{11-2}$$

which results in a receiver input SNR of

$$\left(\frac{S}{N}\right)_R = \frac{1}{N_s}\left(\frac{S}{N}\right)_F = \left(\frac{1}{pS_cN_s}\right)\left(\frac{S}{N}\right)_D \tag{11-3}$$

The amount of power expended by the jammer is a critical parameter. Therefore, it is advantageous to refer the jamming power to the input of the receiver. For CW-tone or FM jamming, the signal-to-jamming ratio (SJR) referred to the receiver input is

$$\left(\frac{S}{J}\right)_R = \left(\frac{A_s^2}{2}\right)/\left(\frac{A_j^2}{2}\right) = \frac{A_s^2}{A_j^2} \tag{11-4}$$

The SJR for noise jamming is

$$\left(\frac{S}{J}\right)_R = \frac{A_s^2}{2N_j} \tag{11-5}$$

If the SJR were required at the frequency-dehopping output or the demodulator input, the respective ratios would be

$$\left(\frac{S}{J}\right)_F = K_s \left(\frac{S}{J}\right)_R \quad \text{(CW-Tone,FM,Noise)} \tag{11-6}$$

and

$$\left(\frac{S}{J}\right)_D = \frac{K_s p S_c}{S_n} \left(\frac{S}{J}\right)_R \quad \text{(Noise)}$$

$$\left(\frac{S}{J}\right)_D = \frac{K_s}{(A)^2} \left(\frac{S}{J}\right)_R \quad \text{(CW-Tone)}$$

$$\left(\frac{S}{J}\right)_D = \frac{K_s}{(A_x)^2} \left(\frac{S}{J}\right)_R \quad \text{(FM)} \tag{11-7}$$

where A and A_x are defined at the end of Chapter X. Of course, if no jamming signal were present in the dehopped bandwidth, then

$$\left(\frac{S}{J}\right)_F = \infty$$

$$\left(\frac{S}{J}\right)_D = \infty \tag{11-8}$$

2. Up to this point, the type of filter has remained unspecified in order to maintain generality. For illustrative purposes the narrowband, bandpass filter considered is a Butterworth filter with

magnitude characteristic

$$A(\omega) = \frac{1}{[1+(\frac{\omega-\omega_c}{\omega_b})^{2K}]^{\frac{1}{2}}} \tag{11-9}$$

and phase characteristic [32]

$$\theta(\omega) = \arctan\left[\frac{b_{K-1}\cdot j^{K-2}\cdot\omega_n^{K-1}+b_{K-3}\cdot j^{K-4}\cdot\omega_n^{K-3}+\ldots+b_1\omega_n}{j^K\cdot\omega_n^K+b_{K-2}\cdot j^{K-2}\cdot\omega_n^{K-2}+\ldots+b_2\cdot j^2\cdot\omega_n^2+1}\right],$$

(K even)

$$= \arctan\left[\frac{j^{K-1}\cdot\omega_n^K + b_{K-2}\cdot j^{K-3}\cdot\omega_n^{K-2}+\ldots+b_1\omega_n}{b_{K-1}\cdot j^{K-1}\cdot\omega_n^{K-1}+b_{K-3}\cdot j^{K-3}\cdot\omega_n^{K-3}+\ldots+b_2\cdot j^2\cdot\omega_n^2+1}\right]$$

(K odd)

where (11-10)

$$j^2 = -1 \quad , \quad \omega_n = \frac{\omega-\omega_c}{\omega_b} \quad , \quad \omega_b = \frac{2\pi}{T_b}$$

$$b_{K-1} = \frac{1}{\sin(\frac{\pi}{2K})} = b_1$$

$$b_{K-2} = \frac{\cos(\frac{\pi}{2K})}{\sin(\frac{\pi}{K})}\cdot b_{K-1} = b_2$$

$$\vdots$$

$$b_{K-a} = \frac{\cos[(a-1)\frac{\pi}{2K}]}{\sin(\frac{a\pi}{2K})}\cdot b_{K-a+1} = b_a \tag{11-11}$$

(3) For maximum generality, the specific type of periodic modulation for the FM jamming signal has not been considered. In other words, the expressions in Chapter X are general enough to include any periodically modulated FM signal. However, in order to make comparisons with previous work [30], the linear-swept (Figure 7) FM signal, whose Fourier series coefficients are found in Appendix A, is considered.

Computational Organization

To carry out the numerical evaluation of the probability-of-error expressions, a computer program has been developed. The program has the extensive capability of accepting a set of signal, interference, and noise parameters, evaluating the error expressions for this set, and plotting the determined error rates. The specific organization of the program follows:

(1) The main program is used as a base from which all calculations are made. Parameter values such as the ranges of SNR and SJR, p, S_c, S_m, W_{fo}, K_s, N_s, M, β, and the Butterworth filter order (K) are all assigned specific values in the main program. The type of jamming signal is also chosen, as well as which variable (SNR or SJR) is to be plotted on the abscissa axis.

(2) Immediately following the input of the specified parameters and only for the CW-tone or FM jamming cases, the main program calculates the maximum envelope value for CW-tone jamming or the required RMS value of the FM jamming envelope. This is accomplished by first determining the appropriate set of Fourier series coefficients, and secondly, making a comparison of those envelope values generated by Eq. (5-26) or an RMS calculation at the maxchip of the envelope in Eq. (5-13). The RMS calculation at the maxchip is made by evaluating Eq. (5-13) at a discrete number of equally-spaced values on the interval $(0,2\pi)$, and then taking the square root of the average of the squared envelope values. See Appendix L for additional information on envelope calculations.

The envelope calculation step may not be required for two reasons: (a) if the jamming signal is noise only; or (b) if the specified parameters are such that the envelope maximum or the RMS of the envelope has been previously determined. For the second reason, such a situation may arise if SNR, SJR, K_s, N_s, or M either individually or simultaneously change and all envelope-related parameters remain fixed.

The actual Fourier series definitions for the

PR waveform and the FM signal require an infinite number of terms. However, for computational purposes, the series are truncated whenever the PR waveform representation reaches 95% of its power and the FM representation reaches 99% of its power. Only 95% is used for the PR waveform since a large number of additional terms are needed to obtain the next 4% of power with negligible increase in representation accuracy.

(3) Once the desired envelope value (if required) is calculated, the error expressions for the appropriate value of M and jamming signal are evaluated. All basic functions requiring evaluation are found through basic library routines or by special, individual subroutines attached to the main program. For example, the functions Q(c,d) and erfc(u) are not contained in a basic computer library but are evaluated by separate subroutines. The Marcum-Q function is calculated by a method proposed by Schnidman [56] with a general accuracy of one part in 10^{10}. An accuracy of one part in 10^{13} is achieved by calculating the complementary error function with a method developed by the Control Data Corporation [57].

The numerical integration routine is a fixed

step-size, Romberg integration scheme. Because the integrands are relatively smooth functions, a fixed rather than an adaptive step-size is possible. To insure good accuracy, an adaptive, Romberg integration routine with a relative accuracy of one part in 10^{10} was used to compare with the fixed step-size routine. A negligible difference resulted from the comparison.

(d) Finally, a CALCOMP plotting routine is used to plot the logarithm of the error rates versus SNR or SJR.

Based on the different analytical techniques utilized for M=2,4, and M>4, multiple cross-checks were made to establish a high degree of confidence in the numerical computations. For example, the bounds for the general M-ary situation (Chapter IX) were used, with M set equal to 2, to test the validity of the individually computed binary case. A similar test was carried out for M=4.

Basis for Parametric Comparison

A reference point, or points, must be established in order to make comparisons and draw conclusions. For this analysis, three reference points have been chosen. The first and primary reference point is the performance of a conventional, binary DPSK system in a white gaussian noise environment (S/J=∞). An advantage of such a reference is the common basis it establishes for all three jamming signals. Because of the interest in confirming the benefits of spread spectrum signaling, the final two reference points are the performance of an FH-DPSK system

and a conventional DPSK system, both of which are subjected to noise, CW-tone, and periodic FM jamming. These references are elaborated on now.

Gaussian Noise Reference

From Eq. (3-1) the jam-free performance of conventional, binary DPSK is

$$Pr(err) = \frac{1}{2} \exp[-\frac{S}{N}]$$

For illustrative purposes this reference is plotted in Figure 26. Because the performance of a DS/FH, binary DPSK system must approach the jam-free performance of Figure 26 for high SJR, Figure 27 is presented to illustrate the limiting effects of the jammed performance.

Reference Without DS

This reference depends on the type of jamming signal present. For each of the three different jamming signals, the system operates in two hopping slots with only one of the slots containing a jamming signal (i.e. $N_s = 2, K_s = 1$). The expressions in Chapter X may be used here with the following required parameter values:

(1) Noise Jamming

$$p = 1$$

$$S_c/S_n = 1$$

(2) CW-Tone Jamming

$$W_{fo} = 0$$

$$A_1 = A_2 = 1$$

(3) Periodic FM Jamming

$$W_{fo} = 0$$

$$\beta = 1$$

$$S_j = 1$$

$$K = 1$$

$$A_1 = A_2 = \text{RMS value of } j_i(t)\Big|_{t=0} \quad \text{where}$$

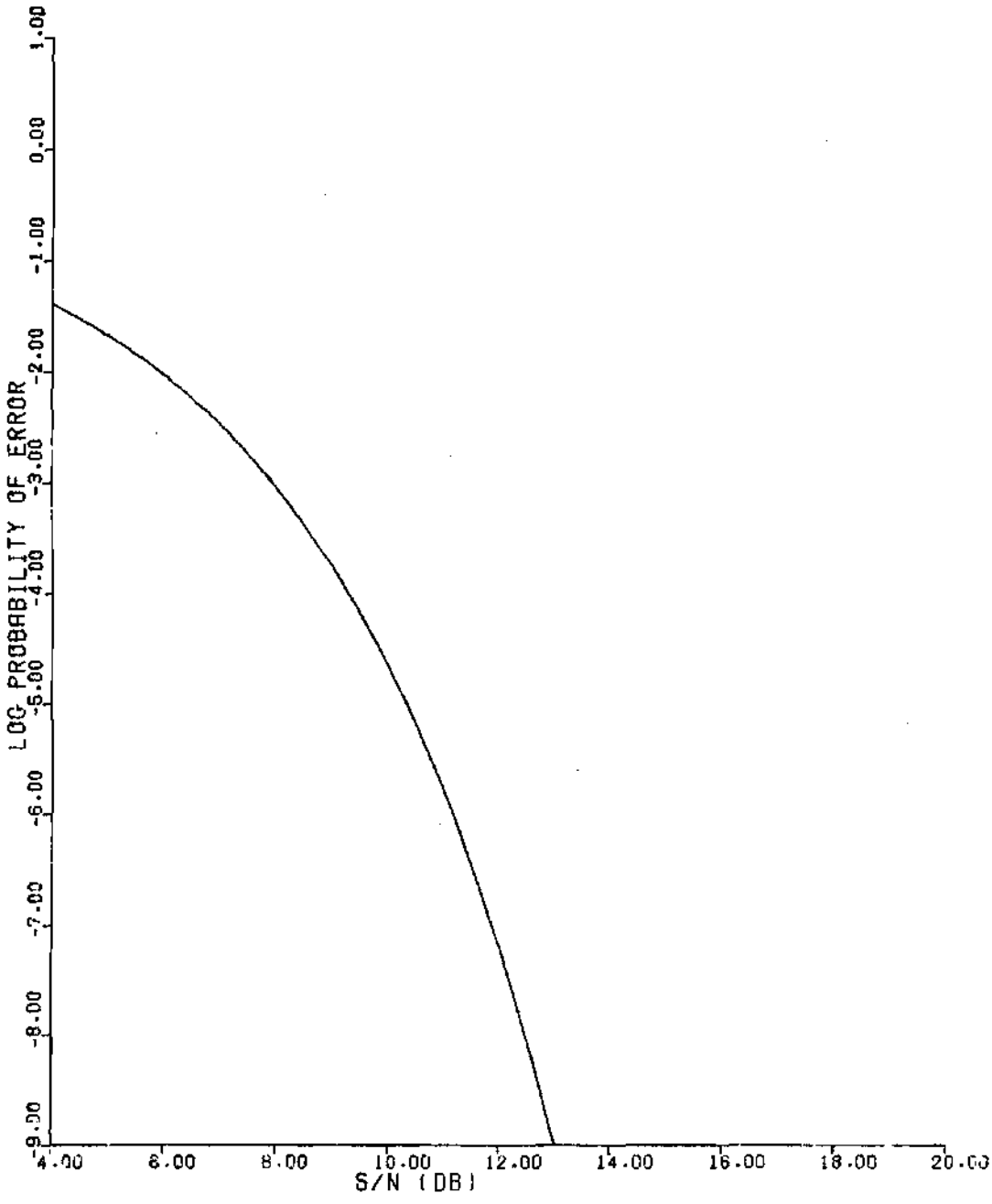

FIGURE 26. Probability of Error vs S/N for Binary DPSK in a White Gaussian Noise Environment (Jamless Case or S/J = ∞)

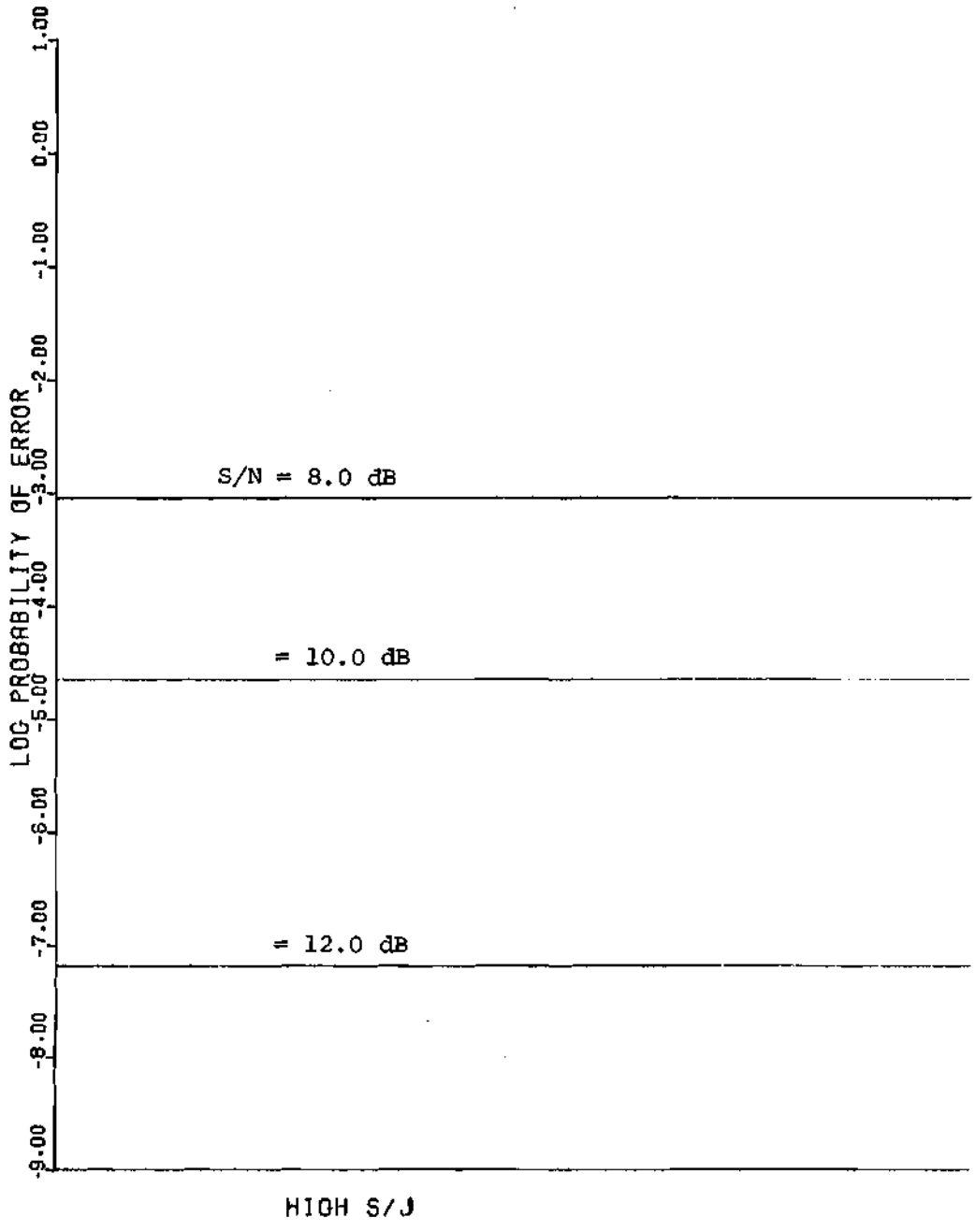

FIGURE 27. Probability of Error for High S/J and DS/FH, Binary DPSK Regardless of the Jamming Type

$$j_i(t)\Big|_{t=0} = \frac{1}{2}\{\sum_{n=-\infty}^{\infty} |a_n| A(w_j+nw_m)\cos(\phi_n - \theta(w_j+nw_m))\}^{\frac{1}{2}}$$

These references for binary FH-DPSK are shown in Figures 28-33. Two sets of references are shown for each jamming signal; the differences residing in the abscissa variable and the parameter variable.

Reference Without DS/FH

Previous results [26,30] are used here in order to establish references for each type of jamming environment. In the noise jamming case, the required binary, DPSK performance-reference is

$$P_{BNR}(err) = \frac{1}{2}\exp\left[-\frac{A_s^2}{2(N+N_j)}\right] \qquad (11\text{-}12)$$

$$= \frac{1}{2}\exp\left[\frac{-(S/N)(S/J)}{(S/J + S/N)}\right]$$

where N_j is the total jamming power and

$$\frac{S}{N} = \frac{A_s^2}{2N}$$

$$\frac{S}{J} = \frac{A_s^2}{2N_j} \qquad (11\text{-}13)$$

For the cochannel, CW-tone situation, the reference is [26]

$$P_{BCWR}(err) = \frac{1}{2}Q\left[\frac{A_j}{\sqrt{N}}, \frac{A_s}{\sqrt{N}}\right]$$

$$= \frac{1}{2}Q\left[\sqrt{2\frac{J}{N}}, \sqrt{2\frac{S}{N}}\right] \qquad (11\text{-}14)$$

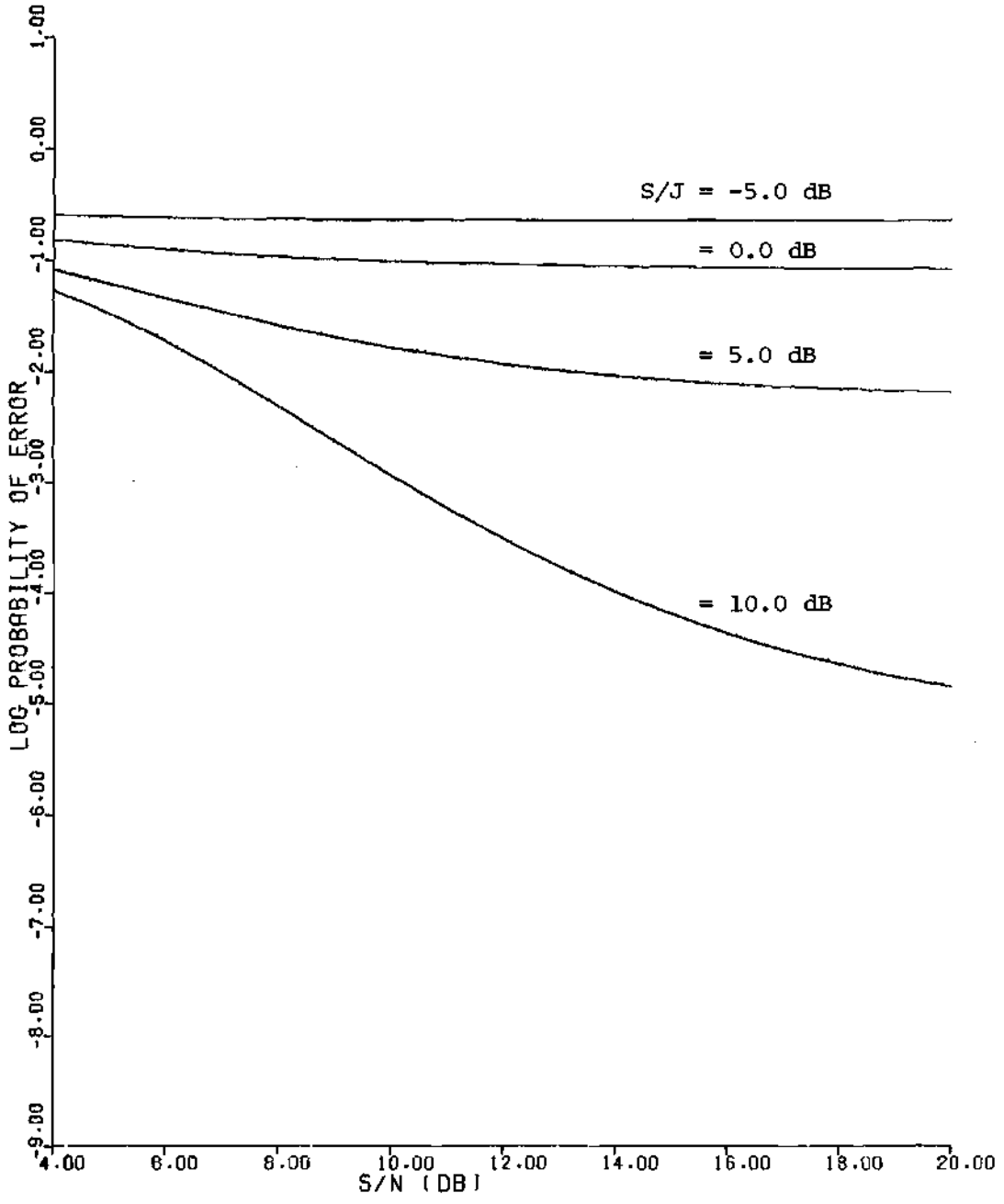

FIGURE 28. Reference Curves Without DS and vs S/N: FH, Binary DPSK; Noise Jamming; N_s=2, K_s=1

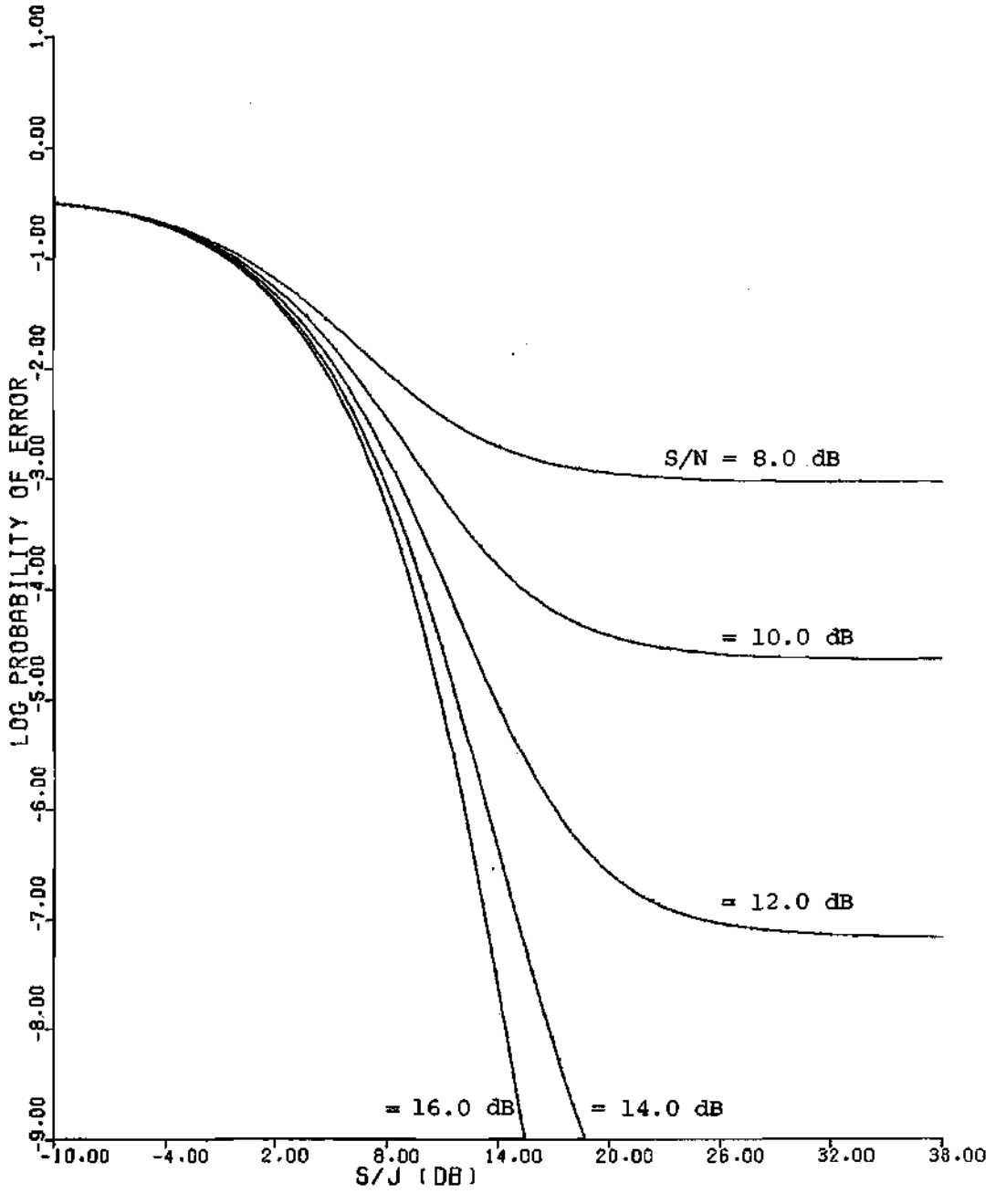

FIGURE 29. Reference Curves Without DS and vs S/J: FH, Binary DPSK; Noise Jamming; N_s=2, K_s=1

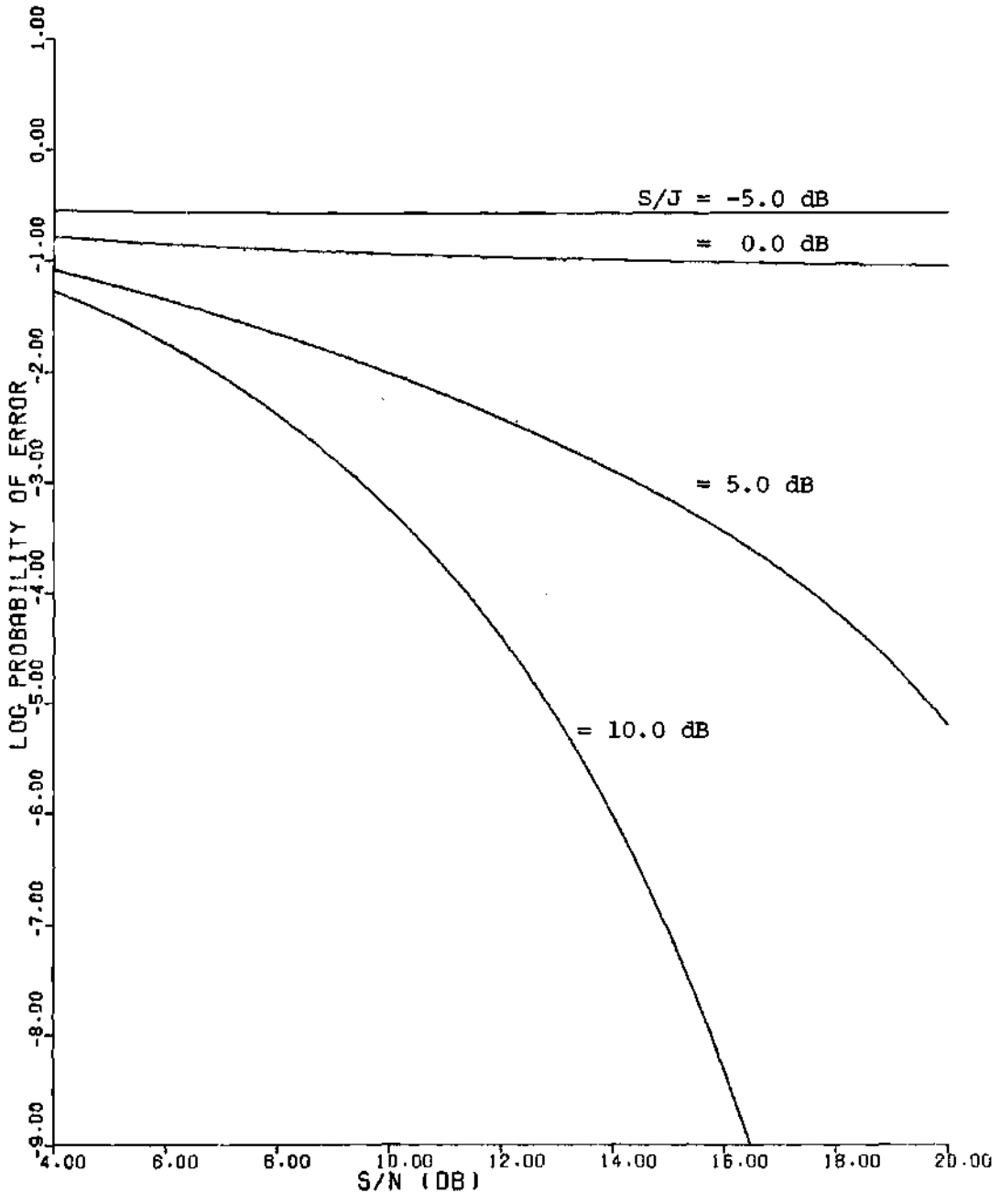

FIGURE 30. Reference Curves Without DS and vs S/N: FH, Binary DPSK; Cochannel, CW-Tone Jamming; N_s=2, K_s=1

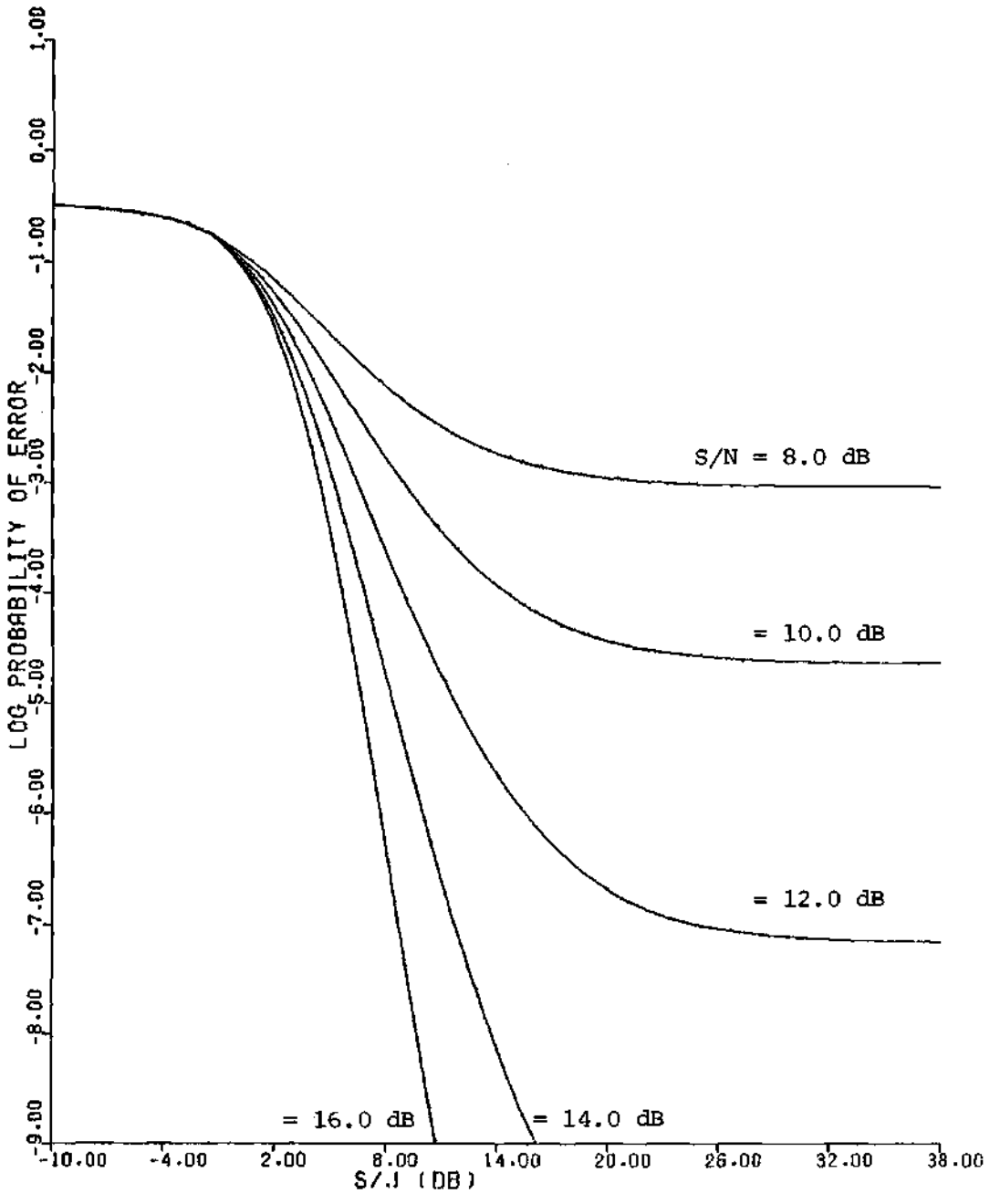

FIGURE 31. Reference Curves Without DS and vs S/J: FH, Binary DPSK; Cochannel, CW-Tone Jamming; N_s=2, K_s=1

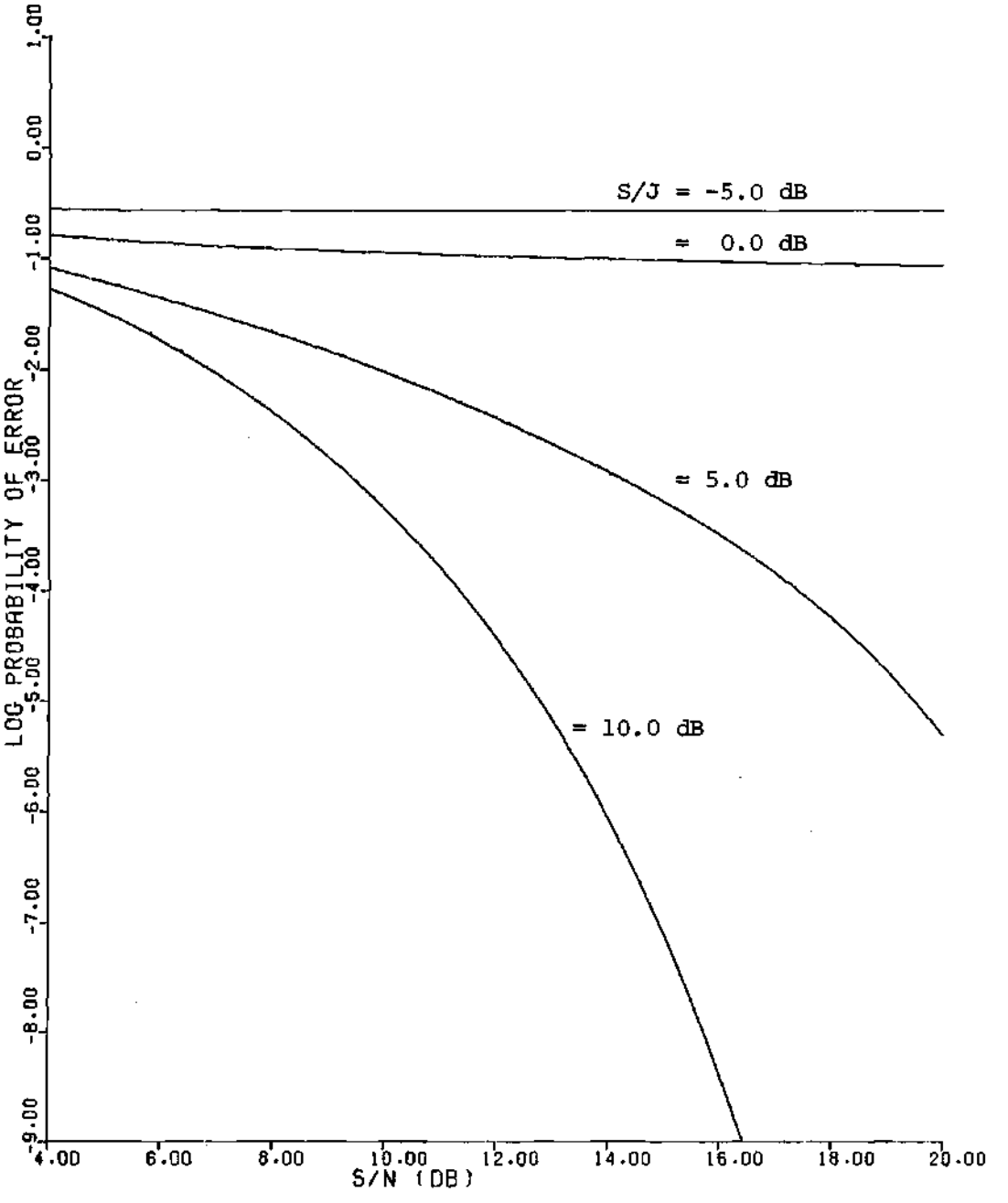

FIGURE 32. Reference Curves Without DS and vs S/N: FH, Binary DPSK; Cochannel, Linear FM Jamming; β=1, S_j=1, K=1, N_s=2, K_s=1

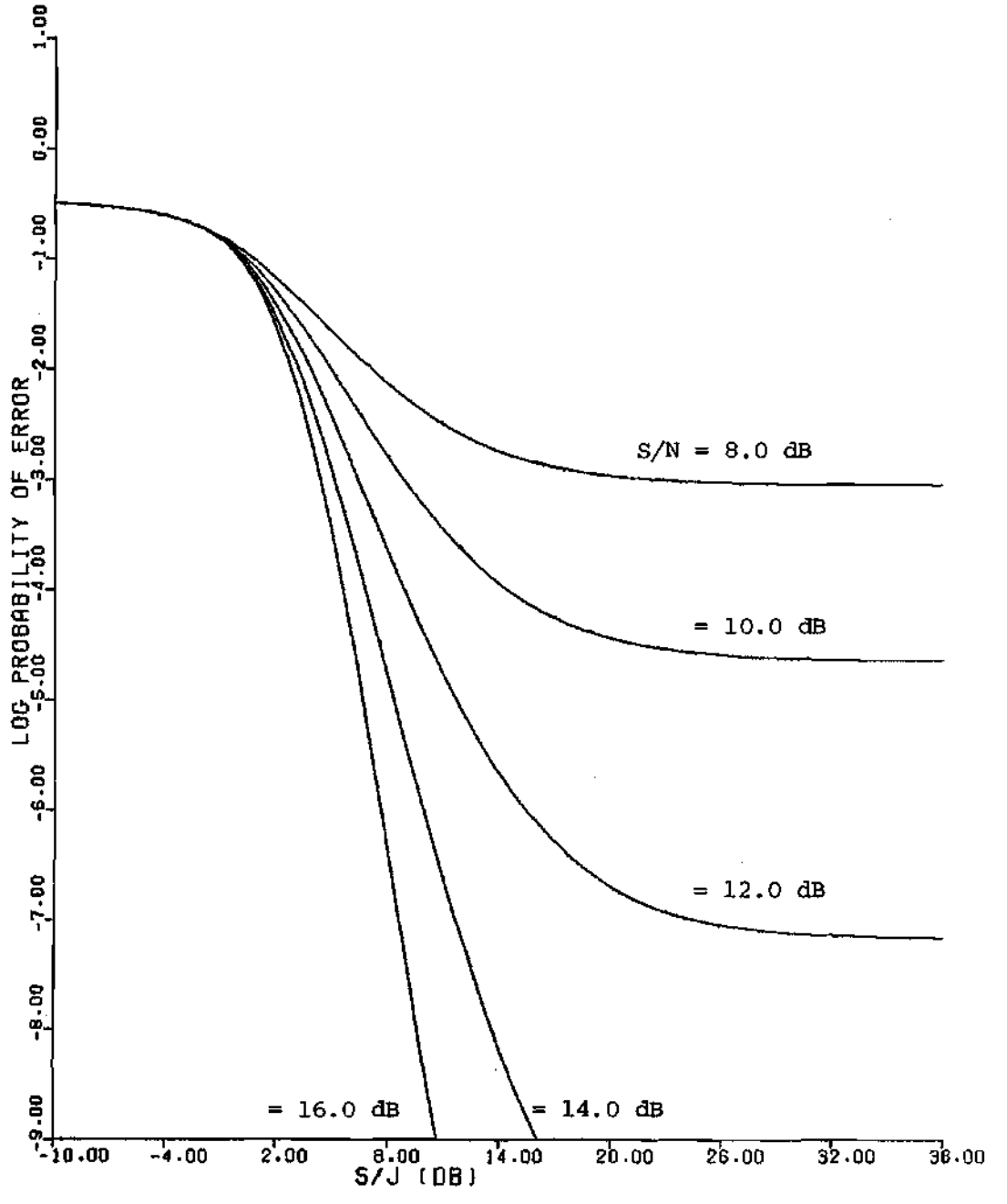

FIGURE 33. Reference Curves Without DS and vs S/J: FH, Binary DPSK; Cochannel, Linear FM Jamming; β=1, S_j=1, K=1, N_s=2, K_s=1

where the jamming-to-noise power ratio (JNR) and the SNR are

$$\frac{J}{N} = \frac{A_j^2}{2N}$$

$$\frac{S}{N} = \frac{A_s^2}{2N} \qquad (11\text{-}15)$$

Finally, and from [30], the performance reference for the periodic FM jamming case is

$$P_{BFMR}(err) = \frac{1}{4\pi} \int_o^{2\pi} Q\left[\frac{A_j}{\sqrt{N}} \cdot A_j(x), \frac{A_s}{\sqrt{N}}\right] dx$$

$$= \frac{1}{4\pi} \int_o^{2\pi} Q\left[\sqrt{2\frac{J}{N}}\ A_j(x)\ ,\ \sqrt{2\frac{S}{N}}\right] dx \qquad (11\text{-}16)$$

where $A_j(x)$ is the envelope of the filtered FM signal as a function of the offset parameter at t=0 and

$$W_{fo} = 0$$

$$\beta = 1$$

$$S_j = 1$$

$$K = 1 \qquad (11\text{-}17)$$

The combined results are illustrated in Figures 34-39 where again two sets of reference curves are plotted for each jamming signal. Notice that in this non-spread situation, noise jamming is more destructive to system performance than CW-tone or periodic-FM for large

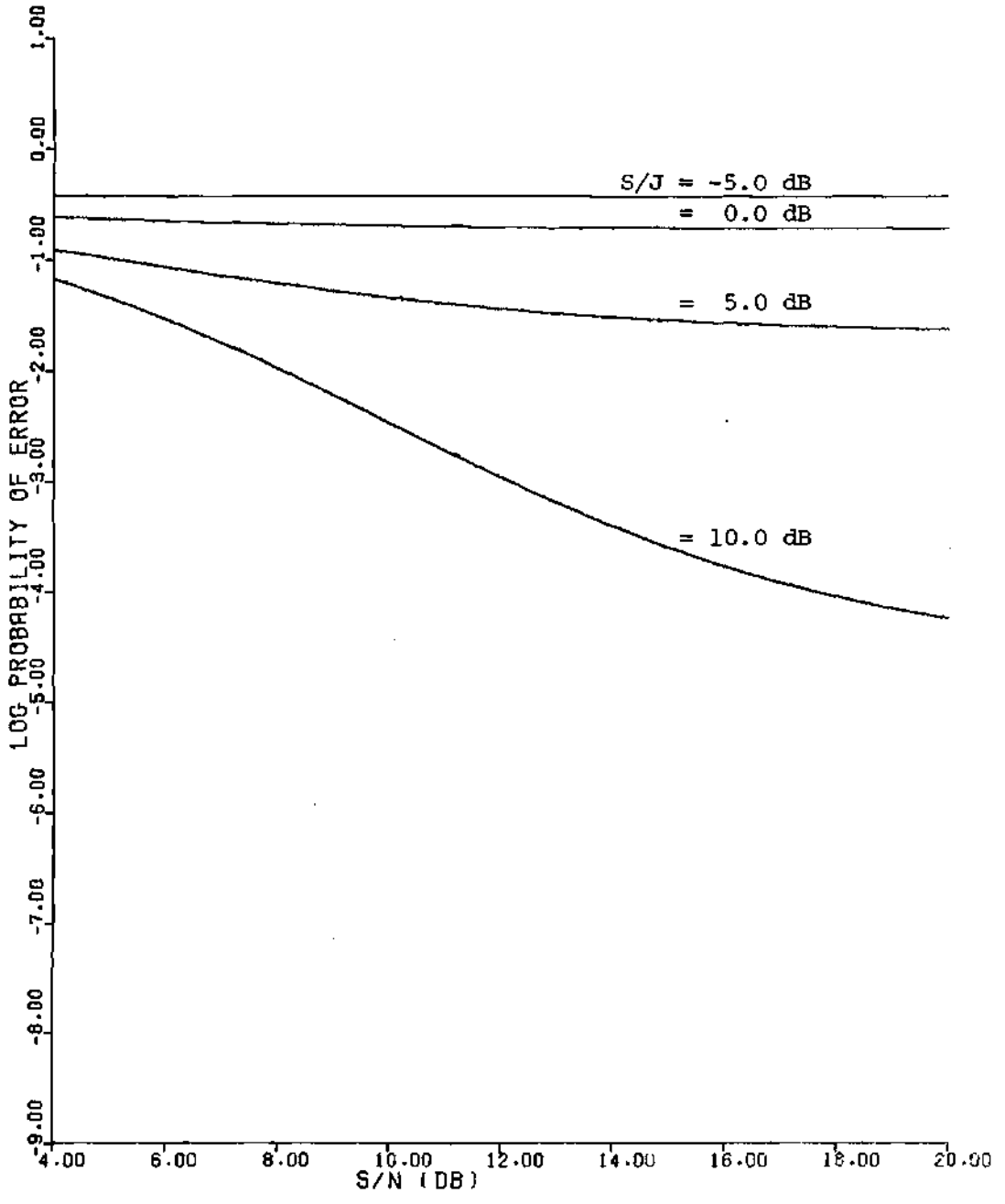

FIGURE 34. Reference Curves Without DS/FH and vs S/N: Binary DPSK; Noise Jamming

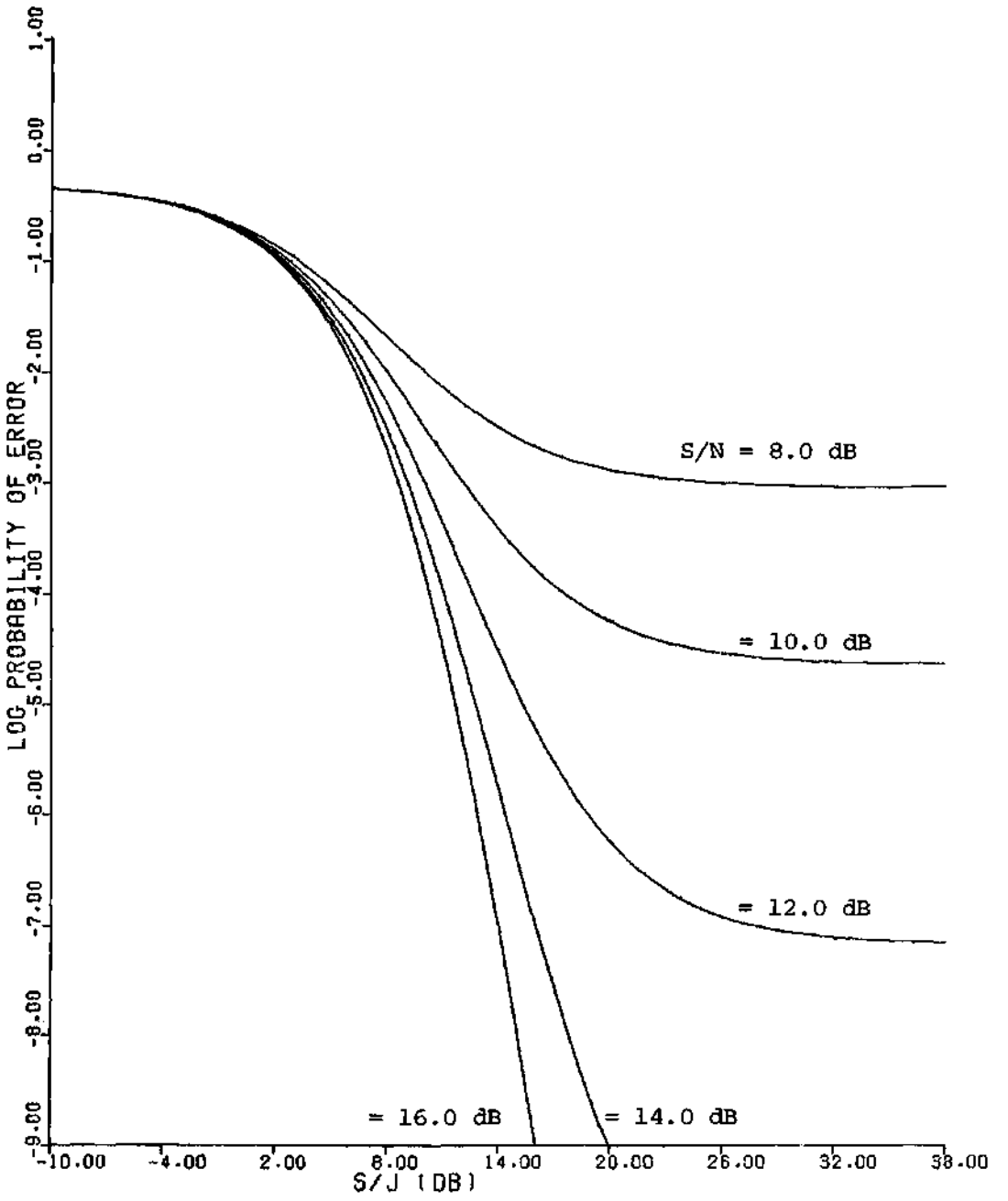

FIGURE 35. Reference Curves Without DS/FH and vs S/J: Binary DPSK; Noise Jamming

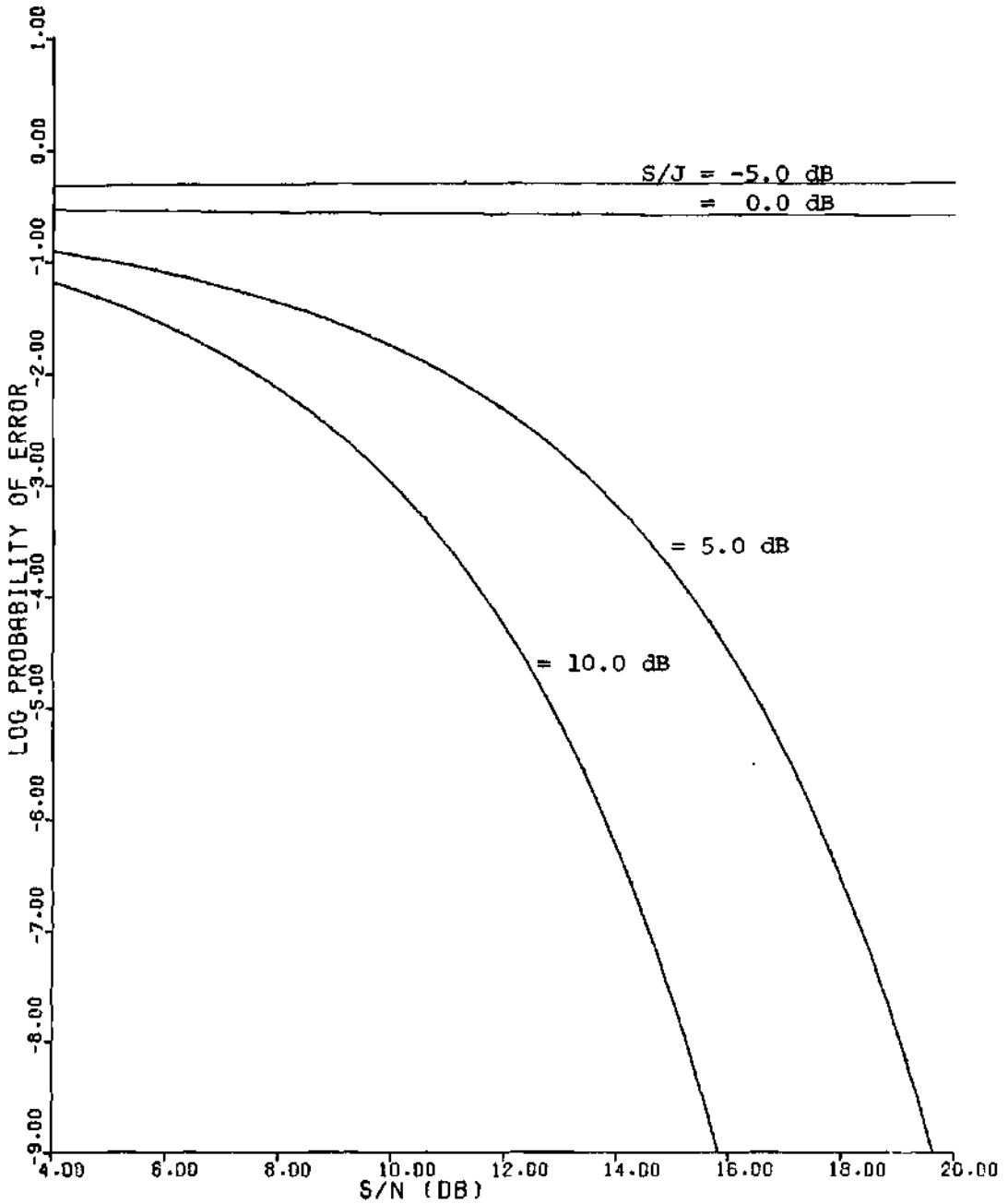

FIGURE 36. Reference Curves Without DS/FH and vs S/N: Binary DPSK; Cochannel, CW-Tone Jamming

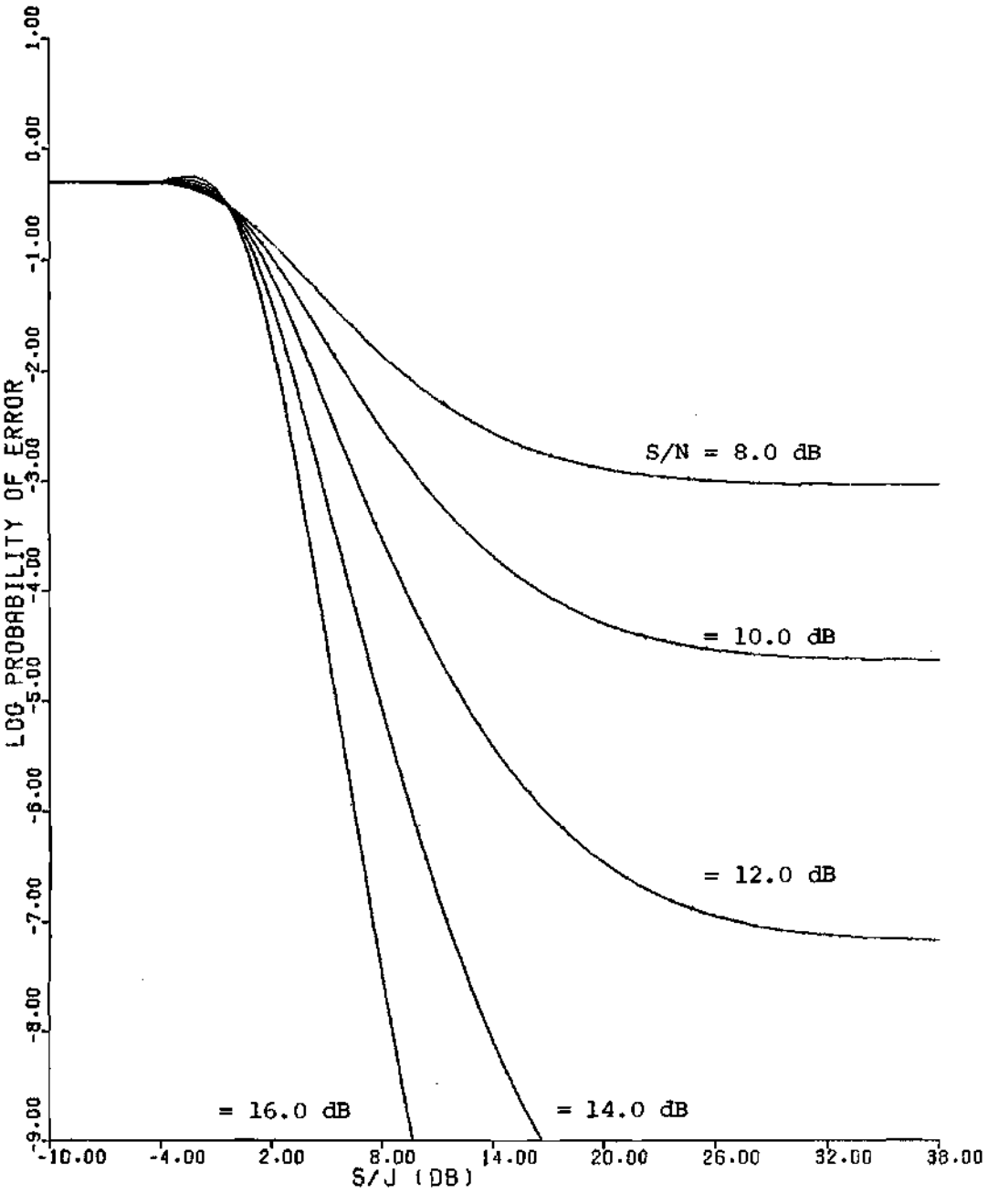

FIGURE 37. Reference Curves Without DS/FH and vs S/J: Binary DPSK; Cochannel, CW-Tone Jamming

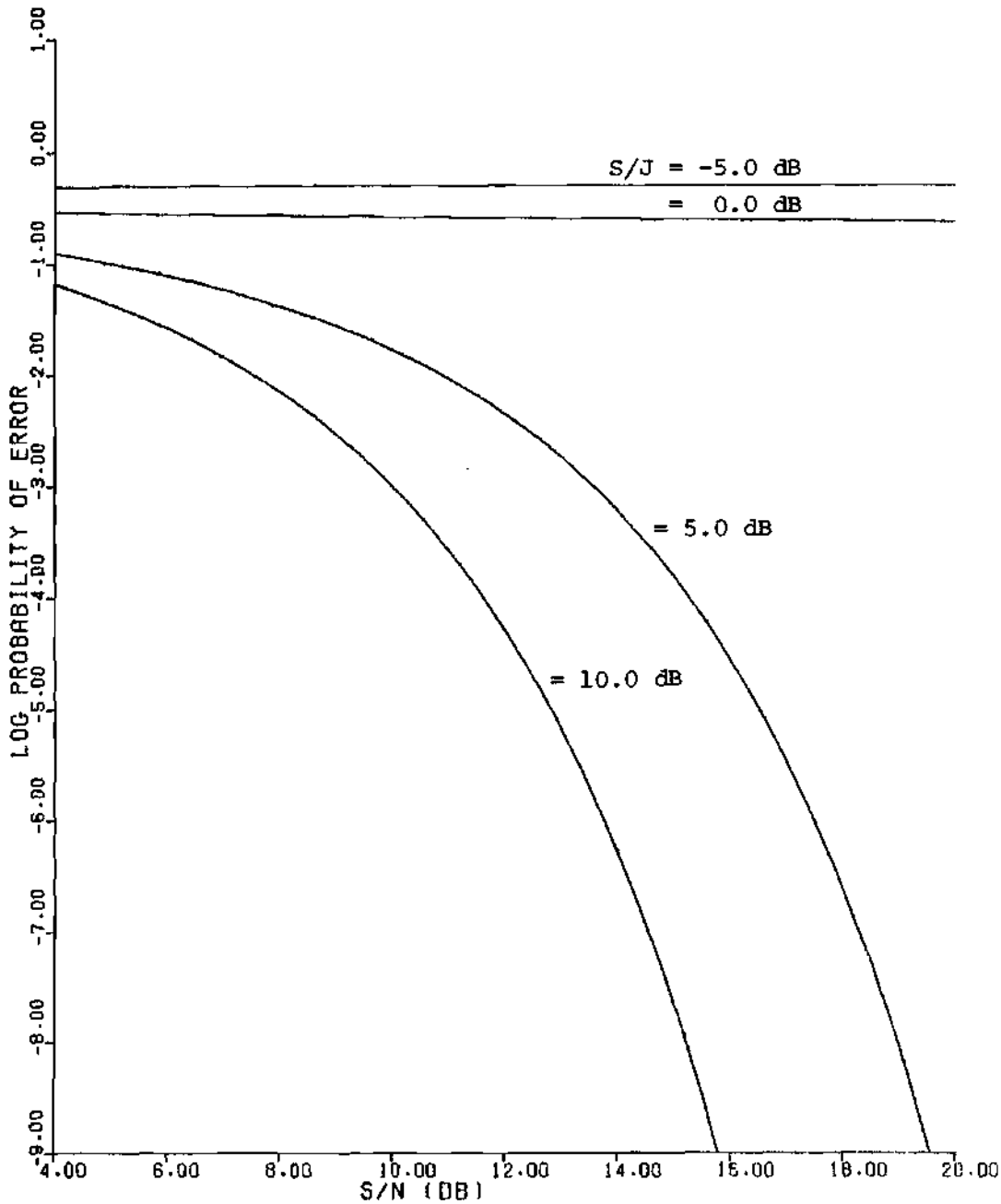

FIGURE 38. Reference Curves Without DS/FH and vs S/N: Binary DPSK; Cochannel, Linear FM Jamming; β=1, S_J=1, K=1

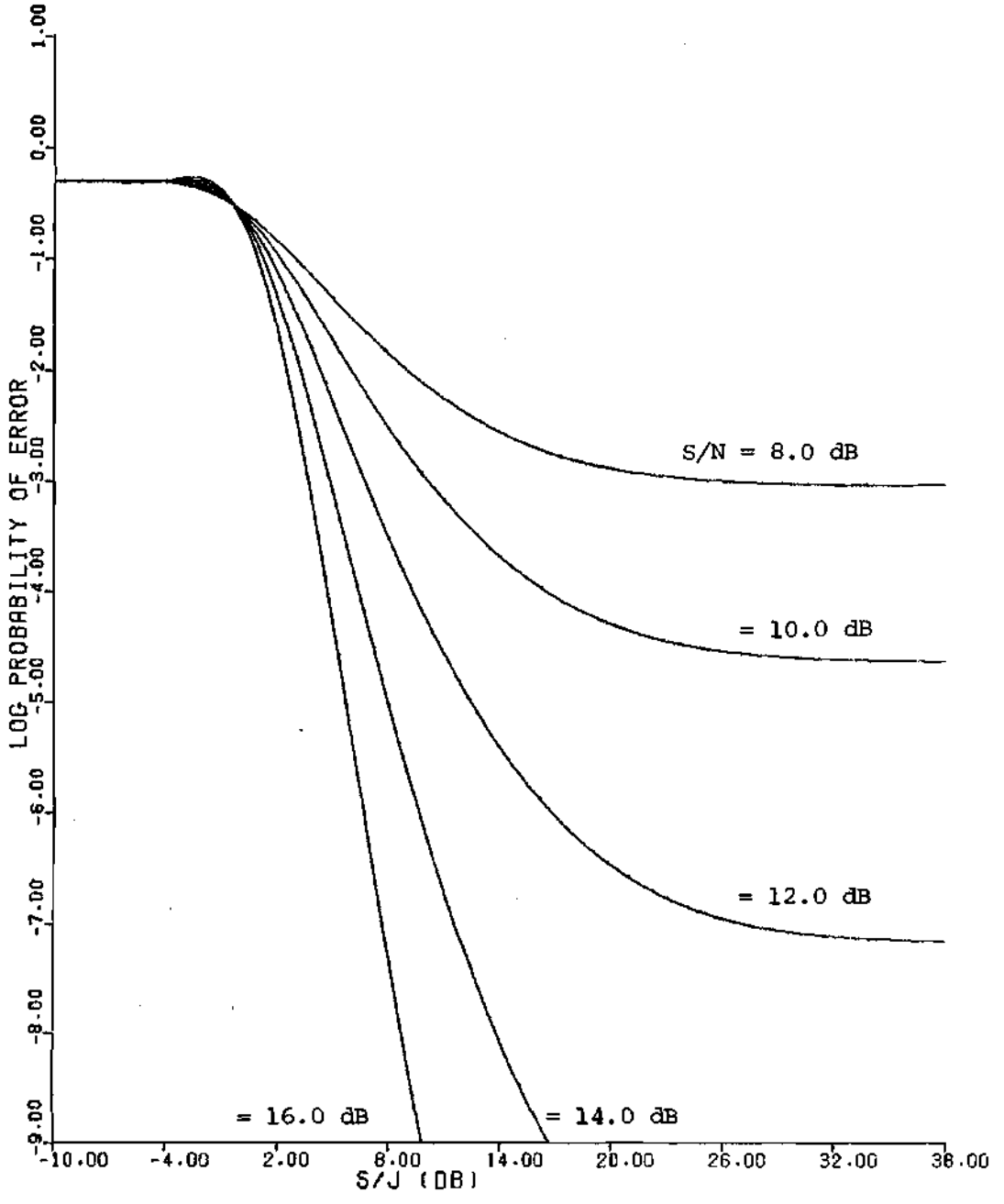

FIGURE 39. Reference Curves Without DS/FH and vs S/J: Binary DPSK; Cochannel, Linear FM Jamming; β=1, S_j=1, K=1

SJR. However, for a low SJR, it is seen that CW-tone and periodic-FM produce larger error rates.

As an interesting sidenote, $P_{BFMR}(err)$ was also calculated by using the RMS approximation method. In other words

$$P_{BFMR}(err) = \frac{1}{2} Q \left[\sqrt{2 \frac{J}{N}} \; A_{RMS} \; , \; \sqrt{2 \frac{S}{N}} \right] \tag{11-18}$$

where

$$A_{RMS} = RMS(A_j(x))$$

The results of this approximation and the actual averaging were nearly indistinguishable.

General Results and Preliminary Conclusions

In order to exemplify some typical results obtainable during an extensive parametric study, Figures 40-45 are presented. As before, there are two sets of curves for each jamming signal. The first set for each jamming signal has an abscissa variable equal to the SNR whereas the second set uses the SJR as the abscissa variable. In all cases the following parameter values are used:

$$\begin{aligned} p &= 31 \\ S_c &= 1 \\ N_s &= 2 \\ K_s &= 1 \end{aligned} \tag{11-19}$$

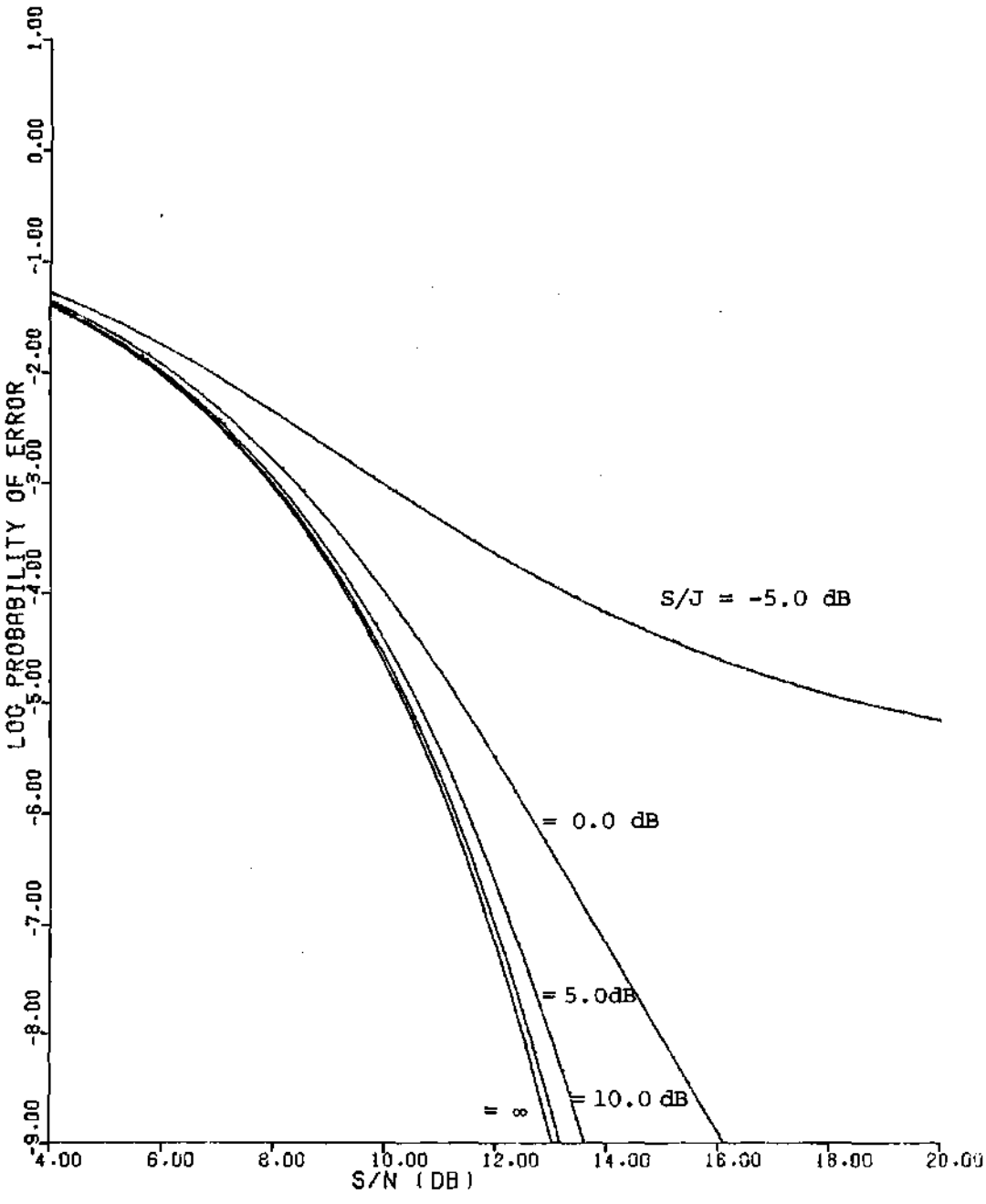

FIGURE 40. Probability of Error vs S/N: DS/FH, Binary DPSK; Noise Jamming; p=31, S_c=1, N_s=2, K_s=1

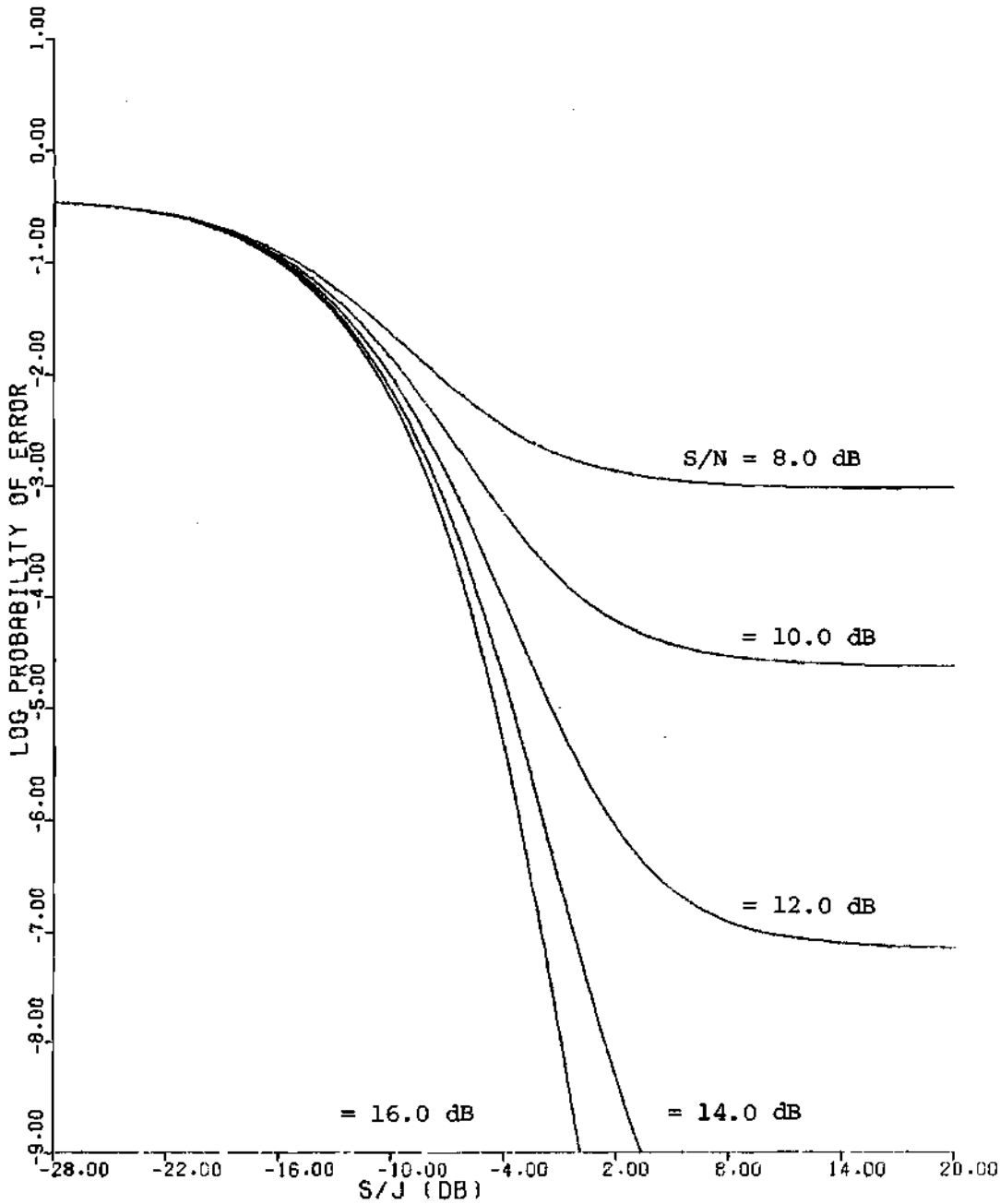

FIGURE 41. Probability of Error vs S/J: DS/FH, Binary DPSK; Noise Jamming; p=31, S_c=1, N_s=2, K_s=1

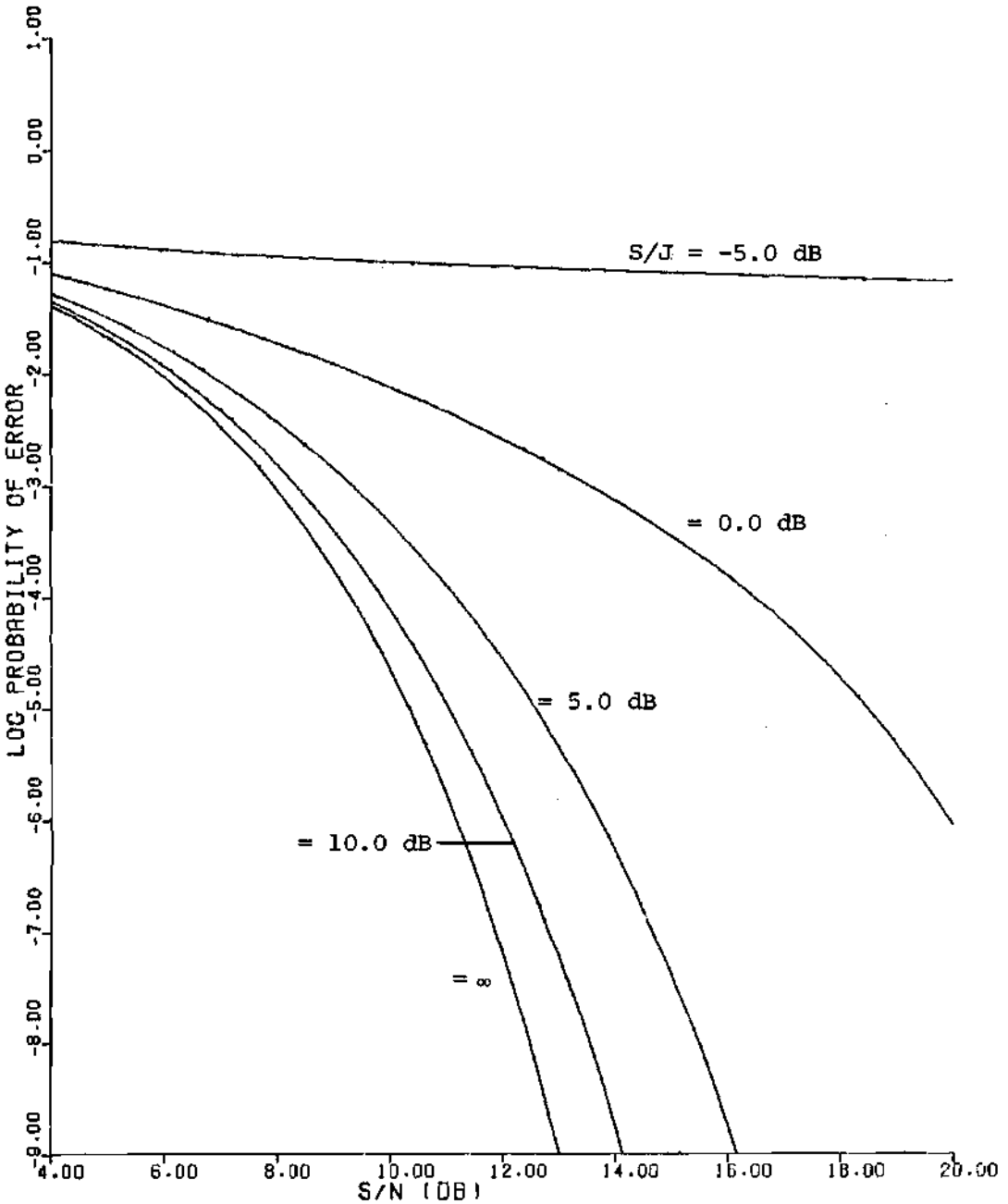

FIGURE 42. Probability of Error vs S/N: DS/FH, Binary DPSK; Cochannel, CW-Tone Jamming; p=31, S_c=1, N_s=2, K_s=1

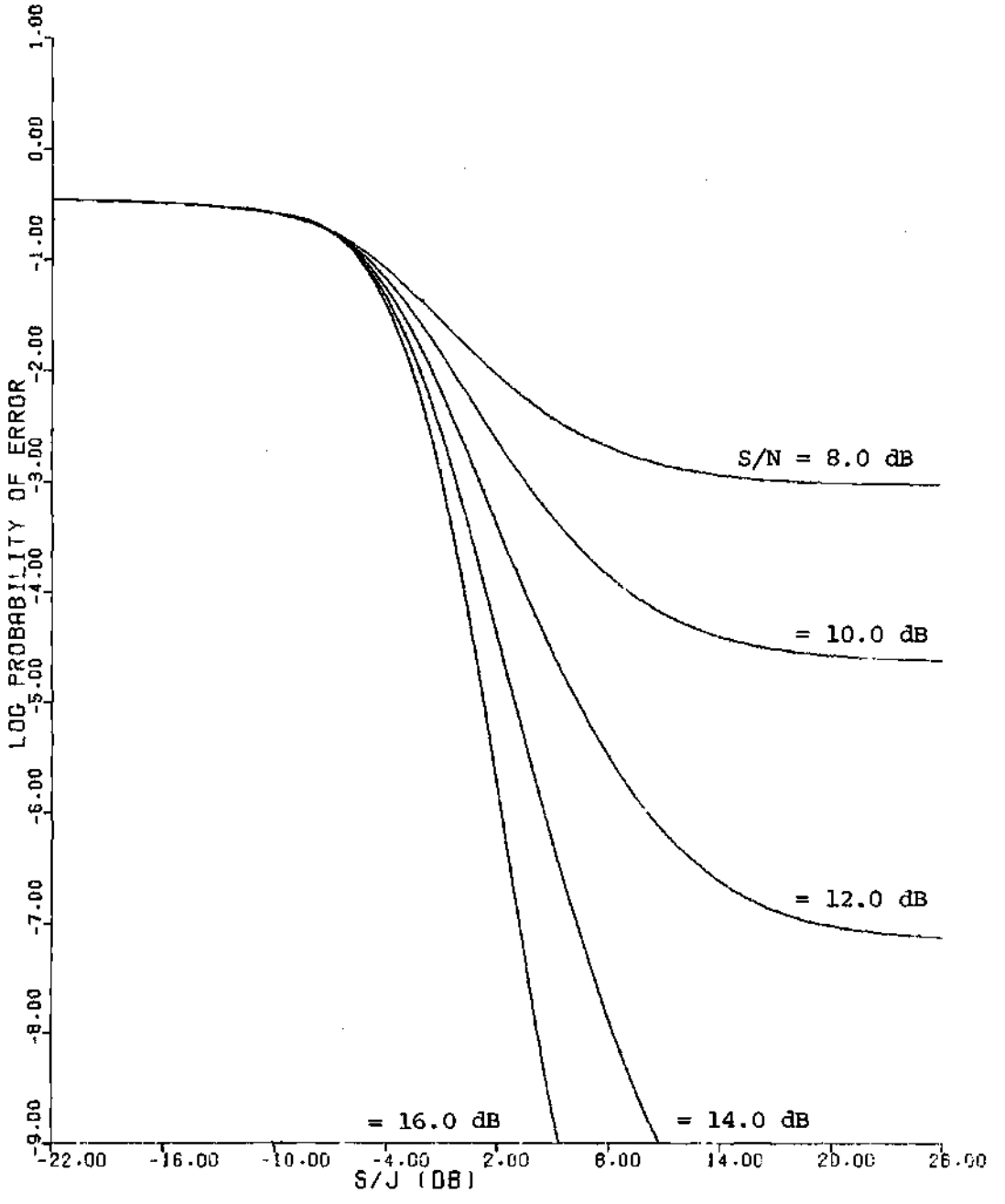

FIGURE 43. Probability of Error vs S/J: DS/FH, Binary DPSK; Cochannel, CW-Tone Jamming; p=31, S_c=1, K=1, N_s=2, K_s=1

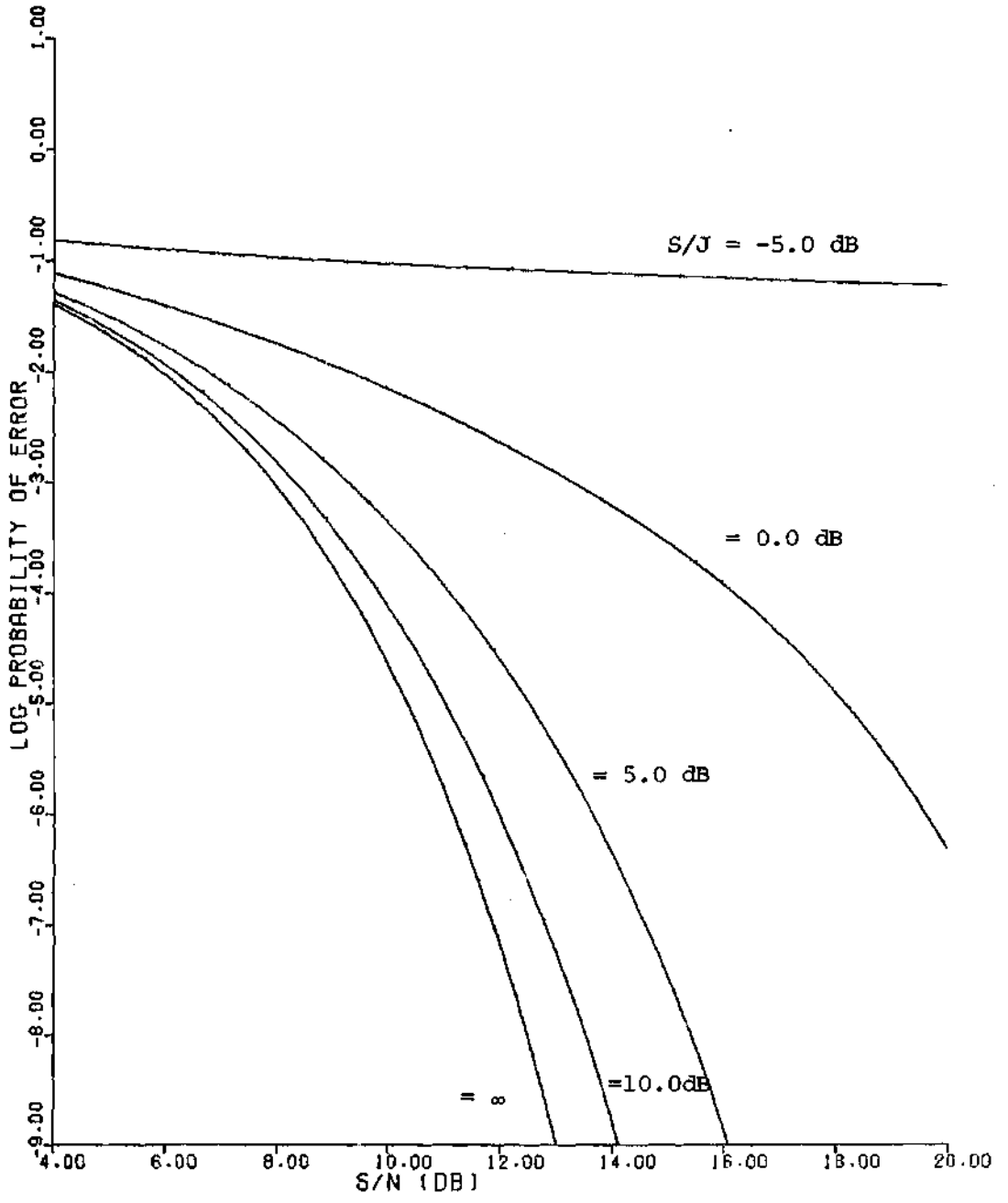

FIGURE 44. Probability of Error vs S/N: DS/FH, Binary DPSK; Cochannel, Linear FM Jamming; p=31, S_c=1, β=1, S_j=1, K=1, N_s=2, K_s=1

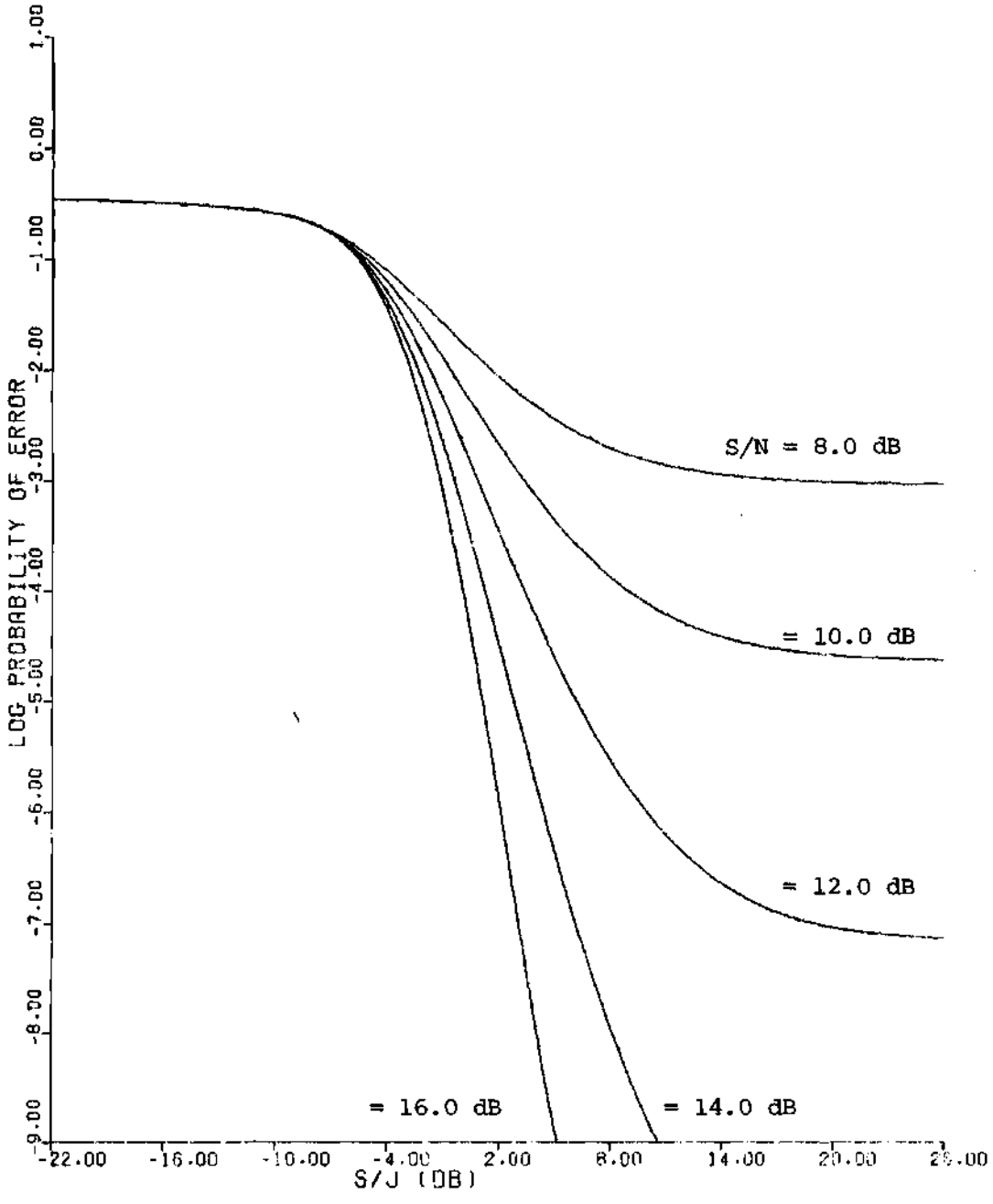

FIGURE 45. Probability of Error vs S/J: DS/FH, Binary DPSK; Cochannel, Linear FM Jamming; p=31, S_c=1, β=1, S_j=1, K=1, N_s=2, K_s=1

The CW-tone and periodic FM jamming signals are both cochannel (W_{fo} = 0) and are filtered by a first order (K=1) Butterworth filter. A unity modulation index (β=1) and a jamming slip ratio (S_j=1) are also used to complete the description of the FM jamming signal.

Jamming Degradation

From Figures 40-45, it is clearly evident that the effects of jamming become quite noticeable for low S/J ratios. For example, a binary DPSK system operating in white gaussian noise only performs at an error rate of $.7 \times 10^{-7}$ for an S/N of 12 dB. At the same S/N this performance is drastically reduced to an error rate of .2 for a non-spread, binary DPSK system (Figure 34), and reduced to an error rate of $.3 \times 10^{-5}$ for a DS/FH, binary DPSK system (Figure 40) upon subjection to a noise jamming environment with S/J = 0 dB. The effectiveness in a jamming environment of the DS/FH system over the non-spread system is certainly demonstrated here since the performance of the DS/FH system is significantly superior. To reach the "jamless" performance level ($.7 \times 10^{-7}$), the DS/FH system subjected to noise jamming (S/J = 0 dB) must increase its signal power by 2 dB (from Figure 40).

The amount of performance reduction exhibited in moving from the "jamless" state to the "jammed" state depends on the type of jamming signal. It was shown above that an error rate increase from $.7 \times 10^{-7}$ to $.3 \times 10^{-5}$ (DS/FH) was obtained for an S/J of 0 dB and an S/N of 12 dB. For the same S/N and S/J but with a CW-tone jamming signal, the resultant "jammed" error rate is $.2 \times 10^{-2}$; a maximum signal power increase of approximately 9 dB would be required to maintain the "jamless" error rate of $.7 \times 10^{-7}$.

Spot vs. Barrage Jamming

As Figures 46 and 47 indicate, a DS/FH system is much more susceptible to a spot jammer (CW-tone) than to a barrage type of jamming (noise). For the spot and barrage jamming modes with S/J = 0 dB, Table 10 presents the amount of signal power increase that would be required to maintain an error rate equivalent to that rate achieved by a "jam-free" system. A considerable amount of additional signal power is required for a specific error rate if the system is being jammed by a CW-tone signal. Additional power is also required in a noise jamming environment but to a much lessor extent. Because the performance curves for the system in a CW-tone environment are upper bounds to the average performance, the power increases in Table 10 are also upper bounds.

Spot vs. Swept-Spot Jamming

Table 11 and Figures 48 and 49 illustrate the comparison of the effectiveness of spot (CW-tone) and swept-spot (FM) jamming on a DS/FH, binary DPSK system. Derived from Figure 48 and Table 10, Table 11 presents upper bounds to the signal power increase required to maintain the same error rate as the "jamless" system for an S/J of 0 dB.

From a jammer's point of view, Table 11 indicates that the effectiveness of the spot and swept-spot jamming signal is nearly identical, with the spot jamming holding a slight edge. A logical reason for a spot jammer to degrade the performance slightly more than the swept-spot resides in the fact that the swept-spot jammer has a larger bandwidth and hence contributes less jamming power in the demodulator bandwidth. However, Table 11 and some results to be discussed shortly indicate that the larger FM bandwidth is not a significant parameter.

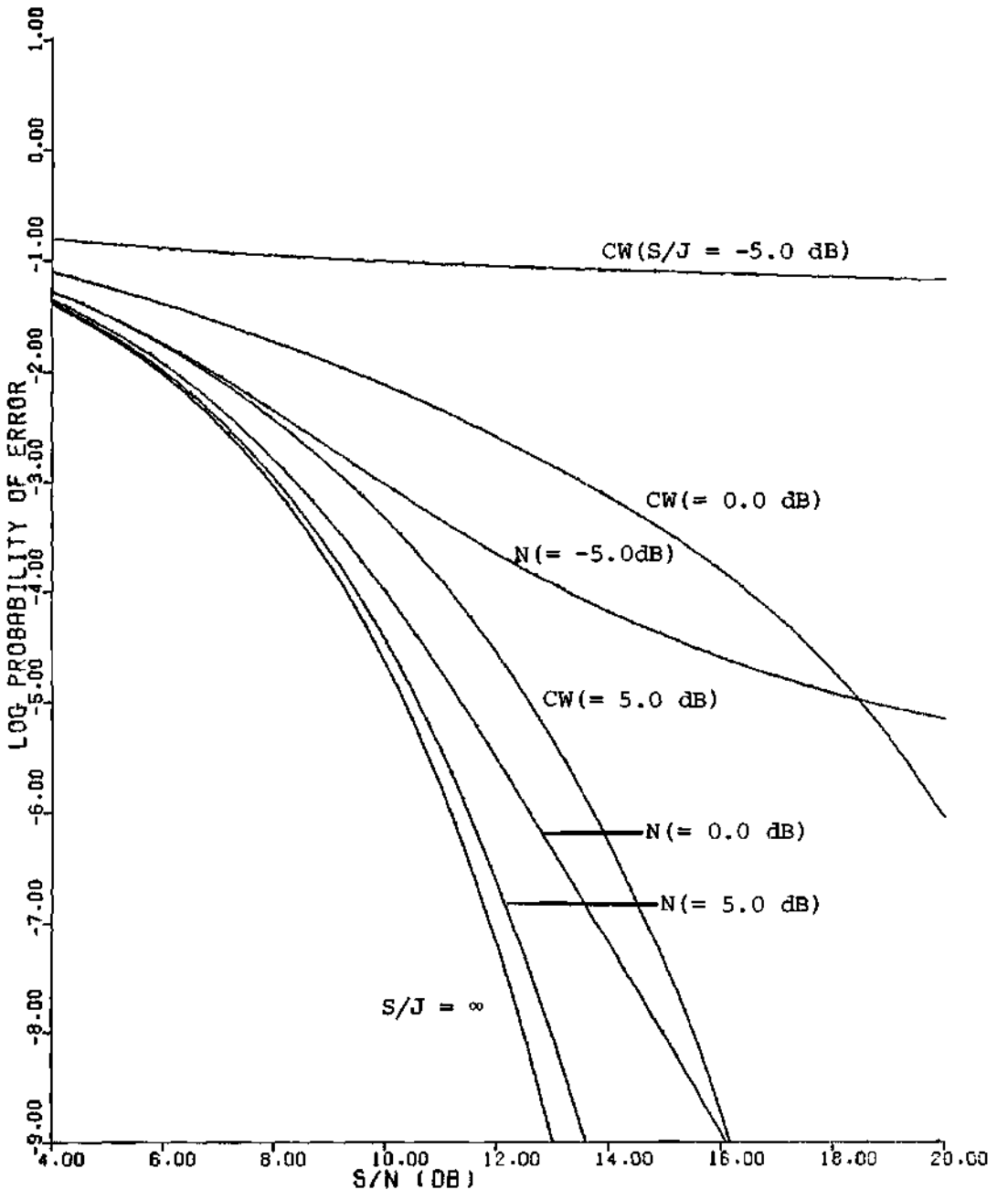

FIGURE 46. Comparison of Spot (Cochannel, CW-Tone) and Barrage (Noise) Jamming Error Rates vs S/N: DS/FH, Binary DPSK; p=31, S_c=1, K=1, N_s=2, K_s=1

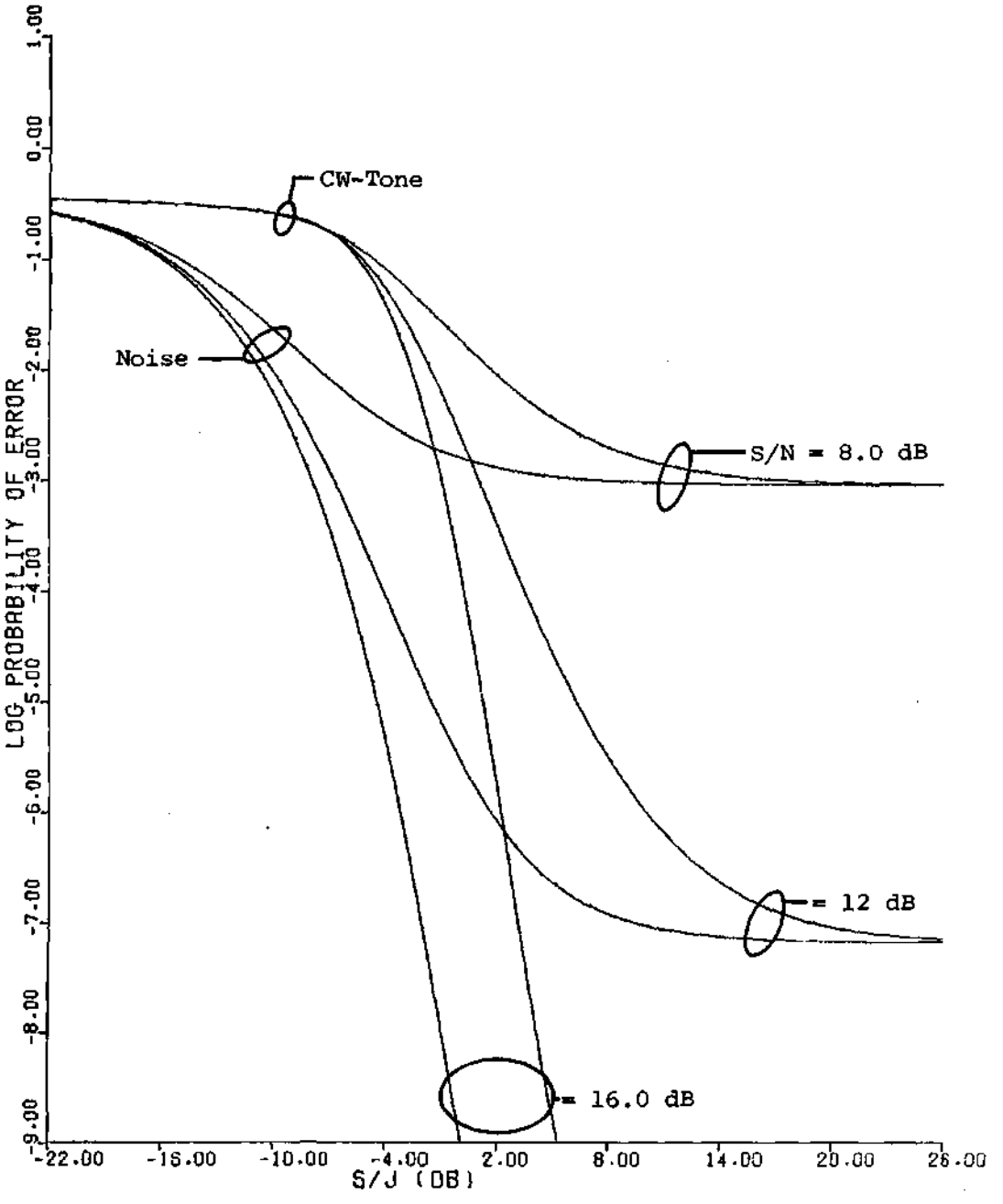

FIGURE 47. Comparison of Spot (Cochannel, CW-Tone) and Barrage (Noise) Jamming Error Rates vs S/J: DS/FH, Binary DPSK; p=31, S_c=1, K=1, N_s=2, K_s=1

TABLE 10. Signal Power Increase Required to Maintain the Jam-Free Error Rate in a Spot and Barrage Jamming Environment with S/J = 0 dB

$\frac{S}{N}$ (dB)	JAM-FREE ERROR RATE	SIGNAL POWER INCREASE (dB)	
		NOISE	CW-TONE (MAX)
4	$.4 \times 10^{-1}$	0.0	2.0
6	$.9 \times 10^{-2}$	0.5	3.5
8	$.9 \times 10^{-3}$	0.7	5.8
10	$.2 \times 10^{-4}$	1.0	7.8
12	$.7 \times 10^{-7}$	2.0	9.0

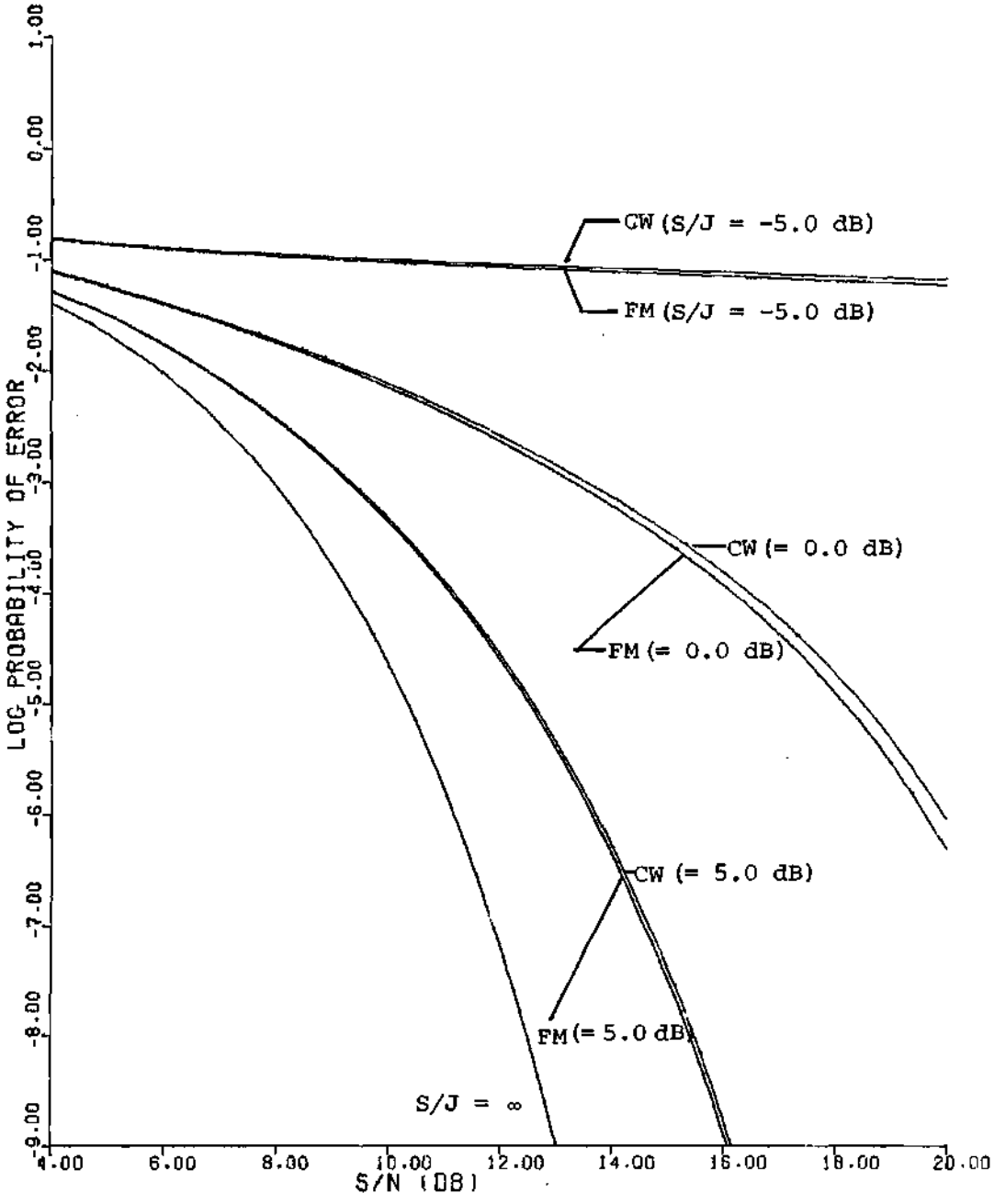

FIGURE 48. Comparison of Spot (Cochannel, CW-Tone) and Swept-Spot (Cochannel, Linear FM) Jamming Error Rates vs S/N: DS/FH, Binary DPSK; p=31, S_c=1, β=1, S_j=1, K=1, N_s=2, K_s=1

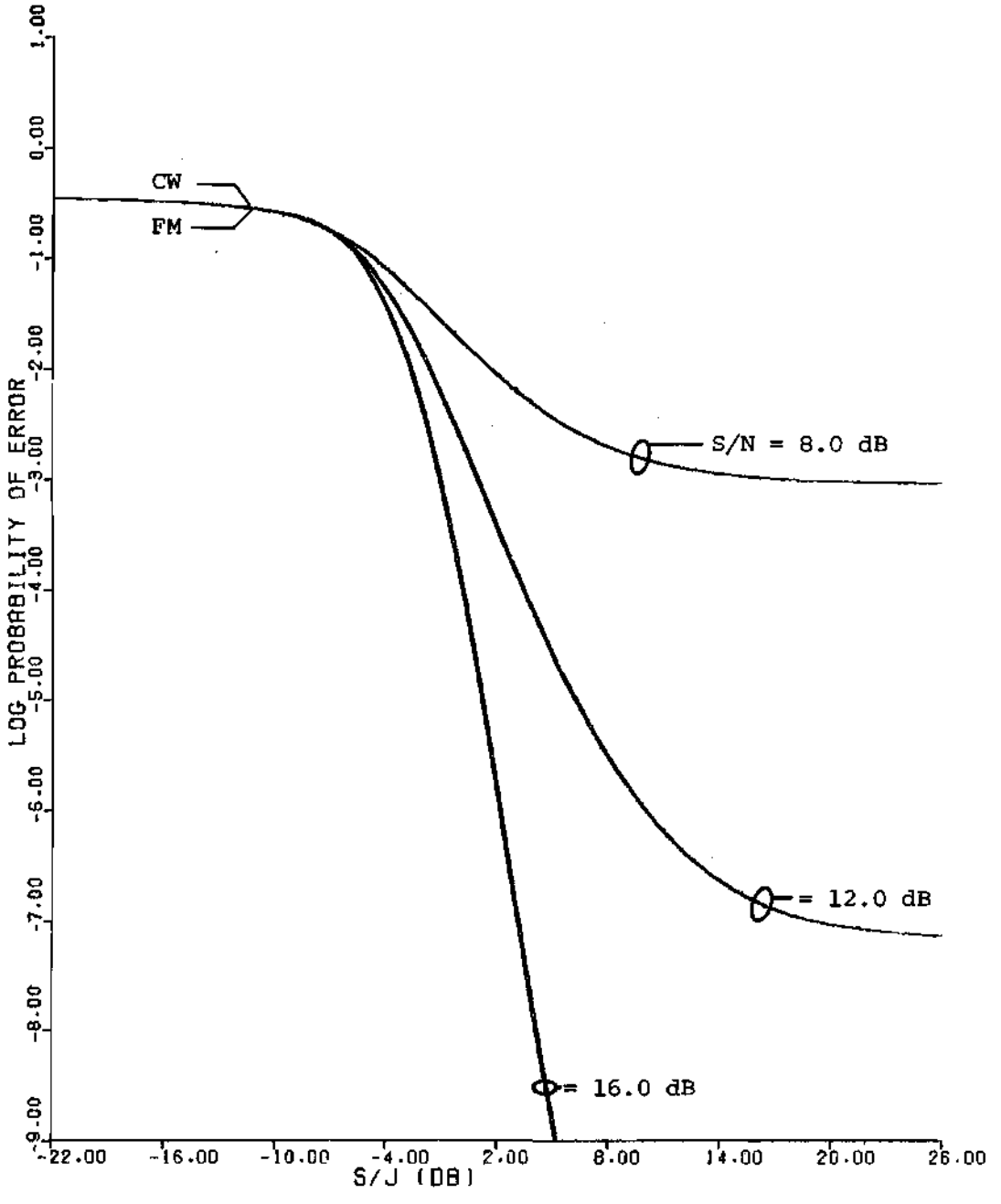

FIGURE 49. Comparison of Spot (Cochannel, CW-Tone) and Swept-Spot (Cochannel, Linear FM) Jamming Error Rates vs S/J: DS/FH, Binary DPSK; p=31, S_c=1, β=1, S_j=1, K=1, N_s=2, K_s=1

TABLE 11. Signal Power Increase Required to Maintain the Jam-Free Error Rate in a Spot and Swept-Spot Jamming Environment With S/J = 0 dB

		SIGNAL POWER INCREASE (dB)	
$\frac{S}{N}$ (dB)	JAM-FREE ERROR RATE	CW-TONE (MAX)	FM (MAX)
4	$.4 \times 10^{-1}$	2.0	2.0
6	$.9 \times 10^{-2}$	3.5	3.5
8	$.9 \times 10^{-3}$	5.8	5.8
10	$.2 \times 10^{-4}$	7.8	7.5
12	$.7 \times 10^{-7}$	9.0	8.8

Limitation of Jamming Efficiency

As the SJR becomes large, the jamming effects become overshadowed by the thermal noise effects and the error rate becomes limited by that rate achieved by the "jam-free" system. Therefore, a jammer cannot always reduce his power and expect to maintain a significant degree of effectiveness. This limiting is best illustrated in those plots using the SJR as the abscissa variable, in particular Figures 41, 43, 45, 47, and 49.

In a constant SNR situation, the limiting effect provides an upper limit to the practical amount of spread spectrum processing gain. This will be discussed in more detail later.

As an added note, unless the thermal noise term is allowed to remain in the analysis, the limiting effect will not be produced and an assumed error rate for large SJR may very well be smaller than what actually occurs. Therefore, a complete analytical description, and, as shown here, a practical discussion must consider the thermal noise effects.

Code Rate Dependence

A significant parameter in the DS spread spectrum portion of the system is the PR code rate, R_c. As seen in Chapter II, the code rate is the fundamental factor in determining the DS-spread bandwidth and ultimately the DS processing gain. There are two parameters which determine the code rate. These are the code frequency, ω_p, and the number of chips (p) per code period. In fact

$$R_c = \frac{1}{T_c} = \frac{pw_p}{2\pi}$$

As for the processing gain (P.G.), the assumed gain, or rule-of-thumb, is defined as

$$(P.G.)_a \triangleq \frac{\text{DS Spread Bandwidth}}{\text{Information Bandwidth}}$$

$$= \frac{2R_c}{2R_I}$$

$$= \frac{T_b}{T_c} = \left(\frac{2\pi}{w_b}\right)\left(p\,\frac{w_p}{2\pi}\right) = pS_c$$

Figures 50 and 51 illustrate the system error rate dependence on the code rate by using p as a parameter with the code slip ratio fixed at one (S_c=1). In both figures S/N is 12 dB and the "No DS/FH" and "No DS" basis curves are included for comparison.

When the jammer is of the barrage (noise) type, the binary, DS/FH DPSK error rate is as shown in Figure 50 for a number of values of p. A dramatic increase in system performance (decrease in error rate) when using DS spread spectrum is evident from this figure. For example an error rate of $.47 \times 10^{-1}$ (S/J = 2 dB) is achievable without the DS spreading. Upon introducing the DS technique with p=31 (S_c=1), the error rate is significantly reduced to $.85 \times 10^{-6}$ for the same S/J of 2 dB.

From Figure 48 and using the "No DS" curve as the basis, the true, DS processing gain, $(P.G.)_t$, may be determined and then compared

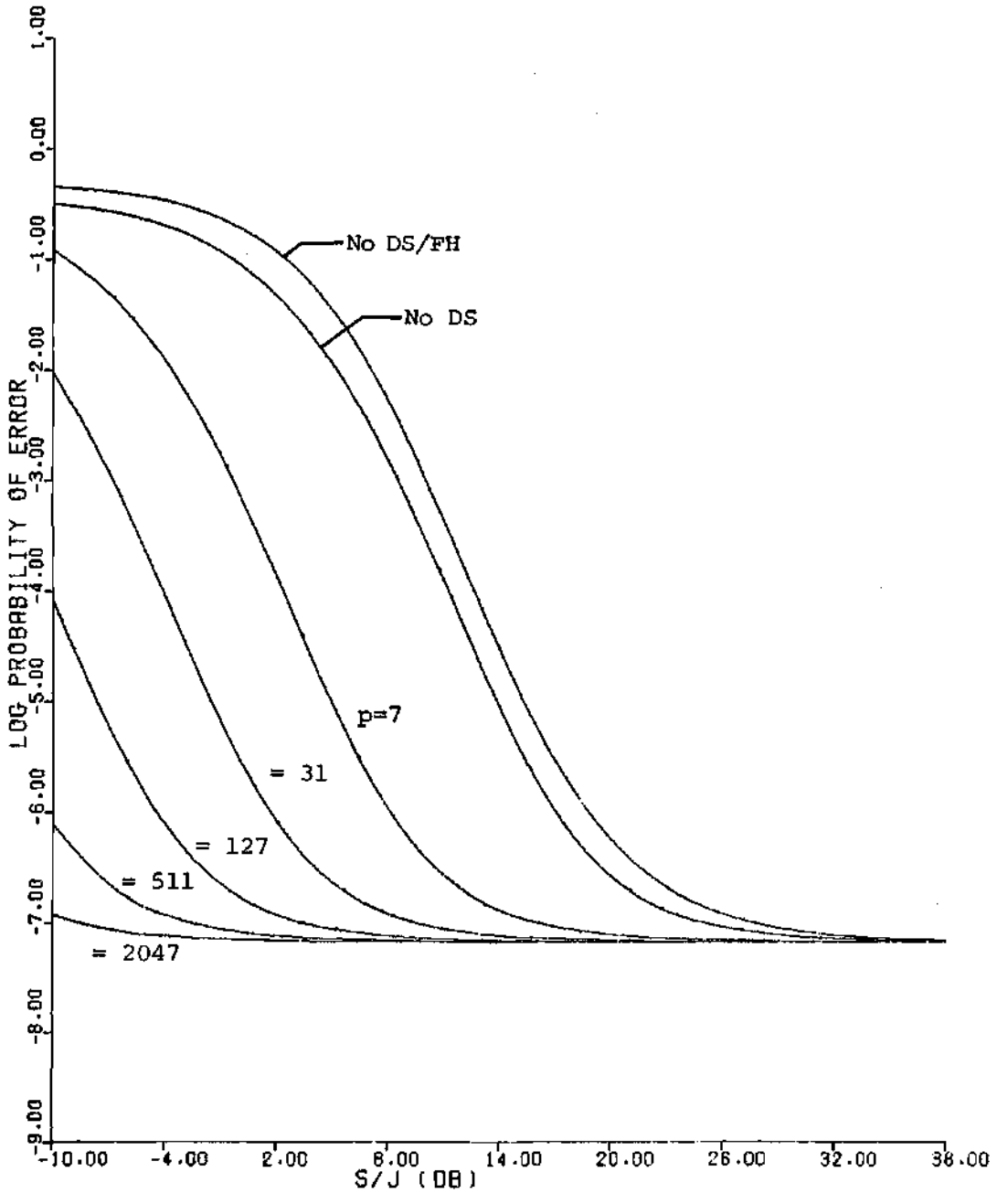

FIGURE 50. Dependence of the Probability of Error vs S/J on the Code Rate (~p): DS/FH, Binary DPSK; Noise Jamming; S/N=12 dB S_c=1, N_s=2, K_s=1

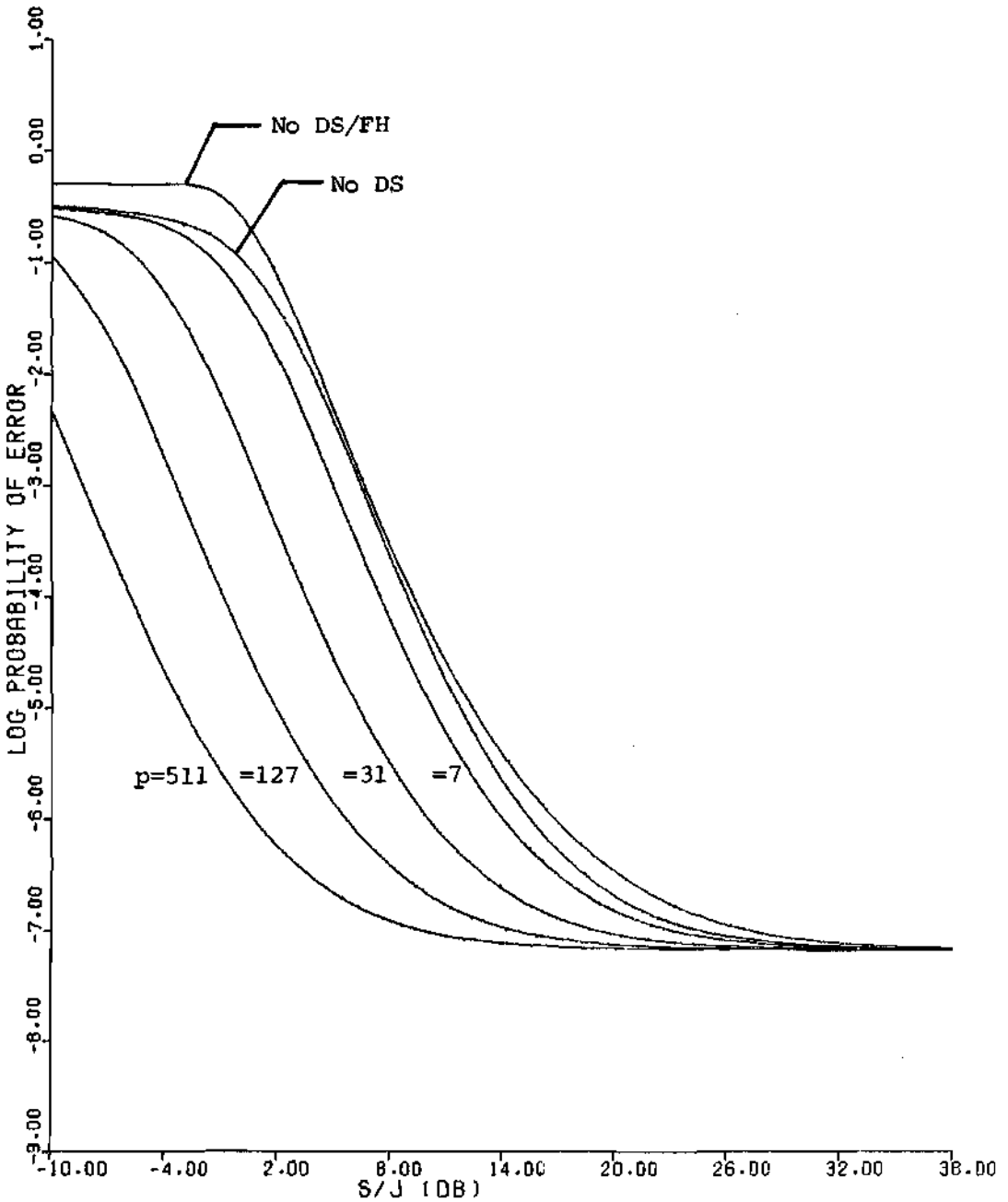

FIGURE 51. Dependence of the Probability of Error vs S/J on the Code Rate (~p): DS/FH, Binary DPSK; Cochannel, CW-Tone Jamming; S/N=12 dB, S_c=1, K=1, N_s=2, K_s=1

to the assumed processing gain. These results are summarized in Table 12 for an error rate of 10^{-5}.

In the strictest sense, the assumed processing gain definition must generally be written as

$$(P.G.)_a = \frac{2R_c+2R_I}{2R_I}$$

since the multiplication of the conventional DPSK signal (bandwidth $\approx 2R_I$) and the PR waveform (bandwidth $\approx 2R_c$) at the transmitter results in a DS-spread signal whose spread bandwidth is actually $2R_c+2R_I$. In the majority of situations $R_c >> R_I$, thus reducing the more general definition to the rule-of-thumb used here. As a result of using the rule-of-thumb for the assumed processing gain, the true, DS processing gains in the noise jamming situation are greater than the assumed gains.

Figure 51 is similar to Figure 50 but is concerned with the spot (CW-tone) mode of jamming rather than the barrage mode. Again, an increase in system performance is seen as a result of using a DS spread spectrum technique. Without DS spreading, an error rate of only $.38 \times 10^{-1}$ (S/J = 2 dB) is achievable, whereas with DS spreading the error rate (actually the upper bound to the average error rate) can be reduced to $.39 \times 10^{-3}$ with p=31 (S_c=1). The degree of performance increase for the spot jamming situation is not as significant as that produced in the barrage case. However, this may be partially explained by recalling that the CW-tone error rates are upper bounds rather than average rates as the noise jamming cases are.

TABLE 12. Assumed and True DS Processing Gains for a Noise Jamming Environment with an Error Rate of 10^{-5} and S/N = 12 dB

$p(\sim R_c)$	$(P.G.)_a$ (dB)	$(P.G.)_t$ (dB)
7	8.5	8.6
31	14.9	15.2
127	21.0	21.2

TABLE 13. Assumed and Minimum DS Processing Gains for a Cochannel, CW-Tone Jamming Environment with an Error Rate of 10^{-5} and S/N = 12 dB

$p(\sim R_c)$	$(P.G.)_a$ (dB)	$(P.G.)_{MIN}$ (dB)
7	8.5	1.5
31	14.9	5.4
127	21.0	10.2
511	27.1	15.0

Because the CW-tone error rates are upper bounds, what has been referred to as the true processing gain is now in fact a minimum processing gain. From Figure 51 the minimum processing gain as a function of p has been determined and is compared to the assumed processing gain in Table 13 for an error rate of 10^{-5}.

In comparing Tables 12 and 13, the assumed and true processing gains are nearly identical for the noise jamming case but are quite different for the CW-tone jamming situation. Again, a partial reason for the difference in processing gains for the CW-tone case is the fact that upper bounds rather than average error rates are used. In general, however, the true processing gain does occur between the assumed and minimum processing gains. In other words, the actual (true) processing gain and the assumed processing gain still differ, regardless of using the average or upper bound error rate. Clearly, care must be exercised in using the assumed processing gain as a performance criterion.

It has been stated previously that the thermal noise places a practical upper limit on the available DS processing gain. Because of complexity, a system should use the smallest code rate possible to maintain the required error rate. Suppose a barrage jamming signal is corrupting the binary, DS/FH DPSK system with enough power such that S/J = 8 dB (S/N = 12 dB). The corresponding error rates for the five values of p in Figure 50 are presented in Table 14. Assume as before that an increase in p is analogous to an increase in R_c. Due to thermal noise, the error rates for p = 127, 511, and 2047 are nearly identical. In fact, the "jam-free" thermal noise performance rate is $.7 \times 10^{-7}$. Therefore, where the system performance in a jamming situation begins

TABLE 14. Thermal-Noise-Limiting Error Rate for S/J = 8 dB and S/N = 12 dB

$p(\sim R_c)$	ERROR RATE
7	11.0×10^{-7}
31	1.2×10^{-7}
127	$.8 \times 10^{-7}$
511	$\sim.7 \times 10^{-7}$
2047	$.7 \times 10^{-7}$

to reach the performance level for thermal noise, there is no need to increase the code rate any further since the increase would cause greater system complexity with no achievable benefits in system performance.

Hopping Slot Dependence and Partial-Band Jamming Effects

Considerable variation in system/jamming strategies can be exhibited by showing the dependence of the system error rate on the number of jammed slots (K_s) and the number of hopping slots (N_s). The error rate dependence on K_s and N_s for barrage (noise) and spot (CW-tone) jamming is illustrated in Figures 52 and 53, and Figures 54 and 55, respectively.

With the jamming strategy fixed (K_s fixed) and for both of the above jamming types, an increase in system performance (error rate decrease) is clearly evident when the number of hopping slots is increased. For example, in a noise jamming environment with S/J = -6 dB, the error rate is reduced from $.53 \times 10^{-3}$ to $.59 \times 10^{-5}$ when the number of hopping slots is increased from 2 to 50 and K_s remains at 1. This same increase in system performance always exists whenever the number of hopping slots is increased, provided the jamming strategy remains unchanged.

Changes in the jamming strategy as N_s increases may cause the error rate reduction to be smaller than that achieved by a fixed jamming strategy. This situation is depicted in curves F, G, and H of Figure 52 below an S/J of -24 dB and curves F, G, and H of Figure 54 below an S/J of -18 dB. More impressively and because of the changes in the jamming strategy, curves F and H of Figure 54 indicate a degraded system performance below an S/J of -24 dB despite the increase in the number

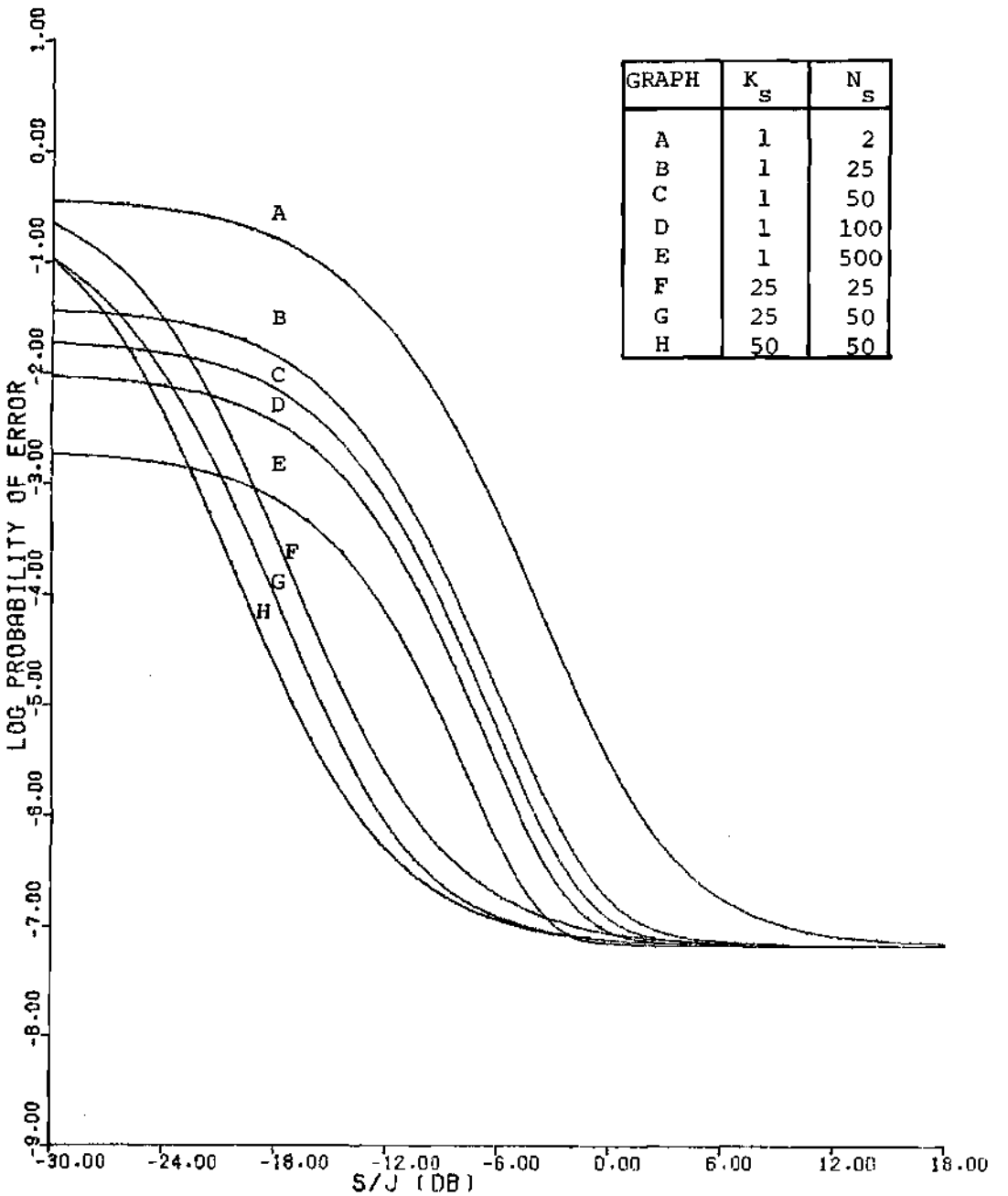

FIGURE 52. Dependence of the Probability of Error vs S/J on N_s and K_s ($1 \le K_s \le 50$): DS/FH, Binary DPSK; Noise Jamming; S/N=12 dB, p=31, S_c=1

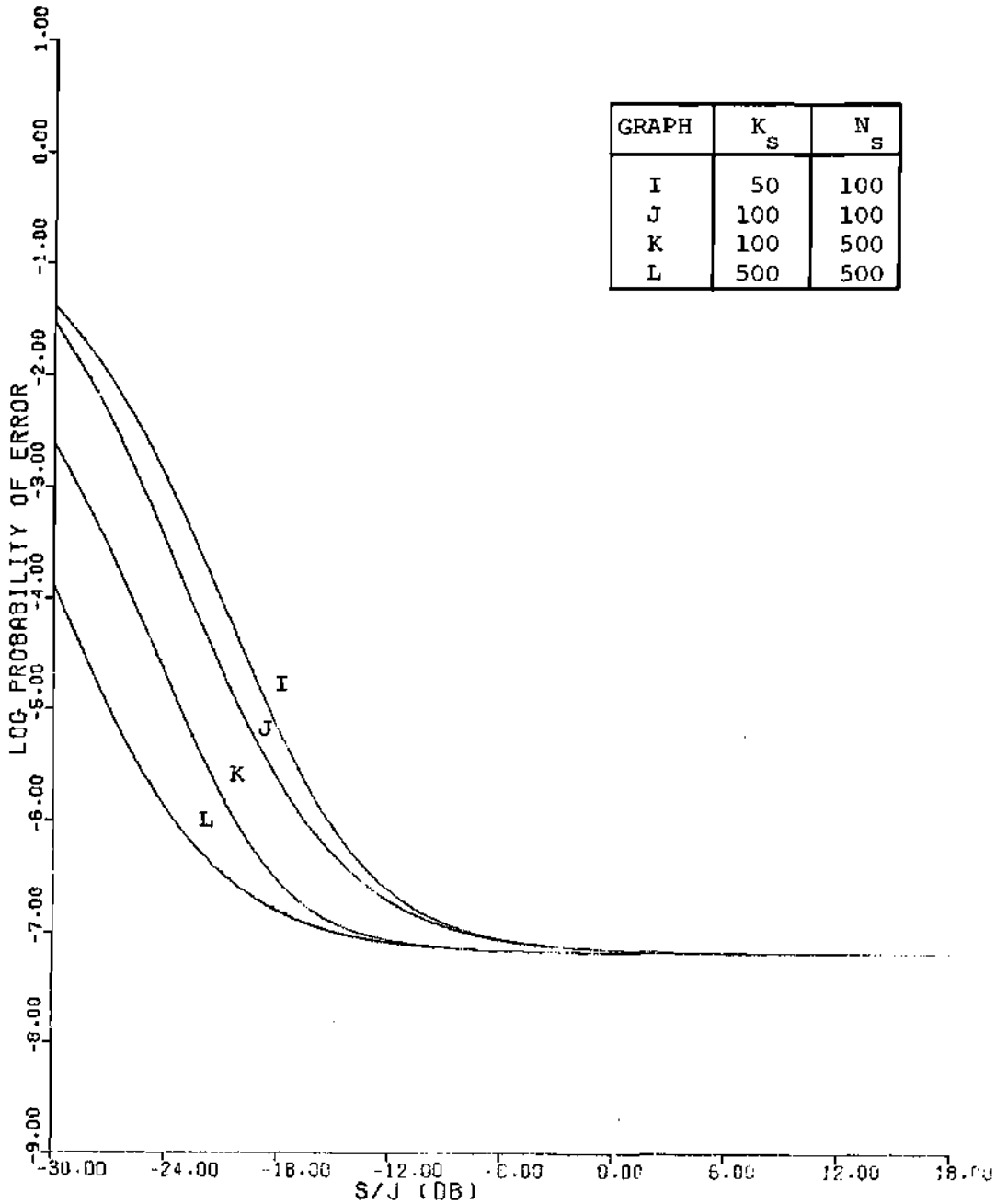

FIGURE 53. Dependence of the Probability of Error vs S/J on N_s and K_s ($50 \leq K_s \leq 500$): DS/FH, Binary DPSK; Noise Jamming; S/N=12 dB, p=31, S_c=1

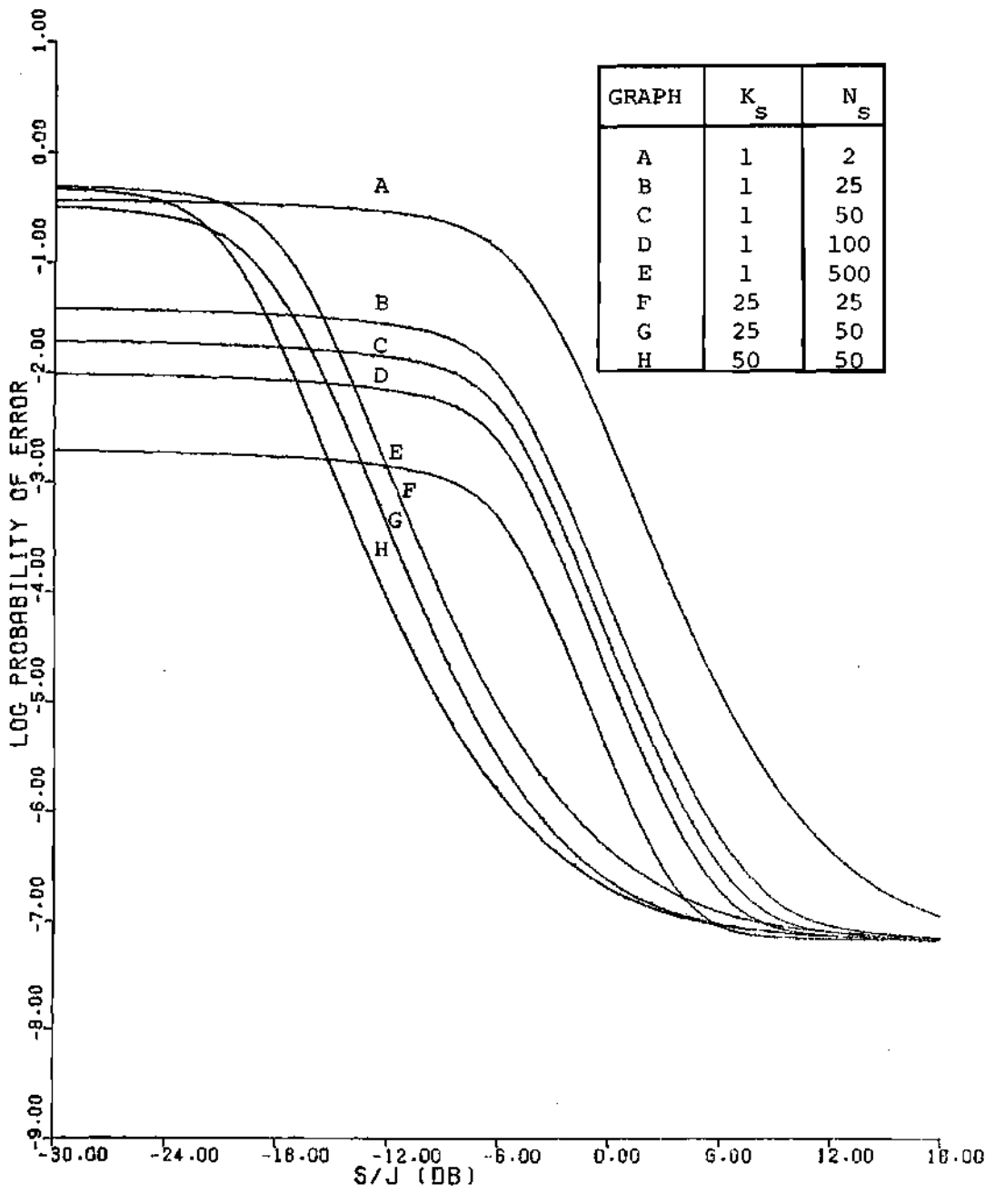

FIGURE 54. Dependence of the Probability of Error vs S/J on N_S and K_S ($1 \le K_S \le 50$): DS/FH, Binary DPSK; Cochannel, CW-Tone Jamming; S/N=12 dB, p=31, S_C=1, K=1

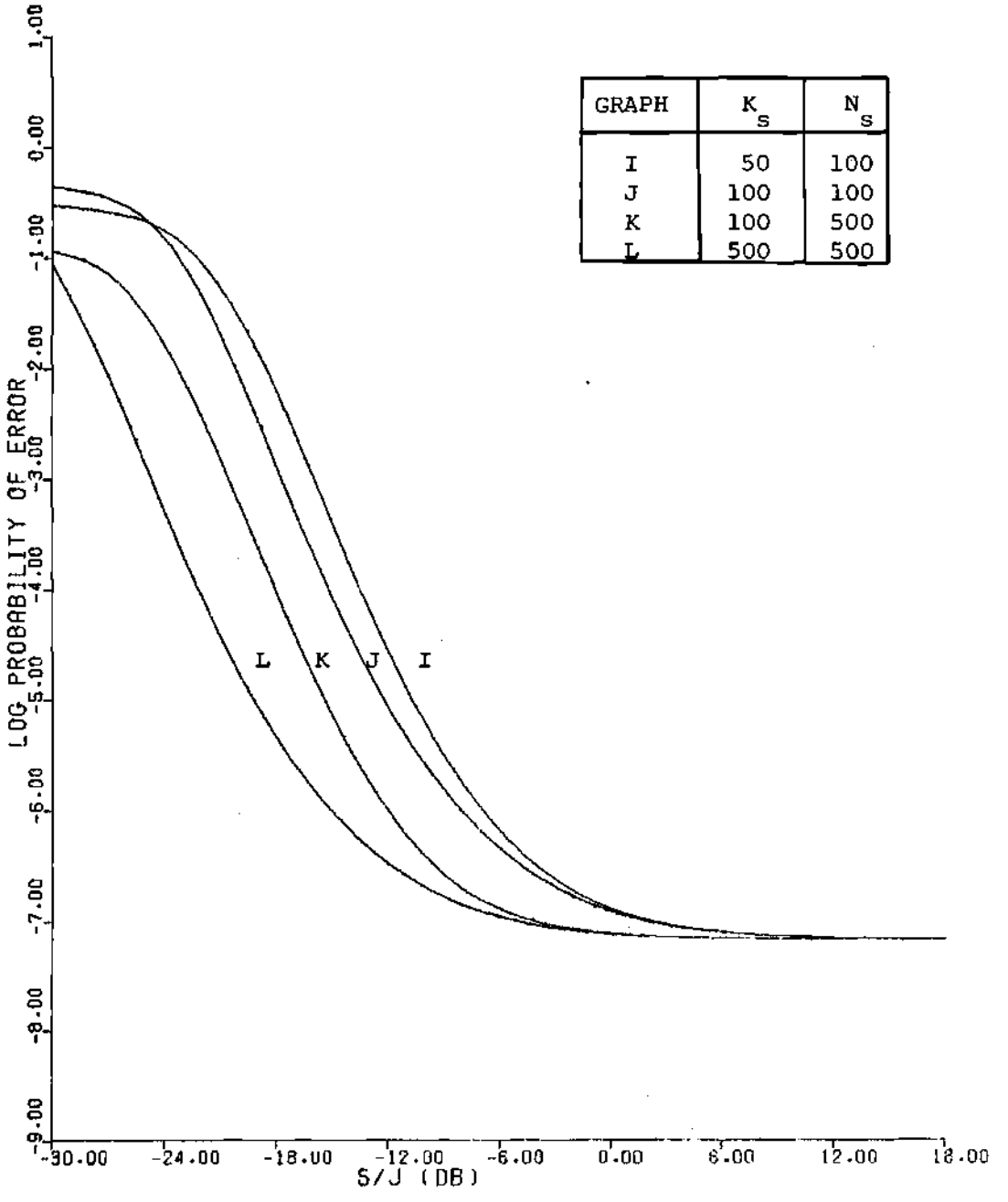

FIGURE 55. Dependence of the Probability of Error vs S/J on N_S and K_S ($50 \leq K_S \leq 500$): DS/FH, Binary DPSK; Cochannel, CW-Tone Jamming; S/N=12 dB, p=31, S_c=1, K=1

of hopping slots. Therefore, an increase in the number of hopping slots cannot always guarantee a better or prescribed system performance since the jamming strategy may change and alter the expected error rate reduction.

From the jamming point-of-view, the strategy implemented is dependent upon the required jammed-error-rate, peak power limitations and average power limitations. The required jammed-error-rate is a function of the modulation scheme (e.g. DS/FH, DPSK) and the critical nature of the information being conveyed by that scheme; the error rate is determined by the jammer to be that rate in which the received information is said to be unintelligible. Determining this subjective jammed-error-rate is not of interest here but rather the use of the rate. For example, suppose the required jammed-error-rate were 10^{-4}. From Figures 52-55, the best (in the sense of least average jamming power) jamming strategy is to jam only one slot, regardless of the number of hopping slots. In this error region, peak power limitations may force the strategy to increase the number of jamming signals although at the expense of a larger average power. If the jammed-error-rate were greater than or equal to 10^{-1}, the results of Figures 52-55 indicate that a jammer may be forced to alter his jamming strategy and increase the number of jamming signals to reach this error rate. In other words, if 25 hopping slots are used and only one slot is jammed, the limiting nature of the error curve (curve B in Figures 52 and 54) for low SJR prevents the jammer from reaching his goal. The jammer, however, may change his strategy and jam a larger number of slots (e.g. K_s=25, curve F) and consequently have the ability to maintain the required error

rate. As seen from this discussion, the jamming strategy is dependent upon a number of parameters, and although this research has presented specific strategies, the research has established the methodology to perform more extensive parametric studies.

The true processing gain for this FH spread spectrum technique sheds more light on this jamming strategy dependence. Tables 15 and 16 illustrate the difference between the true and assumed processing gains for the barrage and spot jamming situations, respectively. The table values are derived from Figures 52-55 for an error rate of 10^{-4} and use the "No DS/FH" curve of Figures 50 and 51 as reference. Since the processing gain here is intended to reflect only the gain due to frequency-hopping, the DS gain must be subtracted out. From Figures 50 and 51 the DS processing gain (p=31) at an error rate of 10^{-4} for noise and CW-tone jamming is, respectively, 15.2 dB and 5.4 dB. In Tables 15 and 16 the results indicate that the assumed processing gain depends heavily on the jamming strategy (partial- or full-band) and the type of jamming signal. In addition, although not indicated in the tables, it can be seen from Figures 52-55 that the actual processing gain also depends on the error rate.

For a full-band jamming environment, however, the actual and assumed processing gains are identical. This equality of processing gains is expected since the jammer maintains the same full-band strategy for all N_s, and as a result must reduce the jamming power per slot if the average jamming power is to remain constant.

In summary, differences exist between the assumed and actual system performance. The factors affecting these differences are the

TABLE 15. Assumed and True FH Processing Gains for a Noise Jamming Environment with an Error Rate of 10^{-4} and S/N = 12 dB

GRAPH	$(P.G.)_a$ (dB)	$(P.G.)_t$ (dB)
A	3.0	1.1
B	14.0	5.6
C	17.0	6.5
D	20.0	7.4
E	27.0	9.8
F	14.0	14.0
G	17.0	15.5
H	17.0	17.0
I	20.0	18.5
J	20.0	20.0
K	27.0	23.3
L	27.0	27.0

TABLE 16. Assumed and True FH Processing Gains for a Cochannel, CW-Tone Jamming Environment with an Error Rate of 10^{-4} and S/N = 12 dB

GRAPH	$(P.G.)_a$ (dB)	$(P.G.)_t$ (dB)
A	3.0	1.4
B	14.0	5.0
C	17.0	5.8
D	20.0	6.6
E	27.0	8.5
F	14.0	14.0
G	17.0	15.4
H	17.0	17.0
I	20.0	18.3
J	20.0	20.0
K	27.0	23.0
L	27.0	27.0

jamming strategy (type, number, and power of jamming signals) with respect to the system strategy and the error rate. For the case in which the jammer jams all slots, regardless of the number of slots, the assumed processing gain is valid. In many cases, however, a knowledgeable jammer realizes that a partial-band jamming strategy is more advantageous to him, and thus the use of the assumed processing gain may be inadequate and misleading. Therefore, caution must be exercised in using and relying on the frequency-hopping processing gain as conventionally defined. With the methods developed here, more accuracy and insight concerning actual system performance is provided.

Frequency Offset Dependence

In many communication situations, a doppler shift causes a carrier frequency to vary about the true carrier frequency. If the desired signal or the jamming signal exhibit some type of doppler shift, the receiver would ultimately offset the jamming carrier from the signal carrier. The same situation arises if both the desired and jamming signals exhibit different doppler shifts. Alternatively, these situations are equivalent to the jamming frequency being offset from the signal frequency when both the jamming and desired systems are operating under non-doppler conditions. To analyze this case, the frequency offset parameter, W_{fo}, defined in Chapter X as

$$W_{fo} \triangleq \frac{\omega_j - \omega_c}{\omega_b}$$

can now take on non zero values. In fact and within the practical

boundaries of the model, W_{fo} may take on any real number.

Figure 56 illustrates the dependence of the system error rate on W_{fo} with the jamming environment being of the spot (CW-tone) type. Surprisingly, Figure 56 indicates that the largest error rate is not achieved for cochannel ($W_{fo} = 0$) interference but rather for a jamming frequency located approximately $\pm 3\omega_b$ from the carrier frequency, ω_c. Furthermore, jamming frequencies of $\omega_c \pm \omega_b$ and $\omega_c \pm 4\omega_b$ also provide larger error rates than that rate for $\omega_j = \omega_c$. It is not until $\omega_j = \omega_c \pm 5\omega_b$ that the error rate becomes smaller than the rate for cochannel interference.

Because the CW-tone error rates are upper bounds, it is not initially clear that this same dependence would occur for average error rates, but in fact it does. The results are not graphically presented but the average error rates do indicate that the maximum system degradation occurs for a jamming frequency of $\omega_c \pm 3\omega_b$ (only p=31 and integer values of W_{fo} are considered). Furthermore, the larger values of W_{fo} show a much more pronounced effect on the average error rates than what is indicated in Figure 56. In fact the average error rate with $\omega_j = \omega_c$ is actually smaller than the average rate with $\omega_j = \omega_c \pm 5\omega_b$, contrary to the upper bounds in Figure 56.

The jamming frequency at which the maximum system degradation occurs depends on the value of p ($\sim R_c$ with S_c fixed). With S_c=1 and considering only integer values of W_{fo}, Table 17 indicates the jamming frequency causing the maximum system degradation as a function of p ($\sim R_c$).

A non-cochannel interference creating a greater system degradation is, at first, seemingly contrary to previous results [30]. Yet,

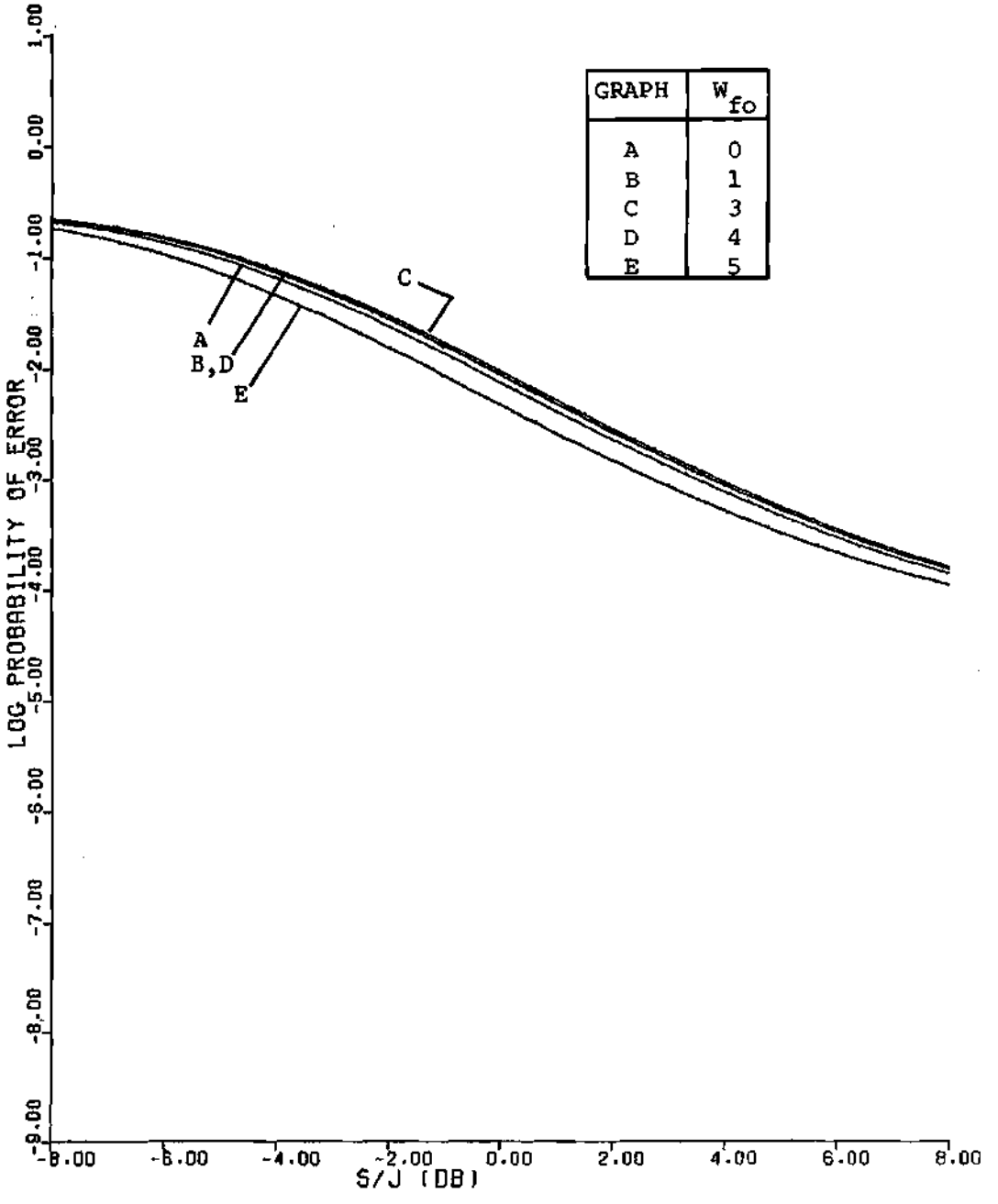

FIGURE 56. Dependence of the Probability of Error vs S/J on the Frequency Offset Parameter, W_{fo}: DS/FH, Binary DPSK; CW-Tone Jamming; p=31, S_c=1, K=1, N_s=2, K_s=1

TABLE 17. CW-Tone Jamming Frequencies Causing the Most System Degradation as a Function of the PR-Code Period

$p(\sim R_c)$	ω_j
7	$\omega_c \pm \omega_b$
15	$\omega_c \pm 2\omega_b$
31	$\omega_c \pm 3\omega_b$
63	$\omega_c \pm 4\omega_b$
127	$\omega_c \pm 6\omega_b$

the previous results did not include a DS spread spectrum scheme. It is this spreading technique which apparently causes the increased system degradation from cochannel to non-cochannel (in all cases the DS scheme produces better system performance than the non-DS scheme). Consider the magnitude spectrum of a spread (p=7), cochannel CW-tone signal in Figure 57. This is identical to the spectrum of the PR-waveform (p=7) before filtering. The spectrum consists of a very low DC term (located here at $\omega = \omega_c$) so that whenever $\omega_j = \omega_c$, there is a small amount of power at the carrier frequency. Translating the envelope by $\pm\omega_p$ (with $S_c = 1$, this is $\pm\omega_b$), however, results in a larger power term at the carrier frequency and hence more system degradation.

FM Modulation Index Dependence

As indicated in [30], a strong dependence of system performance on the modulation index is witnessed. Yet, for the spread spectrum system considered here, this is not the case, as Figures 58 and 59 illustrate. The error rate curves shown in these two figures include the case of β=0 (CW-tone) and a few other non-zero values of β.

In an average sense, the dependence is a little more pronounced since the larger values of β cause larger differences between the upper bound and average error rates. Nevertheless, the dependence is certainly not as great as that witnessed in the non-spread system. This can be explained with the reasoning that the DS spreading (from the signal point of view, this is despreading) portion of the receiver is the dominating factor rather than the "spreading" caused by the increase in β.

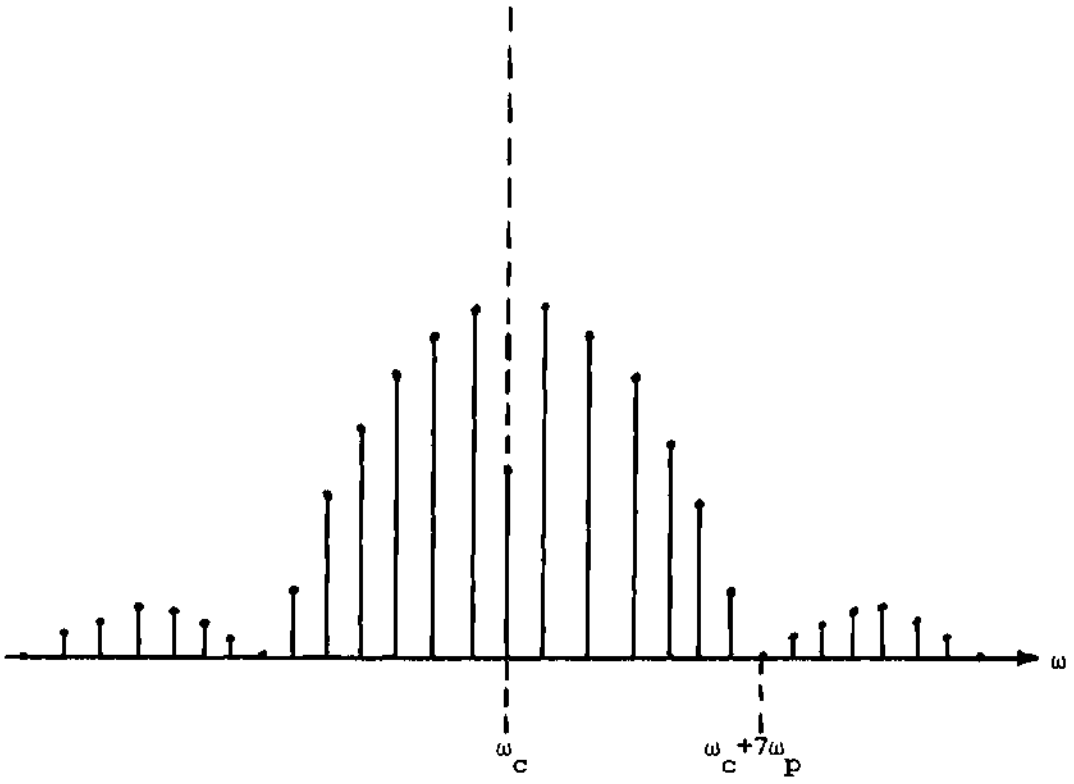

FIGURE 57. Magnitude Spectrum of a Spread, CW-Tone Jamming Signal

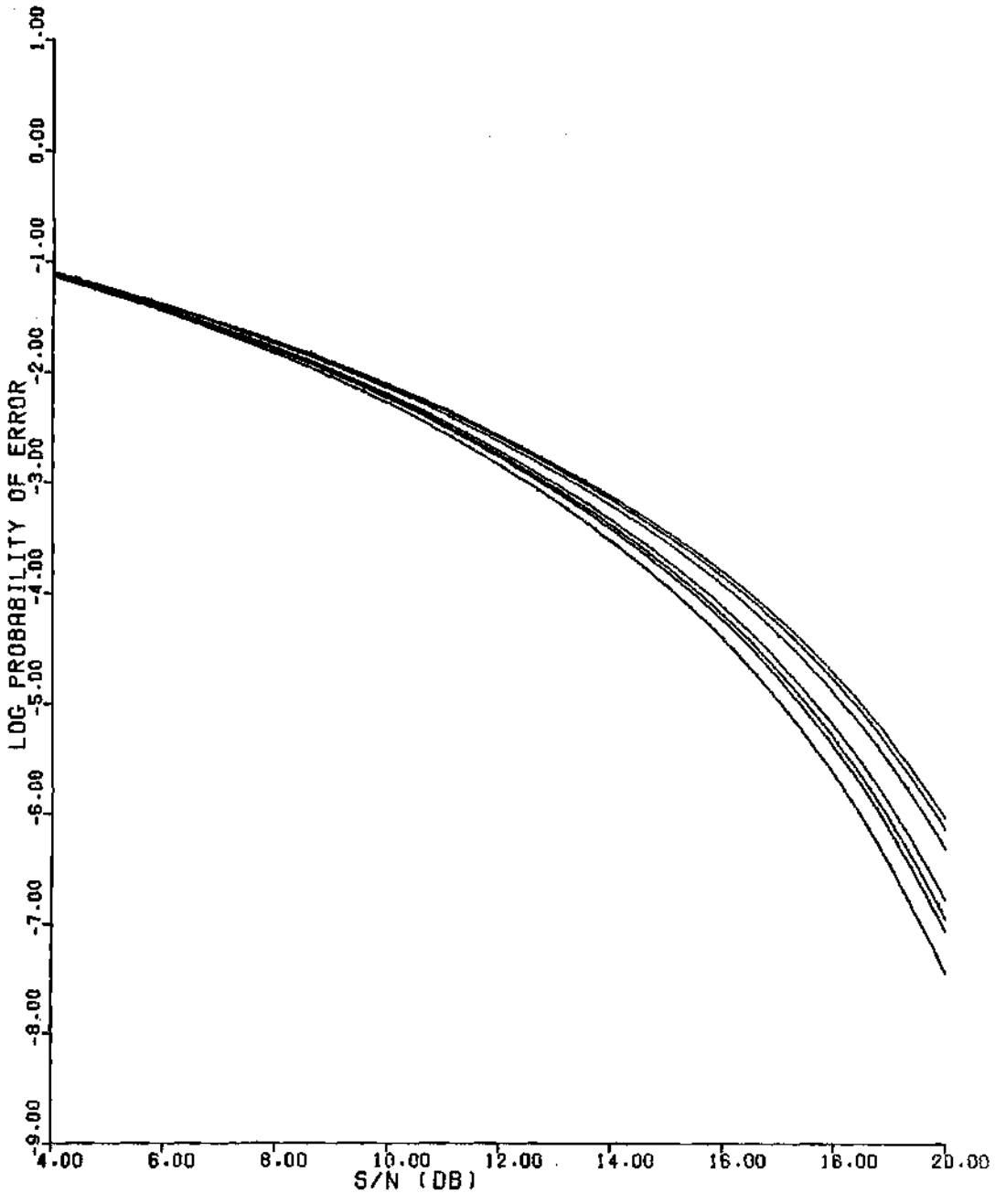

FIGURE 58. Dependence of the Probability of Error vs S/N on β: The Uppermost Curve Represents β=0, and Each Succeeding Curve Represents β=0.5,1,2,3,4,5 With S/J=0 dB, p=31, S_c=1, S_j=1, K=1, N_s=2, K_s=1

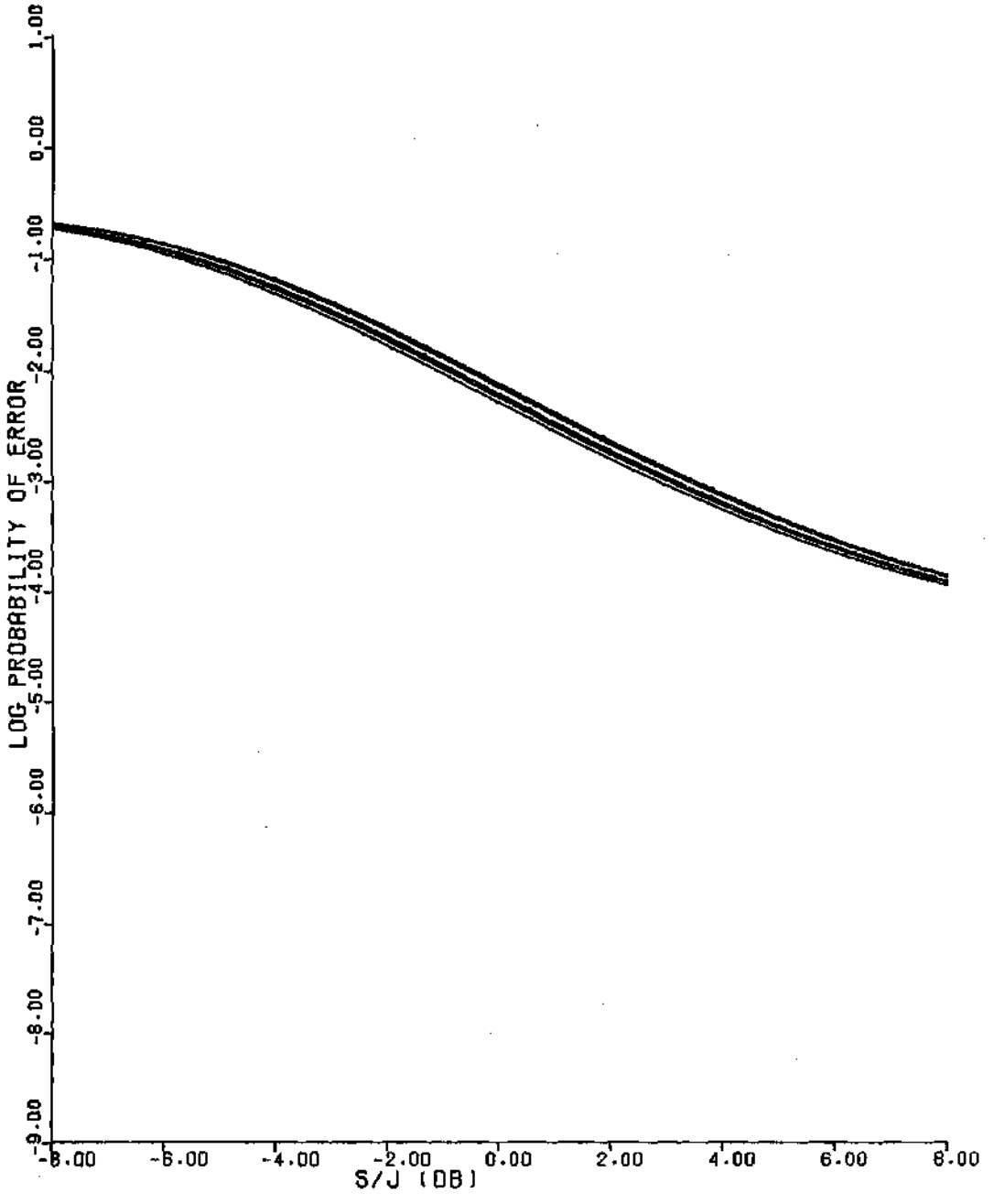

FIGURE 59. Dependence of the Probability of Error vs S/J on β: The Uppermost Curve Represents β=0 and Each Succeeding Curve Represents β=0.5,1,2,3,4,5 With S/N=10 dB, p=31, S_c=1, S_j=1, K=1, N_s=2, K_s=1

Gaussian Approximations

For numerous spread spectrum studies, and in particular DS studies, a frequently used analytical assumption is that the spread interference is equivalent to additional gaussian noise of equal power. With this assumption and the additional gaussian-interference-power denoted as N_j, the noise jamming expressions may be used to approximate the average system performance. The degree of accuracy to which the gaussian approximation is valid depends heavily upon the PR-code period (p), the code slip ratio (S_c), and the method used to calculate the additional power. As for the method, it is possible to use only those spectral lines within the filter bandwidth, or to include all spectral lines outside the bandwidth.

It is not completely valid to compare the gaussian approximation to the results obtained herein since these results are upper bounds rather than average error rates. Nevertheless, for a few cases in which the average may be feasibly calculated, a comparison has been made. Figures 60 and 61 illustrate this comparison for a PR-code period of 15 and 31, respectively. As seen in both cases, the gaussian approximations are, for a large range of S/J, less than the true average. For other ranges of S/J (S/J < -16 dB), the approximations are greater than the true average. Therefore, the general gaussian approximation may give a poor indication of its relationship with respect to the average error rate for the CW-tone jamming signal. In addition, for low S/J and a constant error rate the difference in required signal power can be rather significant.

For the analysis contained herein, the calculated error rate is

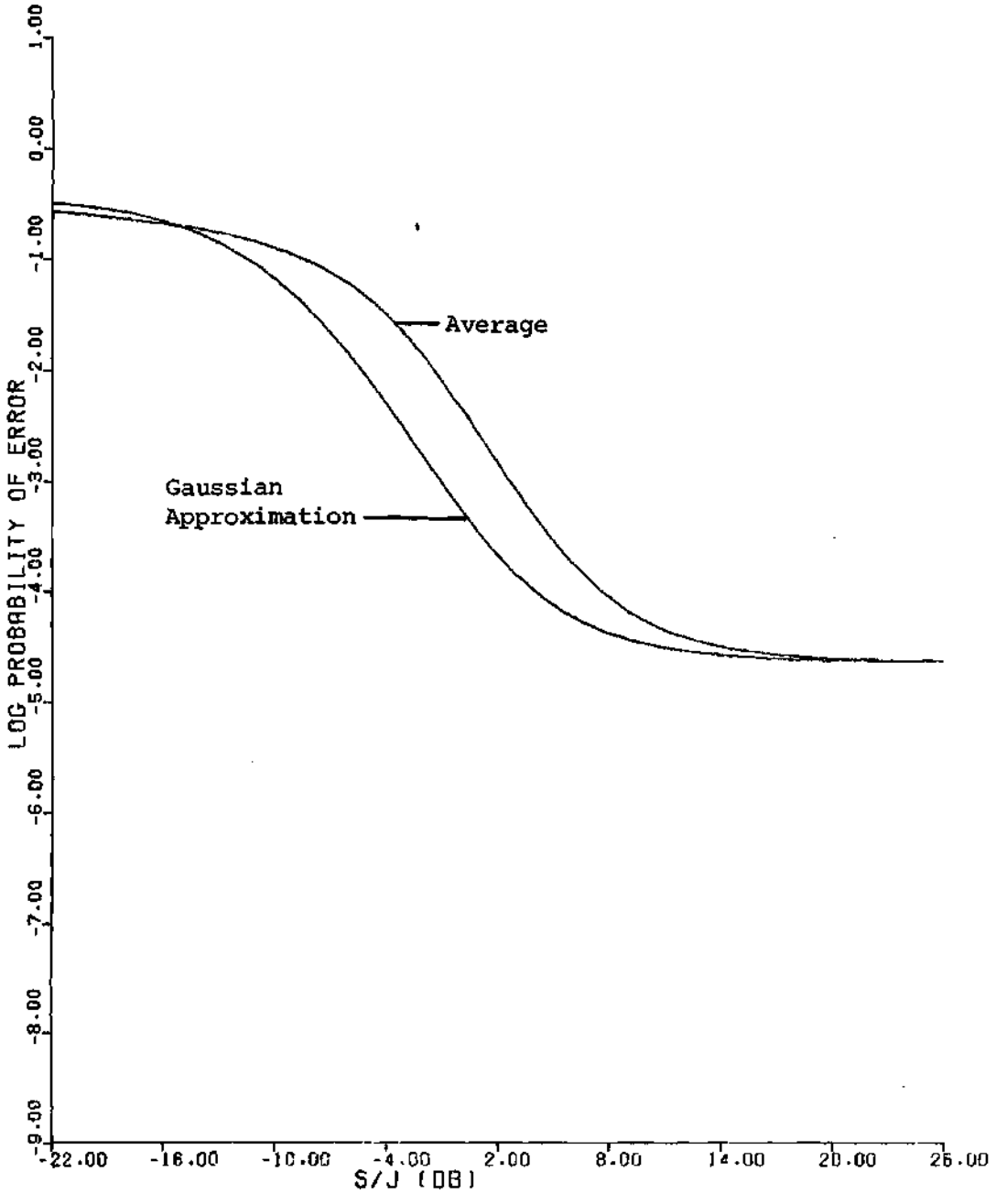

FIGURE 60. Comparison of Gaussian Approximation to Average Error Rate vs S/J: DS/FH, Binary DPSK; Cochannel, CW-Tone Jamming; S/N=10 dB, p=15, S_c=1, K=1, N_s=2, K_s=1

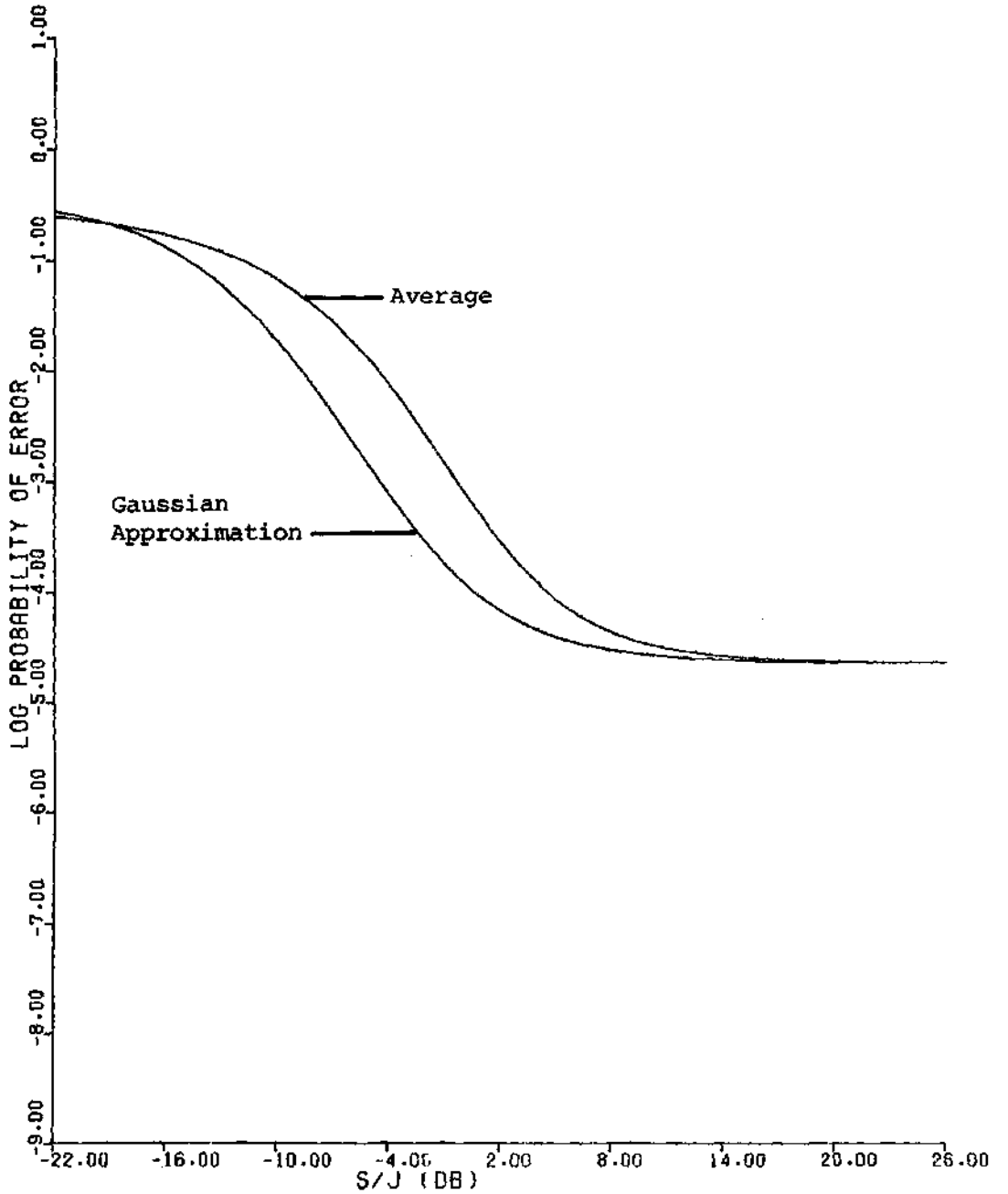

FIGURE 61. Comparison of Gaussian Approximation to Average Error Rate vs S/J: DS/FH, Binary DPSK; Cochannel, CW-Tone Jamming; S/N=10 dB, p=31, S_c=1, K=1, N_s=2, K_s=1

an upper bound for the average error rate for all S/J. For many system evaluations, this type of bounded performance is more useful and desirable than approximations whose degree of accuracy is questionable or unknown.

M-ary DPSK

The results up to this point have included only a binary coding format, although all parametric curves shown previously may be determined for the general M-ary (M>2) format as well. As an illustration of this determination, the upper and lower bounds for M=4 and 8 are shown in Figures 62-65 with the binary case as a reference. Figures 62 and 63 consider the noise jamming case while the error rates for CW-tone jamming are shown in Figures 64 and 65.

For both jamming environments it is evident that a significant degradation in system performance occurs for a small jamming power and a non-binary coding format. In a large jamming power situation, the difference in the performances of the respective coding formats becomes smaller. At any rate, a DPSK system using a coding format other than binary must increase its signal strength to compensate for the additional performance degradation exhibited by that format.

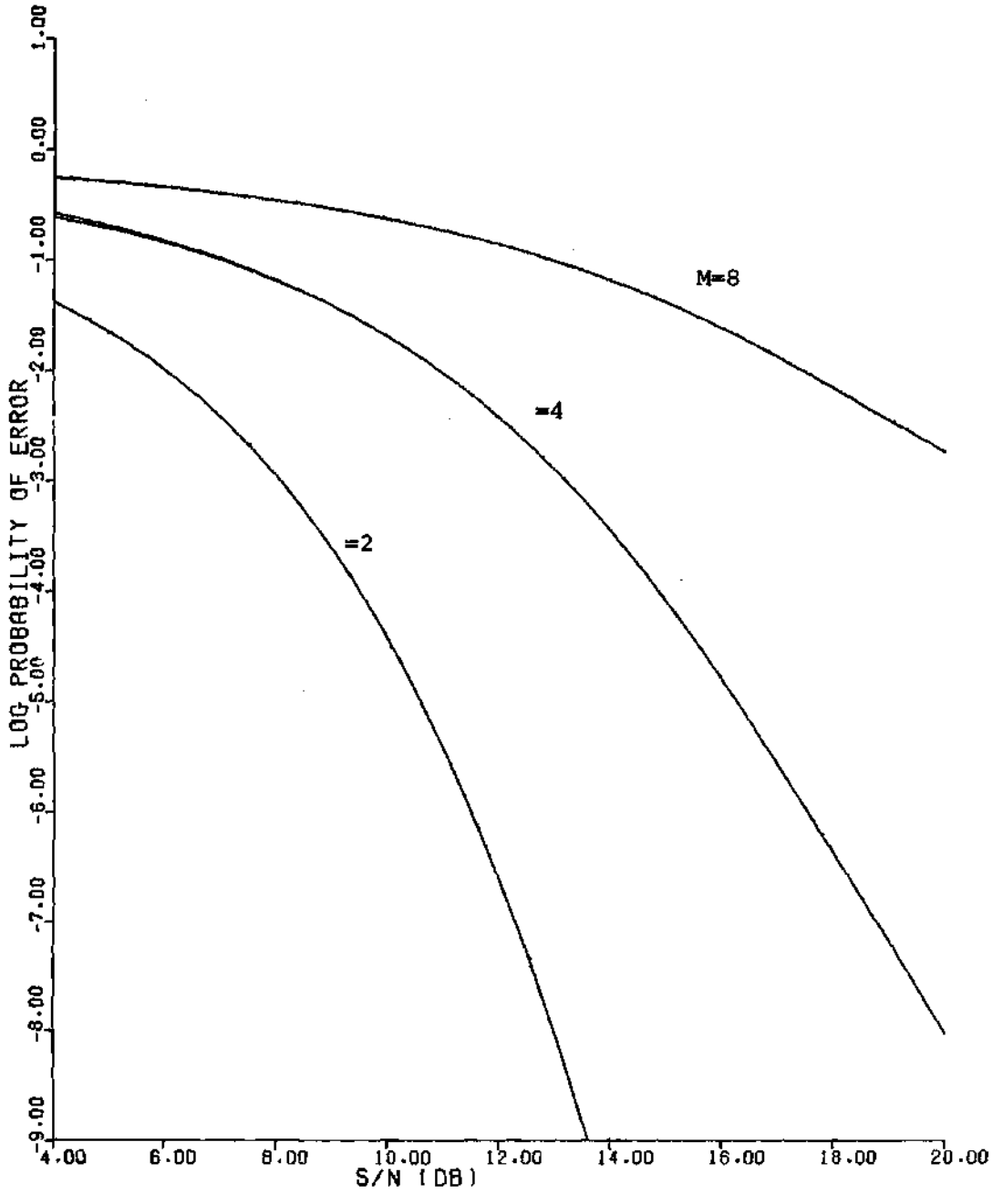

FIGURE 62. Upper and Lower Bounds for M-ary (M=4,8) DPSK: DS/FH; Noise Jamming; S/J=5 dB, p=31, S_c=1, N_s=2, K_s=1

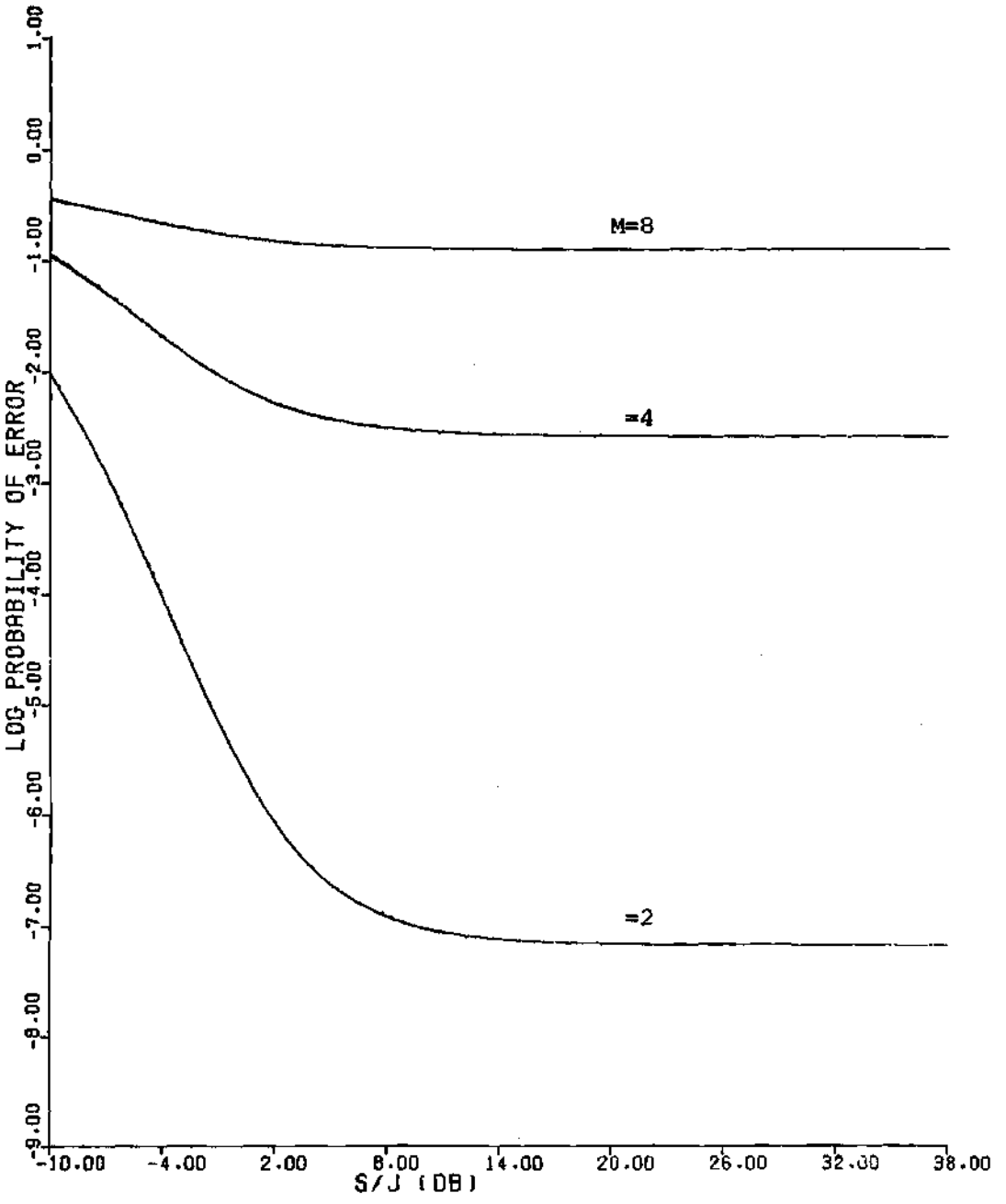

FIGURE 63. Upper and Lower Bounds for M-ary (M=4,8) DPSK: DS/FH; Noise Jamming; S/N=12 dB, p=31, S_c=1, N_s=2, K_s=1

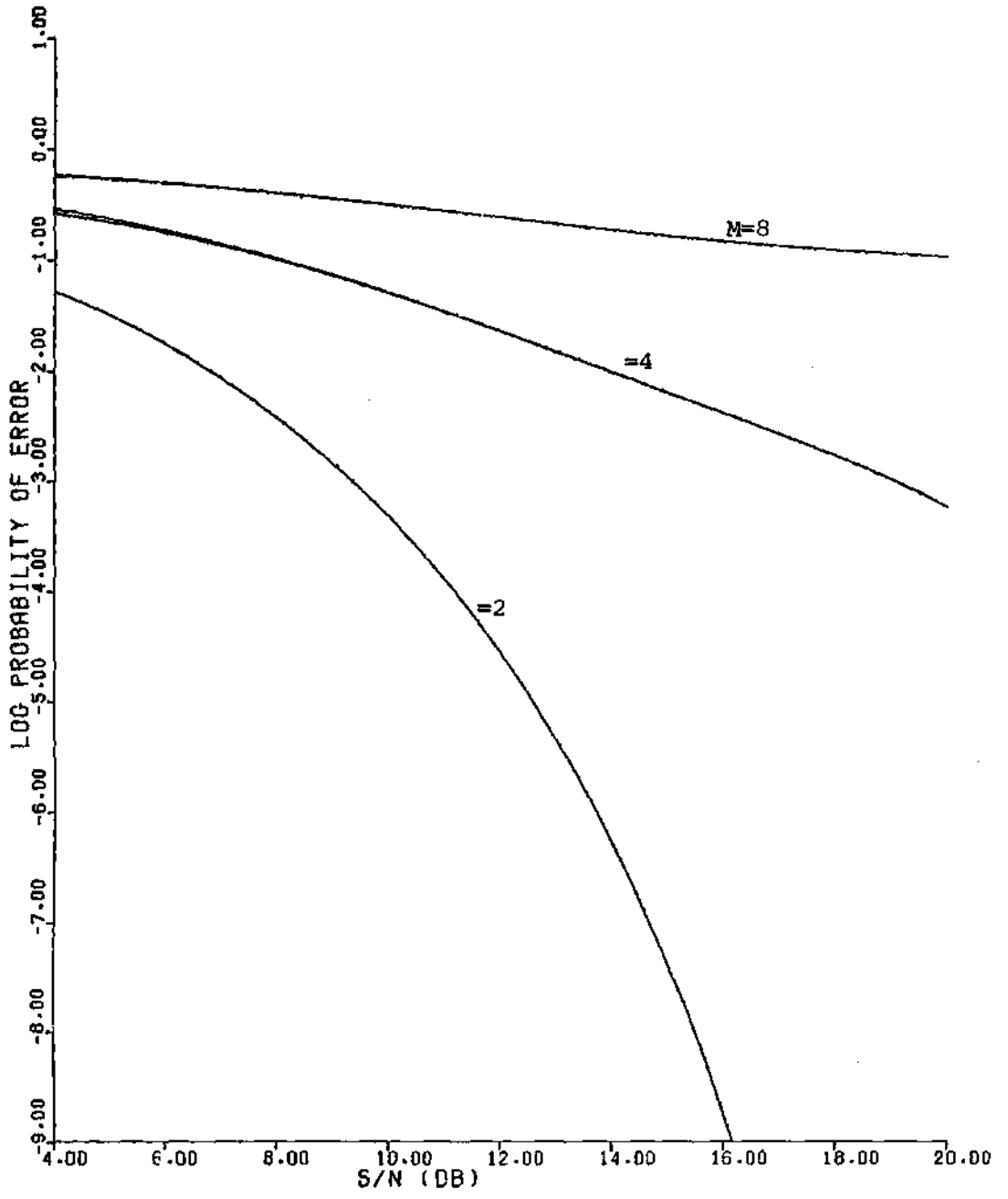

FIGURE 64. Upper and Lower Bounds at the Maxchip for M-ary (M=4,8) DPSK: DS/FH; Cochannel, CW-Tone Jamming; S/J=5 dB, p= 31, S_c=1, K=1, N_s=2, K_s=1

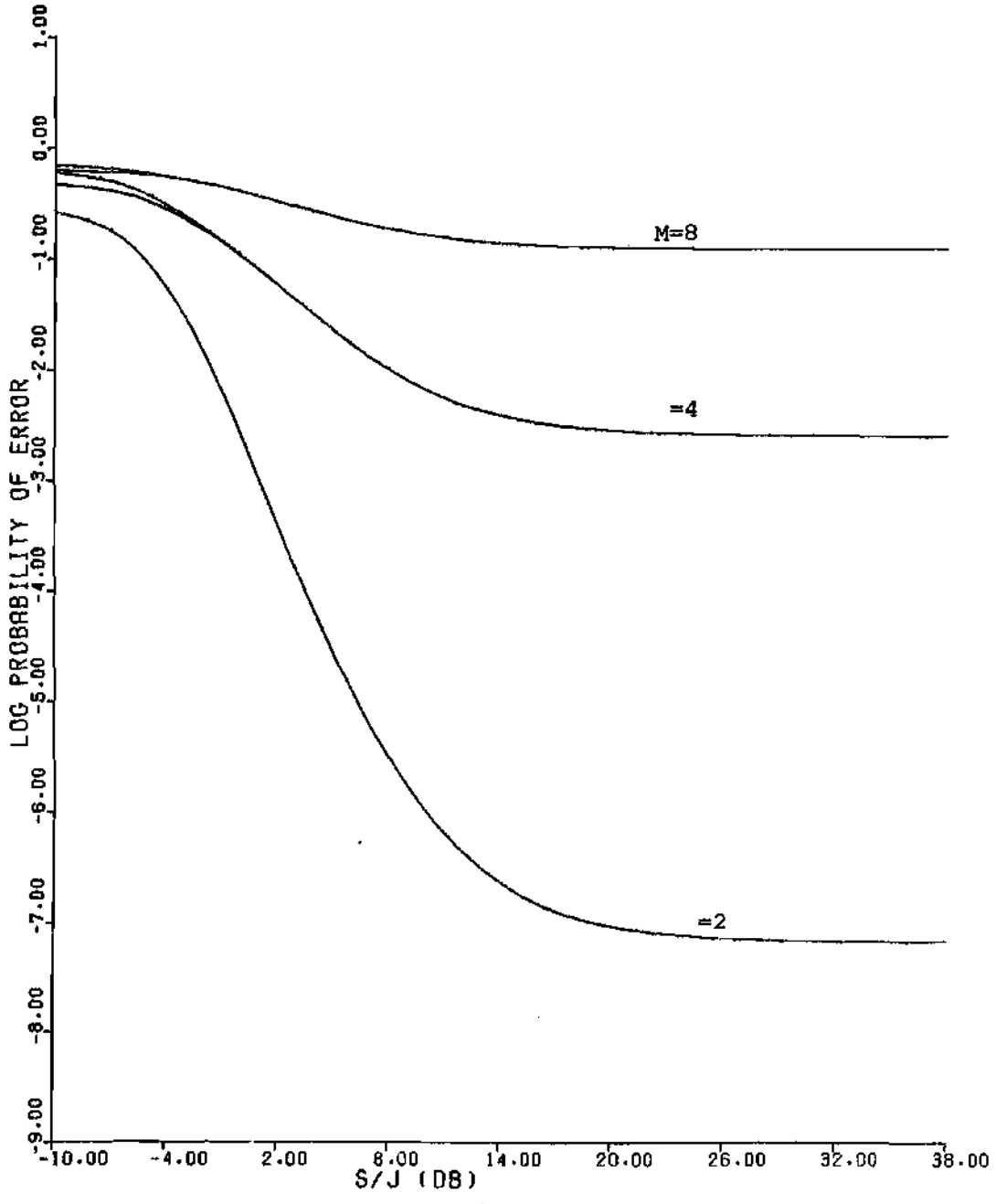

FIGURE 65. Upper and Lower Bounds at the Maxchip for M-ary (M=4,8) DPSK: DS/FH; Cochannel, CW-Tone Jamming; S/N=12 dB, p= 31, S_c=1, K=1, N_s=2, K_s=1

CHAPTER XII

SUMMARY, CONCLUSIONS, AND RECOMMENDATIONS

A theoretical study of the susceptibility of DS/FH, M-ary DPSK to a wide range of jamming threats has been completed. Specific jamming threats included white gaussian noise, CW-tone, and linear-swept FM interference. Probability of error expressions, which describe the system susceptibility, were derived in Chapters VII-IX for the coding formats of binary, quaternary, and general M-ary, respectively. Feasible simplications of these expressions for numerical computation were developed and then shown to produce useful results for parametric studies. These results were graphically and tabularly presented in Chapter XI. Here, and in concise form, are the conclusions of those results.

Transmitter Strategy

As graphically illustrated in Figures 34-39, the performance of an M-ary DPSK communication system can be severely degraded when jammed by deliberate electrical signals. A hybrid scheme of direct sequence (DS) and frequency-hopping (FH) spread spectrum may advantageously be used by the DPSK system to combat such jamming (compare Figures 40-45 with Figures 34-39). The specific spread spectrum parameters depend on the jamming type, power, and strategy. If the jamming power were known to be below a certain level, the code rate could be increased until the thermal-noise-limiting error rate was reached. From Figures 50 and 51,

any code rate increase above that rate would serve only to increase the system complexity without a corresponding gain in system performance. If all parameters are held fixed (jamming parameters included) and the number of hopping slots is increased, the system performance definitely increases. In general, however, the jammer has the ability to change jamming strategy (K_s) and as a result, an increase in the number of hopping slots does not always guarantee a better system performance. This is especially true for a partial-band jamming strategy with large jamming power (see Figures 52-55).

Jamming Strategy

For the hybrid DS/FH spread spectrum transmission system, results indicate that the CW-tone jamming threat is the best ECM signal. Because of its narrow bandwidth, the CW-tone signal has a smaller, DS-spread bandwidth than the noise jamming threat, thus causing significantly more damage to the transmission system. This is clearly evident in Figures 46 and 47. In addition, and from Figures 48 and 49, findings show that the CW-tone and FM jamming threats cause nearly identical upper bounds to the average error rates (CW-tone has a slight jamming edge). Since their individual effectiveness is nearly identical, the jammer is placed in the advantageous position of choosing the CW-tone or FM signal, with the choice based on some useful criterion.

In addition to the choice of the jamming signal, a jammer can also choose to operate in either a partial- or full-band jamming mode. Evidence has been presented that indicates a partial-band strategy is more effective in certain situations (refer to Figures 52-55). The

effectiveness, however, depends on the jammer knowing certain critical transmitter parameters (N_s, signal power). If these parameters are unknown or known inaccurately, the partial-band strategy may be a hinderance as witnessed in Figure 54 for an S/J below -24 dB.

Precise knowledge of the carrier frequency is not very critical in a DS-spread system as opposed to a non-spread system. In fact and as Figure 56 and Table 17 indicate, a non-cochannel interference is slightly more destructive than a cochannel interference.

Processing Gain Definitions

In certain situations, the assumed processing gains for DS and FH are reasonably valid. For DS, the valid situation occurs for a noise jamming environment, while a full-band jamming strategy for all jamming signals allows the valid use of the FH processing gain definition.

It has been demonstrated here that the usually defined gain does not always provide an accurate estimate of actual gain from spread spectrum techniques. For example, small discrepancies occur between the assumed and true, DS processing gains when the system is subjected to CW-tone jamming. Furthermore, Tables 15 and 16 indicate that a partial-band jamming strategy results in significant discrepancies between the assumed and true, FH processing gains. Though it is true that the assumed processing gains do provide maximum achievable gains, care must be exercised in using the processing gain definitions as design criteria for all jamming strategies, signals, and required jammed-error-rates. The techniques and theoretical results obtained here provide the basis for determination of actual gains.

Gaussian Approximations

Equating the spread jamming signal to gaussian noise of equal power and then using the noise-only error expressions provides a possible approximation to the true average error rate. The relationship of the approximation to the average error rate is, however, unknown in general. For some jamming or signal powers, the approximation is less than the average and for other cases, the opposite is true. This is clearly illustrated in Figures 60 and 61. The gaussian approximation does have some computational advantages, but more accuracy and insight is obtained by using the procedures developed in this study. Improved performance, from both signaling and jamming points-of-view, can result from parametric and strategy optimization investigations which are made possible by the methodology described here

Recommendations

The general analysis approach attempted in Chapter VI served only as a motivational tool for the more specific results which were eventually obtained. It remains unclear as to whether a closed form expression actually exists for Eq. (6-30) and hence its derivation continues to be a reasonable research topic. It is this author's opinion however, that the complexity of the marginal density functions for χ_1 and χ_2 may indicate an eventual solution which is purely academic rather than practical.

Computation time is always of great concern to those researchers undertaking studies similar to this work. The accuracy and reduction in computation time produced by the RMS approximation method (FM cases only)

indicate the possibility of using a similar approach in existing and future studies of this kind. For example, Eq. (11-16) (taken from [30]) was significantly simplified to that result in Eq. (11-18) by the RMS method. The accuracy of the simplification was quite favorable as noted below Eq. (11-18). Though it was not attempted in this work, considerable savings in time and computations may be possible if the PR-waveform representation were truncated at 90% of its total power. This depends on the amount of required accuracy, however this additional reduction in accuracy is thought to be minimal.

Extensions of the work performed herein could include other types of spread spectrum schemes and jamming signals (sinusoidal-swept FM, pulsed). In addition, other digital schemes (PSK, NCFSK) could very well rely on the mathematical approaches introduced here.

And finally, there has been little, if any, work performed in optimizing the receiver structure for a fixed jamming environment or optimizing the jamming signal for a fixed receiver structure. Also, the susceptibility of system synchronization to ECM tactics is a relatively new and increasingly important research area.

APPENDIX A

FOURIER SERIES COEFFICIENTS OF LINEAR-SWEPT FM

Even though the analysis is modeled for a general periodic modulation waveform, a linear-swept waveform is considered throughout the computational section for illustrative purposes. The Fourier series coefficients of the linear swept FM signal are required in that section and have been determined to be [30]

$$|a_n| = \frac{1}{2\sqrt{\beta}}\left\{\left[C\left(\frac{\beta-n}{\sqrt{\beta}}\right) + C\left(\frac{\beta+n}{\sqrt{\beta}}\right)\right]^2 + \left[S\left(\frac{\beta-n}{\sqrt{\beta}}\right) + S\left(\frac{\beta+n}{\sqrt{\beta}}\right)\right]^2\right\}^{\frac{1}{2}}$$

and

$$\phi_n = -n\pi - \left(\frac{n^2+\beta^2}{2\beta}\right)\pi + (\beta-n)x - \frac{\beta x^2}{2\pi}$$

$$+ \arctan\left[\frac{S\left(\frac{\beta-n}{\sqrt{\beta}}\right) + S\left(\frac{\beta+n}{\sqrt{\beta}}\right)}{C\left(\frac{\beta-n}{\sqrt{\beta}}\right) + C\left(\frac{\beta+n}{\sqrt{\beta}}\right)}\right]$$

where x is related to the offset parameter through

$$x = \frac{2\pi t_o}{T_m},$$

β is the modulation index, and, S(u) and C(u) are the Fresnel integrals

$$S(u) = \int_0^u \sin(\pi\tau^2/2)d\tau$$

$$C(u) = \int_0^u \cos(\pi\tau^2/2)d\tau$$

There exists a slight discrepancy in the phase between the results in [30] and here. This is due to the fact that in [30], $(-1)^n \exp(-j\phi)$ had inadvertently been assigned a phase of $(-1)^{n+1}\phi$ rather than $-(n\pi + \phi)$.

APPENDIX B

ERROR EXPRESSIONS FOR DS/FH, BINARY DPSK SUBJECTED TO DEPENDENT INTERFERENCE

A more complete description of a DS/FH, binary DPSK signal would include the situation in which the same hopping frequency is used for a number of consecutive signaling intervals. The consequence of such a situation is to make the adjacent-interval interference dependent rather than independent. All data-symbol-conditioned error expressions in the body of this report are applicable for this dependent interference situation but with (FM jamming alone)

$$
\begin{aligned}
A_1 &= A_{jr}(t_s - T_b) \\
A_2 &= A_{jp}(t_s) = A_{jr}(t_s) \\
\phi_1 &= \phi_{jr} + \Phi_{jr}(t_s - T_b) \\
\phi_2 &= \phi_{jr} + \Phi_{jr}(t_s)
\end{aligned}
\tag{B-1}
$$

and

$$
\Delta\phi \triangleq \phi_2 - \phi_1 = \Phi_{jr}(t_s) - \Phi_{jr}(t_s - T_b) \tag{B-2}
$$

Since both intervals are jammed, only the results of the (JR,JP) subcase are needed.

For the FM jamming case, the result in Eq. (7-17) can be used but modified according to Eq. (B-1). The result is

$$P_{BFM}(JR,JP,\bar{H},"0",x_r,\phi_1,\Delta\phi)$$

$$= \frac{1}{2}\left\{1 - Q\left[\frac{1}{2}\sqrt{\frac{m_1^2+m_2^2}{N}} \quad , \quad \frac{1}{2}\sqrt{\frac{m_3^2+m_4^2}{N}}\right]\right.$$

$$\left. + Q\left[\frac{1}{2}\sqrt{\frac{m_3^2+m_4^2}{N}} \quad , \quad \frac{1}{2}\sqrt{\frac{m_1^2+m_2^2}{N}}\right]\right\} \qquad \text{(B-3)}$$

where

$$m_1^2+m_2^2 = 4A_s^2 + 4A_s(A_1\cos\phi_1+A_2\cos\phi_2) + 2A_1A_2\cos(\phi_1-\phi_2) + A_1^2 + A_2^2$$

$$= 4A_s^2 + 4A_s(A_1\cos\phi_1+A_2\cos(\phi_1+\Delta\phi)) + 2A_1A_2\cos\Delta\phi + A_1^2 + A_2^2$$

$$m_3^2+m_4^2 = A_1^2 + A_2^2 - 2A_1A_2\cos(\phi_1-\phi_2)$$

$$= A_1^2 + A_2^2 - 2A_1A_2\cos\Delta\phi \qquad \text{(B-4)}$$

and the event $\bar{H}$ represents the fact that no frequency hop has occurred between adjacent intervals.

Eliminating the x_r, ϕ_1 conditioning results in

$$P_{BFM}(JR,JP,\bar{H},"0",\Delta\phi)$$

$$= \left(\frac{1}{2\pi}\right)^2 \int_0^{2\pi}\int_0^{2\pi} P_{BFM}(JR,JP,\bar{H},"0",x_r,\phi_1,\Delta\phi)\,dx_r\,d\phi_1 \qquad \text{(B-5)}$$

where the dependence of the integrand on x_r is implicitly found in A_1 and A_2 via m_1, m_2, m_3, and m_4.

It can be shown that

$$P_{BFM}(JR,JP,\bar{H},"1",\Delta\phi) = P_{BFM}(JR,JP,\bar{H},"0",\Delta\phi+\pi)$$

giving

$$P_{BFM}(JR,JP,\bar{H},\Delta\phi) = \frac{1}{2}\{P_{BFM}(JR,JP,\bar{H},"0",\Delta\phi) + P_{BFM}(JR,JP,\bar{H},"0",\Delta\phi+\pi)\} \tag{B-6}$$

for the special case of $P_o = P_1 = \frac{1}{2}$.

In a CW-tone jamming environment, Eqs. (B-3) and (B-4) are applicable. Thus

$$P_{BCW}(JR,JP,\bar{H},"0",\phi_1,\Delta\phi) = \frac{1}{2}\left\{1 - Q\left[\frac{1}{2}\sqrt{\frac{m_1^2+m_2^2}{N}}\ ,\ \frac{1}{2}\sqrt{\frac{m_3^2+m_4^2}{N}}\right] + Q\left[\frac{1}{2}\sqrt{\frac{m_3^2+m_2^2}{N}}\ ,\ \frac{1}{2}\sqrt{\frac{m_1^2+m_2^2}{N}}\right]\right\} \tag{B-7}$$

and

$$m_1^2+m_2^2 = 4A_s^2 + 4A_s(A_1\cos\phi_1+A_2\cos(\phi_1+\Delta\phi)) + 2A_1A_2\cos\Delta\phi + A_1^2 + A_2^2$$
$$m_3^2+m_4^2 = A_1^2 + A_2^2 - 2A_1A_2\cos\Delta\phi \tag{B-8}$$

where

$$A_1 \triangleq [A_{jr}(t_s - T_b)]_{cw}$$

$$A_2 \triangleq [A_{jr}(t_s)]_{cw}$$

$$\phi_1 \triangleq \phi_{jr} + [\Phi_{jr}(t_s - T_b)]_{cw}$$

$$\phi_2 \triangleq \phi_{jr} + [\Phi_{jr}(t_s)]_{cw}$$

and

$$\Delta\phi = \phi_2 - \phi_1$$

There are two variables to average out immediately. First

$$P_{BCW}(JR, JP, \overline{H}, "0", \Delta\phi)$$

$$= \frac{1}{2\pi} \int_0^{2\pi} P_{BCW}(JR, JP, \overline{H}, "0", \phi_1, \Delta\phi) d\phi_1 \qquad \text{(B-9)}$$

and secondly

$$P_{BCW}(JR, JP, \overline{H}, \Delta\phi) = \frac{1}{2} \{P_{BCW}(JR, JP, \overline{H}, "0", \Delta\phi)$$

$$+ P_{BCW}(JR, JP, \overline{H}, "0", \Delta\phi + \pi)\} \qquad \text{(B-10)}$$

where again the fact that

$$P_{BCW}(JR,JP,\overline{H},"1",\Delta\phi) = P_{BCW}(JR,JP,\overline{H},"0",\Delta\phi+\pi)$$

has been used.

For the noise jamming situation, the jamming signal was assumed to be gaussian noise with a vanishing correlation function at multiples of the sampling time. Therefore, the noise interference remains independent even when a hop does not occur.

Procedures outlined in Chapter X permit the determination of the upper bound to the average error rate for this dependent interference case. However, an additional parameter needs consideration. This parameter is the phase slippage, $\Delta\phi$, of the spread and filtered jamming signal from one interval to the next. Either this parameter would need to be averaged over (if the distribution were known) or simply chosen to maximize the error rate.

If a $\Delta\phi$-maximization occurs, then the overall effect of the (JR,JP) subcase is

$$[P_{BFM}(JR,JP)]_{max} = Pr(H)[P_{BFM}(JR,JP,H)]_{max} + Pr(\overline{H})[P_{BFM}(JR,JP,\overline{H})]_{max}$$

or

$$[P_{BCW}(JR,JP)]_{max} = Pr(H)[P_{BCW}(JR,JP,H)]_{max} + Pr(\overline{H})[P_{BCW}(JR,JP,\overline{H})]_{max}$$

where $P_{BFM}(JR,JP,H)$ and $P_{BCW}(JR,JP,H)$ are the independent interference results of Chapter VII. If the hopping interval (1/rate) were an integer (I_h) multiple of the signaling interval, then

$$Pr(H) = \frac{1}{I_h}$$

$$Pr(\overline{H}) = \frac{I_h - 1}{I_h}$$

APPENDIX C

FOURIER SERIES COEFFICIENTS OF A PSEUDO-RANDOM WAVEFORM

A pseudo-random (PR) waveform can be expressed as an infinite summation of amplitude-scaled and time scaled pulses x(t), whose general shape is shown in Figure 66. Mathematically, a PR waveform, p(t), may be written as

$$p(t) = \sum_{i=-\infty}^{\infty} a_i x(t-iT_c) \tag{C-1}$$

where the $\{a_i\}$ are ±1 and determined from the output of an (r)-stage, maximal-length shift register having the property that

$$a_i = a_{i+p} \tag{C-2}$$

for all i and $p = 2^r-1$. The property in Eq. (C-2) exemplifies the periodic nature of PR sequences, and more general PR waveforms.

Because of the periodicity of p(t) (period = pT_c), it can be optimally (in the mean-square-convergence sense) expanded into a complex Fourier series. Such an expansion results in

$$p(t) = \sum_{m=-\infty}^{\infty} c_m \exp[j(\frac{2\pi m}{pT_c})t] \tag{C-3}$$

where

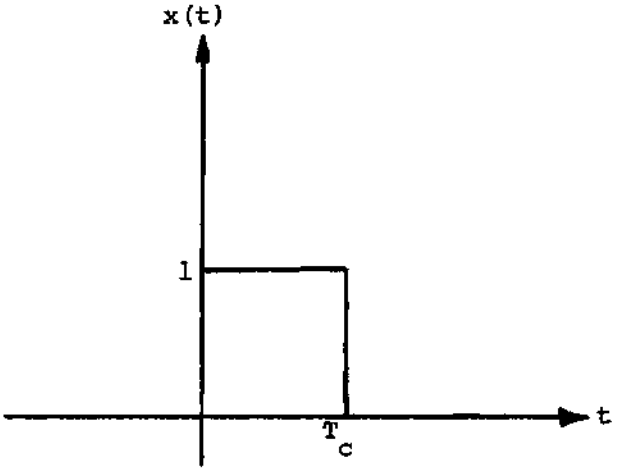

FIGURE 66. Basic Waveshape for Each PR Chip

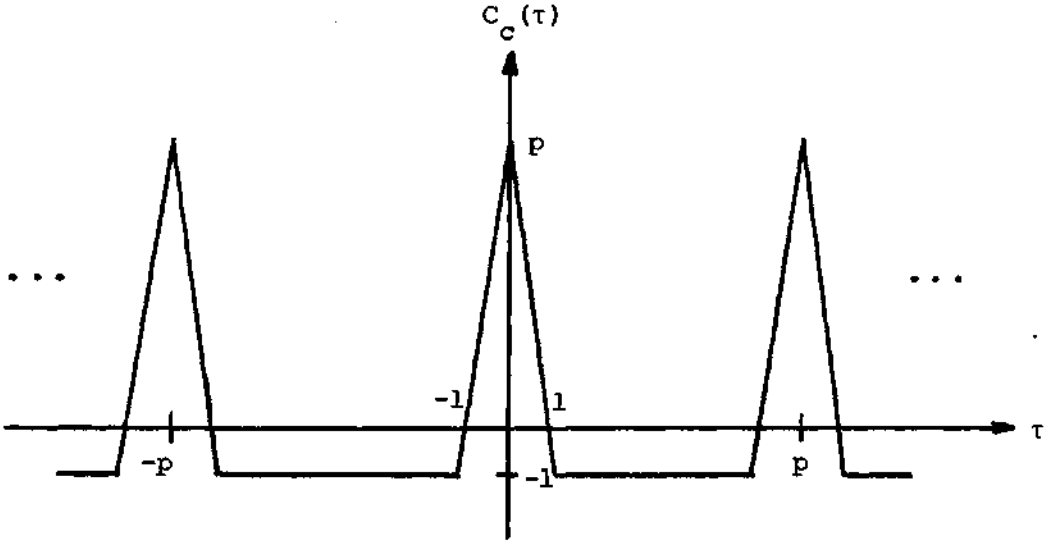

FIGURE 67. Continuous Version of the Unnormalized Autocorrelation Function for a PR Code Sequence Consisting of Elements ± 1

$$c_m = \frac{1}{pT_c} \int_o^{pT_c} p(t)\exp[-j(\frac{2\pi m}{pT_c})t]dt \qquad (C-4)$$

The coefficients, c_m, may also be written as

$$c_m = |c_m|\exp[j\ \phi_m] \qquad (C-5)$$

where

$$|c_m| = (c_m c_m^*)^{\frac{1}{2}} \qquad (C-6)$$

and

$$\phi_m = \arctan\ [\mathrm{Imag}(c_m)/\mathrm{Real}(c_m)] \qquad (C-7)$$

It is the purpose of this appendix to determine the coefficients, c_m.

Substituting Eq. (C-1) into Eq. (C-4) results in

$$c_m = \frac{1}{pT_c} \int_o^{pT_c} (\sum_{i=-\infty}^{\infty} a_i x(t-iT_c))\exp[-j(\frac{2\pi m}{pT_c})t]dt \qquad (C-8)$$

Only one period of p(t) affects the outcome of the integral in Eq. (C-8). Therefore, the summation is made finite over one period and is interchanged with the integration to give

$$c_m = \frac{1}{pT_c} \sum_{i=o}^{p-1} a_i \{\int_o^{pT_c} x(t-iT_c)\exp[-j(\frac{2\pi m}{pT_c})t]dt\} \qquad (C-9)$$

The function $x(t-iT_c)$ is non-zero only over the time interval $(iT_c, (i+1)T_c)$. Thus

$$c_m = \frac{1}{pT_c} \sum_{i=o}^{p-1} a_i \left\{ \int_{iT_c}^{(i+1)T_c} (1) \exp\left[-j\left(\frac{2\pi m}{pT_c}\right) t\right] dt \right\} \qquad \text{(C-10)}$$

The integration in Eq. (C-10) is performed and results in

$$c_m = \frac{1}{pT_c} \sum_{i=o}^{p-1} a_i \left\{ \left(\frac{pT_c}{j2\pi m}\right) \left(\exp\left[-j\left(\frac{2\pi mi}{p}\right)\right] - \exp\left[-j\left(\frac{2\pi m(i+1)}{p}\right)\right]\right)\right\}$$

$$= \frac{1}{2j\pi m} \sum_{i=o}^{p-1} a_i \exp\left[-j\left(\frac{2\pi mi}{p}\right)\right] \left\{1 - \exp\left[-j\left(\frac{2\pi m}{p}\right)\right]\right\}$$

$$= \left(\frac{1}{2j\pi m}\right) \exp\left[-j\left(\frac{\pi m}{p}\right)\right] \left\{\exp\left[j\left(\frac{\pi m}{p}\right)\right] - \exp\left[-j\left(\frac{\pi m}{p}\right)\right]\right\} \cdot \sum_{i=o}^{p-1} a_i \exp\left[-j\left(\frac{2\pi mi}{p}\right)\right]$$

$$= \left(\frac{1}{p}\right) \exp\left[-j\left(\frac{\pi m}{p}\right)\right] \left(\frac{\sin(\pi m/p)}{\pi m/p}\right) \sum_{i=o}^{p-1} a_i \exp\left[-j\left(\frac{2\pi mi}{p}\right)\right]$$

$$= \left(\frac{1}{p}\right) \exp\left[-j\left(\frac{\pi m}{p}\right)\right] \left(\frac{\sin(\pi m/p)}{\pi m/p}\right) \sum_{i=1}^{p} a_i \exp\left[-j\left(\frac{2\pi mi}{p}\right)\right] \qquad \text{(C-11)}$$

where the last step is justified because of Eq. (C-2).

Because of the widespread familiarity with the PR, two-level autocorrelation function, whose continuous version is shown in Figure 67, the relationship between the discrete autocorrelation function,

$C_d(\tau)$, and c_m (specifically $|c_m|$) is now shown. The magnitude-squared of the coefficients in Eq. (C-11) may be written as

$$|c_m|^2 = c_m c_m^*$$

$$= \left|\frac{\sin(\pi m/p)}{\pi m}\right|^2 \left(\sum_{\ell=1}^{p} a_\ell \exp\left[-j\left(\frac{2\pi m\ell}{p}\right)\right]\right)\left(\sum_{i=1}^{p} a_i \exp\left[j\left(\frac{2\pi mi}{p}\right)\right]\right) \tag{C-12}$$

The key step in determining this relationship is to notice that for any L,

$$\sum_{\ell=1}^{p} a_\ell \exp\left[-j\left(\frac{2\pi m\ell}{p}\right)\right] = \sum_{\ell=L+1}^{L+p} a_\ell \exp\left[-j\left(\frac{2\pi m\ell}{p}\right)\right] \tag{C-13}$$

Due to its generality, L may be set equal to i and Eq. (C-13) used in Eq. (C-12) to obtain

$$|c_m|^2 = \left|\frac{\sin(\pi m/p)}{\pi m}\right|^2 \left(\sum_{i=1}^{p} \sum_{\ell=i+1}^{i+p} a_i a_\ell \exp\left[-j\left(\frac{2\pi m}{p}\right)(\ell-i)\right]\right) \tag{C-14}$$

After a summation-variable change ($\ell=\tau+i$), Eq. (C-14) becomes

$$|c_m|^2 = \left|\frac{\sin(\pi m/p)}{\pi m}\right|^2 \left(\sum_{i=1}^{p} \sum_{\tau=1}^{p} a_i a_{i+\tau} \exp\left[-j\left(\frac{2\pi m}{p}\right)\tau\right]\right)$$

$$= \left|\frac{\sin(\pi m/p)}{\pi m}\right|^2 \left(\sum_{\tau=1}^{p} \left\{\sum_{i=1}^{p} a_i a_{i+\tau}\right\} \exp\left[-j\left(\frac{2\pi m}{p}\right)\tau\right]\right)$$

$$= \left|\frac{\sin(\pi m/p)}{\pi m}\right|^2 \left(\sum_{\tau=1}^{p} C_d(\tau) \exp\left[-j\left(\frac{2\pi m}{p}\right)\tau\right]\right) \qquad \text{(C-15)}$$

where

$$C_d(\tau) = \sum_{i=1}^{p} a_i a_{i+\tau} = \{C_c(\tau): \quad \tau=0,\pm1,\pm2, \ldots\}$$

$$= \begin{cases} p & \tau=0,\pm p,\pm 2p, \ldots \\ -1 & \text{elsewhere} \end{cases} \qquad \text{(C-16)}$$

is the unnormalized discrete autocorrelation function of the PR waveform. If m is equal to np (n = 0,±1,±2, . . .), then

$$\sum_{\tau=1}^{p} C_d(\tau) \exp\left[-j\left(\frac{2\pi m}{p}\right)\tau\right] = \sum_{\tau=1}^{p} C_d(\tau)$$

$$= 1 \qquad \text{(C-17)}$$

On the other hand, if m is not equal to np, then

$$\sum_{\tau=1}^{p} C_d(\tau) \exp\left[-j\left(\frac{2\pi m}{p}\right)\tau\right] = C_d(p) + \sum_{\tau=1}^{p-1} (-1) \exp\left[-j\left(\frac{2\pi m}{p}\right)\tau\right]$$

$$= p+1 \qquad \text{(C-18)}$$

With Eqs. (C-17) and (C-18), Eq. (C-15) simplifies to

$$|c_m|^2 = \begin{cases} 1/p^2 & m = 0 \\ 0 & m = \pm p, \pm 2p, \pm 3p, \ldots \\ (p+1)\left|\frac{\sin(\pi m/p)}{\pi m}\right|^2 & \text{otherwise} \end{cases} \qquad \text{(C-19)}$$

The ϕ_m's are written as Eq. (C-7) suggests as

$$\phi_m = \arctan\left\{\frac{-\sin(\pi m/p)\sum_{i=1}^{p} a_i \sin(\frac{2\pi mi}{p} + \frac{\pi m}{p})}{\sin(\pi m/p)\sum_{i=1}^{p} a_i \cos(\frac{2\pi mi}{p} + \frac{\pi m}{p})}\right\}$$

$$= \arctan\left\{\frac{-\sum_{i=1}^{p} a_i \sin(\frac{2\pi mi}{p} + \frac{\pi m}{p})}{\sum_{i=1}^{p} a_i \cos(\frac{2\pi mi}{p} + \frac{\pi m}{p})}\right\}$$

$$+ \pi \cdot \begin{cases} 0 & \ell p \le m < (\ell+1)p \\ & (\ell = 0,2,4,6, \ldots) \\ 1 & (\ell+1)p \le m < (\ell+2)p \end{cases}$$

(C-20)

Note also that

$$\phi_m = -\phi_{-m}$$

$$= \phi_{m+p}$$

The complete PR waveform representation is finally written in

the form

$$p(t) = \sum_{m=-\infty}^{\infty} |c_m| \exp[j(\frac{2\pi m}{pT_c} t + \phi_m)]$$

$$= \sum_{m=o}^{\infty} |c'_m| \cos(m\omega_p t + \phi_m) \qquad \text{(C-21)}$$

where

$$|c'_m| = \begin{cases} 1/p & m = 0 \\ 2\sqrt{p+1} \left| \frac{\sin(\pi m/p)}{\pi m} \right| & m = 1,2,3, \ldots \end{cases} \qquad \text{(C-22)}$$

and

$$\omega_p = \frac{2\pi}{pT_c}$$

APPENDIX D

SPECTRAL-DENSITY-REDUCTION-FACTOR FOR NOISE JAMMING

It is the purpose of this appendix to derive the spectral-density-reduction-factor for the noise jamming signal. A typical low-pass equivalent spectral density of the noise jamming signal is illustrated in Figure 68.

The correlation process forms the product of the noise jamming signal and the PR waveform. Because the jamming signal is assumed to be independent of the PR waveform, the correlation function of this product is equal to the product of the individual correlation functions. Therefore, the spectral density of the product may be determined by evaluating the convolution of the individual spectral densities. One spectral density is given in Figure 68. As for the PR waveform, consider a continuous version of the well-known discrete spectral density. The continuous spectral density of the PR waveform is shown in Figure 69 and mathematically expressed as

$$S_p(f) = T_c\left\{\frac{\sin^2(\pi T_c f)}{(\pi T_c f)^2}\right\} \quad -\infty<f<\infty \tag{D-1}$$

The spread jamming signal has a spectral density denoted as $S_{js}(f)$ and defined by

$$S_{js}(f) = S_j(f) * S_p(f) \tag{D-2}$$

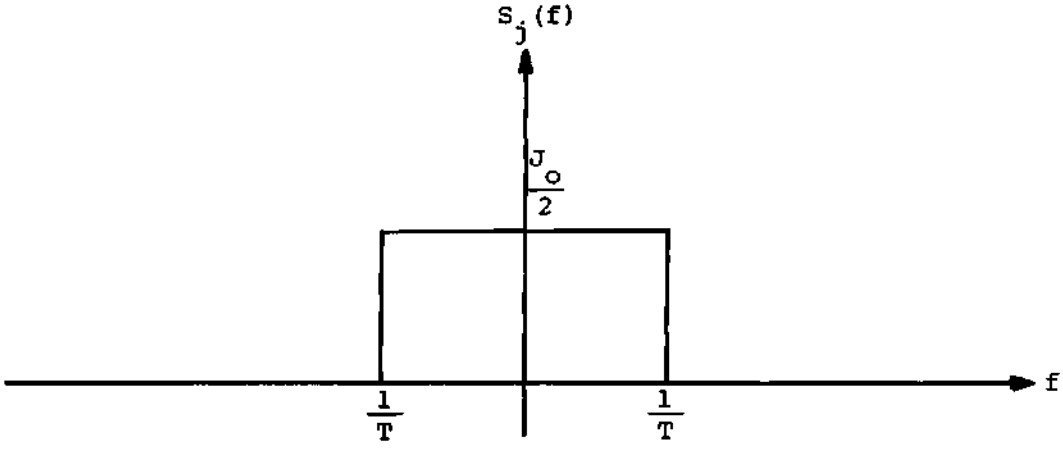

FIGURE 68. Spectral Density of a Wideband Noise Jammer ($\frac{1}{T} \leq \frac{1}{T_c} = R_c$)

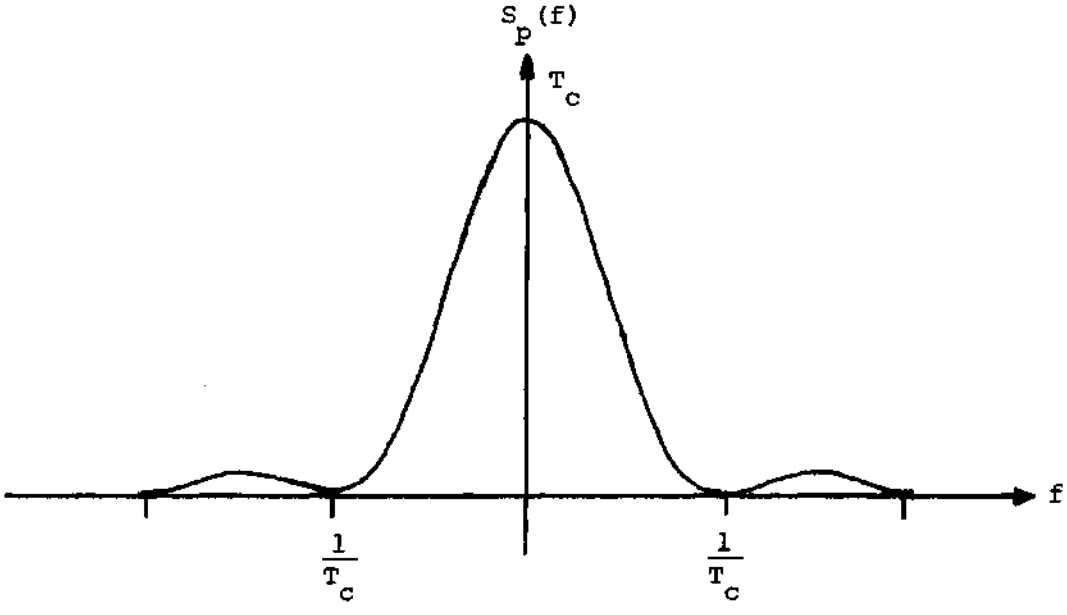

FIGURE 69. Continuous Version of the Well Known Discrete Spectral Density for a PR Waveform of Amplitude ± 1

Notice that if $S_j(f)$ were truly white noise, and denoted as $S_{jw}(f)$, then

$$S_{js}(f) = S_{jw}(f) \ .$$

The convolution of the two functions in Figures 68 and 69 is mathematically written as

$$S_{js}(f) = \int_{-\infty}^{\infty} S_j(f-\lambda) S_p(\lambda) d\lambda$$

$$= \frac{J_o T_c}{2} \int_{-\frac{1}{T}+f}^{\frac{1}{T}+f} \frac{\sin^2(\pi T_c \lambda)}{(\pi T_c \lambda)^2} d\lambda \qquad \text{(D-3)}$$

The change of variable

$$u = \pi T_c \lambda$$

transforms Eq. (D-3) into

$$S_{js}(f) = \frac{J_o}{2\pi} \int_{\pi T_c (f-\frac{1}{T})}^{\pi T_c (f+\frac{1}{T})} \frac{\sin^2 u}{u^2} du \ . \qquad \text{(D-4)}$$

From [58], it is known that

$$\int \frac{\sin^{2m}(u)}{u^2} du = -\binom{2m}{m} \frac{1}{2^{2m} u}$$

$$+ \frac{(-1)^m}{2^{2m-1}} \sum_{k=o}^{m-1} (-1)^{k+1} \binom{2m}{m} \left\{ \frac{\cos[(2m-2k)u]}{u} + (2m-2k)\,si[(2m-2k)u] \right\} \quad \text{(D-5)}$$

where

$$\binom{b}{a} = \frac{b!}{a!(b-a)!}$$

and

$$si(u) = -\int_u^\infty \frac{\sin(t)}{t}\, dt$$

The function si(u) is related to the well known sine integral, Si(u), by

$$Si(u) = \int_o^u \frac{\sin(t)}{t}\, dt$$

$$= si(u) + \frac{\pi}{2} \quad \text{(D-6)}$$

With m=1 in Eq. (D-5), Eq. (D-4) becomes

$$S_{js}(f) = \frac{J_o}{2\pi} \left\{ \frac{\cos[2\pi T_c(f+\frac{1}{T})]}{2\pi T_c(f+\frac{1}{T})} - \frac{\cos[2\pi T_c(f-\frac{1}{T})]}{2\pi T_c(f-\frac{1}{T})} \right.$$

$$+ si[2\pi T_c(f+\frac{1}{T})] - si[2\pi T_c(f-\frac{1}{T})]$$

$$\left. - \frac{1}{2\pi T_c(f+\frac{1}{T})} + \frac{1}{2\pi T_c(f-\frac{1}{T})} \right\} \quad \text{(D-7)}$$

For the special case of interest, $T=T_c$, Eq. (D-5) reduces to

$$S_{js}(f) = \frac{J_o}{2\pi}\left\{\frac{\cos[2\pi T_c f+2\pi]}{2\pi T_c f+2\pi} - \frac{\cos[2\pi T_c f-2\pi]}{2\pi T_c f-2\pi}\right.$$

$$+ \mathrm{si}[2\pi T_c f+2\pi] - \mathrm{si}[2\pi T_c f-2\pi]$$

$$\left. - \frac{1}{2\pi T_c f+2\pi} + \frac{1}{2\pi T_c f-2\pi}\right\} \qquad \text{(D-8)}$$

which is plotted in Figure 70 for frequencies spanning half of the spread bandwidth. Since the correlation process includes a narrowband filter, the spectral density over the bandwidth of the filter will be approximately constant (see Figure 70) with a value of

$$S_{js}(f=0) = \frac{J_o}{2\pi}\{\mathrm{si}(2\pi) - \mathrm{si}(-2\pi)\}$$

$$= \frac{J_o}{2\pi}\{\pi + 2\mathrm{si}(2\pi)\}$$

$$= \frac{J_o}{\pi}\,\mathrm{Si}(2\pi)$$

$$= \frac{J_o}{2} \cdot S_n \qquad \text{(D-9)}$$

where

$$S_n = \frac{2}{\pi}\,\mathrm{Si}(2\pi) = .902823349530 \qquad \text{(D-10)}$$

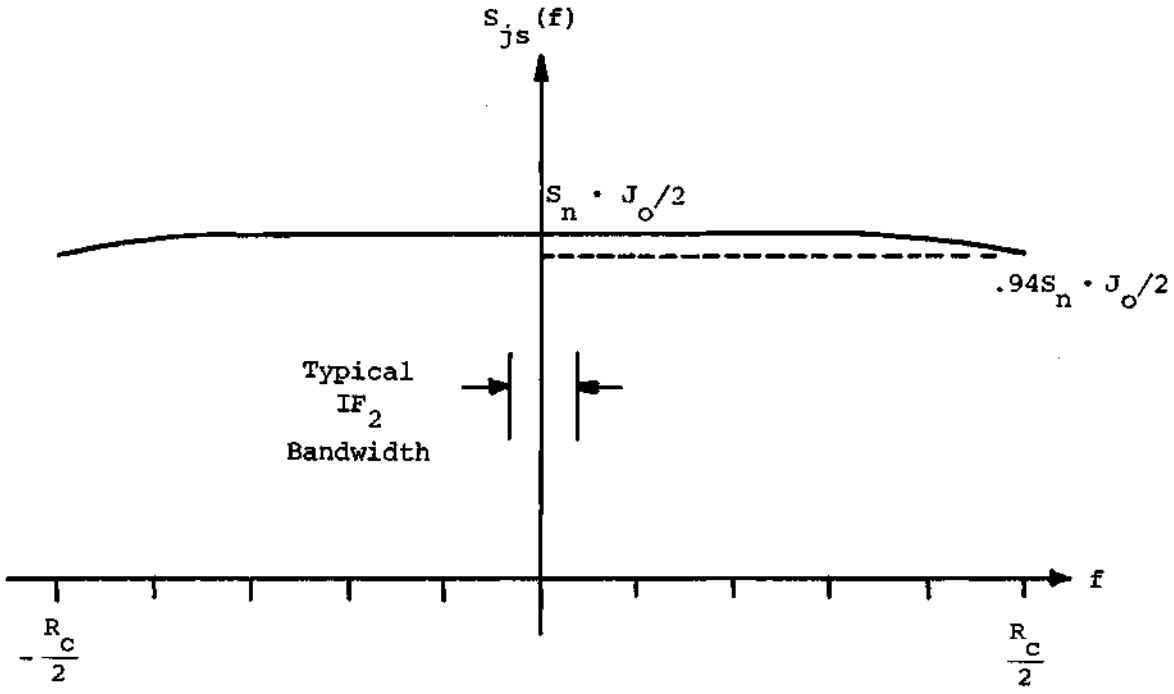

FIGURE 70. Spectral Density of a Spread Noise Jammer Over the Frequency Range $(-\frac{R_c}{2}, \frac{R_c}{2})$

A continuous approximation, rather than the precise discrete spectral density of the PR waveform for each value of p, was used to determine $S_{js}(f=0)$. If the discrete density were used it can be readily seen that

$$S_{js}(f=0) = \frac{J_o}{2} \left(\sum_{m=-(p-1)}^{p-1} |c_m|^2 \right) \qquad \text{(D-11)}$$

Using the results of Appendix C, Eq. (D-11) becomes

$$S_{js}(f=0) = \frac{J_o}{2} \left(\frac{1}{p^2} + 2 \sum_{m=1}^{p-1} |c_m|^2 \right) \qquad \text{(D-12)}$$

$$= \frac{J_o}{2} \left(\frac{1}{p^2} + 2(p+1) \sum_{m=1}^{p-1} \frac{\sin^2(\pi m/p)}{(\pi m)^2} \right)$$

where for p=7

$$S_{js}(f=0) = \frac{J_o}{2}(.9093651853)$$

or

$$S_n = .9093651853 \ .$$

Thus, the continuous version is a valid approximation.

APPENDIX E

PROOF THAT $PR(ERR|JR,\overline{JP}) = PR(ERR|\overline{JR},JP)$

Instead of directly considering the error probabilities, it is equivalent to consider the probabilities of a correct decision where the relations

$$\begin{aligned} Pr(cor|\overline{JR},JP) &= 1 - Pr(err|\overline{JR},JP) \\ Pr(cor|JR,\overline{JP}) &= 1 - Pr(err|JR,\overline{JP}) \end{aligned} \tag{E-1}$$

must hold.

If the reference signal were jammed the double-exposure phasor diagram in Figure (71) is valid. The correct decision probability conditioned on α is

$$\begin{aligned} Pr(cor|JR,\overline{JP},\alpha) &= Pr(\gamma_r + \alpha - \tfrac{\pi}{M} < \gamma_p < \gamma_r + \alpha + \tfrac{\pi}{M}) \\ &= Pr(-\tfrac{\pi}{M} + \alpha < \gamma_p - \gamma_r < \tfrac{\pi}{M} + \alpha) \end{aligned} \tag{E-2}$$

In the case of the jamming affecting only the present signal, Figure (72) can be used to show that the conditioned, correct decision probability is

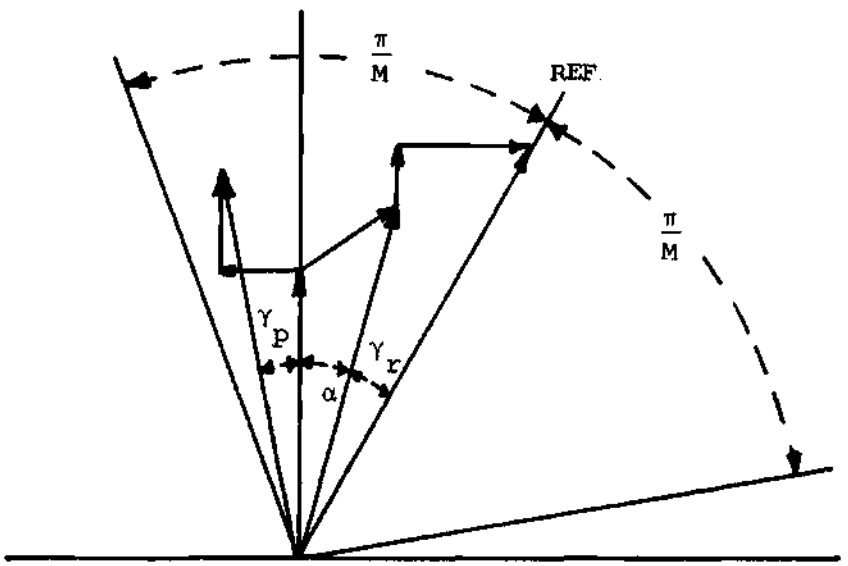

FIGURE 71. Double-Exposure Phasor Diagram for a Jammed Reference Signal (JR)

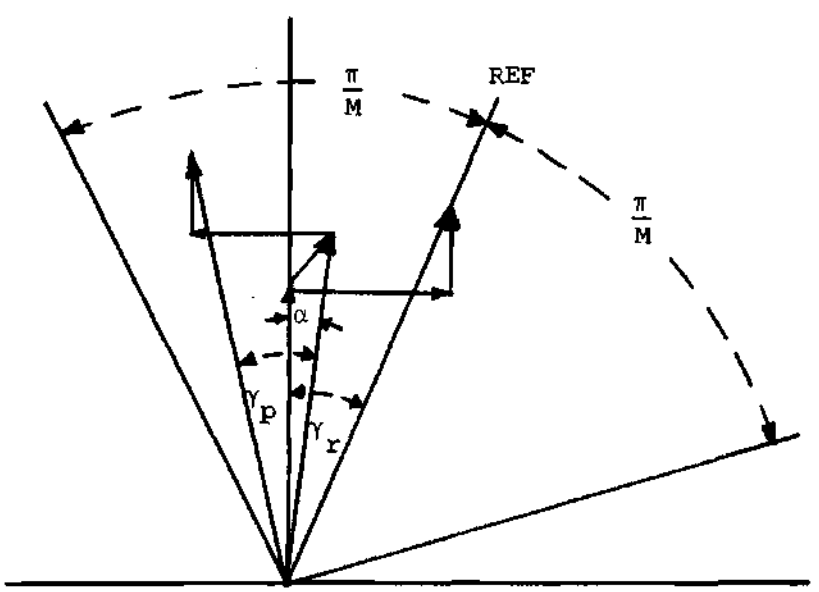

FIGURE 72. Double-Exposure Phasor Diagram for a Jammed Present Signal (JP)

$$\Pr(\text{cor}|\overline{JR},JP,\alpha) = \Pr(\gamma_r - \frac{\pi}{M} < \gamma_p + \alpha < \gamma_r + \frac{\pi}{M})$$

$$= \Pr(-\frac{\pi}{M} - \alpha < \gamma_p - \gamma_r < \frac{\pi}{M} - \alpha)$$

$$= \Pr(-\frac{\pi}{M} + \alpha < \gamma_r - \gamma_p < \frac{\pi}{M} + \alpha) \qquad \text{(E-3)}$$

From Eqs. (E-2) and (E-3), it can be seen that if the density function of $D = \gamma_r - \gamma_p$ is an even function then

$$\Pr(\text{cor}|\overline{JR},JP,\alpha) = \Pr(\text{cor}|JR,\overline{JP},\alpha)$$

and ultimately

$$\Pr(\text{cor}|\overline{JR},JP) = \Pr(\text{cor}|JR,\overline{JP})$$

Therefore, the remainder of this appendix proves that the density function of D is an even function.

The density functions of γ_p and γ_r are well known [16 or Appendix G] and have the individual properties

$$p_{\gamma_p}(\gamma_p) = p_{\gamma_p}(-\gamma_p) \qquad \text{(E-4)}$$

and

$$p_{\gamma_r}(\gamma_r) = p_{\gamma_r}(-\gamma_r) \qquad \text{(E-5)}$$

It is assumed that any conditioning of the density functions for γ_p and γ_r on any random variable (e.g. ϕ_2 or ϕ_1) has been removed. The conditioning or removal of the conditioning does not affect the even properties in Eqs. (E-4) and (E-5).

Denote the probability distribution function of the difference D as

$$P_D(\eta) = Pr(D \leq \eta) = Pr(\gamma_r - \gamma_p \leq \eta)$$

where from Figure (73)

$$P_D(\eta) = Pr(\text{shaded region}) \tag{E-6}$$

Two cases must be considered:

(1) $-2\pi \leq \eta \leq 0$

$P_D(\eta) = Pr(\text{shaded region in Figure (73)})$

$$= \int_{-\pi-\eta}^{\pi} p_{\gamma_p}(\gamma_p) \int_{-\pi}^{\eta+\gamma_p} p_{\gamma_r}(\gamma_r) d\gamma_r d\gamma_p \tag{E-7}$$

(2) $0 \leq \eta \leq 2\pi$

$P_D(\eta) = 1 - Pr(\text{shaded region in Figure (74)})$

$$= 1 - \int_{-\pi}^{\pi-\eta} p_{\gamma_p}(\gamma_p) \int_{\eta+\gamma_p}^{\pi} p_{\gamma_r}(\gamma_r) d\gamma_r d\gamma_p \tag{E-8}$$

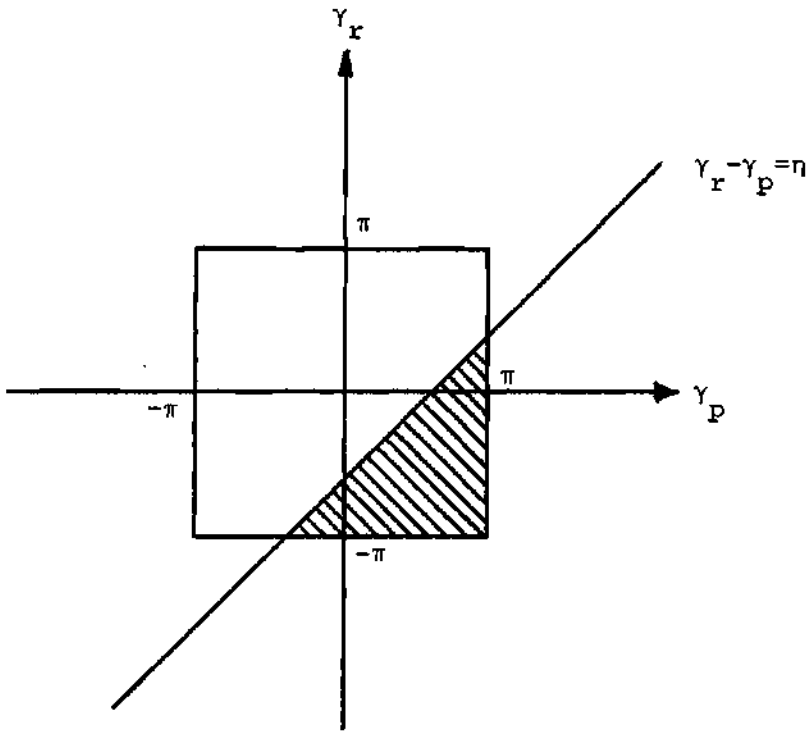

FIGURE 73. Region Containing the Event $\gamma_r-\gamma_p\leq\eta$ for $-2\pi\leq\eta\leq 0$

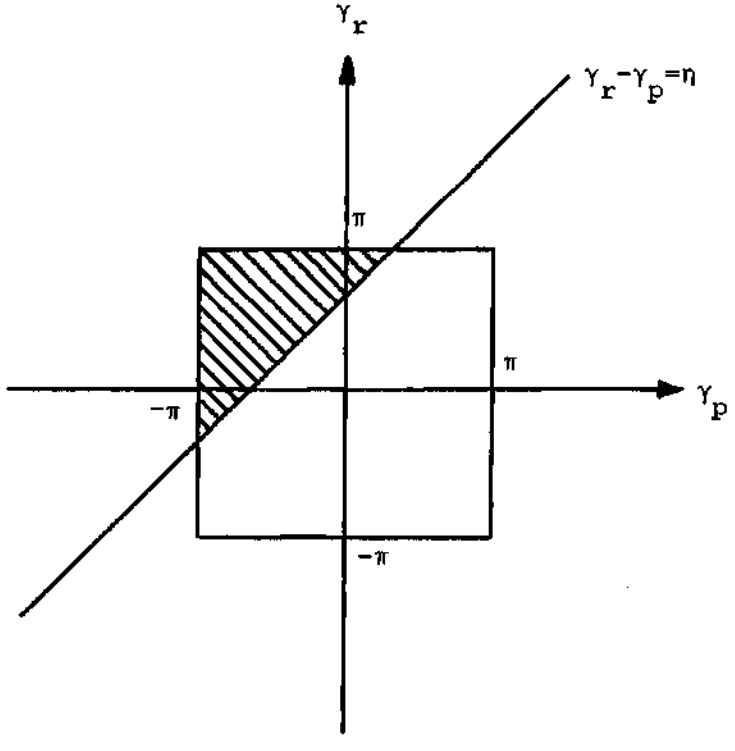

FIGURE 74. Region Containing the Event $\gamma_r-\gamma_p>\eta$ for $0\leq\eta\leq 2\pi$

Determination of $p_D(\eta)$ for $-2\pi \le \eta \le 0$

The probability density function of D for this range of η is, from Eq. (E-7),

$$p_D(\eta) = \frac{d}{d\eta}\,(P_D(\eta))$$

$$= \frac{d}{d\eta}\left\{\int_{-\pi-\eta}^{\pi} p_{\gamma_p}(\gamma_p) \int_{-\pi}^{\eta+\gamma_p} p_{\gamma_r}(\gamma_r)\, d\gamma_r d\gamma_p\right\} \qquad \text{(E-9)}$$

Define $g_1(\gamma_p,\eta)$ to be

$$g_1(\gamma_p,\eta) \triangleq \int_{-\pi}^{\eta+\gamma_p} p_{\gamma_r}(\gamma_r)\, d\gamma_r \qquad \text{(E-10)}$$

Therefore

$$p_D(\eta) = \frac{d}{d\eta}\left\{\int_{-\pi-\eta}^{\pi} p_{\gamma_p}(\gamma_p) g_1(\gamma_p,\eta)\, d\gamma_p\right\}$$

$$= p_{\gamma_p}(-\pi-\eta) g_1(-\pi-\eta,\eta) + \int_{-\pi-\eta}^{\pi} p_{\gamma_p}(\gamma_p)\left(\frac{\partial}{\partial\eta}\, g_1(\gamma_p,\eta)\right) d\gamma_p \qquad \text{(E-11)}$$

From Eq. (E-10), it is seen that

$$g_1(-\pi-\eta,\eta) = \int_{-\pi}^{-\pi} p_{\gamma_r}(\gamma_r)\, d\gamma_r = 0$$

$$\frac{\partial}{\partial\eta}(g_1(\gamma_p,\eta)) = p_{\gamma_r}(\eta+\gamma_p)$$

giving rise to

$$p_D(\eta) = \int_{-\pi-\eta}^{\pi} p_{\gamma_p}(\gamma_p) p_{\gamma_r}(\gamma_p+\eta)\, d\gamma_p \qquad (-2\pi \le \eta \le 0) \qquad \text{(E-12)}$$

Determination of $p_D(\eta)$ for $0 \le \eta \le 2\pi$

Using Eq. (E-8), the probability density function of D for this range of η can be written as

$$p_D(\eta) = \frac{d}{d\eta}(P_D(\eta))$$

$$= \frac{d}{d\eta}\left\{1 - \int_{-\pi}^{\pi-\eta} p_{\gamma_p}(\gamma_p) \int_{\eta+\gamma_p}^{\pi} p_{\gamma_r}(\gamma_r)\, d\gamma_r d\gamma_p\right\} \qquad \text{(E-13)}$$

With the definition

$$g_2(\gamma_p,\eta) \triangleq \int_{\eta+\gamma_p}^{\pi} p_{\gamma_r}(\gamma_r)\, d\gamma_r \qquad \text{(E-14)}$$

the density function in Eq. (E-13) becomes

$$p_D(\eta) = -\frac{d}{d\eta}\left\{\int_{-\pi}^{\pi-\eta} p_{\gamma_p}(\gamma_p) g_2(\gamma_p,\eta)\, d\gamma_p\right\}$$

$$= p_{\gamma_p}(\pi-\eta) g_2(\pi-\eta,\eta) - \int_{-\pi}^{\pi-\eta} p_{\gamma_p}(\gamma_p)\left(\frac{\partial}{\partial\eta} g_2(\gamma_p,\eta)\right) d\gamma_p$$

(E-15)

The properties

$$g(\pi-\eta,\eta) = \int_{\pi}^{\pi} p_{\gamma_p}(\gamma_p)d\gamma_p = 0$$

$$\frac{\partial}{\partial\eta} g_2(\gamma_p,\eta) = -p_{\gamma_r}(\eta+\gamma_p)$$

are now used in Eq. (E-15) to produce

$$p_D(\eta) = \int_{-\pi}^{\pi-\eta} p_{\gamma_p}(\gamma_p)p_{\gamma_r}(\eta+\gamma_p)d\gamma_p \qquad (0\le\eta\le2\pi) \qquad \text{(E-16)}$$

Proof of Evenness Property

If $p_D(\eta)$ is even, then

$$p_D(\eta)\Big|_{-2\pi\le\eta\le0} = p_D(-\eta)\Big|_{0\le\eta\le2\pi}$$

must be shown. From Eq. (E-16) it is seen that

$$p_D(-\eta)\Big|_{0\le\eta\le2\pi} = \int_{-\pi}^{\pi+\eta} p_{\gamma_p}(\gamma_p)p_{\gamma_r}(-\eta+\gamma_p)d\gamma_p \qquad \text{(E-17)}$$

With the change of variable, $u = -\gamma_p$, Eq. (E-17) becomes

$$p_D(-\eta)\Big|_{0\le\eta\le2\pi} = -\int_{\pi}^{-\pi-\eta} p_{\gamma_p}(-u)p_{\gamma_r}(-\eta-u)du$$

$$= \int_{-\pi-\eta}^{\pi} p_{\gamma_p}(u)p_{\gamma_r}(\eta+u)du$$

$$= p_D(\eta)\Big|_{-2\pi \le \eta \le 0}$$

Therefore $p_D(\eta)$ is an even function and consequently

$$\Pr(\text{cor}\,|\,\overline{\text{JR}},\text{JP}) = \Pr(\text{cor}\,|\,\text{JR},\overline{\text{JP}})$$

or

$$\Pr(\text{err}\,|\,\overline{\text{JR}},\text{JP}) = \Pr(\text{err}\,|\,\text{JR},\overline{\text{JP}})$$

APPENDIX F

PRICE'S FUNCTION

In [53], Price evaluated the double integral

$$a^{-\mu}b^{-\nu}\int_0^{\infty} x^{\mu+1}\exp[-\tfrac{1}{2}(x^2+a^2)]I_{\mu}(ax)\,dx \cdot$$

$$\int_0^{rx} y^{\nu+1}\exp[-\tfrac{1}{2}(y^2+b^2)]I_{\nu}(by)\,dy$$

where $I_{\mu}(z)$ is the modified Bessel function of the first kind, order μ, and argument z.

Price denoted the double integral as $P_{\mu,\nu}(a,b;r)$ and found it to be

$$P_{\mu,\nu}(a,b;r) = P_{o,o}(a,b;r)$$

$$+ \exp[-\frac{a^2r^2+b^2r^{-1}}{2R}] \sum_{m=-\nu}^{\mu} C_m(\mu,\nu;r)(\frac{br}{a})^m I_m(\frac{ab}{R})$$

where

$$P_{o,o}(a,b;r) = Q\left(\frac{ar}{\sqrt{1+r^2}}\right),\left(\frac{b}{\sqrt{1+r^2}}\right) -$$

$$(1+r^2)^{-1}\exp\left[-\frac{a^2r^2+b^2}{2(1+r^2)}\right]I_0\left(\frac{abr}{1+r^2}\right)$$

$$C_m(\mu,\nu;r) = \begin{cases} \sum_{k=m}^{\mu} \binom{\nu+k}{k-m} r^{\nu-k+1} R^{-\nu-k-1} - \delta_{m0}\left(\frac{r^2}{1+r^2}\right) & m \geq 0 \\ -C_{-m}(\nu,\mu;r^{-1}) & m \leq -1 \end{cases}$$

$$R = r + r^{-1}$$

$$\delta_{m0} \triangleq \begin{cases} 1 & \text{if } m=0 \\ 0 & \text{otherwise} \end{cases}$$

and $Q(\cdot,\cdot)$ is the Marcum-Q function.

APPENDIX G

DERIVATION OF $p_{\gamma|\phi_1}(\gamma|\phi_1)$

From Figure 9 in Chapter VIII, the independent orthogonal noise components (x_1, y_1) may be rotated and aligned with the phasor $\vec{Z}$. The result of such an alignment is illustrated in Figure 75, where the phasor $\vec{Z}$ has the squared-magnitude

$$|\vec{Z}|^2 = (A_s + A_1\cos\phi_1)^2 + (A_1\sin\phi_1)^2 \ .$$

With the definitions

$$x = x_1 + |\vec{Z}|$$

$$y = y_1$$

and the fact that x_1 and y_1 are independent, zero-mean, gaussian random variables with variance N, the joint density function of x and y may be written directly as

$$p_{x,y|\phi_1}(x,y|\phi_1) = \frac{1}{2\pi N} \exp\left\{-\frac{(x-|\vec{Z}|)^2 + y^2}{2N}\right\} \qquad \text{(G-1)}$$

A change to polar coordinates transforms the x and y characterization into an (r,γ) description, where

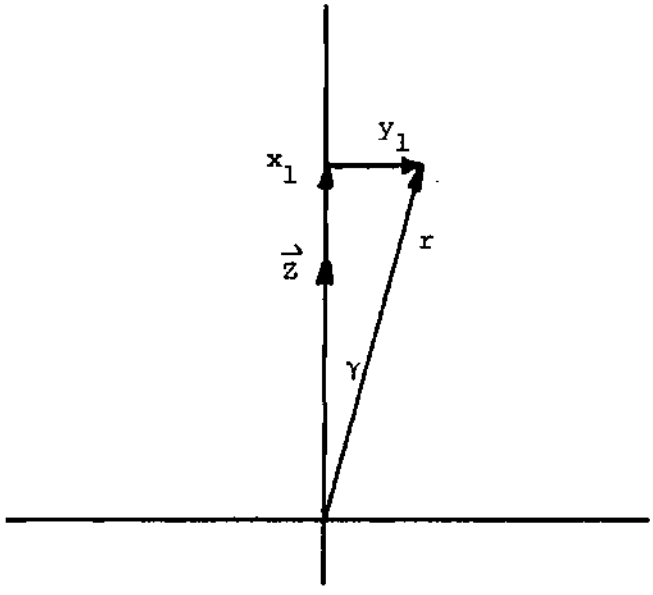

FIGURE 75. Quadrature Noise Components Properly Aligned With The Interference-Corrupted Desired Signal Phasor, $\vec{z}$

$$x = r\cos\gamma$$

$$y = r\sin\gamma$$

thus giving

$$r = \sqrt{x^2+y^2}$$

$$\gamma = \arctan\left(\frac{y}{x}\right)$$

The Jacobian of such a transformation is

$$J(r,\gamma) \triangleq \begin{vmatrix} \frac{\partial x}{\partial r} & \frac{\partial x}{\partial \gamma} \\ \frac{\partial y}{\partial r} & \frac{\partial y}{\partial \gamma} \end{vmatrix} = \begin{vmatrix} \cos\gamma & -r\sin\gamma \\ \sin\gamma & r\cos\gamma \end{vmatrix}$$

$$= r$$

thereby producing a transformed joint density function of the form

$$p_{r,\gamma|\phi_1}(r,\gamma|\phi_1) = p_{x,y|\phi_1}(r\cos\gamma,\ r\sin\gamma|\phi_1)J(r,\gamma)$$

$$= \frac{r}{2\pi N}\exp\left\{-\left[\frac{(r\cos\gamma-|\vec{Z}|)^2 + (r\sin\gamma)^2}{2N}\right]\right\}$$

$$= \frac{r}{2\pi N}\exp\left\{-\left[\frac{r^2 + |\vec{Z}|^2 - 2r|\vec{Z}|\cos\gamma}{2N}\right]\right\} \qquad (G\text{-}2)$$

The desired conditional density function of γ may be determined

by averaging Eq. (G-2) over all values of r. Thus

$$p_{\gamma|\phi_1}(\gamma|\phi_1) = \frac{1}{2\pi N} \exp\left[-\frac{|\vec{Z}|^2}{2N}\right] \int_0^\infty r \exp\left[-\left(\frac{r^2 - 2r|\vec{Z}|\cos\gamma}{2N}\right)\right] dr \qquad \text{(G-3)}$$

With the change of variable

$$\lambda = (r - |\vec{Z}|\cos\gamma)\frac{1}{\sqrt{N}} \quad ,$$

the argument of the exponential in the integrand becomes

$$\frac{1}{2N}\{(\sqrt{N}\lambda + |\vec{Z}|\cos\gamma)^2 - 2(\sqrt{N}\lambda + |\vec{Z}|\cos\gamma)|\vec{Z}|\cos\gamma\}$$

$$= \frac{1}{2N}\{N\lambda^2 - |\vec{Z}|^2\cos^2\gamma\}$$

Therefore

$$p_{\gamma|\phi_1}(\gamma|\phi_1) = \frac{1}{2\pi\sqrt{N}} \exp\left[-\frac{1}{2N}(|\vec{Z}|^2\sin^2\gamma)\right] \cdot$$

$$\int_{\frac{-|\vec{Z}|\cos\gamma}{\sqrt{N}}}^{\infty} (\sqrt{N}\lambda + |\vec{Z}|\cos\gamma) \exp\left[-\frac{\lambda^2}{2}\right] \cdot d\lambda$$

$$= \frac{1}{2\pi} \exp\left[-\frac{1}{2N}(|\vec{Z}|^2\sin^2\gamma)\right] \int_{\frac{-|\vec{Z}|\cos\gamma}{\sqrt{N}}}^{\infty} \lambda \exp\left[-\frac{\lambda^2}{2}\right] d\lambda$$

$$+ \frac{1}{2\pi\sqrt{N}} \left(|\vec{Z}|\cos\gamma\right) \exp\left[-\frac{1}{2N}\left(|\vec{Z}|^2\sin^2\gamma\right)\right] \int_{\frac{-|\vec{Z}|\cos\gamma}{\sqrt{N}}}^{\infty} \exp\left[-\frac{\lambda^2}{2}\right]d\lambda \qquad \text{(G-4)}$$

The first integral of Eq. (G-4) is easily evaluated as

$$\int_{\frac{-|\vec{Z}|\cos\gamma}{\sqrt{N}}}^{\infty} \lambda \exp\left[-\frac{\lambda^2}{2}\right]d\lambda = \exp\left[-\frac{|\vec{Z}|^2\cos^2\gamma}{2N}\right] \qquad \text{(G-5)}$$

With the definition

$$\text{erf}(u) = \frac{2}{\sqrt{\pi}} \int_0^u \exp\left[-t^2\right]dt$$

and the identities

$$\text{erf}(\infty) = 1$$

$$\text{erf}(-u) = -\text{erf}(u)$$

the second integral becomes

$$\int_{\frac{-|\vec{Z}|\cos\gamma}{\sqrt{N}}}^{\infty} \exp\left[-\frac{\lambda^2}{2}\right]d\lambda = \sqrt{2} \int_{\frac{-|\vec{Z}|\cos\gamma}{\sqrt{2N}}}^{\infty} \exp\left[-\lambda^2\right]d\lambda$$

$$= -\sqrt{2} \int_0^{-\frac{|\vec{Z}|\cos\gamma}{\sqrt{2N}}} \exp\left[-\lambda^2\right]d\lambda + \sqrt{2} \int_0^{\infty} \exp\left[-\lambda^2\right]d\lambda$$

$$= \sqrt{\frac{\pi}{2}}\ \mathrm{erf}\left(\frac{|\vec{Z}|\cos\gamma}{\sqrt{2N}}\right) + \sqrt{\frac{\pi}{2}}$$

$$= \sqrt{\frac{\pi}{2}}\ \left\{1 + \mathrm{erf}\left(\frac{|\vec{Z}|\cos\gamma}{\sqrt{2N}}\right)\right\} \qquad \text{(G-6)}$$

The conditional density function of γ is now, via Eqs. (G-5) and (G-6), equal to

$$p_{\gamma|\phi_1}(\gamma|\phi_1) = \frac{1}{2\pi}\exp[-\rho]\left\{1 + \sqrt{\rho\pi}\,\cos\gamma\,\exp[\rho\cos^2\gamma]\,(1 + \mathrm{erf}(\sqrt{\rho}\,\cos\gamma))\right\}$$

where

$$\rho = \frac{|\vec{Z}|^2}{2N} = \frac{1}{2N}[(A_s + A_1\cos\phi_1)^2 + (A_1\sin\phi_1)^2]$$

APPENDIX H

STEPS LEADING TO ROSENBAUM'S EQUIVALENT EXPRESSION

In Chapter IX, details of a number of mathematical steps were omitted in obtaining Eq. (9-6) from Eq. (9-5). The steps were derived by Rosenbaum [22,38] and are presented here for completeness.

Within this derivation, the probability distribution function for the absolute value of the angle θ must be used. The distribution function is denoted as $P_{|\theta|}(\theta)$. Because of the notational similarities this distribution exhibits with the half-plane probability functions, $P_p[\lambda]$ and $P_r[\lambda]$, a mental note at this time of their basic differences should be made to avoid confusion in the steps to follow.

From Eq. (9-5), the starting point is

$$I \triangleq P^u(\text{err}|\text{"0"}, x_r, x_p)$$

$$= \int_{-\pi}^{\pi} p_\theta(\theta)\{P_p[A_s\cos(\theta+\theta_c)] + P_p[A_s\cos(\theta-\theta_c)]\}d\theta \qquad \text{(H-1)}$$

The steps presented here eliminate the probability density function $p_\theta(\theta)$.

The first step is to integrate Eq. (H-1) by parts. With $P_p'[\lambda] \triangleq \frac{d}{d\lambda} P_p[\lambda]$, the factors of this integration are

$$u = P_p[A_s\cos(\theta\pm\theta_c)] \qquad du = -A_s\sin(\theta\pm\theta_c)P_p'[A_s\cos(\theta\pm\theta_c)]d\theta$$

$$dv = 2\, p_{\theta}(\theta)d\theta \qquad\qquad v = P_{|\theta|}(\theta)$$

Equation (H-1) is transformed into

$$I = \{P_{|\theta|}(\theta)(P_p[A_s\cos(\theta+\theta_c)] + P_p[A_s\cos(\theta-\theta_c)])\}\Big|_o^{\pi}$$

$$+ A_s \int_o^{\pi} P_{|\theta|}(\theta)\{\sin(\theta+\theta_c)P_p'[A_s\cos(\theta+\theta_c)] + \sin(\theta-\theta_c)P_p'[A_s\cos(\theta-\theta_c)]\}d\theta \qquad \text{(H-2)}$$

With the identities

$$P_{|\theta|}(0) = 0$$

$$P_{|\theta|}(\pi) = 1$$

and

$$\cos(\pi+\theta_c) = \cos(\pi-\theta_c)\ ,$$

Eq. (H-2) becomes

$$I = 2\, P_p[-A_s\cos\theta_c] + A_s \int_o^{\pi/2} \{P_{|\theta|}(\theta) + P_{|\theta|}(\pi-\theta)\} \cdot$$

$$\{\sin(\theta+\theta_c)P_p'[A_s\cos(\theta+\theta_c)] + \sin(\theta-\theta_c)P_p'[A_s\cos(\theta-\theta_c)]\}d\theta \qquad \text{(H-3)}$$

where, from the last property in Eq. (9-4), the identity $P'_p[\lambda] = P'_p[-\lambda]$ has been used.

Consider Figure 76 wherein a set of boundaries are located $\pm\xi$ radians away from the uncorrupted reference signal. The perpendicular distance from the tip of the uncorrupted reference signal to the boundaries is $A_s\sin(\xi)$. Circularly symmetric noise-plus-interference will cause the reference to deviate by some angle (say θ) from the uncorrupted reference signal. It is evident from Figure 76 that for a half-plane probability function, $P_r[\lambda]$, defined for the reference signal

$$2\,P_r[A_s\sin(\xi)] = Pr\{|\theta|\geq\xi\} + Pr\{|\theta|\geq\pi-\xi\}$$

$$= 1 - P_{|\theta|}(\xi) + 1 - P_{|\theta|}(\pi-\xi) \qquad \text{(H-4)}$$

Therefore

$$P_{|\theta|}(\xi) + P_{|\theta|}(\pi-\xi) = 2(1 - P_r[A_s\sin(\xi)])$$

$$= 2\,P_r[-A_s\sin(\xi)] \qquad \text{(H-5)}$$

where Eq. (9-4) has again been used in the last step of Eq. (H-5).

The result of Eq. (H-5) can now be used in Eq. (H-3) to give

$$I = 2\,P_p[-A_s\cos\theta_c] + 2\,A_s\int_o^{\pi/2} P_r[-A_s\sin\theta]\cdot$$

$$\{\sin(\theta+\theta_c)P'_p[A_s\cos(\theta+\theta_c)] + \sin(\theta-\theta_c)P'_p[A_s\cos(\theta-\theta_c)]\}d\theta \qquad \text{(H-6)}$$

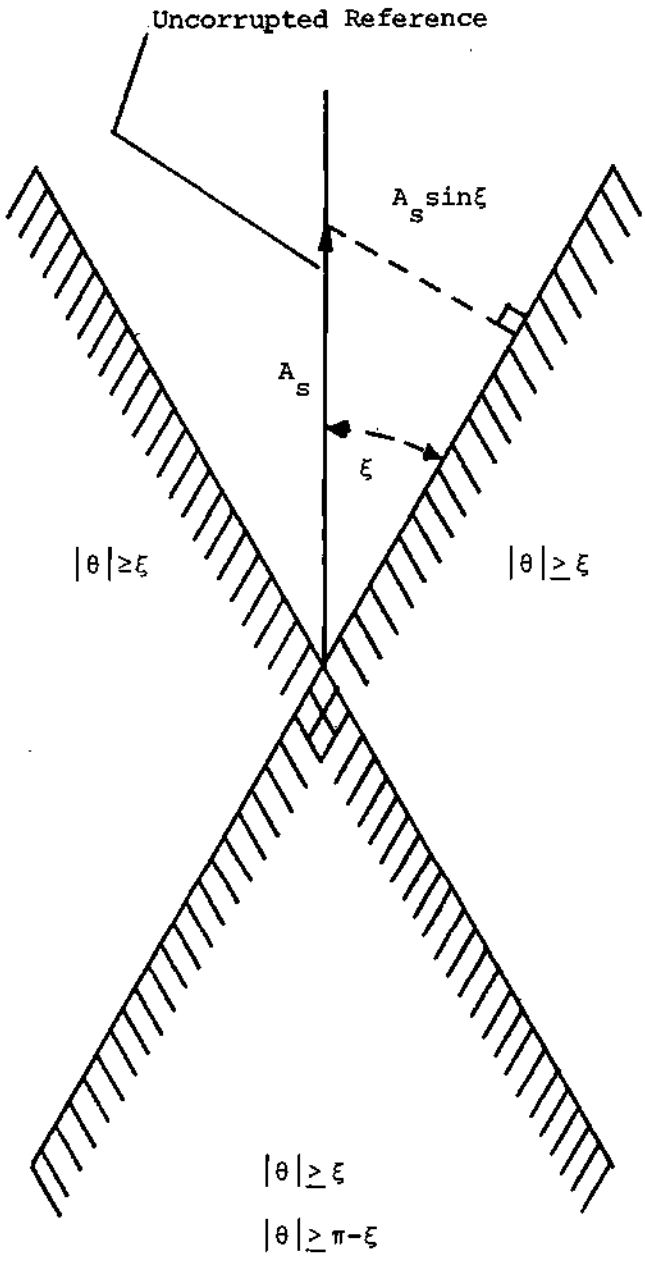

FIGURE 76. Illustration of the Regions Required by Eq. (H-4)

At this point another integration by parts is performed. The factors are

$$u = P_r[-A_s\sin\theta] \qquad du = -A_s\cos\theta\ P_r'[-A_s\sin\theta]d\theta$$

$$dv = \{A_s\sin(\theta+\theta_c)P_p'[A_s\cos(\theta+\theta_c)] + A_s\sin(\theta-\theta_c)P_p'[A_s\cos(\theta-\theta_c)]\}d\theta$$

$$v = -P_p[A_s\cos(\theta+\theta_c)] - P_p[A_s\cos(\theta-\theta_c)]$$

Equation (H-6) becomes

$$I = 2\ P_p[-A_s\cos\theta_c]$$
$$-2\{P_r[-A_s\sin\theta](P_p(A_s\cos(\theta+\theta_c)] + P_p[A_s\cos(\theta-\theta_c)]\}\Big|_0^{\frac{\pi}{2}}$$
$$-2\ A_s\int_0^{\pi/2} P_r'[-A_s\sin\theta]\{P_p[A_s\cos(\theta+\theta_c)] + P_p[A_s\cos(\theta-\theta_c)]\}\cos\theta d\theta \qquad (H-7)$$

With the identities (Eq. (9-4) for the reference signal)

$$P_r'[-A_s\sin\theta] = P_r'[A_s\sin\theta]$$

$$P_r[-A_s\sin(0)] = \frac{1}{2}$$

$$P_p[A_s\cos(\tfrac{\pi}{2}+\theta_c)] + P_p[A_s\cos(\tfrac{\pi}{2}-\theta_c)] = 1$$

Eq. (H-7) reduces to

$$I = 2\,P_r[A_s] - 2\,A_s \int_o^{\pi/2} P'_r[A_s \sin\theta]\{P_p[A_s\cos(\theta+\theta_c)] + P_p[A_s\cos(\theta-\theta_c)]\}\cos\theta\, d\theta$$

as desired.

APPENDIX I

PROOF OF THE EVEN DISTRIBUTION OF ERRORS

Consider the M-ary, double exposure phasor diagram in Figure 77 . The heavy lines (0-A,0-B) are the decision boundaries for this subcase and thus are located at $\pm \frac{\pi}{M}$ radians from the corrupted reference. The angles, α and β, are written in terms of the signal and interference parameters as

$$\alpha = \arctan\left[\frac{A_1 \sin\phi_1}{A_s + A_1 \cos\phi_1}\right] \tag{I-1}$$

$$\beta = \arctan\left[\frac{A_2 \sin\phi_2}{A_s + A_2 \cos\phi_2}\right] \tag{I-2}$$

where ϕ_1 and ϕ_2 are uniformly distributed random variables over the interval $(0,2\pi)$. The variables γ_r and γ_p can be described, respectively, as

$$p_{\gamma_r|\phi_1}(\gamma_r|\phi_1) = \frac{1}{2\pi} \exp[-\rho_r]\{1 + \sqrt{\rho_r \pi}\cos(\rho_r)\exp[\gamma_r \cos^2\gamma_r](1+\mathrm{erf}(\sqrt{\rho_r}\cos\gamma_r))\} \tag{I-3}$$

and

$$p_{\gamma_p|\phi_2}(\gamma_p|\phi_2) = \frac{1}{2\pi}\exp[-\rho_p]\{1+\sqrt{\rho_p \pi}\cos(\gamma_p)\exp[\rho_p \cos^2\gamma_p](1+\mathrm{erf}(\sqrt{\rho_p}\cos\gamma_p))\} \tag{I-4}$$

with

$$\rho_r = \frac{1}{2N}(A_s^2 + A_1^2 + 2A_sA_1\cos\phi_1)$$

and

$$\rho_p = \frac{1}{2N}(A_s^2 + A_2^2 + 2A_sA_2\cos\phi_2)$$

Two error regions, equally-distant from the reference, are shown shaded in Figure 77 and labeled E_1 and E_2. The shaded error region labeled E_1 is located within the angle limits of $\alpha + \gamma_r + \frac{\pi}{M} + \xi$ and $\alpha + \gamma_r + \frac{\pi}{M} + \xi + \eta$ whereas the region labeled E_2 is contained within the angle limits of $\alpha + \gamma_r - \frac{\pi}{M} - \xi - \eta$ and $\alpha + \gamma_r - \frac{\pi}{M} - \xi$.

In order for the lower bound of Chapter IX to be valid, the probability of the interference-plus-noise-corrupted present phasor landing in region E_1 must equal the probability of the phasor landing in region E_2. It is the intent here to prove that

$$\begin{aligned} \Pr(\text{phasor landing in } E_1) &= \Pr(E_1) \\ &= \Pr(E_2) \\ &= \Pr(\text{phasor landing in } E_2) \end{aligned} \qquad \text{(I-5)}$$

From Figure 77 it is evident that

$$\Pr(E_1) = \Pr\{\alpha + \gamma_r + \frac{\pi}{M} + \xi < \gamma_p + \beta < \alpha + \gamma_r + \frac{\pi}{M} + \xi + \eta\}$$

$$= \Pr\{\frac{\pi}{M} + \xi < \gamma_p + \beta - \gamma_r - \alpha < \frac{\pi}{M} + \xi + \eta\} \qquad \text{(I-6)}$$

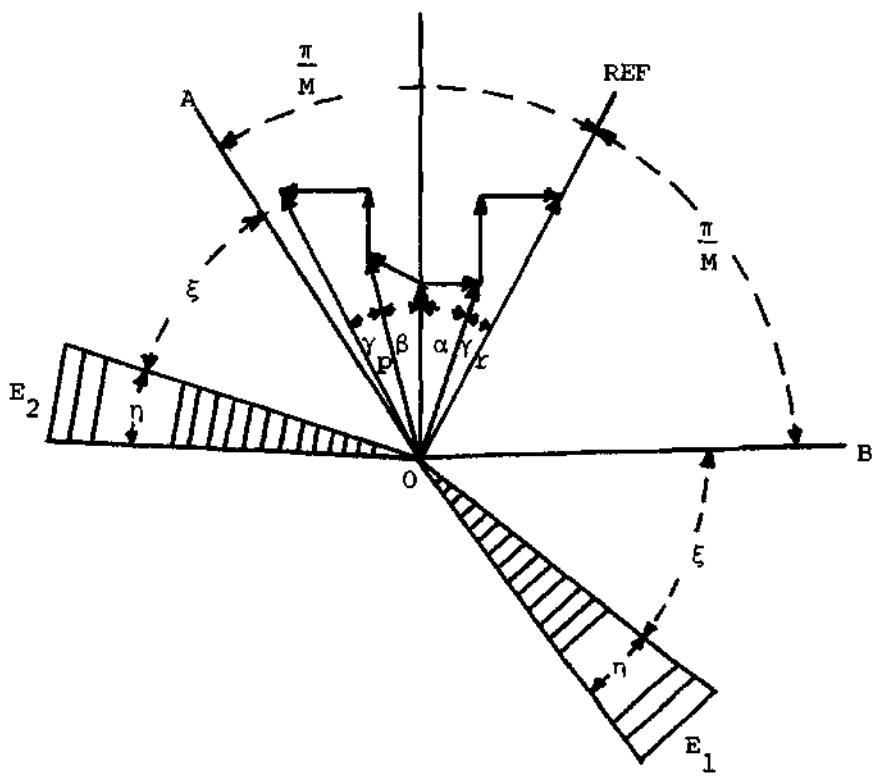

FIGURE 77. Double-Exposure Phasor Diagram Depicting the Equally-Spread Error Regions E_1 and E_2

$$\Pr(E_2) = \Pr\{\alpha + \gamma_r - \frac{\pi}{M} - \xi - \eta < \gamma_p + \beta < \alpha + \gamma_r - \frac{\pi}{M} - \xi\}$$

$$= \Pr\{-\frac{\pi}{M} - \xi - \eta < \gamma_p + \beta - \gamma_r - \alpha < -\frac{\pi}{M} - \xi\} \qquad \text{(I-7)}$$

It follows that if the probability density function of the random variable

$$Z = \gamma_p + \beta - \gamma_r - \alpha$$

is an even function, then Eq. (I-3) is satisfied.

Define two random variables

$$Z_1 \triangleq -(\gamma_r+\alpha) \qquad \text{(I-8)}$$

and

$$Z_2 \triangleq \gamma_p + \beta \qquad \text{(I-9)}$$

having conditional density functions

$$p_{Z_1|\phi_1}(z_1|\phi_1) = p_{\gamma_r|\phi_1}(-z_1-\alpha|\phi_1)$$

$$= p_{\gamma_r|\phi_1}(z_1+\alpha|\phi_1) \qquad \text{(I-10)}$$

and

$$p_{Z_2|\phi_2}(z_2|\phi_2) = p_{\gamma_p|\phi_2}(z_2-\beta|\phi_2) \qquad \text{(I-11)}$$

The random variables Z_1 and Z_2 are independent of each other so that

$$p_{Z|\phi_1,\phi_2}(z|\phi_1,\phi_2) = p_{Z_1|\phi_1}(\cdot|\phi_1) * p_{Z_2|\phi_2}(\cdot|\phi_2)$$

where * denotes convolution. Furthermore

$$p_Z(z) = \left(\frac{1}{2\pi}\right)^2 \int_0^{2\pi}\int_0^{2\pi} \left\{ \int_{-\infty}^{\infty} p_{Z_2|\phi_2}(u|\phi_2) p_{Z_1|\phi_1}(z-u|\phi_1)\,du \right\} d\phi_1 d\phi_2 \tag{I-12}$$

It remains to show that $p_Z(z) = p_Z(-z)$.

The (ϕ_1,ϕ_2) area of integration can be divided into four separate areas, thus transforming Eq. (I-12) into the sum of four triple integrals. The separate areas are:

$$(1)\quad \text{Area 1} = \begin{cases} 0<\phi_1<\pi \\ 0<\phi_2<\pi \end{cases}$$

$$(2)\quad \text{Area 2} = \begin{cases} 0<\phi_1<\pi \\ \pi<\phi_2<2\pi \end{cases}$$

$$(3)\quad \text{Area 3} = \begin{cases} \pi<\phi_1<2\pi \\ 0<\phi_2<\pi \end{cases}$$

$$(4)\quad \text{Area } 4 = \begin{cases} \pi<\phi_1<2\pi \\ \\ \pi<\phi_2<2\pi \end{cases}$$

From Eq. (I-1) and (I-2), each area places certain limits on α and β. In fact,

$$\text{Area } 1 \Longrightarrow \begin{cases} \alpha>0 \\ \beta>0 \end{cases}$$

$$\text{Area } 2 \Longrightarrow \begin{cases} \alpha>0 \\ \beta<0 \end{cases}$$

$$\text{Area } 3 \Longrightarrow \begin{cases} \alpha<0 \\ \beta>0 \end{cases}$$

$$\text{Area } 4 \Longrightarrow \begin{cases} \alpha<0 \\ \beta<0 \end{cases}$$

Assign the triple integration over area j the notation $p_j(z)$. Therefore

$$p_1(z) = \left(\frac{1}{2\pi}\right)^2 \int_0^{\pi}\int_0^{\pi}\left\{\int_{-\infty}^{\infty} p_{Z_2|\phi_2}(u|\phi_2)\,p_{Z_1|\phi_1}(z-u|\phi_1)\,du\right\}d\phi_1 d\phi_2$$

$$= \left(\frac{1}{2\pi}\right)^2 \int_0^{\pi}\int_0^{\pi}\left\{\int_{-\infty}^{\infty} p_{\gamma_p|\phi_2}(u-|\beta|\,|\phi_2)\,p_{\gamma_r|\phi_1}(z-u+|\alpha|\,|\phi_1)\,du\right\}d\phi_1 d\phi_2$$

(I-13)

$$p_2(z) = \left(\frac{1}{2\pi}\right)^2 \int_{\pi}^{2\pi}\int_{o}^{\pi}\left\{\int_{-\infty}^{\infty} p_{\gamma_p|\phi_2}(u+|\beta|\,|\phi_2)\,p_{\gamma_r|\phi_1}(z-u+|\alpha|\,|\phi_1)\,du\right\}d\phi_1 d\phi_2 \tag{I-14}$$

$$p_3(z) = \left(\frac{1}{2\pi}\right)^2 \int_{o}^{\pi}\int_{\pi}^{2\pi}\left\{\int_{-\infty}^{\infty} p_{\gamma_p|\phi_2}(u-|\beta|\,|\phi_2)\,p_{\gamma_r|\phi_1}(z-u-|\alpha|\,|\phi_1)\,du\right\}d\phi_1 d\phi_2 \tag{I-15}$$

and

$$p_4(z) = \left(\frac{1}{2\pi}\right)^2 \int_{\pi}^{2\pi}\int_{\pi}^{2\pi}\left\{\int_{-\infty}^{\infty} p_{\gamma_p|\phi_2}(u+|\beta|\,|\phi_2)\,p_{\gamma_r|\phi_1}(z-u-|\alpha|\,|\phi_1)\,du\right\}d\phi_1 d\phi_2 \tag{I-16}$$

It then follows that

$$p_Z(z) = p_1(z) + p_2(z) + p_3(z) + p_4(z) \tag{I-17}$$

In Eqs. (I-15) and (I-16), let $u \to -u$, use the evenness properties of $p_{\gamma_p|\phi_2}(\cdot\,|\phi_2)$ and $p_{\gamma_r|\phi_1}(\cdot\,|\phi_1)$, and the evenness of $\cos(\cdot)$ around π, to respectively obtain

$$p_3(z) = \left(\frac{1}{2\pi}\right)^2 \int_{o}^{\pi}\int_{\pi}^{2\pi}\left\{\int_{-\infty}^{\infty} p_{\gamma_p|\phi_2}(u+|\beta|\,|\phi_2)\,p_{\gamma_r|\phi_1}(-z-u+|\alpha|\,|\phi_1)\,du\right\}d\phi_1 d\phi_2$$

$$= p_2(-z) \tag{I-18}$$

and

$$p_4(z) = \left(\frac{1}{2\pi}\right)^2 \int_{\pi}^{2\pi}\int_{\pi}^{2\pi}\left\{\int_{-\infty}^{\infty} p_{\gamma_p|\phi_2}(u-|\beta|\,|\phi_2)\,p_{\gamma_r|\phi_1}(-z-u+|\alpha|\,|\phi_1)\,du\right\}d\phi_1 d\phi_2$$

$$= p_1(-z) \qquad \text{(I-19)}$$

Hence, with Eqs. (I-18) and (I-19), Eq. (I-17) becomes

$$p_Z(z) = p_1(z) + p_2(z) + p_2(-z) + p_1(-z)$$

and thus the even property of $p_Z(z)$ is proven and Eq. (I-5) holds.

Although the (JR,JP) subcase was considered here, similar steps can be performed for the remaining subcases, with the results reflecting the conclusions formed above.

APPENDIX J

DETERMINATION OF THE GENERAL LOWER BOUND FOR M EVEN

The general lower bound for arbitrary M (even) was stated in Eq. (9-17) without proof. It is the purpose of this appendix to develop Eq. (9-17).

Consider the M decision regions shown in Figure 78. Without a loss of generality, it is assumed that the received signal must be contained within the shaded region for a correct decision to be made. There are M-1 remaining decision regions that comprise the entire error region. Bisect each of these M-1 error regions into two equal subregions as illustrated by the dashed lines in Figure 78. Begin from the shaded region and move clockwise through M-1 subregions; label these subregions R_1, R_2, . . . , R_{M-1}. Similarly, move counterclockwise from the shaded region and label the corresponding M-1 subregions R'_1, R'_2, . . . , R'_{M-1}. Let P_{R_j} be the probability that the received signal falls in the error subregion R_j, and $P_{R'_j}$ be the probability that the received signal falls in the error subregion R'_j.

From Figure 78 it is seen that

$$Pr(err) = \sum_{j=1}^{M-1} (P_{R_j} + P_{R'_j}) \qquad (J-1)$$

The upper bound discussed in Chapter IX may also be written in terms of these subregional probabilities. In fact

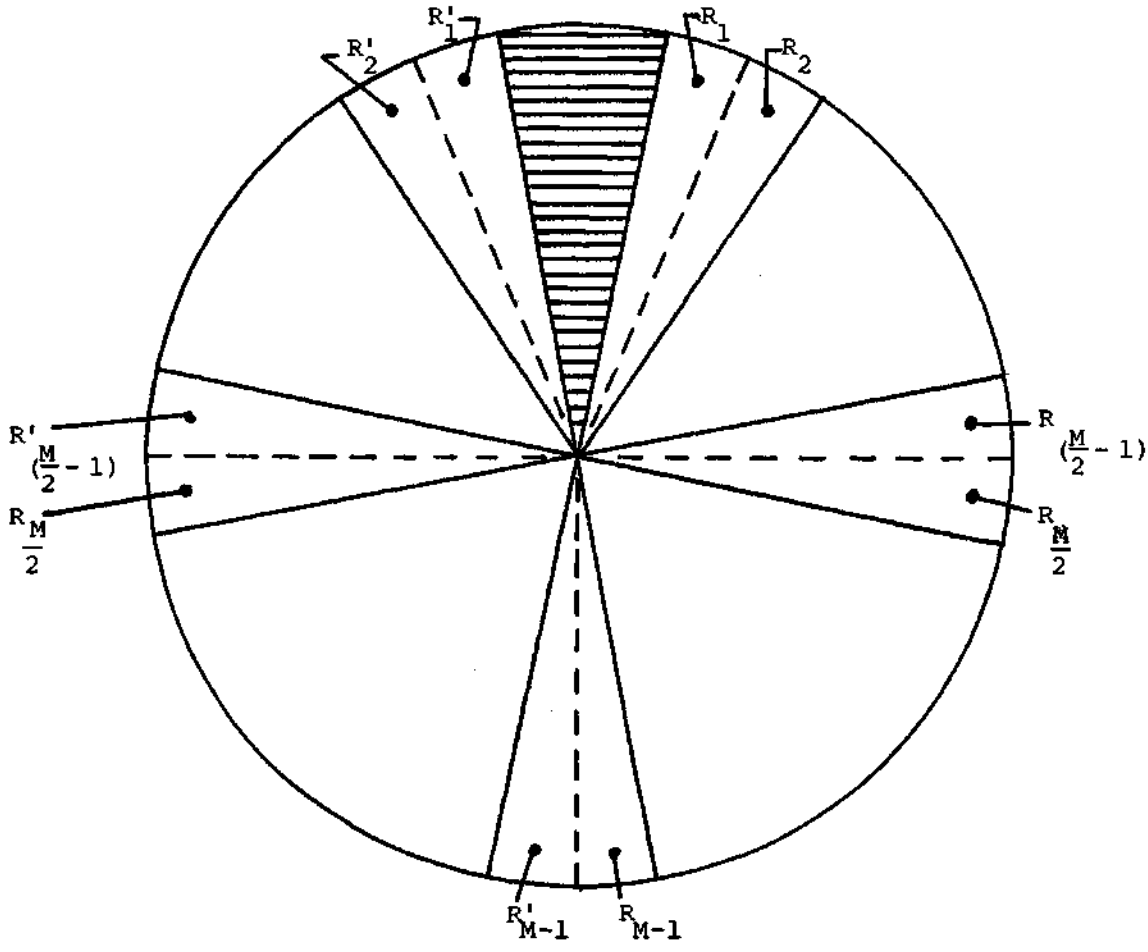

FIGURE 78. Illustration of the M-ary Decision Regions With the Appropriately Defined Error Sub-regions

$$P^{u}(\text{err}) = \sum_{j=1}^{M-2} (P_{R_j} + P_{R'_j}) + 2(P_{R_{(M-1)}} + P_{R'_{(M-1)}}) \qquad \text{(J-2)}$$

Consider the probability

$$P \triangleq P^{u}(\text{err}) - \frac{2}{M} \{ \sum_{j=\frac{M}{2}}^{M-1} (P_{R_j} + P_{R'_j}) \} \qquad \text{(J-3)}$$

Because of the symmetry in Figure 78, and the results of Appendix I

$$P_{R_j} = P_{R'_j} \qquad \text{(all j)} \quad , \qquad \text{(J-4)}$$

thus Eq. (J-3) becomes

$$P = P^{u}(\text{err}) - \frac{4}{M} \sum_{j=\frac{M}{2}}^{M-1} P_{R_j} \qquad \text{(J-5)}$$

The result of substituting Eq. (J-2) into Eq. (J-5) is

$$P = \sum_{j=1}^{M-2} (P_{R_j} + P_{R'_j}) + 2(P_{R_{(M-1)}} + P_{R'_{(M-1)}}) - \frac{4}{M} \sum_{j=\frac{M}{2}}^{M-1} P_{R_j}$$

$$= \sum_{j=1}^{\frac{M}{2}-1} P_{R_j} + (1 - \frac{4}{M}) \sum_{j=\frac{M}{2}}^{M-2} P_{R_j} + (2 - \frac{4}{M}) P_{R_{(M-1)}} + 2P_{R'_{(M-1)}} + \sum_{j=1}^{M-2} P_{R'_j}$$

(J-6)

With Eq. (J-4), equate one of the $P_{R'_{(M-1)}}$ probabilities to

$P_{R_{(M-1)}}$ to obtain

$$P = \sum_{j=1}^{\frac{M}{2}-1} P_{R_j} + (1 - \frac{4}{M}) \sum_{j=\frac{M}{2}}^{M-2} P_{R_j} + (2 - \frac{4}{M}) P_{R_{(M-1)}}$$

$$+ P_{R_{(M-1)}} + P_{R'_{(M-1)}} + \sum_{j=1}^{M-2} P_{R'_j}$$

$$= \sum_{j=1}^{\frac{M}{2}-1} P_{R_j} + (1 - \frac{4}{M}) \sum_{j=\frac{M}{2}}^{M-2} (P_{R_j} + \frac{4}{M-4} \cdot P_{R_{(M-1)}})$$

$$+ P_{R_{(M-1)}} + P_{R'_{(M-1)}} + \sum_{j=1}^{M-2} P_{R'_j} \qquad \text{(J-7)}$$

Since the subregion $R_{(M-1)}$ is further away from the error-free region it is less likely to contain the received signal than is subregion R_j for $j<M-1$. In other words

$$P_{R_j} > P_{R_{(M-1)}} \qquad (j<M-1)$$

Therefore Eq. (J-7) is upper bounded by

$$P < \sum_{j=1}^{\frac{M}{2}-1} P_{R_j} + (1 - \frac{4}{M}) \sum_{j=\frac{M}{2}}^{M-2} (P_{R_j} + \frac{4}{M-4} P_{R_j})$$

$$+ P_{R_{(M-1)}} + P_{R'_{(M-1)}} + \sum_{j=1}^{M-2} P_{R'_j}$$

or

$$P < \sum_{j=1}^{M-1} (P_{R_j} + P_{R'_j}) = Pr(err) \qquad (J-8)$$

Equation (J-8) says that P is a lower bound to the true probability of error so

$$P^{\ell}(err) = P = P^{u}(err) - \frac{2}{M} \sum_{j=\frac{M}{2}}^{M-1} (P_{R_j} + P_{R'_j})$$

$$= P^{u}(err) - \frac{2}{M} P_B(err) \qquad (J-9)$$

where the binary error probability, $P_B(err)$, is equal to

$$P_B(err) = \sum_{j=\frac{M}{2}}^{M-1} (P_{R_j} + P_{R'_j})$$

APPENDIX K

CONDITIONS FOR ENVELOPE PERIODICITY

A simplification of Eq. (10-3) is possible provided the envelope of the spread and filtered jamming signal returns to its initial value after N_r signaling intervals. For such a repetition, the infinite averaging is reduced to a finite averaging over N_r signaling intervals and p phase shifts. Therefore, the conditions under which the envelope is periodic over a period $N_r T_b$ must be obtained in order to insure the finite averaging.

Referring back to Eqs. (5-9) and (5-10), it can be seen that the envelope $A_{ji}(t)$ is periodic provided the time functions $\rho_1(t)$ and $\rho_2(t)$ are jointly periodic. By joint periodicity it is meant that the periods of $\rho_1(t)$ and $\rho_2(t)$ are integrally related. The joint period, if in fact it exists, must be equal to the period of $A_{ji}(t)$.

The actual existence of the joint period is determined by investigating the frequency content of $\rho_1(t)$ and $\rho_2(t)$ separately. For $\rho_1(t)$, the set of frequencies is

$$\{\omega_1\} = \{\omega_j - \omega_c + n\omega_m + m\omega_p\} \qquad \text{(K-1)}$$

with $n = 0, \pm 1, \pm 2, \ldots$, and $m = 0, 1, 2, \ldots$. The frequency offset parameter W_{fo}, the jamming slip ratio S_j, and the code slip ratio S_c are, respectively, defined as

$$W_{fo} \triangleq \frac{\omega_j - \omega_c}{\omega_b} \tag{K-2}$$

$$S_j \triangleq \frac{\omega_m}{\omega_b} \tag{K-3}$$

and

$$S_c \triangleq \frac{\omega_p}{\omega_b} \tag{K-4}$$

As a result, the set of frequencies for $\rho_1(t)$ becomes

$$\{\omega_1\} = \{(\frac{\omega_j - \omega_c}{\omega_b} + n\frac{\omega_m}{\omega_b} + m\frac{\omega_p}{\omega_b})\omega_b\}$$

$$= \{(W_{fo} + nS_j + mS_c)\omega_b\} \tag{K-5}$$

Consider the joint class of jamming signals and PR waveforms for which the frequency offset parameter, the jamming slip ratio, and the code slip ratio are rational numbers. In other words,

$$W_{fo} = N_1 + \frac{u_1}{v_1}$$

$$S_j = N_2 + \frac{u_2}{v_2}$$

$$S_c = N_3 + \frac{u_3}{v_3} \tag{K-6}$$

where

$$N_1 = 0,\pm1,\pm2, \ldots$$

$$N_i = 0,1,2, \ldots \qquad (i=2,3)$$

$$u_i, v_i = 0,1,2, \ldots \qquad (i=1,2,3)$$

and

$$u_i < v_i \qquad (i=1,2,3)$$

This joint class is not rigidly restrictive since any irrational number can be closely approximated to any degree of accuracy by a rational number. Furthermore, the rational frequency offset includes the important cases of cochannel ($N_1=u_1=0$), band edge ($|N_1|=1, u_1=0$) and interchannel ($|N_1|>1$) interference.

The frequency content of $\rho_1(t)$ for this special class becomes

$$\{\omega_1\} = \{(N_1 + \frac{u_1}{v_1} + nN_2 + \frac{nu_2}{v_2} + mN_3 + \frac{mu_3}{v_3})\omega_b\} \qquad (K-7)$$

The smallest frequency may not always be considered the fundamental frequency since higher frequencies may not be harmonically related to it. However, a fundamental frequency does exist and is equal to

$$\omega_{f_1} = \frac{\omega_b}{v_1 v_2 v_3} .$$

The corresponding fundamental period is then

$$T_{f_1} = \frac{2\pi}{\omega_{f_1}} = \frac{2\pi}{\omega_b} (v_1 v_2 v_3) \tag{K-8}$$

Similarly for $\rho_2(t)$, the set of frequencies for the same class is

$$\{\omega_2\} = \{(N_1 + \frac{u_1}{v_1} + nN_2 + \frac{nu_2}{v_2} - mN_3 - \frac{mu_3}{v_3})\omega_b\} \tag{K-9}$$

It is again apparent that the fundamental frequency is

$$\omega_{f_2} = \frac{\omega_b}{v_1 v_2 v_3}$$

and a fundamental period

$$T_{f_2} = \frac{2\pi}{\omega_{f_2}} = \frac{2\pi}{\omega_b} (v_1 v_2 v_3) = T_{f_1} \tag{K-10}$$

From Eq. (K-10), the joint period T_f is

$$T_f = T_{f_1} = T_{f_2} = \frac{2\pi}{\omega_b} (v_1 v_2 v_3) \tag{K-11}$$

This states that the envelope is periodic with period T_f and will return to its initial value after T_f seconds. In order for the envelope to repeat b times every c signaling intervals, then

$$bT_f = cT_b$$

$$= b \frac{2\pi}{\omega_b} (v_1 v_2 v_3) = bT_b(v_1 v_2 v_3)$$

giving

$$\frac{c}{b} = v_1 v_2 v_3$$

Therefore the averaging process may be simplified to an average over $N_r = v_1 v_2 v_3$ time samples and p phase shifts for each time sample.

Furthermore, if W_{fo}, S_j, and S_c were

$$\begin{aligned} W_{fo} &= N_1 \qquad (N_1 = \text{integer}) \\ S_j &= N_2 \qquad (N_2 = \text{positive integer}) \\ S_c &= N_3 \qquad (N_3 = \text{positive integer}) \end{aligned} \tag{K-12}$$

then $u_1=u_2=u_3=0$. The choice of v_1,v_2, and v_3 is arbitrary, so let $v_1 = v_2=v_3=1$. For this special case

$$T_f = \frac{2\pi}{\omega_b} = T_b$$

and $\frac{c}{b} = 1$, which states that the envelope repeats once every signaling interval. Thus, in the notation introduced in Chapter X,

$$A_{jr}(nT_b,k_p) = A_{jr}((n-1)T_b,k_p)$$

and

$$A_{jp}(nT_b,k_p) = A_{jp}((n-1)T_b,k_p)$$

In the case of the CW-tone jamming signal, the same parameter values in Eqs. (K-6) or (K-12) (excluding S_j) produce the required periodic amplitudes.

APPENDIX L

ENVELOPE CALCULATIONS

As p becomes larger, the amount of computation time required to evaluate the CW-tone, envelope maximum or the FM, RMS value of the envelope becomes a large percentage of the overall computation time. At this time though, it is important to emphasize that no additional, envelope computation time is required once the values have been calculated for the specific interference parameters; the same envelope values are continually used for all ranges and changes of SNR, SJR, K_s, N_s, and M. In other words, once an envelope value is calculated, a large number of parameter variations may occur without a new envelope calculation.

As computers become faster and more powerful, the computation time will certainly decrease, but until then an alternate method of envelope calculation is quite advantageous for the extreme cases. In a strict mathematical sense, the new method to be presented is an unproven technique, however, for every case considered thus far, the method is substantiated and can be explained heuristically.

Consider for the time being the calculation of the spread and filtered, cochannel, CW-tone envelope. There are a total of p (corresponding to the p possible PR chips) envelope values to calculate and compare. Interestingly enough, the envelope maximum always occurs at a time near or coinciding with a long string of consecutive 1's or 0's of the PR sequence (+1 or -1 of the PR waveform). A possible reason for

such a happening is that during a long string of unchanged bits, the jamming signal is increasing in amplitude (charging up). There are no changes during this period to prevent the jamming amplitude from increasing. For example, the PR-code sequence for p=7 is 1110100, and the envelope maximum for a spread and filtered, cochannel, CW-tone jamming signal is located at the end of the third bit (the end of the longest string of consecutive 1's).

In some instances, the maximum does not necessarily occur <u>at</u> the end of the longest string of 1's but rather <u>near</u> one of the longer string of consecutive bits. This is illustrated in the case of p=127 where the bits found in locations 91-111 are 00100010000010010011. The consecutive string of six 0's is the second longest string of consecutive bits (seven 1's is the longest) but the additional 0's near this string act as additional "charging" intervals for the jamming signal. In fact the envelope maximum for a spread (p=127) and filtered, cochannel, CW-tone signal occurs at the end of the 109^{th} bit. Therefore, the envelope calculation method proposed here is to choose those bit locations which have the greatest possibility of "charging up" the jamming signal and calculate the envelope for those locations only.

The most probable bit locations may be found at or near the longest string of consecutive 1's or 0's. Good beginning choices would be those locations at which the last 1 occurs for the longest string of 1's and at which the last 0 occurs for the longest string of 0's. From there, notice the bit variations around these longer strings. If there are some strings of identical bits around the longest strings, and separated from these longest strings by a small number of different

bits, the ends of these strings would be very good second choices. As an example, consider those bits from locations 91-111 for p=127. Notice that immediately following the string of six 0's, the sequence 10010011 occurs. The two strings of two 0's will cause the envelope to increase more than the 1's preceding them decrease it. Thus, the end of each string of two 0's here would be a good choice. At the end of the second string of two 0's, the consecutive 1's drastically reduce the envelope. Whenever there are rapid bit changes, a possible location is rather unlikely.

The search method proposed here is not a mathematically proven search, yet for every case considered thus far, the location of the maximum has been successfully chosen in this manner. The only drawback of this method is that it is not clear that the method works for non-cochannel interference. Therefore, the envelope maximum for non-cochannel, CW-tone interference must be determined in the conventional brute-force manner.

It has also become apparent that the FM, RMS value is evaluated at the same maxchip which the maximum value for a CW-tone envelope is found. Therefore, the RMS calculation time can be reduced by using the same maxchip location as that used by the CW-tone calculations. Incidently, this phenomenon seems to occur regardless of the value of W_{fo}.

It must be emphasized here that these methods are not generally proven schemes but rather engineering methods which have been successfully demonstrated in a large number of specific cases. The calculations of the maximum and RMS envelope values can most certainly be carried out exactly, but as the confidence in the above heuristically

proven method increases, the methods will become computationally more attractive.

BIBLIOGRAPHY

1. D. Mennie, "Communications and Microwave Technology," IEEE Spectrum, vol. 14, no. 1, p. 48, Jan. 1977.

2. F. T. Hutson, "UHF AFSAT/LES-8/9 Dual Modem," NAECON 1975 Record, pp. 371-376, 1975.

3. R. C. Dixon, "Why Spread Spectrum," IEEE Communications Society Magazine, vol. 13, no. 4, pp. 21-25, July 1975.

4. R. C. Dixon, Spread Spectrum Systems, New York, NY: John Wiley and Sons, 1976.

5. AGARD-LS-58, Spread Spectrum Communications, Lecture Series No. 58, July 1973 (AD-766-914).

6. Proceedings of the 1973 Symposium on Spread Spectrum Communications, Technical Document 271, Naval Electronics Systems Command, Naval Electronics Laboratory Center, San Diego, CA, March 1973 (AD-915-852).

7. N. G. Davies, "Performance and Synchronization Considerations," AGARD-LS-58, Spread Spectrum Communications, Lecture Series No. 58, July 1973 (AD-766-914).

8. R. F. Cobb and W. P. Osborne, "Hardware Implementation of a Spread Spectrum Modulator/Demodulator for the Space Shuttle Orbiter," National Telecommunications Conference, Dallas, TX, 1976.

9. R. Yost, "Synchronization of Digital Communication Systems," Interim Technical Report, School of Electrical Engineering, Georgia Institute of Technology, Atlanta, GA, for Headquarters-U.S. Air Force, Contract No. F30602-75-0118, December 1976.

10. E. J. Nossen, "Fast Frequency Hopping Synthesizer," Proceedings of the 1973 Symposium on Spread Spectrum Communications, Technical Document 271, Naval Electronics Systems Command, Naval Electronics Laboratory Center, San Diego, CA, pp. 51-63, March 1973 (AD-915-852).

11. "JTIDS/TIES Consolidate Tactical Communications," Electronic Warfare, pp. 45-53, September/October 1977.

12. J. W. Seyl and M. H. Kapell, "Application of Spread Spectrum to the Shuttle Orbiter Communication System," 1976 National Telecommunications Conference Record, pp. 32.1-1-32.1-5, December 1976.

13. B. H. Batson and R. W. Moorehead, "The Space Shuttle Orbiter Telecommunications System," IEEE Communications Society Magazine, vol. 14, no. 3, pp. 18-23, May 1976.

14. B. G. Glazer, "Spread Spectrum Concepts - A Tutorial," Proceedings of the 1973 Symposium on Spread Spectrum Communications, Technical Document 271, Naval Electronics Systems Command, Naval Electronics Laboratory Center, San Diego, CA, pp. 5-8, March 1973 (AD-915-852).

15. R. H. Pettit, "On the Use of Processing Gain as a Performance Measure for Spread-Spectrum Systems," Proceedings of IEEE Region 3 Southeastern Convention, pp. 185-188, April 4-6, Williamsburg, VA.

16. S. Stein and J. J. Jones, Modern Communication Principles with Application to Digital Signaling, New York, NY: McGraw-Hill Book Company, 1967.

17. M. L. Doelz, E. T. Heald, and D. L. Martin, "Binary Data Transmission Techniques for Linear Systems," Proceedings of the IRE, vol. 45, no. 5, pp. 656-661, May 1957.

18. M. L. Doelz, "Special Techniques for Detection in Noise," Collins Eng. Rep. (CER-W272) Burbank, CA, presented at IRE Subsection, Monmouth County, NJ, January 1953.

19. J. G. Lawton, "Comparison of Binary Data Transmission Systems," Proceedings of the Second National Conference on Military Electronics, pp. 54-61, 1958.

20. C. R. Cahn, "Performance of Digital Phase-Modulation Communication Systems," IRE Transactions on Communication Systems, vol. CS-7, pp. 3-6, May 1959.

21. A. S. Rosenbaum, "PSK Error Performance with Gaussian Noise and Interference," The Bell System Technical Journal, vol. 48, pp. 413-442, February 1968.

22. A. S. Rosenbaum, "Binary PSK Error Probabilities with Multiple Cochannel Interferences," IEEE Transactions on Communication Technology, vol. COM-18, no. 3, pp. 241-253, June 1970.

23. V. K. Prabhu, "Error Rate Considerations for Coherent Phase-Shift Keyed Systems with Cochannel Interference," The Bell Systems Technical Journal, vol. 49, pp. 743-767, March 1969.

24. D. Middleton, An Introduction to Statistical Communication Theory, New York, NY: McGraw-Hill Book Company, 1960, pp. 614-615.

25. J. J. Jones, "Multichannel FSK and DPSK Reception with Three-Component Multipath," IEEE Transactions on Communication Technology, vol. COM-16, no. 6, pp. 808-821, December 1968.

26. J. J. Jones, "FSK and DPSK Performance in a Mixture of CW-tone and Random Noise Interference," IEEE Transactions on Communication Technology, vol. COM-18, pp. 693-695, October 1970.

27. J. J. Bussgang and M. Leiter, "Error Performance of Differential Phase-Shift Transmission over a Telephone Line," IEEE Transactions on Communication Technology, vol. COM-16, no. 3, pp. 411-418, June 1968.

28. O. Shimbo, M. I. Celebiler, and R. J. Fang, "Performance Analysis of DPSK Systems in Both Thermal Noise and Intersymbol Interference," IEEE Transactions on Communication Technology, vol. COM-19, no. 6, pp. 1179-1188, December 1971.

29. J. Goldman, "Multiple Error Performance of PSK Systems with Co-channel Interference and Noise," IEEE Transactions on Communications Technology, vol. COM-19, no. 4, pp. 420-430, August 1971.

30. C. A. Lowery, Jr., "Susceptibility of Binary DPSK to Periodic FM Interference," Ph.D. dissertation, School of Electrical Engineering, Georgia Institute of Technology, Atlanta, GA, 1974.

31. R. H. Pettit, "Error Probability for NCFSK with Linear FM Jamming," IEEE Transactions on Aerospace and Electronic Systems, vol. AES-8, no. 5, pp. 609-614, September 1972.

32. R. H. Pettit, "Susceptibility Analysis of Binary NCFSK with Generalized Jamming," Interim Technical Report, School of Electrical Engineering, Georgia Institute of Technology, Atlanta, GA, for HqUSAF, Contract No. F30602-75-0118, October 1975.

33. J. G. Lawton, "Theoretical Error Rates of Differentially Coherent Binary and Kineplex Data Transmission Systems," Proceedings of the IRE, vol. 47, pp. 333-334, February 1959.

34. C. R. Cahn, "Comparison of Coherent and Phase-Comparison Detection of a Four-Phase Digital Signal," Proceedings of the IRE, vol. 47, p. 1662, September 1959.

35. J. T. Fleck and E. A. Trabka, "Error Probabilities of Multi-state Differentially Coherent Phase-Shift Keying Systems in the Presence of White Gaussian Noise," Detect Memo. No. 2A in "Investigation of Digital Data Communication Systems," J. G. Lawton, ed., Cornell Aeronautical Laboratory, Inc., Ithaca, NY, Report No. UA-1420-S-1; January 1961 (AD-256-584).

36. E. Arthurs and H. Dym, "On the Optimum Detection of Digital Signals in the Presence of White Gaussian Noise - A Geometric Interpretation and a Study of Three Basic Data Transmission Systems," IRE Transactions on Communication Systems, vol. CS-10, pp. 336-372, December 1962.

37. J. H. Halton and A. D. Spaulding, "Error Rates in Differentially Coherent Phase Systems in Non-Gaussian Noise," IEEE Transactions on Communication Technology, vol. COM-14, no. 5, pp. 594-601, October 1966.

38. A. S. Rosenbaum, "Error Performance of Multiphase DPSK with Noise and Interference," IEEE Transactions on Communication Technology, vol. COM-18, no. 6, pp. 821-824, December 1970.

39. V. Castellani, L. L. Presti, and M. Pent, "Performance of Multi-level DCPSK System in the Presence of Both Interchannel and Intersymbol Interference," Electronic Letters, vol. 10, no. 7, pp. 111-112, April 1974.

40. V. K. Prabhu, "Error-Rate Considerations for Digital Phase-Modulation Systems," IEEE Transactions on Communication Technology, vol. COM-17, no. 1, pp. 33-42, February 1969.

41. Microwave Journal Staff, "Microwave Components for EW Systems," Microwave Journal, vol. 20, no. 1, p. 16, January 1977.

42. S. W. Houston, "Modulation Techniques for Communication. Part 1: Tone and Noise Jamming Performance of Spread Spectrum M-ary FSK and 2, 4-ary DPSK Waveforms," NAECON 1975 Record, pp. 51-58, 1975.

43. H. Schmidt and P. L. McAdam, "Modulation Techniques for Communications. Part 2: Anti-Jam Performance of Spread Spectrum Coded Systems," NAECON 1975 Record, pp. 59-65, 1975.

44. R. H. Pettit, "Frequency-Hopping ECCM for Binary NCFSK with Generalized Jamming," Interim Technical Report, School of Electrical Engineering, Georgia Institute of Technology, Atlanta, GA, for HqUSAF, Contract No. F30602-75-0118, December 1975.

45. C. J. Waylan, "Detection of Fast, Noncoherent, Frequency-Hopped FSK," IEEE Transactions on Communications, vol. COM-23, no. 5, pp. 543-546, May 1975.

46. Veloris A. Marshall, III, "Theoretical Performance Models for a Coherent Frequency-Hopped/Pseudonoise Modem," MS Thesis, Air Force Institute of Technology, Wright-Patterson Air Force Base, Ohio, December 1975 (AD-A019-840).

47. J. L. Katz, "Performance of Spread Spectrum Modulation in a Multipath Environment," Technical Note 1972-28, Lincoln Laboratory, MIT, for Air Force Systems Command, USAF, Contract No. F19628-73-C-0002, July 1972.

48. P. C. Jain, "Performance of Hard-Limited Spread-Spectrum Transmission Systems," SRI Project 1328, Stanford Research Institute, Menlo Park, CA, for Rome Air Development Center, Griffiss Air Force Base, New York, Contract No. F30602-71-C-0338, April 1972.

49. D. J. Gooding, "Final Report - Modulation Study," Technical Report 6070-01, Stein Associates, Inc., Waltham, MA, for Naval Air Development Command, Warminster, PA, Contract No. N62269-76-M-2163, October 1975 (AD-A017-465).

50. P. M. Hopkins and R. S. Simpson, "Probability of Error in Pseudonoise (PN)-Modulated Spread Spectrum Binary Communication Systems," IEEE Transactions on Communications, vol. COM-23, no. 4, pp. 467-472, April 1975.

51. R. V. Ridings, C. R. Reeves, J. P. Aasterud, "Modulation Waveform Study," CDRL Item No. A002 (RADC-TR-77), Texas Instruments, Inc., Dallas, TX, for Rome Air Development Center, Griffiss Air Force Base, New York, Contract No. F30602-72-C-0102, March 1973 (AD-761-522).

52. A. Papoulis, Probability, Random Variables, and Stochastic Processes, New York, NY: McGraw-Hill Book Company, 1965.

53. R. Price, "Some Non-Central F-Distributions Expressed in Closed Form," Biometrika, vol. 51, no. 1 and 2, pp. 107-122, 1964.

54. H. L. Van Trees, Detection, Estimation, and Modulation Theory-Part I, New York, NY: John Wiley and Sons, Inc., 1968.

55. R. W. Lucky, "A Survey of the Communication Theory Literature," IEEE Transactions on Information Theory, vol. IT-19, no. 5, pp. 725-739, November 1973.

56. D. A. Schnidman, "Evaluation of the Q-Function," IEEE Transactions on Communications, vol. COM-22, no. 3, pp. 342-346, March 1974.

57. "Program ERF," Math Science Library, Level 404 , Version 1.0, Control Data Corporation.

58. I. S. Gradshteyn and I. M. Ryzhik, Tables of Integrals, Series, and Products, New York, NY: Academic Press, 1965.

VITA

Richard Alan Yost was born on October 27, 1951 in Fort Wayne, Indiana to Harold E. and Dortha A. Yost. He married his high school sweetheart, Sharon Lee Layton on August 17, 1974.

Mr. Yost attended and graduated from Fort Wayne's North Side High School in 1970. From 1970 to 1974 he attended Purdue University and received the Bachelor of Science Degree in Electrical Engineering With Distinction.

Graduate studies were begun at the Georgia Institute of Technology in 1974 where he was awarded the 1974-75 President's Fellowship and the following year, the 1975-76 Schlumberger Fellowship. He received his M.S.E.E. degree in 1975 and since then has been a graduate research assistant and a graduate teaching assistant.